

Expression, purification and characterisation of  
typical 2-Cys peroxiredoxins from Southern bluefin  
tuna (*Thunnus maccoyii*), Atlantic salmon (*Salmo  
salar*) and Yellowtail kingfish (*Seriola lalandi*)

Drew L. Sutton

B.Med.Sci., B.Sc. (Hons)

A thesis submitted in fulfilment of the requirements for the degree  
of Doctor of Philosophy

School of Biological Sciences  
Faculty of Science and Engineering  
Flinders University



# Table of Contents

Summary	i
Declaration	iii
Acknowledgements	iv

## Chapter 1

### Introduction

1.1 Reactive oxygen species	2
1.2 Sources of ROS	2
1.3 Role of ROS in cell damage and disease	6
1.4 Role of ROS in normal cell function	8
1.5 Decomposition of ROS	10
1.6 Oxidative stress in fish	16
1.7 Oxidative stress in farmed finfish and its impact on the industry	17
1.8 Enzymatic antioxidant defences in finfish	18
1.9 Aims and scope of this study	19

## Chapter 2

### Common materials and methods

2.1 <i>Escherichia coli</i> strain descriptions	22
2.2 pET-30a vector map	22
2.3 <i>Escherichia coli</i> growth conditions	24
2.4 Cryopreserved <i>Escherichia coli</i> cell stock preparation	24
2.5 DNA purification	24
2.6 Agarose gel electrophoresis of DNA	25
2.7 Polymerase Chain Reaction (PCR) - based amplification of DNA	26
2.8 DNA sequencing	26
2.9 <i>Escherichia coli</i> transformation	26
2.10 Polymerase Chain Reaction (PCR) - based colony screening	27
2.11 Recombinant protein expression	28
2.12 Sodium Dodecyl Sulphate Polyacrylamide Gel Electrophoresis	29
2.13 Immunoblotting	31
2.14 Nickel affinity chromatography purification of recombinant proteins	31
2.15 Peroxiredoxin enzyme assays	33
2.16 Gel filtration chromatography	34

2.17 Differential centrifugation	34
2.18 Protein crystallisation	35
2.19 Protein crystal harvesting and X-ray crystallography analysis	36

### Chapter 3

Expression, purification, and characterisation of a peroxiredoxin 2 from southern bluefin tuna (*Thunnus maccoyii*)

3.1 Introduction	38
3.2 Materials and Methods	40
3.2.1 Gene construct	40
3.2.2 Sequencing of pET-30a-SBT-Prx construct	40
3.2.3 Optimisation of recombinant SBT Prx 2 protein expression	41
3.2.4 Large scale recombinant SBT Prx 2 protein expression	41
3.2.5 Ni-affinity purification of SBT Prx 2 protein	42
3.2.6 SBT Prx 2 kinetic assays	42
3.2.7 Gel filtration chromatography of SBT Prx 2 protein	42
3.2.8 SBT Prx 2 Cys mutant cloning, expression and purification	43
3.2.9 SBT Prx 2 antibody preparation and evaluation	45
3.2.10 Crystallisation of SBT Prx 2 protein	47
3.3 Results	52
3.3.1 Sequencing of pET-30a-SBT Prx construct	52
3.3.2 SBT Prx protein sequence analysis	52
3.3.3 Optimisation of recombinant SBT Prx 2 protein expression	59
3.3.4 Large scale recombinant expression of SBT Prx 2 protein	61
3.3.5 Ni-affinity purification of SBT Prx 2 protein	65
3.3.6 Development of the Prx kinetic assay	67
3.3.7 SBT Prx 2 kinetics	73
3.3.8 Gel filtration chromatography of SBT Prx 2 protein	77
3.3.9 SBT Prx 2 Cys mutant cloning, expression, purification and characterisation	81
3.3.10 SBT Prx 2 antibody preparation and evaluation	103
3.3.11 Crystallisation of SBT Prx 2 protein	107
3.4 Discussion	119

## Chapter 4

Expression, purification, and characterisation of a peroxiredoxin 1 from Atlantic salmon (*Salmo salar*)

4.1 Introduction	138
4.2 Materials and Methods	140
4.2.1 Gene Construct	140
4.2.2 Sequencing of pET-30a-AS Prx construct	140
4.2.3 Optimisation of recombinant AS Prx 1 protein expression	141
4.2.4 Large scale recombinant AS Prx 1 protein expression	141
4.2.5 Ni-affinity purification of AS Prx 1 protein	142
4.2.6 AS Prx 1 kinetic assays	142
4.2.7 Gel filtration chromatography of AS Prx 1 protein	142
4.2.8 Crystallisation of AS Prx 1 protein	143
4.3 Results	144
4.3.1 Sequencing of pET-30a-AS Prx construct	144
4.3.2 AS Prx protein sequence analysis	144
4.3.3 Optimisation of recombinant AS Prx 1 protein expression	151
4.3.4 Large scale recombinant expression of AS Prx 1 protein	153
4.3.5 Ni-affinity purification of AS Prx 1 protein	157
4.3.6 AS Prx 1 kinetics	159
4.3.7 Gel filtration chromatography of AS Prx 1 protein	161
4.3.8 Crystallisation of AS Prx 1 protein	163
4.4 Discussion	168

## Chapter 5

Expression, purification and characterisation of a peroxiredoxin 4 from yellowtail kingfish (*Seriola lalandi*)

5.1 Introduction	174
5.2 Materials and Methods	176
5.2.1 Gene Construct	176
5.2.2 Sequencing of pET-30a-YTK Prx 4 construct	176
5.2.3 Site-directed mutagenesis of pET-30a-YTK Prx 4 construct	177
5.2.4 Preparation of constructs with truncated YTK Prx 4 inserts	178
5.2.5 Expression and purification of YTK Prx 4-197, 231 and 264 proteins	180

5.2.6 Gel filtration chromatography of YTK Prx 4-197 and 231 proteins	181
5.3 Results	182
5.3.1 Sequencing of pET-30a-YTK Prx 4 construct	182
5.3.2 Site directed mutagenesis of pET-30a-YTK Prx 4 construct	184
5.3.3 Sequence analysis of predicted N-terminal YTK Prx 4 signal peptides	186
5.3.4 Preparation of constructs with truncated YTK Prx 4 inserts	187
5.3.5 Large scale expression of YTK Prx 4-197, 231 and 264 protein	189
5.3.6 Ni-affinity purification of YTK Prx 4-197, 231 and 264 proteins	194
5.3.7 Gel filtration chromatography of YTK Prx 4-197 and 231 proteins	198
5.4 Discussion	203
<b>Chapter 6</b>	
General discussion and conclusion	210
<b>References</b>	216
<b>Appendix</b>	
Crystallisation suite composition tables	
1.1 Qiagen® NeXta® Classic Suite	234
1.2 Qiagen® NeXta® PEGs Suite	239
1.3 Qiagen® NeXta® MPD Suite	243
1.4 Hampton Research Crystal Screen	247
1.5 Hampton Research Crystal Screen 2	250

## Summary

The typical 2-Cys peroxiredoxins (Prxs) are a family of highly conserved proteins that are ubiquitously distributed throughout all phyla. Within the cell, they detoxify various peroxide substrates and thus contribute to regulation of the redox environment. The function and structure of typical 2-Cys Prxs has been well characterised in mammals, yeast, protists and bacteria but not in fish. In the present study, I present the functional and structural characterisation of a selection of typical 2-Cys Prxs from three finfish species that are important in Australian aquaculture. These finfish species include *Thunnus maccoyii* (southern bluefin tuna, SBT), *Salmo salar* (Atlantic salmon, AS) and *Seriola lalandi* (yellowtail kingfish, YTK).

The SBT and AS Prx deduced amino acid sequences contain features including peroxidatic and resolving Cys residues that are highly conserved among typical 2-Cys Prxs. Phylogenetic analysis of these amino acid sequences revealed that the AS Prx was most likely a Prx 1 isoform while the SBT Prx was most likely a Prx 2 isoform. Previously, the YTK Prx deduced amino acid sequence was found to contain the highly conserved features of typical 2-Cys Prxs in addition to an N-terminal extension. The N-terminal amino acid extension is a defining feature of Prx 4 isoforms and encodes an endoplasmic reticulum signal peptide. Analysis of the YTK Prx 4 N-terminal amino acid extension revealed that the putative signal peptide was most likely encoded by the first 33 amino acids. The deduced amino acid sequences of all three finfish Prx isoforms also contained the GGLG motif associated with the sensitivity of eukaryotic typical 2-Cys Prx proteins to overoxidation and consequent inactivation by peroxide substrates.

Functional characterisation of purified recombinant SBT Prx 2 and AS Prx 1 revealed that both proteins exhibited thioredoxin-dependent peroxidase activity. At low concentrations of peroxide substrate ( $\leq 120 \mu\text{M}$ ), the SBT Prx 2 protein

displayed positive cooperativity, a unique feature among typical 2-Cys Prxs. In contrast, at increasing high concentrations of peroxide substrate (0.5-2.0 mM), the peroxidase activity of the SBT Prx 2 and AS Prx 1 proteins was progressively lost. Consistent with other eukaryotic typical 2-Cys Prx 1 and Prx 2 isoform comparisons, the AS Prx 1 protein displayed a greater susceptibility to inactivation by increasing high concentrations of peroxide substrate compared to the SBT Prx 2 protein.

Analysis of the native molecular mass of purified recombinant SBT Prx 2, AS Prx 1 and YTK Prx 4 proteins revealed differences in oligomeric structure that were influenced by changes in the redox environment and protein concentration. Under reducing and oxidising conditions, the native molecular mass of the SBT Prx 2 and YTK Prx 4 proteins (minus its predicted N-terminal signal peptides) remained relatively unchanged. However, prolonged storage of the SBT Prx 2 protein promoted the formation of large aggregates consistent with a dimer of decamers. In contrast to the SBT Prx 2 and YTK Prx 4 proteins, the oligomeric properties of the AS Prx 1 protein were strongly influenced by the redox environment. Under reducing conditions, the AS Prx 1 protein existed predominantly as decamers while under oxidising conditions its structure was destabilised, resulting in the formation of insoluble aggregates. At comparable protein concentrations, the AS Prx 1 and YTK Prx 4 (minus its predicted N-terminal signal peptides) existed predominantly as decamers while the SBT Prx 2 existed predominantly as dimers. However, at a higher protein concentration, the native molecular mass of the SBT Prx 2 shifted from dimer to higher order oligomeric structures including decamers.

## Declaration

"I certify that this document does not incorporate without acknowledgement any material previously submitted for a degree or diploma in any University; and that to the best of my knowledge does not contain any material previously published by another person except where due reference is made in the text"

## Authority Access

This document may be made available for loan and limited copying in accordance with the Copyright Act, 1968.

Signed

Drew L. Sutton



## Acknowledgements

The production of this thesis is the culmination of my PhD studies which has only been achievable with the guidance, support and friendship of my colleagues, and love and support of my family and friends.

To my primary supervisor, Associate Professor Kathy Schuller, I am privileged to have had the opportunity to work with you as a member of your research team. At every step of the way you have unconditionally offered me your time, guidance and support for which I am extremely grateful. I would also like to extend a sincere thanks to my co-supervisor, Associate Professor Ian Menz, for his technical counsel, enthusiasm and support.

Over the course of my PhD studies I have had the privilege of working alongside many great colleagues, some of whom have become good friends. First and foremost, I would like to thank Dr Melissa Gregory for her friendship, support and technical counsel. It was a pleasure to have studied with you. I would also like to thank the following members of the molecular research cluster for their assistance and friendship; Dr Bart Eijkelkamp, Dr Peter Bain, Dr Melissa Pitman, Dr Simon Williams, Dr Patrick Laffy, Dr Melani Sulda, Dr Crystal Sweetman, Dr Chevaun Smith, Mr Nicholas Warnock, Ms Emma de Courcy-Ireland, Ms Bianca Kyriacou, Mr Pradeep Sornaraj and Ms Lexi Young.

Not only have I had great support and guidance from colleagues throughout my PhD studies, I have also been exceptionally lucky to have had the love and support of my family and friends. To my wife Dana, parents Grant and Sue, sister Wendy and extended family, I sincerely thank you for your constant love, patience and kind words of encouragement. I love you all so much. These same thanks are extended to my wonderful circle of friends. Thank you all for helping me through the difficult times and sharing in the celebration of the successful times.

# Chapter 1

Introduction

## 1.1 Reactive oxygen species

Oxygen ( $O_2$ ) is an essential molecule required by all aerobic organisms (Halliwell, 1978). Its role within aerobic organisms is to act as the terminal electron acceptor at complex IV of the mitochondrial electron transport chain (Errede et al., 1978). In its ground state,  $O_2$  is a relatively un-reactive molecule. However, in its step-wise reduction to water, requiring a total of four electrons, several reactive partially reduced intermediates are produced. These reactive  $O_2$  species (ROS) include super oxide ( $\cdot O_2^-$ ), hydrogen peroxide ( $H_2O_2$ ), and the hydroxyl radical ( $\cdot OH$ ) (Scandalious, 1993). In a regulated environment, ROS play a variety of important roles in normal cellular function, including defence against invading organisms and cell signalling (Rada and Leto, 2008). Conversely, in an unregulated environment, accumulated ROS can non-specifically and rapidly react with biomolecules, causing molecular damage such as DNA mutation, protein oxidation and lipid peroxidation (Lambeth, 2004).

## 1.2 Sources of ROS

Within cells, ROS are produced by several organelles including mitochondria, endoplasmic reticulum and peroxisomes. It is generally accepted that the mitochondrial electron transport chain is an important and significant source of ROS (Cochemé and Murphy, 2009). Early studies of sub-mitochondrial particles and intact isolated mitochondria revealed that they produced  $H_2O_2$  (Jensen, 1966; Chance and Oshino, 1971). The  $H_2O_2$  produced from sub-mitochondrial particles was later found to be derived in part from the dismutation of  $\cdot O_2^-$  (Loschen et al., 1974). Superoxide dismutates to form  $H_2O_2$  and water in a spontaneous process that is enhanced by the superoxide dismutase enzyme (McCord and Fridovich, 1969). Superoxide itself is generated from the interaction of  $O_2$  with an electron leaking

from the mitochondrial electron transport chain (Cochemé and Murphy, 2009). Within isolated mitochondria, significant  $\cdot\text{O}_2^-$  production can occur in two modes of operation. Firstly,  $\cdot\text{O}_2^-$  is produced from Complex I when mitochondria are not making ATP and consequently have a high proton-motive force and a reduced coenzyme Q pool. Secondly, when there is a high NADH/NAD<sup>+</sup> ratio in the matrix. Conversely, when mitochondria are actively generating ATP, and consequently have a lower proton-motive force and NADH/NAD<sup>+</sup> ratio,  $\cdot\text{O}_2^-$  is still produced albeit at a far lower rate (Reviewed in Murphy, 2009). Analysis of isolated mitochondria from *Drosophila melanogaster* revealed that in the presence of antimycin, an inhibitor of the cytochrome c reductase portion of Complex III, glycerol-3-phosphate dehydrogenase and centre o of Complex III had the greatest capacity to produce  $\cdot\text{O}_2^-$  on the cytosolic side of the inner membrane whilst on the matrix side of the inner membrane only Complex I produced a significant amount of  $\cdot\text{O}_2^-$ . In the absence of antimycin, both glycerol-3-phosphate dehydrogenase and Complex I remained sites of  $\cdot\text{O}_2^-$  production but centre o of Complex III did not (Miwa et al., 2003). Despite the fairly complete understanding of the magnitude and source of ROS production in isolated mitochondria, there is still relatively little known about this in the mitochondria of living organisms (Cochemé and Murphy, 2009).

The membranes of the endoplasmic reticulum have been shown to be a site of  $\text{H}_2\text{O}_2$  production. Investigation into oxidation of drugs by liver microsomes revealed that the oxidation of triphosphopyridine nucleotide (nicotinamide adenine dinucleotide phosphate) by triphosphopyridine nucleotide oxidase (nicotinamide adenine dinucleotide phosphate oxidase) resulted in the production of  $\text{H}_2\text{O}_2$  (Gillette et al., 1956). Later, the microsomal oxidation of nicotinamide adenine dinucleotide phosphate (NADPH), in the absence of hydroxylating substrates, was found to produce  $\text{H}_2\text{O}_2$  in an almost quantitative fashion. It was reasoned that NADPH-

cytochrome c reductase was the most likely candidate responsible for the microsomal production of  $H_2O_2$  (Boveris et al., 1972).

Peroxisomes were first isolated by De Duve and Baudhuin (1966) and found to contain  $H_2O_2$  producing oxidases in addition to catalase, a  $H_2O_2$  degrading enzyme. The main sources of  $H_2O_2$  production in peroxisomes are oxidases that transfer hydrogen from their respective substrates to  $O_2$ . These oxidases include Acyl-CoA, D-Amino acid, D-Aspartate,  $\alpha$ -Hydroxyacid, Pipecolic acid, Polyamine and Urate oxidases (reviewed in Schrader and Fahimi, 2004). Of the various metabolic processes that these oxidases are involved in, the most important in terms of  $H_2O_2$  production is the  $\beta$ -oxidation of fatty acids performed by the Acyl-CoA oxidases (Schrader and Fahimi, 2004). Peroxisomes have also been found to be sources of  $\cdot O_2^-$  production. Xanthine oxidase, a key enzyme in purine metabolism, is capable of reducing  $O_2$  to produce  $\cdot O_2^-$  (Harrison, 2002; McCord and Fridovich, 1968).

In addition to the intracellular enzyme-mediated sources of ROS, there are several environmental sources of ROS and pro-oxidants that stimulate the production of ROS. These environmental sources include transition metals (Stohs and Bagchi, 1995) and radiation (Stadtman and Levine, 2000). Transition metals, including iron, copper, cadmium, chromium, lead, mercury, nickel and vanadium, exhibit the ability to catalyse the production of ROS. The basic mechanism of ROS production is the same for these transition metal ions and involves Fenton-like chemistry that is governed by the Haber-Weiss reaction (reviewed in Stohs and Bagchi, 1995).

Fenton (1894) observed that in the presence of  $H_2O_2$  and a ferrous iron salt, tartaric acid was oxidised to yield a strong violet coloured solution upon addition of caustic alkali. It was later proposed that iron salts catalyse the decomposition of  $H_2O_2$  to produce the highly oxidising  $\cdot OH$  radical in a net reaction that is now referred to as the Haber-Weiss reaction (Haber and Weiss, 1934; Kehrer, 2000). The Haber-Weiss reaction consists of two steps with the first involving an interaction between ferric

iron ( $\text{Fe}^{3+}$ ) and  $\cdot\text{O}_2^-$  to produce ferrous iron ( $\text{Fe}^{2+}$ ) and  $\text{O}_2$ . The second step consists of an interaction between  $\text{Fe}^{2+}$  and  $\text{H}_2\text{O}_2$  to produce  $\text{Fe}^{3+}$ , a hydroxyl anion ( $\text{OH}^-$ ) and  $\cdot\text{OH}$ . The iron-catalysed Haber-Weiss reaction, which makes use of Fenton chemistry, is considered to be the major mechanism by which  $\cdot\text{OH}$  is produced in biological systems (Kehrer, 2000).

Low energy photons, such as visible and ultraviolet light, participate in photochemical reactions that produce intracellular and environmental ROS. Upon colliding with a low energy photon, the energy levels of electrons in organic molecules are increased enabling subsequent chemical reactions to take place. These reactions may involve hydrogen abstraction resulting in the formation of a radical that can react with  $\text{O}_2$  to produce a peroxy radical. Alternatively, these reactions may be directly with  $\text{O}_2$ , generating singlet oxygen that can attack substrates and form peroxides, hydroperoxides or endoperoxides (Riley, 1994). The occurrence of hydrogen peroxide in surface seawater was first reported by Van Baalen and Marler (1966) and was speculated to be a result of photochemical reactions occurring in the seawater itself. Later, this was confirmed when it was found that the rate of  $\text{H}_2\text{O}_2$  production in surface seawater exhibited a linear increase relative to solar flux in the presence of superoxide dismutase (Petasne and Zika, 1987).

Ionising radiation, such as gamma ( $\gamma$ )-rays, generate ROS via radiolysis of water (reviewed in Pikaev and Ershov, 1967), direct ionisation of molecules (Riley, 1994) and activation of NADPH oxidase (Narayanan et al., 1997). In the absence of an electron donor, radicals derived from ionised molecules can react with  $\text{O}_2$  to produce peroxy radicals that undergo a variety of subsequent reactions (Riley, 1994). It has been well established that exposure to ionising radiation results in cellular damage and a biological response that occurs in both irradiated and non-irradiated cells within the same population, in what has been termed the 'bystander response'. Non-

irradiated cells in the vicinity of irradiated cells or exchanged into growth media derived from irradiated cells display biological responses and the same levels of genetic change and lethality as irradiated cells (reviewed in Azzam et al., 2003). The addition of superoxide dismutase, a scavenger of  $\cdot\text{O}_2^-$ , to the growth media of human lung fibroblasts prior to being  $\alpha$ -irradiated was found to inhibit the ionising radiation-induced bystander response, providing the first experimental evidence for the involvement of ROS (Lehnert and Goodwin, 1997). It was subsequently shown by the same group that  $\alpha$ -particles induce the production of  $\cdot\text{O}_2^-$  and  $\text{H}_2\text{O}_2$  in irradiated cells through the activation of plasma-bound NADPH oxidase (Narayanan et al., 1997).

### 1.3 Role of ROS in cell damage and disease

At physiological concentrations, ROS play an important role in normal cell function. However, in excess they give rise to a state of oxidative stress (Nordberg and Arner, 2001). Under oxidative stress conditions, the integrity of various cell components, such as protein, deoxyribonucleic acid (DNA) and lipids is threatened.

#### 1.3.1 Interactions of ROS with proteins

ROS-mediated oxidation of proteins leads to the conversion of histidine residues to 2-oxohistidine, tryptophan residues to kynurenine or *N*-formylkynurenine, tyrosine residues to dihydroxy derivatives, methionine residues to methionine sulfoxide or methionine sulfone derivatives, leucine and valine residues to hydroxyl derivatives, cysteine residues to disulphide derivatives, and lysine, arginine and proline residues to carbonyl derivatives. Carbonyl derivatives can further react with the  $\alpha$ -amino group of lysine residues in the same or another protein molecule to form intra- or inter-molecular protein cross-linked derivatives (Stadtman and Levine, 2000). Elevated levels of protein carbonyls, and hence oxidised proteins, are associated with a number of aging-related diseases and correlate well with their progression.

An increase in the level of oxidised proteins is associated with Alzheimer's disease, Parkinson's disease, adult onset (Type II) diabetes, rheumatoid arthritis, muscular dystrophy, cataractogenesis, induction of renal tumours, bronchopulmonary dysplasia, amyloidosis, chronic ethanol ingestion, acute carbon tetrachloride toxicity, amyotrophic lateral sclerosis and the progerias (reviewed in Stadtman and Levine, 2000).

### 1.3.2 Interactions of ROS with DNA

ROS-mediated damage of DNA occurs through attack on the bases or the deoxyribosyl backbone of DNA (Marnett, 2000). Of the various forms of ROS,  $\cdot\text{OH}$  reacts with DNA by addition to the double bonds of DNA bases and by abstraction of a hydrogen atom from the methyl group of thymine and each of the carbon-hydrogen bonds of 2'-deoxyribose. There are over 20 DNA base products that occur as a result of interaction with ROS and free radical species (reviewed in Cooke et al., 2003). A consequence of oxidative base abnormalities is mutation which is a crucial step in carcinogenesis. Having said this, there are many pathological conditions in which the level of oxidative DNA damage is elevated with no increased incidence of carcinogenesis (reviewed in Cooke et al., 2003).

### 1.3.3 Interaction of ROS with lipids

Lipid peroxidation is initiated by the abstraction of a hydrogen atom from a methylene carbon in the side chain of a fatty acid by a sufficiently reactive chemical species (Halliwell and Chirico, 1993). The reactive chemical species capable of hydrogen abstraction include the hydroxyl radical ( $\cdot\text{OH}$ ), alkoxyl radical ( $\text{RO}\cdot$ ), peroxy radical ( $\text{ROO}\cdot$ ), and possibly the hydroperoxyl radical ( $\text{HO}_2\cdot$ ) but not  $\text{H}_2\text{O}_2$  or  $\cdot\text{O}_2^-$  (Gutteridge, 1995). Polyunsaturated fatty acids (PUFAs) are, because of their multiple double bonds, highly susceptible to attack by ROS (Nordberg and Arnér, 2001). By contrast, both monounsaturated and saturated fatty acids are more



resistant to attack by ROS (Halliwell and Chirico, 1993). Upon abstraction of a methylene carbon hydrogen atom, a fatty acid undergoes a molecular rearrangement that results in the formation of a conjugated diene. Reaction between a conjugated diene and O<sub>2</sub> produces a peroxy radical, itself able to abstract a hydrogen atom from another fatty acid and thus start a chain reaction. The end products of the chain reaction are a variety of hydroperoxides and cyclic peroxides (Gutteridge, 1995). Peroxy radicals can also combine together if they meet or attack membrane proteins (Halliwell and Chirico, 1993). The consequences of extensive lipid peroxidation in biological membranes are loss of fluidity, falls in membrane potential, increased permeability to H<sup>+</sup> and other ions, and eventual rupture of the membrane (Gutteridge, 1995).

#### 1.4 Role of ROS in normal cell function

ROS are an important component of the innate immune system and cell signalling network. The ability of host macrophages and neutrophils to kill foreign cells depends on a number of mechanisms including the production of ROS by gp91phox, now known as NADPH oxidase-2 (Nox2) (Butler et al., 2010; Gough and Cotter, 2011). Within stimulated neutrophils, the catalytic Nox2 subunit combines with the regulatory p22phox subunit to produce the membrane-associated flavohemoprotein cytochrome *b*<sub>558</sub> (Babior, 1995; Lambeth, 2004). This complex combines with several cytosolic subunits (p47phox, p67phox, p40phox), as well as the small GTPase RAC (RAC2 and/or RAC1), to assemble the active oxidase (Uhlinger et al., 1993; Babior, 1995; Lambeth, 2004). The six transmembrane domains of the Nox2 subunit form a channel in the plasma membrane allowing successive transfer of electrons (Gough and Cotter, 2011). On the cytosolic side of the membrane, electrons are transferred sequentially from NADPH to flavin adenine dinucleotide (FAD) to haem and finally used to reduce O<sub>2</sub> in the phagosome (Lambeth, 2004; Gough and Cotter, 2011). The reduction of O<sub>2</sub> to produce  $\cdot\text{O}_2^-$ ,

termed the respiratory burst, results in the termination of foreign cells in the phagosome (Babior, 1995; Gough and Cotter, 2011). Nox2 and its homologues are also expressed in non-phagocytic cells and are a major source of  $H_2O_2$  in cells stimulated with various growth factors and cytokines including platelet-derived growth factor (PDGF), epidermal growth factor (EGF), insulin, tumor necrosis factor- $\alpha$  (TNF $\alpha$ ), interleukin-1 (IL-1) and several others. This ligand-induced production of ROS affects numerous intracellular signalling pathways involved in cell growth, differentiation and death (reviewed in Thannickal and Fanburg, 2000; Rhee, 2006).

Despite the accumulation of supporting evidence, the role of ROS as important intracellular signalling molecules has remained controversial (Rhee, 2006; D'Autréaux and Toledano, 2007). This is due to the apparent paradox between the specificity required for signalling and the highly reactive nature of ROS. Signalling specificity on a macromolecular level stems from the recognition that occurs between the complementary shapes of a ligand and its receptor. By contrast, signalling involving ROS occurs at the atomic level through chemical reactions with specific atoms in target proteins. The distinct biological properties of the different forms of ROS, including chemical reactivity, half-life and lipid solubility, provide a source of signalling specificity. For example,  $\cdot O_2^-$  can rapidly react with the iron-sulphur cluster redox centre of the *Escherichia coli* transcription factor SoxR due to its high electrostatic attraction, whereas  $H_2O_2$  can only mildly react due to its uncharged nature. Similarly, the unique chemical nature of the ROS target can also provide signalling specificity. For example, all characterised  $H_2O_2$ -specific regulatory mechanisms involve the oxidation of unique Cys residues with the exception of the transcription factor peroxide operon regulator (PerR), which uses an iron centre (D'Autréaux and Toledano, 2007). Additionally, specific Cys residues can be targeted based on differences in relative reactivity. The relative reactivity of a target thiol group is influenced by its chemical context and has been shown to be inversely

related to its pK (Winterbourn and Metodiewa, 1999). For example, at pH 7.4 the thiol group of penicillamine (pK 7.9) was the most reactive, whilst the thiol group of *N*-acetylcysteine (pK 9.5) was only mildly reactive.

## 1.5 Decomposition of ROS

The level of intracellular ROS, dictated by the relative rates of generation and decomposition, is tightly regulated to enable normal cell function and prevent oxidative stress. The rate of ROS decomposition is under the control of the antioxidant defence mechanisms of the cell. According to Halliwell and Gutteridge (1989), an antioxidant is defined as “any substance that, when present at low concentrations compared with that of an oxidisable substrate, significantly delays or inhibits oxidation of that substrate”. The antioxidant defence mechanisms of the cell can be divided into two distinct groups based on whether they are non-enzymatic or enzymatic. Non-enzymatic antioxidants in the lipid phase include tocopherols (a constituent of vitamin E) and carotenes, while in the aqueous phase they include ascorbate (vitamin C), glutathione (GSH) and other compounds (Sies, 1997). The antioxidant activity of tocopherols consists of the inhibition of lipid peroxidation in biological membranes by scavenging chain-propagating peroxy radicals (ROO·). This scavenging activity stems from their chromanol nucleus, where a phenolic hydroxy group donates a hydrogen atom to the peroxy radical to form hydroperoxide and a chromanoxyl radical (Serbinova et al., 1991). The chromanoxyl radical is reduced by external reductants that include ascorbate and thiols (Sies, 1997). The antioxidant activity of ascorbate is derived from the high reducing potential of its carbon-carbon double bond. Ascorbate readily donates hydrogen and electrons to a variety of oxidants, including O<sub>2</sub> free radicals, peroxides, and ·O<sub>2</sub><sup>-</sup> (May, 1998). The antioxidant properties of carotenes lie in their ability to physically quench singlet oxygen and trap peroxy radicals (Paiva and Russell, 1999). These antioxidant reactions occur via an extended system of conjugated double bonds

(reviewed in Sies and Stahl, 1995). Lastly, GSH scavenges free radicals via donation of a hydrogen atom from its thiol group. The oxidised thiol group is readily reduced by ascorbate to regenerate GSH (Chaudière and Ferrari-Iliou, 1999).

The enzymatic antioxidant defence mechanisms of the cell include superoxide dismutases (SODs), catalases (CATs), glutathione peroxidases (GPxs) and peroxiredoxins (Prxs). SODs catalyse the reduction of  $\cdot\text{O}_2^-$  to  $\text{H}_2\text{O}_2$  and  $\text{O}_2$  using an active site transition metal ion (McCord and Fridovich, 1969). The cytosolic and extra-cellular SOD isoforms contain copper and zinc ions, while the mitochondrial SOD isoform contains manganese ions (Weisiger and Fridovich, 1973; Marklund, 1984). The catalytic activity of CAT is also derived from a transition metal ion. The iron-containing ferriprotoporphyrin groups of CAT catalyse the decomposition of  $\text{H}_2\text{O}_2$  to  $\text{H}_2\text{O}$  and  $\text{O}_2$  in a two-step reaction (Kirkman and Gaetani, 2007). CAT is so efficient at catalysing these reactions that it cannot be saturated by  $\text{H}_2\text{O}_2$  at any concentration ( $k_{\text{cat}} = 4 \times 10^7 \text{ sec}^{-1}$ ) (Matés, 2000; Garrett and Grisham, 2008).

In contrast to SOD and CAT, the antioxidant activity of GPxs is dependent upon active site selenocysteine (Se-Cys) or cysteine (Cys) residues. In mammals, up to eight distinct GPxs have been detected. GPx-1, 2, 3, 4 and 6 contain an active site Se-Cys residue, while in the remaining variants, the Se-Cys is replaced by a Cys residue. Of the different GPx isoforms, only GPx-1, 3 and 4 have been characterised to any significant extent. Using GPx-1 as an example, the catalytic mechanism involves oxidation of the active site Se-Cys (Se-Cys-H) by a hydroperoxide substrate to yield Se-Cys-OH and the corresponding alcohol. Se-Cys-OH reacts with glutathione to form Se-Cys-OH-GSH, which subsequently undergoes a condensation reaction to produce the half reduced intermediate Se-Cys-SG and water. The Se-Cys-SG intermediate reacts with a second molecule of GSH to yield Se-Cys-SG-GSH, which subsequently rearranges to give Se-Cys-H-GSSG. Finally,

dissociation of oxidised glutathione (GSSG) reconstitutes Se-Cys-H, enabling subsequent rounds of hydroperoxide decomposition (Toppo et al., 2009).

In addition to GPx-5, 7 and 8, Prxs also contain an active site Cys residue capable of reducing peroxide substrates. This catalytic activity is a defining feature of Prxs and is also the basis on which they were discovered. The first member of the Prx family was identified in *Saccharomyces cerevisiae* as an unknown protein capable of preventing the oxidative inactivation of glutamine synthetase. The protection afforded by this protein against a thiol-containing oxidation system was found to be independent of CAT, GPx and SOD activity, and at this time was believed to be attributed to the elimination of sulphur radicals. As a result, the protein was named thiol specific-antioxidant (TSA) (Kim et al., 1988).

Insight into the physiological role of TSA was made by investigating the growth properties of a yeast mutant containing a disrupted TSA gene. Disruption of the TSA gene had no effect on cell viability under aerobic or anaerobic conditions compared to a wild-type strain but it did have an effect on growth rate. Under aerobic conditions, the TSA mutant was slower to grow and this was more pronounced upon inclusion of methyl viologen, a redox cycling drug, in the culture medium. Additionally, the TSA mutant was found to be more sensitive than a wild-type strain to t-butyl hydroperoxide, H<sub>2</sub>O<sub>2</sub> or cumyl hydroperoxide. The TSA mutant phenotype strongly suggested an antioxidant role for TSA (Chae et al., 1993).

A significant level of amino acid identity was found to exist between the TSA from yeast and the alkyl hydroperoxide reductase (AhpC) from *Salmonella typhimurium* and *Escherichia coli*. Subsequent database searches identified >23 proteins from organisms of all kingdoms that shared significant sequence identity to TSA and AhpC, thus defining a large new family of antioxidant enzymes. At this time, three additional members of the AhpC/TSA family were identified at the cDNA level and

they included natural killer enhancing factor (NKEF) A and B from human. As the nomenclature suggests, NKEF proteins were identified based on their ability to enhance Natural Killer (NK) cell cytotoxicity against different cells (Shau et al., 1994). Alignment of the AhpC/TSA sequences revealed that one Cys residue was conserved in all family members and the majority also possessed a second conserved Cys residue. Based on this, the AhpC/TSA family was divided into 2-Cys and 1-Cys subgroups (Chae et al., 1994a). The role of these conserved Cys residues was investigated in the yeast TSA by individual replacement with serine residues. Gel electrophoresis under non-reducing conditions revealed that the wild-type TSA existed as a dimer, whereas both Cys mutants existed as monomers. This suggested that dimer formation required a disulphide linkage, resulting in a head-to-tail arrangement of two monomer subunits. The N-terminal Cys residue, but not the C-terminal Cys residue, was found to be essential for TSA activity. Given that TSA was found to lack redox cofactors, such as heme, flavin, and metal ions, it was proposed that the N-terminal Cys residue was likely to be the site of oxidation by substrates (Chae et al., 1994b).

Clues to the substrate specificity of TSA and the agent responsible for its reduction came from the characterisation of the AhpC protein and its reducing partner AhpF. It was proposed that the reduced form of AhpC converted alkyl hydroperoxides to the corresponding alcohol by oxidation of its two conserved Cys residues, resulting in the formation of a disulphide bond. The regeneration of reduced AhpC was suggested to involve the sequential transfer of reducing equivalents from NAD(P)H to the FAD cofactor of AhpF, then to the two conserved Cys residues of AhpF, and finally to the two conserved Cys residues of AhpC. The overall reaction mechanism resulted in the coupling of peroxide reduction to NAD(P)H oxidation (Jacobson et al., 1989). In light of the homology between TSA and AhpC, it was suggested that TSA may also act on peroxide substrates and be regenerated by an enzyme with a

similar function to AhpF. This was proven to be the case when it was found that the TSA from yeast was capable of reducing  $\text{H}_2\text{O}_2$  and alkyl-hydroperoxide in the presence of two yeast proteins, thioredoxin (Trx) and thioredoxin reductase (TrxR), at the expense of NADPH. Based on these results the TSA naming was no longer applicable and was replaced with thioredoxin peroxidase (TPx). This naming was chosen to reflect the fact that this was the first peroxidase found to use thioredoxin as an intermediate hydrogen donor (Chae et al., 1994c). However, upon finding that a mammalian 1-Cys member of the AhpC/TPx family relied on GSH rather than Trx as the intermediate hydrogen donor, the TPx naming was replaced with peroxiredoxin (Prx) (reviewed in Fisher, 2011). The new Prx nomenclature was chosen to represent the family of peroxidases in which peroxide substrate reduction was catalysed by a Cys residue (Rhee and Woo, 2011).

Although Prxs were initially identified in yeast, it was in mammalian cells that multiple isoforms were first reported and characterised. As alluded to above, Prxs are classified as 1-Cys or 2-Cys depending on the number of Cys residues involved in catalysis. The 2-Cys Prxs can be further classified as typical or atypical based on reaction mechanism. Thus, there are three distinct classes of Prxs that include 1-Cys, typical 2-Cys and atypical 2-Cys (Rhee et al., 2005). In mammalian cells, there are a total of six expressed Prx isoforms (Prx 1-6) that are composed of four typical 2-Cys Prxs (Prx 1-4), one atypical 2-Cys Prx (Prx 5) and one 1-Cys Prx (Prx 6).

In common to the catalytic mechanism of all three classes of Prx, the detoxification of peroxide substrates involves oxidation of the peroxidatic Cys residue ( $\text{Cys-S}_\text{P}\text{H}$ ) to Cys sulfenic acid ( $\text{Cys-S}_\text{P}\text{OH}$ ). The mechanism by which  $\text{Cys-S}_\text{P}\text{OH}$  is recycled back to  $\text{Cys-S}_\text{P}\text{H}$  is unclear for 1-Cys Prxs but is the defining difference between typical and atypical 2-Cys Prxs (Rhee et al., 2005). The  $\text{Cys-S}_\text{P}\text{OH}$  of typical and atypical 2-Cys Prxs reacts with a second Cys residue, referred to as the resolving Cys ( $\text{Cys-S}_\text{R}\text{H}$ ), to form a disulphide bond. In the case of typical 2-Cys Prxs, the

resolving Cys is conserved while in atypical 2-Cys Prxs it is not. The disulphide bond that occurs in atypical 2-Cys Prxs is intramolecular. Thus, the functional catalytic unit of an atypical 2-Cys Prx is a monomer. By contrast, the disulphide bond that occurs in typical 2-Cys Prxs is intermolecular. Thus, the functional catalytic unit of a typical 2-Cys Prx is a dimer. The reaction cycle of typical and atypical 2-Cys Prxs is completed upon the reduction of the disulphide bond by an electron donor such as Trx.

The catalytic cycle of typical 2-Cys Prxs is also associated with transient structural changes. Under reduced conditions, typical 2-Cys Prx homodimers associate to form toroid shaped oligomers. Oxidation of Cys-S<sub>P</sub>H to Cys-S<sub>P</sub>OH by a peroxide substrate induces localised unfolding of the loop-helix motif it is contained within, enabling disulphide bond formation to occur with Cys-S<sub>R</sub>H. These structural changes disrupt the dimer-dimer interface, resulting in dissociation of the oligomer into its dimer subunits. Conversely, reduction of the disulphide bond by Trx facilitates reconstitution of the dimer-dimer interfaces, enabling reassembly of the oligomer (Wood et al., 2003b). The exact physiological reason for this complicated decamer-dimer transition remains unclear but it has been shown that decamers are better peroxidases whereas dimers are more readily reduced by Trx (Hall et al., 2009). To further complicate this, Cys-S<sub>P</sub>H can, under some circumstances, be sequentially oxidised by two peroxide substrates before disulphide bond formation can occur with Cys-S<sub>R</sub>H. Under these circumstances, Cys-S<sub>P</sub>H is over-oxidised to Cys-sulphinic acid (Cys-S<sub>P</sub>O<sub>2</sub>H) and prevented from forming a disulphide bond with Cys-S<sub>R</sub>H (Wood et al., 2003a). The formation of Cys-S<sub>P</sub>O<sub>2</sub>H was thought to be an irreversible catalytic dead-end until the discovery of the sulphiredoxin (Srx) family of reductases. Srxs catalyse the reduction of Cys-S<sub>P</sub>O<sub>2</sub>H to Cys-S<sub>P</sub>OH, enabling Trx to reduce Cys-S<sub>P</sub>OH to Cys-S<sub>P</sub>H and restore catalytic activity (Jönsson and Lowther, 2007).



## 1.6 Oxidative stress in fish

Fish are exposed to several sources of oxidative stress that are specific to their environment. These sources of oxidative stress include pollutants, naturally occurring toxins and parasite infections. Some of the pollutants that have been shown to induce oxidative stress in fish include various pesticides and pulp mill effluent (Jos et al., 2005). For example, exposure of the freshwater fish *Channa punctatus* (Bloch) to the insecticide deltamethrin was found to increase lipid peroxidation, the level of GSH and ascorbic acid, and GPx activity in kidney and liver (Sayeed et al., 2003). Similarly, exposure of the freshwater catfish *Heteropneustes fossilis* (Bloch) to paper mill effluent was found to be associated with increased tissue-specific oxidative damage and increased respiratory burst activity in peritoneal and head kidney phagocytes. Interestingly, these results suggested that the paper mill effluent induced oxidative stress via an immune response (Fatima et al., 2000).

The cyanobacterium *Microcystis aeruginosa* produces microcystins, a family of cyclic peptide toxins, which have been shown to induce oxidative stress in fish. Tilapia fish (*Oreochromis* sp.) fed commercial fish food supplemented with cyanobacteria were found to have significantly higher levels of lipid peroxidation, SOD activity and GPx activity, compared to control fish that were fed just the commercial fish food (Jos et al., 2005).

Parasite infection has also been shown to induce oxidative stress in fish, resulting in tissue damage and increased levels of enzymatic antioxidant activity (Martínez-Álvarez et al., 2005). For example, muscle extracts prepared from catfish (*Rhadia quelen*) infected with the trematode *Clinostomum detrunctum* were found to have significantly higher levels of lipid peroxidation compared to muscle extracts prepared from uninfected fish. It was suggested that the increased lipid peroxidation found in

infected fish occurred as a result of oxidative stress induced by an immune response (Belló et al., 2000). Investigation into various oxidative stress markers in common carp infected with *Ptychobothrium* sp. (Cestoda) revealed a four-fold increase in GPx activity in head kidney tissue compared to uninfected fish. The significant increase in GPx activity was suggested to be an adaptive response to oxidative stress induced by the parasite infection (Dautremepuits et al., 2003).

## 1.7 Oxidative stress in farmed finfish and its impact on the industry

In addition to intracellular and environmental sources of oxidative stress, farmed finfish are also vulnerable to oxidative stress induced by peroxidised ingredients within feed. The feed of farmed finfish is high in lipid content, making it susceptible to lipid peroxidation which can occur during production or as a result of improper storage. Lipid peroxides within feed can be transferred to the tissues of farmed finfish initiating peroxidative damage (Mourente et al., 2000). The tissues of farmed finfish are themselves susceptible to peroxidative damage because they contain high levels of lipid. The high level of lipid in finfish tissues is not only due their high lipid diets, it is also due to relative inactivity (Alvarez et al., 1998). Farmed finfish are relatively inactive because the sea cages or tanks in which they are kept offer limited space for movement.

Exposure of farmed finfish to lipid peroxides in feed can result in disease and mortality. For example, Atlantic salmon (*Salmo salar*) fed a diet high in lipid peroxides and  $\alpha$ ,  $\beta$ -unsaturated aldehydes were found to develop lipid liver degeneration (LLD) (Roald et al., 1981). At this time, the link between rancid feed consumption and the development of LLD was not verified but it appeared to be caused by the oxidation of lipids into toxic compounds. The early clinical manifestations of LLD included reduced appetite and abnormal swimming

movements whilst advanced disease was characterised by impaired equilibrium, fish swimming on their sides and death.

Oxidative stress affects the finfish farming industry not only through its contribution to disease and increased mortality rates, but also through its impact on the quality, and hence the value, of finfish muscle products. The value of finfish muscle products, such as fillets, is dictated by colour, aroma and texture, all of which are heavily influenced by lipids. Failure to prevent lipid peroxidation in these products is associated with deterioration of colour, development of rancid odours and flavours, detrimental changes in texture and reduced shelf life (Alvarez et al., 1998; Fitzgerald and Bremner, 1998). Thus, the minimisation of oxidative stress in farmed finfish, through a better understanding of antioxidant defence mechanisms, can benefit the industry through increased productivity of higher quality, more valuable end products.

## 1.8 Enzymatic antioxidant defences in finfish

There have been numerous studies investigating the effects of various biotic and abiotic factors on the levels of antioxidant enzyme activity in finfish. The biotic and abiotic factors investigated include phylogenetic position, age, feeding behaviour, diet (lipid, vitamin and mineral content), swimming behaviour, environmental conditions (Light, salinity and temperature), feed restriction and deprivation, anoxia, hyperoxia, xenobiotic exposure, metal exposure (copper, cadmium and mercury) and parasite infection (reviewed in Martínez-Álvarez et al., 2005). In contrast to the vast number of these studies, there have been relatively few detailed functional and structural characterisations of finfish antioxidant enzymes (Thompson et al, 2006). Functional and structural characterisations of GPx proteins have been performed in rainbow trout (Bell et al., 1984), carp (Nakano et al., 1992), Japanese sea bass (Nagai et al., 2002) and southern bluefin tuna (Thompson et al., 2006). Similarly,

functional and structural characterisations of SOD proteins have been performed in cod (Bartkowiak et al., 1981), carp (Vig et al., 1989), black porgy (Lin et al., 2000) and red seabream (Ken et al., 2002). However, in contrast to GPx and SOD proteins, 2-Cys Prx proteins have only been characterised in three finfish species, southern bluefin tuna (Sutton et al., 2010), Atlantic salmon (Loo et al., 2012) and yellowtail kingfish (Loo et al., 2010). All of these characterisations were performed within our research group, two of which form part of this study.

## 1.9 Aims and scope of this study

The overall aim of this study was to address the lack of detailed functional and structural characterisations of typical 2-Cys Prx proteins from farmed finfish by recombinantly expressing, purifying and characterising a selection of these proteins from three finfish species important in Australian aquaculture. These three finfish species were *Thunnus maccoyii* (southern bluefin tuna), *Salmo salar* (Atlantic salmon) and *Seriola lalandi* (yellowtail kingfish).

Chapter 3 describes the published sequence analysis, recombinant expression, purification and characterisation of a Prx 2 protein from southern bluefin tuna (SBT) (Sutton et al., 2010). This chapter also includes further structural analyses of the SBT Prx 2 protein using gel filtration chromatography and site directed mutagenesis.

Chapter 4 describes the published sequence analysis, recombinant expression and purification of a Prx 1 protein from Atlantic salmon (AS) (Loo et al., 2012). This chapter also includes analysis of the AS Prx 1 protein structure using gel filtration chromatography and kinetic characterisation of the AS Prx 1 protein at high substrate concentrations.

Chapter 5 describes the recombinant expression and purification of three putative forms of a Prx 4 protein from yellowtail kingfish (YTK). This chapter also includes

structural analysis of the three putative forms of the YTK Prx 4 protein using gel filtration chromatography.

Chapter 6 draws together and compares the findings from Chapters 3, 4 and 5.

# Chapter 2

Common materials and methods

## 2.1 *Escherichia coli* strain descriptions

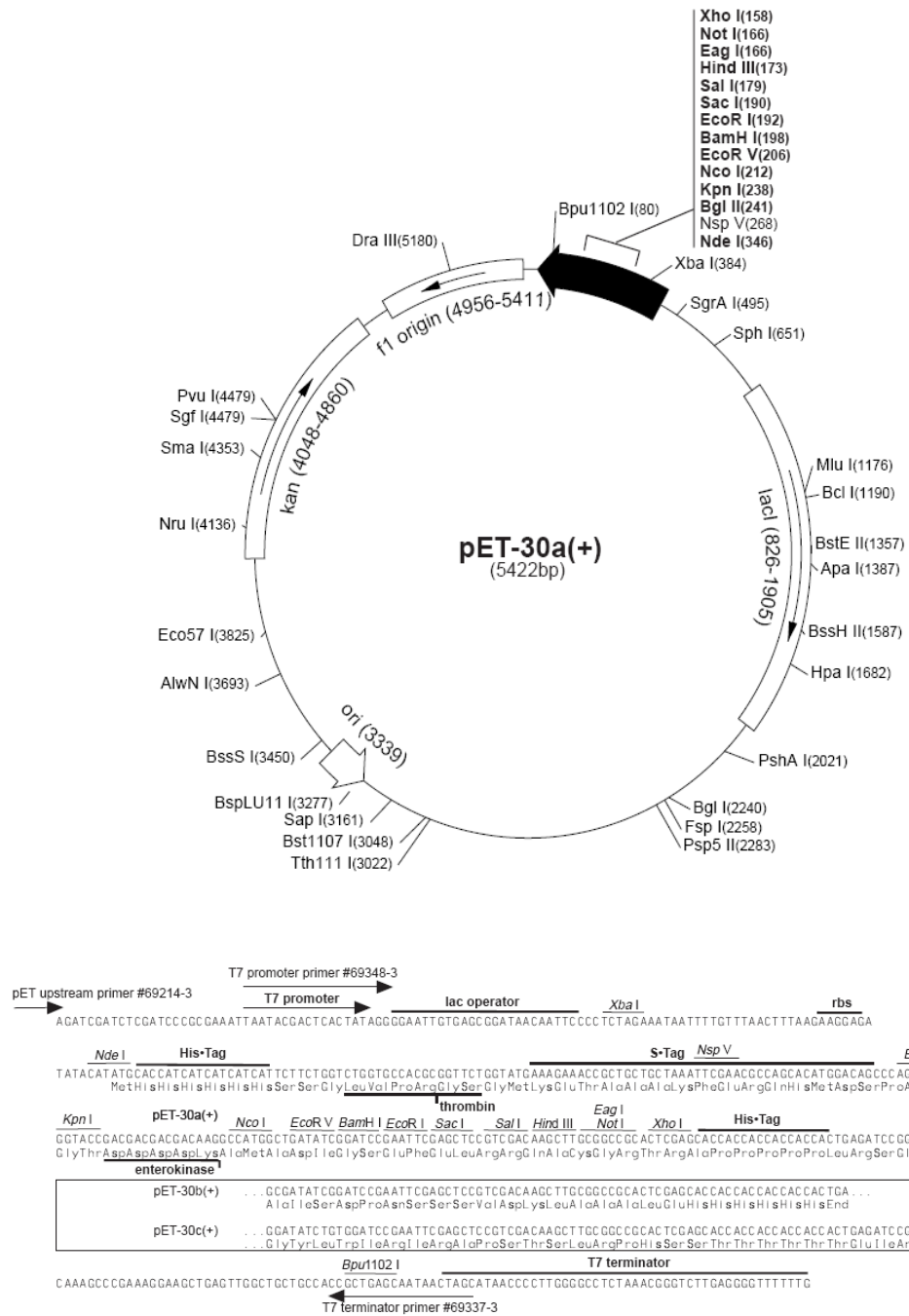
The *E. coli* strains DH5 $\alpha$  and BL21 (DE3) were used throughout this study. Details of these strains are outlined in Table 2.1.

**Table 2.1** *E. coli* strain descriptions, suppliers and antibiotic resistance.

<i>E. coli</i> Strain	Strain Description	Supplier	Antibiotic Resistance
DH5 $\alpha$	$\Phi$ 80d <i>lacZ</i> $\Delta$ M15, <i>rec A1</i> , <i>end A1</i> , <i>gyr A96</i> , <i>thi-1</i> , <i>hsdR17</i> ( <i>rk</i> <sup>-</sup> , <i>mk</i> <sup>+</sup> ), <i>supE44</i> , <i>relA1</i> , <i>deoR</i> , $\Delta$ ( <i>lacZYA-argF</i> )U169	Invitrogen™	None
BL21(DE3)	B F <i>dcm ompT hsdS</i> ( <i>rB<sup>-</sup>mB</i> ) <i>gal</i> $\lambda$ (DE3)	Stratagene	None

## 2.2 pET-30a vector map

The Novagen® pET-30a vector was used for protein expression throughout this study. A map of the pET-30a vector including details of its multiple cloning site is shown Fig. 2.1. The pET-30a vector features a T7*lac* promoter and resistance to kanamycin (30  $\mu$ g mL<sup>-1</sup>).



**Fig. 2.1.** Novagen® pET-30a vector map and multiple cloning site details (TB095 pET-30a-c(+)) Vector Map 1998, EMD4Biosciences, US, viewed 24 January 2011, [http://www.emdchemicals.com/life-science-research/pet-30a-plus-dna/EMD\\_BIO-69909/p\\_2tOb.s1OkacAAAEjWhI9.zLX?attachments=VMAP](http://www.emdchemicals.com/life-science-research/pet-30a-plus-dna/EMD_BIO-69909/p_2tOb.s1OkacAAAEjWhI9.zLX?attachments=VMAP)).



## 2.3 *Escherichia coli* growth conditions

Luria-Bertani (LB) broth was used as the growth medium for all *E. coli* cultures and was prepared according to Sambrook et al. (1989). Solid medium for plating was prepared by mixing agar into LB broth to give a final concentration of 1.5% (w/v). All *E. coli* growth media were sterilized by autoclaving for 15 min using a fluid cycle unless otherwise stated. Where appropriate 0.22 µM filter sterilized antibiotics were incorporated into cooled LB media immediately prior to the pouring of plates or use in liquid culture. The cell and vector specific antibiotics and their working concentrations are outlined in Sections 2.1 and 2.2, respectively. The culturing of *E. coli* was performed at 37°C unless otherwise stated. All manipulation of plates and liquid cultures was performed in a UV sterilised laminar flow cabinet.

## 2.4 Cryopreserved *Escherichia coli* cell stock preparation

Cryopreserved stocks of *E. coli* cells were produced according to the Novagen® pET Systems Manual (9<sup>th</sup> Edition). According to the protocol, *E. coli* cells were grown in liquid LB medium until an OD<sub>600</sub> of 0.6-0.8 was reached. At this point 0.9 mL of culture was removed and mixed with 0.1 mL of 0.22 µM filter sterilized 80% (v/v) glycerol. *E. coli* glycerol cell stocks were stored at -70°C.

## 2.5 DNA purification

### 2.5.1 DNA clean-up

Linear and plasmid DNA was cleaned-up using a Promega™ Wizard® SV Gel and PCR Clean-Up System. The kit was used as per the manufacturer's instructions following the DNA purification by centrifugation protocol.

## 2.5.2 Plasmid DNA purification

Plasmid DNA was purified using a Promega™ Wizard® Plus SV Minipreps DNA Purification System. Purification of plasmid DNA was performed according to the manufacturer's instructions using 10 mL of *E. coli* culture, prepared according to Section 2.3, per plasmid preparation.

## 2.5.3 Purified DNA quantification

The concentration of purified DNA was quantified using a Thermo Scientific NanoDrop spectrophotometer following the manufacturer's instructions.

## 2.6 Agarose gel electrophoresis of DNA

Agarose gels (1-2% w/v) were prepared by mixing the appropriate amount of agarose in 50 mL of 1X TAE buffer made from a 50X stock solution containing 50 mM EDTA, 2 M Tris-base and 5.7% (v/v) glacial acetic acid, pH 8. The agarose was dissolved in the 1X TAE buffer by heating in a microwave. Prior to pouring, the agarose gel was mixed with approximately 5 µL of a concentrated ethidium bromide stock solution or Invitrogen™ SYBR® Safe DNA gel stain. The molten agarose gel was then poured into a gel casting apparatus that had been fitted with a plastic comb to provide sample wells. Once the gel had set it was removed from the casting apparatus and transferred to an agarose gel tank where it was immersed in 1X TAE buffer. DNA samples to be analysed were mixed with 6X Promega™ loading dye to give a final concentration of 1X. Both the DNA samples and an appropriate DNA size marker were loaded into the agarose gel and the gel was run at 100 volts. The DNA within agarose gels was visualised using a Bio-Rad® UV transilluminator 2000 combined with a Bio-Rad® Digi Doc Digital Camera package.

## 2.7 Polymerase Chain Reaction (PCR) - based amplification of DNA

PCR-based amplification of DNA was performed using an Applied Biosystems™ GeneAmp® PCR System 2400 or 2700 in 200 µL dome-cap PCR tubes (Axygen, CA, USA). For the purpose of cloning, the PCR mixture contained 1X Phusion® HF buffer and 1 U Phusion® DNA polymerase (Finnzymes), 200 µM dNTPs, 100 ng of template DNA and 200 ng of forward and reverse primer in a final volume of 50 µL.

## 2.8 DNA sequencing

DNA sequencing was conducted by the Australian Genome Research Facility (St Lucia, Queensland). Each plasmid sample to be sequenced was prepared by combining 200 ng of plasmid DNA with the appropriate forward primer in one reaction and the appropriate reverse primer in a second reaction. The final concentration of primer in each reaction was 1 µM. The Novagen® T7 terminator and promoter primers were used to sequence across the multiple cloning region of the pET-30a vector. The coding sequence for the T7 primers was accessed from the Novagen website (<http://www.emdbiosciences.com/html/NVG/home.html>) and the primers were manufactured by Geneworks (Adelaide, South Australia). Sequencing results were aligned with the expected DNA sequence using Sequencher™ 4.1.4 software produced by Gene Codes.

## 2.9 *Escherichia coli* transformation

Frozen competent *Escherichia coli* Invitrogen™ subcloning Efficiency™ DH5α™ and Novagen® BL21 (DE3) cells were thawed on wet ice and then gently mixed by finger-flick. The competent cells were divided into 50 µL aliquots in 1.5 mL tubes and each aliquot had 1-10 ng of plasmid DNA in a volume of 1-5 µL added to it. The competent cells with plasmid DNA were gently mixed by finger-flick then incubated

on wet ice. The incubation time for the *E. coli* DH5 $\alpha$ <sup>™</sup> and BL21 (DE3) transformation reactions was 30 min and 5 min, respectively. The *E. coli* DH5 $\alpha$ <sup>™</sup> and BL21 (DE3) transformation reactions were heated for 20 s and 30 s, respectively, in a water bath set at 42°C. Immediately following heating the transformation reactions were incubated on wet ice for 2 min. The *E. coli* DH5 $\alpha$ <sup>™</sup> and BL21 (DE3) transformation reactions were removed from ice and mixed with 950  $\mu$ L and 250  $\mu$ L of room temperature SOC medium, respectively. The SOC medium contained 2% tryptone, 0.5% yeast extract, 10 mM sodium chloride, 2.5 mM potassium chloride, 10 mM magnesium chloride, 10 mM magnesium sulphate and 20 mM glucose. Both the *E. coli* DH5 $\alpha$ <sup>™</sup> and BL21 (DE3) transformation reactions were incubated at 37°C for 1 hour on a rotating platform shaker set at 200 revolutions per minute. The transformation reactions were spread-plated (20-200  $\mu$ L) on to LB agar plates containing the appropriate selective antibiotics that are outlined for each cell type and plasmid in Sections 2.1 and 2.2, respectively. The inoculated plates were incubated at 37°C until colonies of 2-3 mm in diameter had grown.

## 2.10 Polymerase Chain Reaction (PCR) - based colony screening

*E. coli* colonies were screened for vector containing an insert of the expected size using PCR. PCR colony screening was performed as described in the Novagen<sup>®</sup> pET Systems Manual (9<sup>th</sup> edition) using the Promega<sup>™</sup> GoTaq<sup>®</sup> Flexi DNA polymerase system. Briefly, half of each colony to be screened was picked off an agar plate with a sterile pipette tip and used to inoculate 50  $\mu$ L of sterile water in a 1.5 mL micro-centrifuge tube. The cells were dispersed throughout the water by vortexing and subsequently given a burst of centrifugation to bring the contents to the bottom of the tube. The cells were lysed by heating at 99°C for 5 min and the cell debris cleared by centrifugation at 12,000 *g* and 25°C for 1 min. The PCR mixture contained 1 X Promega GoTaq<sup>®</sup> Flexi Buffer, 2 mM MgCl<sub>2</sub>, 0.2 mM dNTPs,

0.25  $\mu$ M T7 promoter and terminator primers, 1.25 U Promega GoTaq<sup>®</sup> DNA polymerase and 10  $\mu$ L of template DNA (cleared cell lysate) in a final volume of 50  $\mu$ L. The PCR mixture was prepared in 200  $\mu$ L dome-cap PCR tubes (Axygen, CA, USA) and cycling performed in an Applied Biosystems<sup>™</sup> GeneAmp<sup>®</sup> PCR System 2400 or 2700. The PCR cycling conditions were 1 cycle of denaturation at 94°C for 3 min followed by 35 cycles of (denaturation at 94°C for 1 min, annealing at 55°C for 1 min and extension at 72°C for 1 min), followed by 1 cycle of final extension at 72°C for 10 min. The products of PCR colony screening were analysed by agarose gel electrophoresis according to Section 2.6.

## 2.11 Recombinant protein expression

Cryopreserved *E. coli* cell stocks or fresh transformants were plated on to LB agar plates and incubated overnight at 37°C. Following incubation, well separated colonies were PCR screened as described above in Section 2.10. Colonies found to contain an appropriate sized vector insert were used to inoculate 10-100 mL of LB medium and incubated overnight at 37°C with shaking. Cells cultured overnight were harvested by centrifugation, resuspended in fresh LB medium and used to inoculate 50-500 mL of LB medium in an appropriate sized glass conical flask or 4L of LB medium in a New Brunswick fermentor. The dilution of overnight culture into fresh medium used was 1 in 50. Growth conditions of cells cultured in the New Brunswick fermentor included 0.22  $\mu$ M filtered air delivered at a rate of 7L/min. The rate of cell culture agitation used in the fermentor was regulated according to growth time (150 rpm at 0-0.5 h, 250 rpm at 0.5-1 h, 350 rpm at 1-1.5 h and 400 rpm at 1.5 h-induction). After induction of protein expression the agitation rate was increased to 500 rpm where it remained until the cells were harvested. Cells grown in glass conical flasks were agitated at 100-200 rpm on a rotating platform shaker. Cell cultures in both the fermentor and conical flasks were grown for approximately 2.5 h at which time the OD<sub>600</sub> was measured and routinely found to be 0.75-1. At this point

approximately 10 mL of culture was removed. Of the 10 mL of culture, a 1 mL aliquot was harvested by centrifugation at 5000 *g* and 25°C for 10 min and stored at -20°C for subsequent sodium dodecyl sulphate polyacrylamide gel electrophoresis (SDS-PAGE) and immunoblot analysis. This sample was used to assess the protein composition of the culture prior to induction of recombinant protein expression. Of the remaining 10 mL of culture, several cryopreserved cell stocks were prepared according to Section 2.4. This enabled clones that gave high recombinant protein expression levels to be used for subsequent experiments. Recombinant protein expression was induced in the remaining culture *via* the addition of isopropyl  $\beta$ -D-1-thiogalactopyranoside (IPTG) to give a final concentration of 0.4 mM. Recombinant protein expression was induced for 3 h unless otherwise stated. At completion of the induction, a 1 mL aliquot of cells was removed from the culture and harvested by centrifugation as outlined above. This sample was used to assess the protein composition of the culture post-induction to determine the level of recombinant protein expression. The remainder of the culture was harvested by centrifugation in 50 mL tubes for smaller cultures (3800 *g* and 25°C for 10 min) or 250 mL bottles for larger cultures (5000 *g* and 25°C for 10 min). Cell pellets were stored at -70°C.

## 2.12 Sodium Dodecyl Sulphate Polyacrylamide Gel Electrophoresis

Sodium dodecyl sulphate polyacrylamide gel electrophoresis (SDS-PAGE) was performed using a Bio-Rad<sup>®</sup> Mini Protean<sup>®</sup> II apparatus according to the manufacturers instructions. The SDS-PAGE resolving gel was prepared by combining 0.375 M Tris-HCl (pH 8.8), 0.1 % (w/v) SDS, 10 % (v/v) Acrylamide-Bis, 0.4 % (v/v) N,N,N',N'-Tetramethylethylenediamine (TEMED) and 0.05 % (w/v) ammonium persulphate in a total volume of 10 mL. The resolving gel was transferred into a Bio-Rad<sup>®</sup> casting apparatus, overlaid with iso-propanol and left to polymerise for approximately 15 minutes. Upon polymerisation of the resolving

gel, the iso-propanol was removed by rinsing with distilled water. The SDS-PAGE stacking gel was prepared by combining 0.125 M Tris-HCl (pH 6.8), 0.1 % (w/v) SDS, 4 % (v/v) Acrylamide-Bis, 0.2 % (v/v) TEMED and 0.05 % (w/v) ammonium persulphate in a total volume of 5 mL. Immediately after overlaying the resolving gel with stacking gel, a sample well mold was inserted into the stacking gel. The stacking gel was left to polymerise for approximately 15 min. Upon polymerisation of the stacking gel, the completed SDS-PAGE gel was transferred into a Bio-Rad<sup>®</sup> Mini Protean<sup>®</sup> II apparatus and the sample well mold removed from the stacking gel. The Bio-Rad<sup>®</sup> Mini Protean<sup>®</sup> II apparatus was then filled with SDS-PAGE running buffer until the SDS-PAGE gel was completely immersed. The SDS-PAGE running buffer contained 0.2 M glycine, 25 mM Tris-base and 0.1 % (w/v) SDS.

Protein samples were prepared for SDS-PAGE by being mixed with an equal volume of SDS-PAGE loading buffer and heated at 99°C for 5 minutes. The SDS-PAGE loading buffer contained 0.05 M Tris-HCl (pH 6.8), 2 % (w/v) SDS, 10 % (v/v) glycerol, 2 mM EDTA, 50 mM DTT, 12 M urea and a few grains of bromophenol blue. Whole cell protein extracts were prepared for SDS-PAGE by re-suspending cell pellets in SDS-PAGE loading buffer that had been diluted by half with distilled water. The re-suspended cells were lysed by heating at 99°C for 5 minutes then cell debris cleared by centrifugation at 12,000 g and 25°C for 1 min.

SDS-PAGE gels were run at 170 volts until the BioRad<sup>®</sup> prestained SDS-PAGE broad range standards were suitably separated. Completed SDS-PAGE gels were used for Coomassie blue staining or immunoblotting. Coomassie blue staining was performed overnight at room temperature on a shaking platform. The Coomassie blue stain contained 0.25% (w/v) Coomassie blue, 10% (v/v) acetic acid and 45% (v/v) methanol. Background Coomassie blue stain was removed by incubating the stained gel in a de-stain solution containing 10% acetic acid and 45% methanol.

## 2.13 Immunoblotting

Following SDS-PAGE, proteins were transferred to Pall BioTrace<sup>®</sup> NT nitrocellulose membrane using a Bio-Rad<sup>®</sup> Mini Trans-Blot<sup>®</sup> tank system containing 50 mM Tris-base, 380 mM glycine, 0.1% (w/v) SDS and 20% (v/v) methanol. The transfer was conducted at 0.2 Amps for 1 h at 25°C. Probing of recombinant and native proteins was performed as described in the Qiagen<sup>®</sup> Qiaexpress<sup>®</sup> Detection and Assay Handbook using rabbit anti-6X His polyclonal antibodies (Rockland) or rabbit anti-southern bluefin tuna peroxiredoxin 2 polyclonal antibodies (prepared as part of this study) used at a dilution of 1/1000, followed by goat anti-rabbit IgG (H&L) polyclonal antibodies conjugated to horseradish peroxidase (Rockland) used at a dilution of 1/2000. Chemiluminescent detection of proteins was performed using a Pierce SuperSignal<sup>®</sup> West Pico Chemiluminescence kit according to the manufacturer's instructions. The chemiluminescent signal of immuno-reactive proteins was captured with X-ray film (Kodak<sup>®</sup> X-omat) or digitally using a BioRad<sup>®</sup> VersaDoc<sup>™</sup> Model 4000 imaging system. X-ray films were developed using a Kodak<sup>®</sup> X-omat 1000 developer.

## 2.14 Nickel affinity chromatography purification of recombinant proteins

Recombinant proteins were expressed in *E. coli* BL21 (DE3) cells and purified by nickel affinity chromatography using a 6X His-tag introduced by the pET-30a expression vector. Pellets of *E. coli* cells over-expressing recombinant protein, that had been stored at -70°C, were resuspended in 15 mL of binding buffer containing 20 mM Tris-base (pH 7.5), 0.5 M NaCl, 5 mM imidazole and 5 mM DTT. The volume of the resuspended cells was made up to 40 mL with binding buffer and then homogenised using a glass/Teflon Potter Elvehjem homogeniser. The homogenised cells were lysed with three passes in an Avestin<sup>®</sup> EmulsiFlex-C5 homogenizer



operated at ~15,000 psi (~103 MPa). The cell lysate was centrifuged at 145,000 *g* and 4°C for 45 min and the clarified supernatant was loaded onto a Ni-sepharose column (GE™ Healthcare; 38 mm x 15 mm) equilibrated with binding buffer. The protein content of the column flow through and eluate was monitored by measuring the change in absorbance at 280 nm using an LKB Bromma 8300 Uvicord II and recorded using a Rikadenki multipen recorder. The column was washed with 10 column volumes of binding buffer followed by 40 column volumes of binding buffer containing 20 mM imidazole. The His-tagged recombinant protein was eluted from the column with binding buffer containing 500 mM imidazole. Various fractions from the Ni-affinity purification were analysed by SDS-PAGE and immunoblotting as per Sections 2.12 and 2.13, respectively. The protein eluted with binding buffer containing 500 mM imidazole (i.e. the fractions containing the recombinant protein) was concentrated to 2.5 mL using a Sartorius centrifugal concentrator with a 5 kDa molecular weight cut-off. The concentrated protein was exchanged into a buffer lacking imidazole (see relevant chapter materials and methods for buffer composition) using a GE™ healthcare PD-10 desalting column. The GE™ healthcare PD-10 desalting column was equilibrated with 25 mL of exchange buffer, and then the 2.5 mL of the concentrated protein solution was loaded on to the desalting column. The buffer exchanged protein was eluted from the desalting column by loading 3.5 mL of exchange buffer. The buffer exchanged protein was concentrated as outlined above to the desired protein concentration. The protein concentration was quantified by the method of Bradford (1976) using the BioRad® Protein Assay Dye Reagent and bovine serum albumin as the protein standard. The purified recombinant protein was either used immediately or frozen in liquid nitrogen and stored at -70°C until needed.

## 2.15 Peroxiredoxin enzyme assays

The peroxiredoxin (Prx) enzyme assay was based on the method of Rahlfs and Becker (2001). Prx-dependent peroxide substrate reduction was coupled to nicotinamide dinucleotide phosphate (NADPH) oxidation in the presence of *E. coli* thioredoxin (Trx) and thioredoxin reductase (TrxR) supplied by Sigma-Aldrich®. All assays were performed at 25°C in a temperature-controlled 96-well plate reader set at a wavelength of 340 nm. The non-rate limiting kinetic assay contained 100 mM 4-(2 Hydroxyethyl) piperazine-1-ethanesulfonate (HEPES)-NaOH buffer (pH 7.5), 20 µM Trx, TrxR (5.0 U mL<sup>-1</sup>), 250 µM NADPH, 120 µM peroxide substrate and varying amounts of purified protein in a final volume of 100 µL. When the peroxide substrate concentration was varied, the Trx concentration was held constant at 20 µM. When the Trx concentration was varied, the peroxide substrate concentration was held constant at 120 µM. The kinetic assays were initiated by addition of Prx protein.

At higher peroxide substrate concentrations, the rate of NADPH oxidation in the absence of Prx protein was significant. To correct for this, the SBT Prx-independent rate of NADPH oxidation was subtracted from the rate obtained with all assay components present. To calculate the rate of reaction, the  $\Delta\text{Abs}_{340\text{nm}}$  v.s. time was graphed and linear regression was performed to determine a line of best fit using GraphPad Prism® software. The slope of the line of best fit was used to calculate the rate of the reaction ( $\mu\text{mol NADPH min}^{-1} \text{ mL}^{-1} \text{ sample}$ ) using the Beer-Lambert law. One unit of Prx enzyme activity is defined as the amount required to oxidise 1 µmol of NADPH min<sup>-1</sup>.

## 2.16 Gel filtration chromatography

The molecular mass of Ni-affinity purified recombinant proteins was analysed by gel filtration chromatography using a 10 mm x 30 cm Superdex™ 200 HR column (Amersham-Pharmacia Biotech) attached to an ÄKTA™ Explorer Fast Protein Liquid Chromatography system (Amersham-Pharmacia Biotech). The gel filtration column was equilibrated at 0.75 mL min<sup>-1</sup> and run at 0.3 mL min<sup>-1</sup>. The gel filtration column was calibrated with carbonic anhydrase (29 kDa), bovine serum albumin (66 kDa), alcohol dehydrogenase (150 kDa), α-amylase (200 kDa), apoferritin (443 kDa), thyroglobulin (669 kDa) and blue dextran (2000 kDa) molecular mass markers from Sigma-Aldrich®.

## 2.17 Differential centrifugation

The differential centrifugation protocol was based on the method of Higgins and Hames (2003) and Lodish et al. (2008). Cell pellets were resuspended in a buffer containing 20 mM Tris-base (pH 7.5), 0.5 M NaCl, 5 mM imidazole and 5 mM DTT, and homogenised using a glass/Teflon Potter Elvehjem homogeniser. The homogenised cells were lysed with three passes in an Avestin® EmulsiFlex-C5 homogenizer operated at ~15,000 psi (~103 MPa). The whole cell protein extract was centrifuged at 12,000 g and 4°C for 15 min to pellet cellular debris and insoluble protein. The 12,000 g centrifugation supernatant was removed and retained and the pellet resuspended in a volume of 5% (w/v) SDS equal to the volume of the removed supernatant. The 12,000 g centrifugation supernatant was further centrifuged at 100,000 g and 4°C for 1 hr. The 100,000 g centrifugation supernatant was removed and retained and the pellet resuspended in a volume of 5% (w/v) SDS equal to the volume of the removed supernatant. Samples of the supernatant and resuspended pellet from the 12,000 g and 100,000 g centrifugations were analysed

by SDS-PAGE and immunoblotting according to Sections 2.12 and 2.13, respectively.

## 2.18 Protein crystallisation

### 2.18.1 Small scale protein crystallisation trials

Small scale protein crystallisation trials were performed using sitting drop vapour diffusion in 96 well Intelli-plates™ (Art Robbins Instruments®). Crystallisation screening solutions were supplied by Qiagen® and Hampton Research in a 96 deep well block format (See Appendix for composition tables). An Art Robbins Instruments® Crystal Phoenix Liquid Handling System was used to transfer crystallisation solutions from deep well blocks into Intelli-Plates™ and to setup the crystallisation drops. The reservoir volume used in small scale crystallisation trials was 100 µL. The volume of protein solution and screen solution used in the crystallization drop varied (see legends to relevant tables and figures). Small scale crystallisation trial plates were immediately sealed after setup and were housed and imaged in a TriTek CrystalPro™ HT – Multi-Plate Hotel and Imager kept at a constant temperature of 22°C.

### 2.18.2 Large scale protein crystallisation trials

Large scale protein crystallisation trials were performed using sitting drop vapour diffusion in 24-well Cryschem plates (Hampton Research). Crystallisation screening solutions were supplied by Hampton Research in a 10 mL tube format or prepared from stock chemicals. The reservoir volume used in large scale protein crystallisation trials was 0.5 mL. The volume of protein solution and reservoir solution used in the crystallization drop varied (see legends to relevant tables and figures). Large scale crystallisation trials were incubated at a constant temperature of 22°C.

## 2.19 Protein crystal harvesting and X-ray crystallography analysis

Nylon CryoLoops™ (Hampton Research) were mounted onto copper pins with a magnetic base in accordance with the guidelines set out by the Australian Synchrotron (Clayton, Victoria). All manipulations of the mounted loops were performed with a magnetic wand. Crystals were harvested from crystallisation drops using mounted loops and either directly frozen in liquid nitrogen or transferred through a series of crystallisation solutions containing an increasing concentration of cryo-protectant, then frozen in liquid nitrogen. Frozen crystals were transferred into a Stanford Automated Mounting (SAM) cassette for storage and transportation to the synchrotron. The temperature of the SAM cassette was maintained at  $-196^{\circ}\text{C}$  during storage and transportation using a liquid nitrogen dry-shipper. Mounted crystals were either transferred into the synchrotron beam-line using the automated mounting robot or mounted in the beam-line manually. The X-ray beam was centred on the mounted loop, then the loop was rotated  $+90^{\circ}\Phi$  (angle of rotation perpendicular to the axis that the pin containing the mounted crystal lies upon) and the X-ray beam re-centred on the loop. Images of mounted crystals were captured with the beam attenuated to 90%, detector set at 400 mm, beam stop set at 50 mm combined with exposure times of 1-5 s.

# Chapter 3

Expression, purification, and characterisation  
of a peroxiredoxin 2 from southern bluefin  
tuna (*Thunnus maccoyii*)

### 3.1 Introduction

Human Prx 2 was originally identified and characterised without reference to antioxidant function as a cytosolic factor from red blood cells that enhanced the activity of natural killer cells (Shau et al., 1994). As such, it was referred to as natural killer enhancing factor B (NKEF B) (Shau et al., 1993). Later, the human NKEF B protein was also found to possess antioxidant function by providing protection to protein and DNA against oxidative damage (Sauri et al., 1995). Based on this antioxidant activity and a high degree of amino acid sequence identity, the human NKEF B was found to belong to a large new family of antioxidant enzymes referred to as peroxiredoxins (Prxs) (Rhee et al., 2005). As a cytosolic typical 2-Cys Prx, the human NKEF B has been classified and is widely referred to in the literature as a Prx 2.

In finfish, the NKEF B rather than the Prx 2 nomenclature has been assigned to genes because this is the role in which they have been investigated. NKEF B genes have been characterised in three finfish species including pufferfish (*Tetraodon nigroviridis*), carp (*Cyprinus carpio*) and gilthead sea bream (*Sparus aurata*) (Dong et al., 2007; Huang et al., 2009; Pérez-Sánchez et al., 2011). The pufferfish NKEF B open reading frame (ORF) was found to be 597 bp in length, encoding 198 amino acids. Similarly, the carp and gilthead sea bream NKEF B ORFs were found to be 594 bp in length, encoding 197 amino acids. Phylogenetic analyses of all three finfish NKEF B deduced amino acid sequences revealed that they clustered together with other finfish NKEF B sequences and were closely related to mammalian NKEF B/Prx 2 sequences. The three finfish NKEF B deduced amino acid sequences were found to contain two VCP motifs and an additional Cys residue at position 70, all of which are characteristic features of mammalian NKEF B/Prx 2 amino acid sequences. However, the pufferfish and gilthead sea bream NKEF B deduced

amino acid sequences were also found to contain a Cys residue at position 75 that was not present in mammalian NKEF B/Prx 2 sequences. The pufferfish, carp and gilthead sea bream NKEF B genes were found to be constitutively expressed in a range of different tissues (Dong et al., 2007; Huang et al., 2009; Pérez-Sánchez et al., 2011). In carp and pufferfish, the highest level of NKEF B gene expression was observed in kidney. Although the level of NKEF B gene expression in gilthead sea bream kidney was not tested it was found to be relatively high in liver, eye and brain tissues. The effect of immuno-stimulants on the level of NKEF B gene expression in various tissues was found to be similar in carp and pufferfish but differed in gilthead sea bream. For example, NKEF B gene expression in carp infected with spring viraemia of carp virus (SVCV) and pufferfish stimulated with lipopolysaccharide was induced in spleen, maintained in liver and inhibited in kidney and head kidney. In contrast, NKEF B gene expression in gilthead sea bream exposed to *Enteromyxum leei* was induced in head kidney while in infected fish it was maintained.

Despite the comprehensive characterisation of finfish NKEF B genes, there have been no investigations into the antioxidant function or structure of the corresponding proteins. In the current study I present the first functional and structural characterisation of a Prx 2 protein from the finfish, southern bluefin tuna (SBT) (*Thunnus maccoyii*). A portion of the SBT Prx 2 protein characterisation presented in the current study has been published and includes the amino acid sequence analysis, phylogenetic analysis, recombinant expression, Ni-affinity purification, molecular mass determination and kinetic characterisation at different peroxide and Trx concentrations (Sutton et al., 2010). The current study also details further analysis of the SBT Prx 2 protein structure using gel filtration chromatography and site directed mutagenesis.



## 3.2 Materials and Methods

### 3.2.1 Gene construct

*Escherichia coli* BL21 (DE3) cells containing a plasmid construct composed of a Novagen pET-30a backbone and a putative southern bluefin tuna peroxiredoxin open reading frame (ORF) insert (referred to as pET-30a-SBT Prx) were generated and kindly provided by Grace Loo (School of Biological Sciences, Flinders University) (Sutton et al., 2010). In brief, the cloning of the putative SBT Prx ORF initially involved identification of two highly conserved regions in the amino acid sequences of several fish and mammal Prxs. Based on these highly conserved regions, PCR primers were designed to amplify an internal fragment of the SBT Prx cDNA using cDNA synthesised from SBT liver tissue RNA. Using the sequence of this internal fragment, the 5' and 3' ends of the SBT Prx cDNA were able to be amplified by rapid amplification of cDNA ends (RACE)-PCR. Based on the complete SBT Prx cDNA sequence, PCR primers were designed to amplify the SBT Prx ORF and incorporate *Nco*I and *Bam*HI restriction enzyme sites into the 5' and 3' ends, respectively. The SBT Prx ORF and pET-30a expression vector (Novagen<sup>®</sup>) were digested with the *Nco*I and *Bam*HI restriction enzymes and ligated to produce the pET-30a-SBT Prx construct. The pET30a-SBT Prx construct was transformed into *Escherichia coli* BL21 (DE3) cells and provided to me as a glycerol stock that had been stored at -70°C.

### 3.2.2 Sequencing of pET-30a-SBT Prx construct

Plasmid DNA was prepared from two colonies of *E. coli* BL21 (DE3) cells containing the pET-30a-SBT Prx construct as per Section 2.5.2 and the inserts were subsequently sequenced according to Section 2.8. The SBT Prx nucleotide sequence (GenBank accession no. EU093980) was retrieved from the National

Center for Biotechnology Information (NCBI) database and the ORF was identified by analysing the translation of all six reading frames performed using the Flip 6 program located in the Biomanager ([www.angis.org.au](http://www.angis.org.au)) suite of programs. The SBT Prx ORF was aligned with the pET-30a-SBT Prx construct insert sequences using Gene Codes Corporation Sequencher™ software.

### 3.2.3 Optimisation of recombinant SBT Prx 2 protein expression

Small scale SBT Prx 2 recombinant protein expression was performed with two colonies of *E. coli* BL21 (DE3) cells containing the pET-30a-SBT Prx 2 construct according to Section 2.11. After 3 h induction, a 1 mL sample from each culture was removed, centrifuged at 5000 g and 25°C for 10 min and the resulting cell pellets stored at -20°C. The remaining culture was left to be induced for a total of 18 h. Following the 18 h induction another 1 mL sample of each culture was removed, centrifuged at 5000 g and 25°C for 10 min and the resulting cell pellets stored at -20°C. The level of SBT Prx 2 protein expression in the un-induced, 3 h induced and 18 h induced cell pellets was investigated by SDS-PAGE and immunoblotting according to Sections 2.12 and 2.13, respectively.

### 3.2.4 Large scale recombinant SBT Prx 2 protein expression

Three colonies of *E. coli* BL21 (DE3) cells were screened for the pET-30a-SBT Prx 2 construct using the PCR protocol outlined in Section 2.10. A negative control PCR reaction was included in the PCR screening and it contained 0.22 µm filter sterilised water in the place of lysed cell supernatant as template. The PCR screening products were analysed by agarose gel electrophoresis as per Section 2.6. A colony of *E. coli* BL21 (DE3) cells containing the pET-30a-SBT Prx 2 construct was used for large scale protein expression as per Section 2.11 using a 4 L fermentor vessel.

The level of SBT Prx 2 protein expression was assessed by SDS-PAGE and immunoblotting according to Sections 2.12 and 2.13, respectively.

### 3.2.5 Ni-affinity purification of SBT Prx 2 protein

SBT Prx 2 protein was purified from *E. coli* BL21 (DE3) cells expressing the pET-30a-SBT Prx 2 construct by Ni-affinity chromatography according to Section 2.14. Following Ni-affinity purification, the SBT Prx 2 protein was exchanged into a buffer containing 20 mM Tris-base (pH 7.5), 150 mM NaCl and 5 mM DTT, concentrated and then either used immediately or frozen in liquid nitrogen and stored at -70°C until needed.

### 3.2.6 SBT Prx 2 kinetic assays

To identify non-rate limiting assay conditions, a series of assays were performed with varying concentrations of the SBT Prx 2 protein, *E. coli* thioredoxin (Trx) and *E. coli* thioredoxin reductase (TrxR) proteins (see legends to tables and figures). Otherwise, these assays were conducted as described in Section 2.15.

### 3.2.7 Gel filtration chromatography of SBT Prx 2 protein

The native molecular mass of Ni-affinity purified SBT Prx 2 protein (prepared according to Section 3.2.5) was analysed by gel filtration chromatography according to Section 2.16 under reducing and oxidising conditions. For gel filtration chromatography analysis under reducing conditions, 200 µL of Ni-affinity purified SBT Prx 2 protein (12 mg mL<sup>-1</sup>) was loaded onto a gel filtration column that had been equilibrated with a buffer containing 20 mM Tris-base (pH 7.5), 150 mM NaCl and 5 mM DTT. For gel filtration chromatography analysis under oxidising conditions, Ni-affinity purified SBT Prx 2 protein was exchanged into a buffer containing 20 mM Tris-base (pH 7.5) and 150 mM NaCl. Following buffer exchange,

200  $\mu\text{L}$  of concentrated Ni-affinity purified SBT Prx 2 ( $12 \text{ mg mL}^{-1}$ ) was loaded onto a gel filtration column that had been equilibrated with the same buffer that was used for the protein buffer exchange.

To investigate the effect of storage on native molecular mass, SBT Prx 2 protein was purified by Ni-affinity chromatography according to Section 3.2.5 and concentrated to  $30 \text{ mg mL}^{-1}$ . The concentrated SBT Prx 2 solution was stored at  $4^\circ\text{C}$  for 0, 12 and 132 h. At each of these time points, 200  $\mu\text{L}$  containing 6 mg of protein was loaded onto a gel filtration column that had been equilibrated with a buffer containing 20 mM Tris-base (pH 7.5) and 150 mM NaCl.

### 3.2.8 SBT Prx 2 Cys mutant cloning, expression and purification

Site directed mutagenesis (SDM) was performed using PCR. The nucleotide to be mutated was positioned in the centre of the SDM primer with at least 10 bp of complementary DNA sequence flanking each side. To avoid non-specific amplification, the SDM primers were designed to have a melting temperature of approximately  $60^\circ\text{C}$ . The melting temperature of the primers was estimated using the IDT SciTools OligoAnalyzer 3.1 available at [www.idtdna.com/analyzer/applications/oligoanalyzer/](http://www.idtdna.com/analyzer/applications/oligoanalyzer/). Where possible a G-C rich 3' clamp was incorporated into the SDM primers to increase stability of the primer-target DNA complex, enabling more efficient priming of the DNA polymerase elongation reaction. The SDM primers were designed to mutate the Cys residues at positions 51 and 75 to Ser residues (referred to as C51S and C75S, respectively) in the SBT Prx 2 protein. The pET-30a-SBT-Prx 2 plasmid template DNA was prepared according to Section 2.5.2. The SDM PCR reactions contained 1X Phusion<sup>®</sup> HF buffer and 1 U Phusion<sup>®</sup> DNA polymerase (Finnzymes), 200  $\mu\text{M}$  deoxyribonucleotide triphosphates (dNTPs), 3% (v/v) dimethyl sulfoxide (DMSO), 100 ng of pET-30a-SBT-Prx 2 template DNA and 100 ng of forward and reverse

SDM primer in a final volume of 50  $\mu$ L. PCR cycling was carried out in a GeneAmp<sup>®</sup> Applied Biosystems<sup>™</sup> Thermocycler. The PCR conditions were 1 cycle of denaturation at 98<sup>°</sup>C for 30 s followed by 25 cycles of (denaturation at 98<sup>°</sup>C for 10 s, annealing at 60<sup>°</sup>C for 20 s and extension at 72<sup>°</sup>C for 3.5 min), followed by 1 cycle of final extension at 72<sup>°</sup>C for 5 min. The C75S SDM PCR products were purified using a Promega<sup>™</sup> Wizard<sup>®</sup> SV Gel and PCR Clean-Up System according to the manufacturer's instructions. The purified C75S SDM PCR products were digested with the restriction enzyme *DpnI* supplied by New England Biolabs<sup>®</sup> (NEB<sup>®</sup>). The digestion solution contained 1X NEB<sup>®</sup> buffer 4, 60 U *DpnI* and approximately 2  $\mu$ g of plasmid DNA in a final volume of 50  $\mu$ L. The digestion was carried out at 37<sup>°</sup>C for 4 h followed by 80<sup>°</sup>C for 20 min to heat inactivate the *DpnI* restriction enzyme. The C75S SDM PCR products were analysed by agarose gel electrophoresis according to Section 2.6 before and after *DpnI* digestion.

The C51S SDM PCR was repeated as outlined above except that annealing temperatures of 60, 60.9, 62.9, 65.5, 68.4 and 69.8<sup>°</sup>C were trialled. The PCR products were analysed by agarose gel electrophoresis according to Section 2.6. The products produced by the PCR reaction that had an annealing temperature of 65.5<sup>°</sup>C were purified and digested with the *DpnI* restriction enzyme as described above.

The C51S and C75S SDM PCR products that were digested with the *DpnI* restriction enzyme were transformed into Invitrogen<sup>™</sup> sub-cloning efficiency *E. coli* DH5 $\alpha$  cells as outlined in Section 2.9. Colonies of the C51S and C75S pET-30a-SBT-Prx 2 transformants were used to produce purified plasmid according to Section 2.5.2. The inserts in the purified plasmids were sequenced according to Section 2.8.

The purified C51S and C75S pET-30a-SBT-Prx 2 constructs were used to transform Novagen<sup>®</sup> *E. coli* BL21 (DE3) cells according to Section 2.9. Putative transformants

were screened by PCR using the T7 promoter and terminator primers as described in Section 2.10. The resulting PCR products were analysed by agarose gel electrophoresis according to Section 2.6.

Large scale protein expression was performed with *E. coli* BL21 (DE3) cells containing the C51S and C75S pET-30a-SBT-Prx 2 constructs as per Section 2.11 using 500 mL cultures set up in 2 L Erlenmeyer flasks. The level of C51S and C75S SBT Prx 2 protein expression was assessed using SDS-PAGE and immunoblotting as outlined in Sections 2.12 and 2.13, respectively.

Ni-affinity column chromatography purification of C51S and C75S SBT Prx 2 protein was performed as outlined in Section 2.14. Following Ni-affinity purification, the C51S and C75S SBT Prx 2 proteins were exchanged into a buffer containing 20 mM Tris-base (pH 7.5), 150 mM NaCl and 5 mM DTT, concentrated and then either used immediately or frozen in liquid nitrogen and stored at -70°C until needed.

### 3.2.9 SBT Prx 2 antibody preparation and evaluation

Polyclonal antibodies were raised against Ni-affinity purified SBT Prx 2 protein in a New Zealand White rabbit. The SBT Prx 2 protein was purified by Ni-affinity chromatography and exchanged into a buffer containing 20 mM Tris-base (pH 7.5), 150 mM NaCl and 5 mM DTT as per Section 2.14. The rabbit was initially immunised with an emulsion containing 0.5 mL of Ni-affinity purified SBT Prx 2 protein solution combined with 0.5 mL of Freund's complete adjuvant, giving a final protein concentration of 1 mg mL<sup>-1</sup>. Subsequent immunisations were performed at fortnightly intervals using the same antigenic solution except that the Freund's complete adjuvant was replaced with Freund's incomplete adjuvant. A total of seven immunisations were performed with 10 mL of blood collected before each immunisation. Each of the 10 mL blood samples and the terminal bleed were left overnight at 4°C to allow for clotting of the red blood cells. The clotted blood was

centrifuged at 3800 *g* and 4°C for 5 min to isolate the serum. The serum was divided into small aliquots and stored at -70°C.

The anti-SBT Prx 2 antibody titre of the rabbit serum samples was assessed using immunoblotting. Whole cell protein extracts from *E. coli* expressing the SBT Prx 2 protein were transferred to nitrocellulose membrane following SDS-PAGE and probed with each of the rabbit serum samples and anti-His antibodies as a positive control using the method described in Section 2.13. Both the anti-SBT Prx 2 antiserum and anti-His antibodies were used at a dilution of 1/1000 while the horseradish peroxidase antibody conjugate was used at a dilution of 1/2000.

The specificity of the SBT Prx 2 antibody was assessed using immunoblotting of whole cell protein extracts produced from SBT, yellow-tail kingfish and barramundi tissue. Small portions of fish tissue that had been stored at -70°C were thawed on ice and suspended in an ice cold extraction buffer containing 50 mM HEPES (pH 7.5), 150 mM NaCl, 10 mM DTT, 1 mM phenylmethanesulfonyl fluoride (PMSF) and 1 mM EDTA. The ratio of buffer (mL) to fish tissue (g) used was 2:1. The fish tissue samples were homogenised in extraction buffer using a Polytron® homogeniser (Kinematica, Switzerland) at 4°C. The homogenised fish tissue samples were centrifuged at 3,800 *g* and 4°C for 30 min. The 3,800 *g* supernatant was then transferred to a 1.5 mL tube and centrifuged at 16,000 *g* and 4°C for 20 min. The 16,000 *g* supernatant was transferred to a 1.5 mL tube and its protein concentration was quantified as outlined in Section 2.14. The fish tissue protein extracts were analysed using SDS-PAGE and immunoblotting according to Sections 2.12 and 2.13, respectively.

### 3.2.10 Crystallisation of SBT Prx 2 protein

#### 3.2.10.1 Identification of SBT Prx 2 protein crystallisation conditions

Potential crystallisation conditions for the SBT Prx 2 protein were screened for using small scale protein crystallisation as described in Section 2.18.1. The crystallisation solutions used in the small scale crystallisation trials included the Qiagen<sup>®</sup> NeXtal<sup>®</sup> Classic and PEG suites (see Appendix for composition tables). Crystallisation drops contained 250 nL of Ni-affinity purified SBT Prx 2 protein solution at a concentration of 26 mg mL<sup>-1</sup> combined with 250 nL of crystallisation solution. A small scale crystallisation trial was set up immediately following Ni-affinity column purification and another after 5 days storage at 4°C. The small scale crystallisation trial plates were observed 3 days after setup using a polarised light microscope.

#### 3.2.10.2 Up-scaling and optimisation of crystallisation conditions

A crystallisation screen containing 60-80% (v/v) ( $\pm$ )-2-Methyl-2,4-pentanediol (MPD) in 5% (v/v) increments and pH 7-8 in 0.5 pH unit increments was used to set up a large scale crystallisation trial as outlined in Section 2.18.2. The large scale crystallisation trial consisted of 2  $\mu$ L crystallisation drops containing equal volumes of crystallisation solution and SBT Prx 2 protein solution at a concentration of 10 mg mL<sup>-1</sup>. The SBT Prx 2 protein solution had been stored for 10 days at 4°C following Ni-affinity purification. This large scale crystallisation trial was repeated using SBT Prx 2 protein immediately following Ni-affinity purification.

#### 3.2.10.3 Effect of varying the ratio of protein solution volume to crystallisation solution volume on large scale crystallisation outcome

Large scale crystallisation trials were set up where the ratio of protein solution volume to crystallisation solution volume was systematically varied. The ratios tested are shown in Table 3.1. The crystallisation solution contained 0.1 M HEPES



(pH 8) and 65% (v/v) MPD. The large scale crystallisation trials were set up in three replicate Cryschem plates, with each plate containing each crystallisation condition in duplicate. The three replicate plates were incubated at different temperatures. The temperatures tested were 4°C, 22°C and 37°C.

**Table 3.1.** Large scale crystallisation drop composition. Each crystallisation drop contained a different ratio of protein solution volume to crystallisation solution volume.

Condition	Protein (% of drop)	Protein (mg mL <sup>-1</sup> )	Crystallisation Solution (% of drop)	Crystallisation Solution MPD (% v/v)
1	77	19.25	23	14.95
2	67	16.75	33	21.45
3	60	15.00	40	26.00
4	56	14.00	44	28.60
5	44	11.00	56	36.40
6	40	10.00	60	39.00
7	33	8.25	67	43.55
8	29	7.25	71	46.15

#### 3.2.10.4 Small scale crystallisation optimisation

Small scale crystallisation optimisation was performed using the crystallisation solutions developed in the first round of large scale crystallisation trials (refer to Section 3.2.10.2). These crystallisation solutions contained 60-80% (v/v) MPD in 5% (v/v) increments and pH 7-8 in 0.5 pH unit increments. The crystallisation solutions were transferred to a 96 deep well block in duplicate and used to set up a small scale crystallisation trial as per Section 2.18.1. The crystallisation drops contained 0.25  $\mu\text{L}$  of Ni-affinity purified SBT Prx 2 protein solution at a concentration of 25 mg  $\text{mL}^{-1}$  and 0.25  $\mu\text{L}$  of crystallisation solution. The crystallisation plate was inspected using a polarised light microscope and observations were recorded at 5 and 14 days post-setup.

#### 3.2.10.5 Broadening the search for crystallisation conditions that utilise MPD

To further investigate the use of MPD as a crystallisation precipitant and expand the search for appropriate crystallisation conditions, the SBT Prx 2 protein was screened against the Qiagen<sup>®</sup> NeXtal<sup>®</sup> MPD suite (see Appendix for composition table) using a small scale crystallisation trial as described in Section 2.18.1. Each MPD suite crystallisation condition was used to set up two different crystallisation drop sizes of 0.5 and 2.5  $\mu\text{L}$ . Both crystallisation drop sizes contained equal volumes of protein and crystallisation solutions. The concentration of the SBT Prx 2 protein solution was 20 mg  $\text{mL}^{-1}$ .

#### 3.2.10.6 Effect of lithium sulphate on the large scale crystallisation outcome

A crystallisation screen containing 10-30% (v/v) MPD in 5% (v/v) increments, 0 M or 0.2 M  $\text{Li}_2\text{SO}_4$  and 0.1 M Tris-base (pH 8.5) was used to set up a large scale

crystallisation trial as outlined in Section 2.18.2. The large scale crystallisation trial consisted of 4  $\mu\text{L}$  crystallisation drops composed of equal volumes of crystallisation solution and SBT Prx 2 protein solution. The concentration of the SBT Prx 2 protein solution was  $20 \text{ mg mL}^{-1}$ .

### 3.2.10.7 Effect of increased MPD concentration combined with high pH on the large scale crystallisation outcome

The effects of increased MPD concentration and pH, in the presence of lithium sulphate, on the crystallisation of the SBT Prx 2 protein were investigated using the large scale crystallisation format. The crystallisation solutions contained 30-55% (v/v) MPD in 5% (v/v) increments, 0.2 M  $\text{Li}_2\text{SO}_4$  and 0.1 M Tris-base (pH 8.5). When preparing the crystallisation solution containing 55% (v/v) MPD, it was noticed that two distinct phases formed, presumably lithium sulphate and MPD. The crystallisation solution was able to be homogenised by thorough mixing, however, upon being left undisturbed the two phases re-formed. In light of this the 55% (v/v) MPD crystallisation solution was excluded from the experiment. The large scale crystallisation trial was set up as outlined in Section 2.18.2 and consisted of 4  $\mu\text{L}$  crystallisation drops that were composed of equal volumes of crystallisation solution and SBT Prx 2 protein solution. The concentration of the SBT Prx 2 protein solution was  $20 \text{ mg mL}^{-1}$ .

### 3.2.10.8 X-ray crystallography analysis of crystals

All of the crystals grown in small and large scale crystallisation trials were harvested and prepared for X-ray crystallography analysis according to Section 2.19. Due to the cryo-protectant property of MPD, all crystals were able to be harvested from crystallisation drops and directly frozen in liquid nitrogen. X-ray crystallography analysis of crystals was performed as outlined in Section 2.19.

## 3.3 Results

### 3.3.1 Sequencing of pET-30a-SBT Prx construct

The SBT Prx 2 nucleotide sequence (GenBank accession no. EU093980) was found to contain 5'- and 3'- untranslated regions in addition to the ORF. To identify the ORF the nucleotide sequence was translated in all six reading frames. The +2 reading frame translation was found to produce the longest uninterrupted ORF which contained within it the two characteristic peroxiredoxin 'VCP' motifs (Montemartini et al., 1999). Alignment of the SBT Prx ORF with the pET-30a-SBT Prx construct insert sequence identified a single base mismatch occurring 579 bp from the 5' terminus of the SBT Prx ORF. The mismatch was between an unknown nucleotide (N) in the SBT Prx ORF and an adenine (A) in the pET-30a-SBT Prx insert. Therefore, the unknown nucleotide in the SBT Prx ORF was identified as an adenine. Identification of this base changed the corresponding codon from TTN to TTA and therefore the corresponding amino acid from an unknown residue to a leucine residue. A translated nucleotide alignment revealed that the SBT Prx insert sequence in the pET-30a expression vector was in frame and in the correct orientation relative to the start site for translation.

### 3.3.2 SBT Prx protein sequence analysis

An alignment of the SBT Prx deduced amino acid sequence with NKEF A (Prx 1) and NKEF B (Prx 2) amino acid sequences from other fish and from a selection of mammals revealed a high degree of sequence conservation (Fig. 3.1). The conserved regions included the F-motif (FTFVCPTEI) containing the peroxidatic Cys residue (C<sup>52</sup>) and the hydrophobic region (VCPAGW) containing the resolving Cys residue (C<sup>173</sup>). These features, especially the peroxidatic and resolving Cys residues, are characteristic of typical 2-Cys Prxs (Wood et al., 2003a; König et al.,

2003). Thus, it was clear that the SBT Prx sequence was also a typical 2-Cys Prx sequence.

In addition to the peroxidatic and resolving Cys residues, the SBT Prx sequence also contained an additional Cys residue (C<sup>76</sup>) which appears to be a unique feature of the fish NKEF B sequences. This additional Cys residue was first noted by Dong et al. (2007) in their comparison of pufferfish NKEF A and B sequences.

Interestingly, in the human NKEF B sequence, this Cys residue is replaced by a Val residue.

The SBT sequence also contained the highly conserved GGLG motif (residues 95-98, underlined in Fig. 3.1). This motif is common to most eukaryotic typical 2-Cys Prxs but it is lacking from most prokaryotic typical 2-Cys Prxs (Wood et al., 2003a). In mammals, the GGLG motif is associated with a highly conserved YF motif (residues 194-195, broken underlining in Fig. 3.1). Interestingly, in most of the fish species in the alignment, the YF motif was replaced by an FF motif except for common carp which had the YF motif and SBT which had an LF motif. Thus, in most of the fish species, tyrosine was replaced by phenylalanine whereas in SBT it was replaced by leucine.

**Fig. 3.1.** A multiple sequence alignment of SBT Prx with other members of the Prx family from fish, mammals and fleshy prawn. The alignment was performed using ClustalX software (Larkin et al., 2007) and shading was done using GeneDoc software (Nicholas et al., 1997). The degree of amino acid conservation is indicated by 3 levels of shading with black, dark grey and light grey shading indicating 100, 80 and 60% conservation, respectively. The two active site motifs containing the redox active Cys residues are boxed. The conserved 'GGLG' and 'XF' motifs are highlighted with a solid and a dashed line, respectively. GenBank nucleotide sequence accession numbers for the protein sequences are as follows. Southern bluefin tuna Prx 2, EU093980; Turbot NKEF B, DQ472128; Pufferfish NKEF B, DQ323504; Zebrafish NKEF B-like, BC076347; Rat Prx 1, D30035; Rainbow trout NKEF A, AF250194; Human NKEF A, X67951; Mouse Prx 1, AK083243; Pufferfish NKEF A, DQ003333; Carp NKEF A, AB010959; Zebrafish NKEF A-like, BC091459; Human NKEF B, BC003022; Rat Prx 2, BC058481; Mouse Prx 2, AK008433; Fleshy prawn Prx 1, DQ205423.

```

Southern bluefin tuna Prx II : MSSGNAKIGR*APDFKSTAVV20-DGF*FDIKLSDYKGYVV40FFYPLDFTFVCPT*EIVAFS : 59
Turbot NKEF B : MSSGNAKIGM*APDFKATAVV-DGEFVEIKLSDYR*GKYVVFFYPLDFTFVCPT*EIVAFS : 59
Pufferfish NKEF B : MSSGSAKIGQ*APDFATAVV-DGQF*FDLRLSDYR*GKYVVFFYPLDFTFVCPT*EIVAFS : 59
Zebrafish NKEF B-like : MSAGNAKIGQ*APQFKATAVV-DGQF*FDIQ*LSDYR*GKYVVFFYPLDFTFVCPT*EIVAFS : 59
Rat Prx I : MSSGNAKIGH*APSEKATAVMPDGF*FDISLSDYK*GKYVVFFYPLDFTFVCPT*EIVAFS : 60
Rainbow trout NKEF A : MAAGKARIGH*LAPGETAKAVMPDGF*FDISMSDYR*GKYVVFFYPLDFTFVCPT*EIVAFS : 60
Human NKEF A : MSSGNAKIGH*APNEKATAVMPDGF*FDISLSDYK*GKYVVFFYPLDFTFVCPT*EIVAFS : 60
Mouse Prx I : MSSGNAKIGY*APNEKATAVMPDGF*FDISLSEYK*GKYVVFFYPLDFTFVCPT*EIVAFS : 60
Pufferfish NKEF A : MAAGKAQIGK*LAPDFATAVMPDGF*FHD*LKLSDYR*GKYVVFFYPLDFTFVCPT*EIVAFS : 60
Carp NKEF A : MAAGKAHIGR*APDFATAVMPDGF*FDL*SLSEYK*GKYVVFFYPLDFTFVCPT*EIVAFS : 60
Zebrafish NKEF A-like : MAAGNAHIGR*APDFATAVMPDGF*FGDVRLSDYK*GKYVVFFYPLDFTFVCPT*EIVAFS : 60
Human NKEF B : MASGNAHIGR*APDFATAVAV-DGAF*FEVKLSDYK*GKYVVFFYPLDFTFVCPT*EIVAFS : 59
Rat Prx II : MASGNAHIGR*APDFATAVAV-DGAF*FEIKLSDYR*GKYVVFFYPLDFTFVCPT*EIVAFS : 59
Mouse Prx II : MASGNAQIGK*APDFATAVAV-DGAF*FEIKLSDYR*GKYVVFFYPLDFTFVCPT*EIVAFS : 59
Fleshy prawn Prx I : MSNTVPAIQK*APVFKGTAVV-DGQF*FEISLE*YK*GKYVIF*FFYPLDYTFVCPT*EIVAFS : 59

```

```

Southern bluefin tuna Prx II : DRAEEFRSIC*QEVIC80CSIDSHF*SHLAWINTPRK100GGGLSMK*IPLIADLT*TIISRDYGV120LK : 119
Turbot NKEF B : DRAEEFRSMQ*QEVIC80CSVDSHF*SHLAWINTPRK100GGGLGTM*IPLVADLT*TIISRDYGV120LK : 119
Pufferfish NKEF B : DRVQDFRSIN*QEVIC80CSIDSHF*HLAWINTPRK100GGGLGEM*IPLVADLT*TSISKDYGV120LK : 119
Zebrafish NKEF B-like : ERAAEFRKIG*VELI80AASTDSHF*SHLAWINTPRK100GGGLGSM*NIPLVADLT*QISIRDYGV120LK : 119
Rat Prx I : DRAEEFKKLN*QVIGASVDSHF*CHLAWINTPRK100GGGLGPM*NIPLVSDPKRTIAQDYGV120LK : 120
Rainbow trout NKEF A : DAAEEFRKIG*QEVIGASVDSHF*CHLAWINTPRK100GGGLGAM*NIPLVADLT*RSISTDYGV120LK : 120
Human NKEF A : DRAEEFKKLN*QVIGASVDSHF*CHLAWINTPRK100GGGLGPM*NIPLVSDPKRTIAQDYGV120LK : 120
Mouse Prx I : DRAEEFKKLN*QVIGASVDSHF*CHLAWINTPRK100GGGLGPM*NIPLVSDPKRTIAQDYGV120LK : 120
Pufferfish NKEF A : DAAEDFRKIG*QEVIAASVDSHF*SHLAWINTPRK100GGGLGTM*IPLVSDTRHISTDYGV120LK : 120
Carp NKEF A : DAVEEFRKIN*QEVIGASVDSHF*CHLAWINTPRK100GGGLGMM*VPLVADSLRSISQDYGV120LK : 120
Zebrafish NKEF A-like : DAAEFRKIN*QEVIGASVDSHF*CHLAWITKTPRK100GGGLGPM*VPLVADLT*RSISKDYGV120LK : 120
Human NKEF B : NRAAEFRKLG*QEVIGVSDSQF*HLAWINTPRK100GGGLGPL*NIPLVADVT*RLSEYGV120LK : 119
Rat Prx II : DHAEDFRKLG*QEVIGVSDSQF*HLAWINTPRK100GGGLGPL*NIPLVADVT*KSLSQDYGV120LK : 119
Mouse Prx II : DHAEDFRKLG*QEVIGVSDSQF*HLAWINTPRK100GGGLGPL*NIPLVADVT*KSLSQDYGV120LK : 119
Fleshy prawn Prx I : DRVEEFRKIG*QEVVAC80STDSHF*SHLAWINTPRK100GGGLGTM*IPLVAD*KSMVAKTYGV120LK : 119

```

```

Southern bluefin tuna Prx II : EDDGIAYRGLFVID*DKGILRQITINDLPVGRSVDE140TLRLVQAFQ*HTDKHGEVCPAGWK180FG : 179
Turbot NKEF B : EDDGIAYRGLFVID*DKGILRQITINDLPVGRSVDES140LRLIQAFQ*HTDKHGEVCPAGWK180FG : 179
Pufferfish NKEF B : EDDGIAYRGLFVID*DKGILRQITVNDLPVGRSVDE140TLRLVQAFQ*HTDKYGEVCPAGWK180FG : 179
Zebrafish NKEF B-like : EDEGIAYRGLFVID*DKGILRQITINDLPVGRSVDE140TLRLVQAFQ*HTDKYGEVCPAGWK180FG : 179
Rat Prx I : ADEGISFRGLFII*DKGILRQITINDLPVGRSVDE140TLRLVQAFQ*HTDKHGEVCPAGWK180FG : 180
Rainbow trout NKEF A : EDEGIAYRGLFII*DKGILRQITINDLPVGRSVDE140TLRLVQAFQ*HTDKHGEVCPAGWK180FG : 180
Human NKEF A : ADEGISFRGLFII*DKGILRQITVNDLPVGRSVDE140TLRLVQAFQ*HTDKHGEVCPAGWK180FG : 180
Mouse Prx I : ADEGISFRGLFII*DKGILRQITINDLPVGRSVDE140TLRLVQAFQ*HTDKHGEVCPAGWK180FG : 180
Pufferfish NKEF A : EDEGIAYRGLFII*DKGILRQITINDLPVGRSVDE140TLRLVQAFQ*HTDKHGEVCPAGWK180FG : 180
Carp NKEF A : EDEGIAYRGLFII*DKGILRQITINDLPVGRSVDE140TLRLVQAFQ*HTDKHGEVCPAGWK180FG : 180
Zebrafish NKEF A-like : EDEGIAYRGLFII*DKGILRQITINDLPVGRSVDE140TLRLVQAFQ*HTDKHGEVCPAGWK180FG : 180
Human NKEF B : TDEGIAYRGLFII*DKGILRQITVNDLPVGRSVDE140TLRLVQAFQ*HTDEHGEVCPAGWK180FG : 179
Rat Prx II : NDEGIAYRGLFII*DKGILRQITVNDLPVGRSVDE140TLRLVQAFQ*HTDEHGEVCPAGWK180FG : 179
Mouse Prx II : NDEGIAYRGLFII*DKGILRQITVNDLPVGRSVDE140TLRLVQAFQ*HTDEHGEVCPAGWK180FG : 179
Fleshy prawn Prx I : EDEGIAYRGLFVID*DKQD140LRQVITINDLPVGRVD160DE180TLRLVQAFQ*HTDEHGEVCPAGWK180FG : 179

```

```

Southern bluefin tuna Prx II : SATII*PDVERSKDLFSKQ- : 197
Turbot NKEF B : SDTII*PDVERSKAFFSKQ- : 197
Pufferfish NKEF B : SDTIV*PDVERSKIEFSKQN : 198
Zebrafish NKEF B-like : SDTIV*PDVQSKIEFSKQ- : 197
Rat Prx I : SDTIK*PDVNRKSEYFSKQK : 199
Rainbow trout NKEF A : SDTIK*PDVQKSKDEFSKQQ : 199
Human NKEF A : SDTIK*PDVQKSKSEYFSKQK : 199
Mouse Prx I : SDTIK*PDVNRKSEYFSKQK : 199
Pufferfish NKEF A : SDTIK*PDVQKSKIEFSKH- : 198
Carp NKEF A : KDTIK*PDVQSKDIEFSKQH : 199
Zebrafish NKEF A-like : KDTIK*PDVQSKDEFSKQN : 199
Human NKEF B : SDTIK*PNVDDSKSEYFSKHN : 198
Rat Prx II : SDTIK*PNVDDSKSEYFSKHN : 198
Mouse Prx II : SDTIK*PNVDDSKSEYFSKHN : 198
Fleshy prawn Prx I : AKTMD*ADPAGSKEMFQNE : 198

```

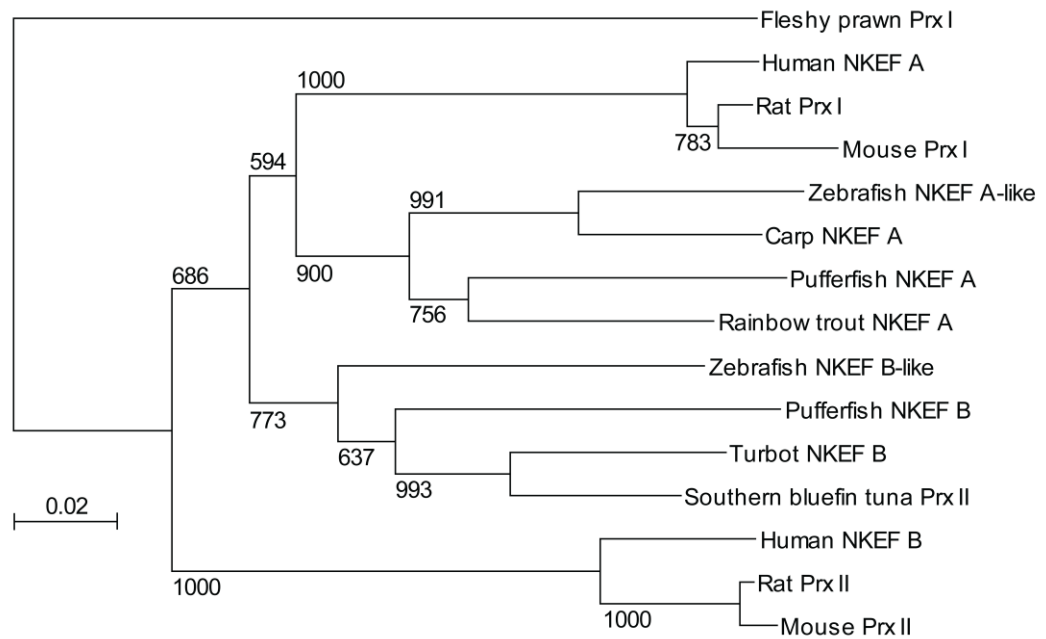


Pairwise comparisons of deduced amino acid sequences revealed that the SBT Prx sequence was more similar to NKEF B (Prx 2) sequences than NKEF A (Prx 1) sequences (Table 3.2). In particular, it was most similar to NKEF B sequences from turbot (92% identity) and pufferfish (86% identity) and a NKEF B-like sequence from zebrafish (86% identity).

**Table 3.2.** Amino acid sequence identity matrix comparing SBT Prx with other members of the 2-Cys Prx family from fish, mammals and fleshy prawn. The ClustalX amino acid sequence alignment shown in Fig. 3.1 was analysed using BioEdit (Hall, 1999).

	Southern bluefin tuna Prx2	Turbot NKEF B	Pufferfish NKEF B	Zebrafish NKEF B-like	Rat Prx 1	Rainbow trout NKEF A	Human NKEF A	Mouse Prx 1	Pufferfish NKEF A	Carp NKEF A	Zebrafish NKEF A-like	Human NKEF B	Rat Prx 2	Mouse Prx 2	Fleshy prawn Prx 1
Southern bluefin tuna Prx 2	100	92	86	86	81	80	80	80	80	79	78	77	77	76	74
Turbot NKEF B		100	85	85	80	80	79	78	80	77	77	77	78	77	71
Pufferfish NKEF B			100	83	77	81	77	75	79	80	79	76	78	77	71
Zebrafish NKEF B-like				100	80	82	80	79	81	80	80	76	76	76	72
Rat Prx 1					100	82	97	97	79	83	81	77	76	76	71
Rainbow trout NKEF A						100	83	80	88	88	87	76	77	77	70
Human NKEF A							100	95	80	83	81	77	76	76	70
Mouse Prx 1								100	77	82	79	76	75	74	69
Pufferfish NKEFA									100	84	84	75	76	77	69
Carp NKEFA										100	92	76	77	76	70
Zebrafish NKEF A-like											100	77	77	76	67
Human NKEF B												100	94	93	71
Rat Prx 2													100	99	70
Mouse Prx 2														100	70
Fleshy prawn Prx 1															100

Fig. 3.2 shows a phylogenetic tree illustrating the evolutionary relationships between fish and mammalian NKEF A and B (Prx 1 and 2) sequences with fleshy prawn as the out-group to root the tree. The phylogenetic analysis produced four distinctly separate clusters which were mammalian Prx 1, fish Prx 1, fish Prx 2 and mammalian Prx 2. As expected, the SBT Prx 2 sequence clustered together with the turbot and pufferfish NKEF B sequences and the zebrafish NKEF B-like sequence. Based on the various lines of evidence presented above, we have classified the SBT Prx cDNA as a NKEF B (Prx 2).



**Fig. 3.2.** A phylogenetic tree showing the relationships between the SBT Prx and other members of the Prx family from fish, mammals and fleshy prawn (included as an out-group). The alignment shown in Fig. 3.1 was analysed by ClustalX using the Neighbor-Joining method (Saitou and Nei, 1987) to generate the tree. The horizontal branch length is proportional to the rate of amino acid substitution per site. The numbers represent bootstrap values calculated from 1000 replicates.

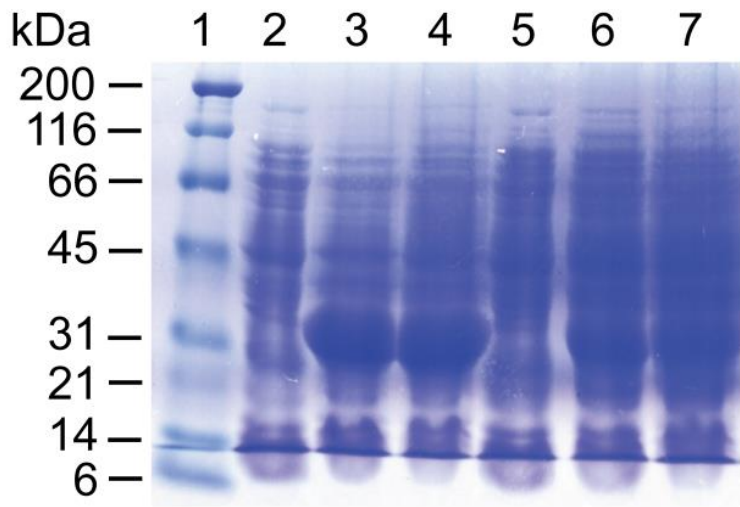
### 3.3.3 Optimisation of recombinant SBT Prx 2 protein expression

Whole cell protein extracts produced from un-induced, 3 h induced and 18 h induced *E. coli* BL21 (DE3) cells containing the pET-30a-SBT Prx 2 construct were analysed by SDS-PAGE and immunoblotting (Fig. 3.3). The Coomassie blue stained SDS-PAGE gel revealed a prominent protein band of approximately 27 kDa was produced by both cell cultures after 3 h and 18 h induction. The molecular mass of this highly abundant protein was consistent with the expected size of the recombinant SBT Prx 2 monomer and its putative identity was confirmed by immunoblotting with anti-His antibodies. Comparison of the intensity of the SBT Prx 2 monomer band after 3 h and 18 h induction of both cultures revealed no difference, indicating that a maximum yield of recombinant SBT Prx 2 protein was obtained after 3 h induction. Therefore, the SBT Prx 2 protein was able to be expressed with a high abundance after 3 h induction and increasing the induction time to 18 h had no effect on yield.

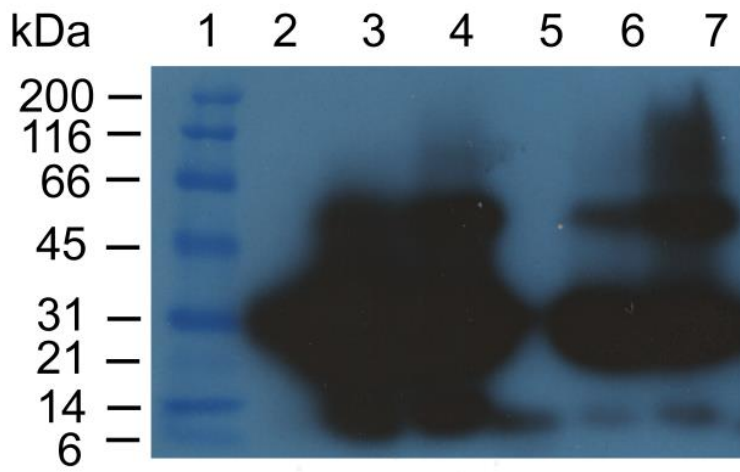
In addition to the 27 kDa SBT Prx 2 monomer, two additional protein species with approximate molecular masses of 10 and 55 kDa were detected by immunoblotting. The 10 kDa species is not consistent with any expected size of the SBT Prx 2 protein and may be a degradation product or it may indicate non-specific detection by the anti-His antibodies. The size of the 55 kDa protein species is consistent with a recombinant SBT Prx 2 dimer. A single faint band of 27 kDa was detected in the un-induced whole cell protein extracts of both colonies. These bands are presumably the result of background protein expression brought about by a basal level of T7 RNA polymerase activity despite the transcription of the SBT Prx 2 gene being under the tight control of a T7 *lac* promoter.

**Fig. 3.3.** Reducing SDS-PAGE (A) and immunoblotting analysis using X-ray film (B) and BioRad® VersaDoc™ imaging system (C) of whole cell protein extracts produced from two cultures of *E. coli* BL21(DE3) cells that contained the pET-30a-SBT Prx 2 construct. The immunoblotting analysis was performed with rabbit anti-6X His polyclonal antibodies (Rockland). Samples of both cell cultures were taken prior to induction, 3 h post-induction and 18 h post-induction. Lane 1, molecular mass markers; Lane 2, un-induced whole cell protein extract from colony 1; Lane 3, 3 h post-induction whole cell protein extract from colony 1; Lane 4, 18 h post-induction whole cell protein extract from colony 1; Lane 5, un-induced whole cell protein extract from colony 2; Lane 6, 3 h post-induction whole cell protein extract from colony 2; Lane 7, 18 h post-induction whole cell protein extract from colony 2.

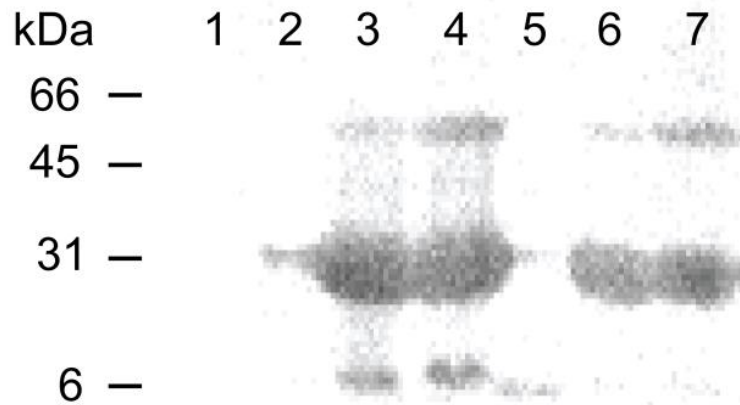
A



B



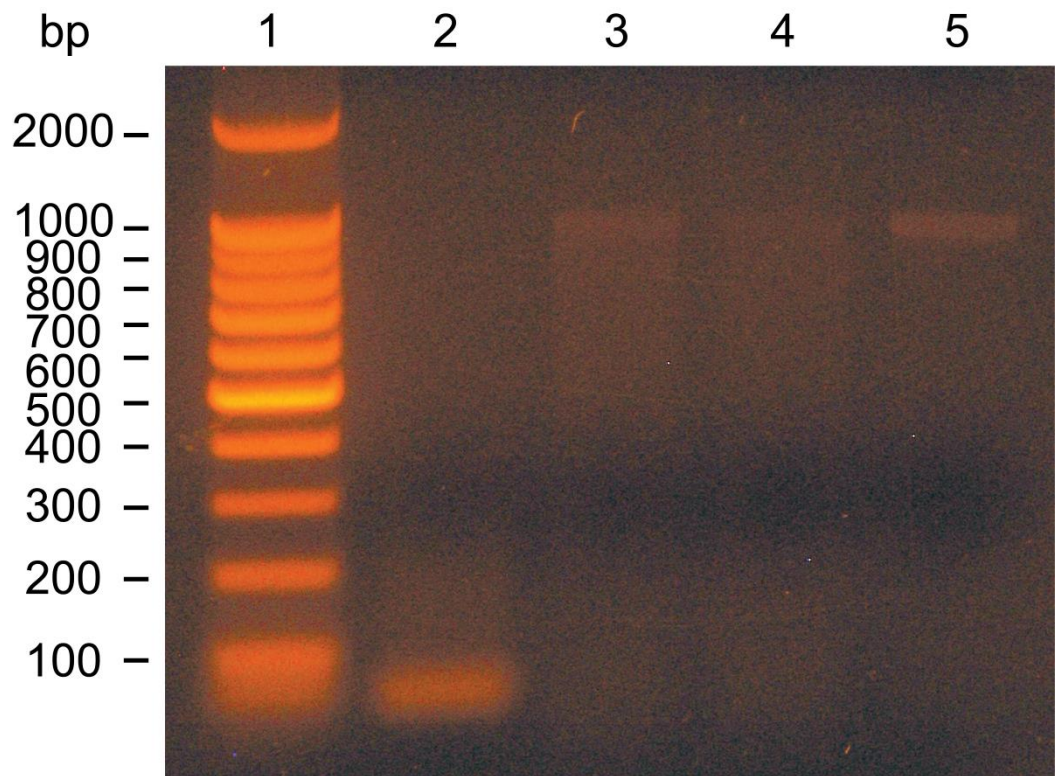
C



### 3.3.4 Large scale recombinant expression of SBT Prx 2 protein

Prior to large scale protein expression, three colonies of *E. coli* BL21 (DE3) cells were PCR screened for the pET-30a-SBT Prx 2 construct. The resulting PCR screening products were analysed by agarose gel electrophoresis (Fig. 3.4). All three colonies produced PCR screening products of approximately 1000 bp which is consistent with the expected size of the pET-30a multiple cloning region containing an SBT Prx 2 insert sequence. The negative control PCR reaction containing water as template produced no PCR products except for primer dimers.



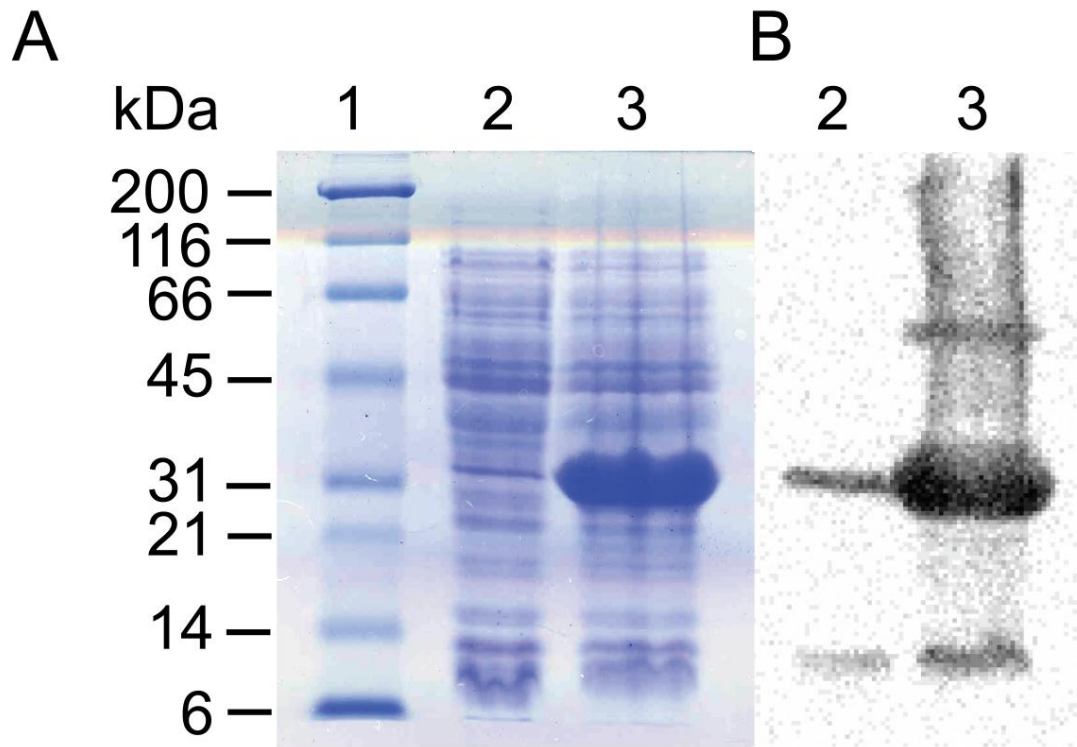


**Fig. 3.4.** Agarose gel electrophoresis of PCR colony screening products produced from three colonies of *E. coli* BL21 (DE3) cells containing the pET-30a-SBT Prx 2 construct. The multiple cloning region of each colony was amplified using T7 promoter and terminator plasmid specific primers. Lane 1, DNA size standards; Lane 2, negative control PCR products; Lane 3, colony 1 PCR products; Lane 4, colony 2 PCR products; Lane 5, colony 3 PCR products.

A colony of *E. coli* BL21 (DE3) cells found to contain the pET-30a-SBT Prx 2 construct was used for large scale protein expression. Whole cell protein extracts produced from un-induced and 3 h-induced cultures were analysed by SDS-PAGE and immunoblotting (Fig. 3.5).

SDS-PAGE analysis of the whole cell protein extract produced from cells that had been induced for 3 h revealed a prominent band of approximately 27 kDa. The molecular mass of the prominent protein band was consistent with the expected molecular mass of SBT Prx 2 monomer. The immunoblot confirmed that the 27 kDa protein species was the His-tagged SBT Prx 2. Therefore, expression of the SBT Prx 2 protein was able to be up-scaled whilst maintaining a high level of expression.

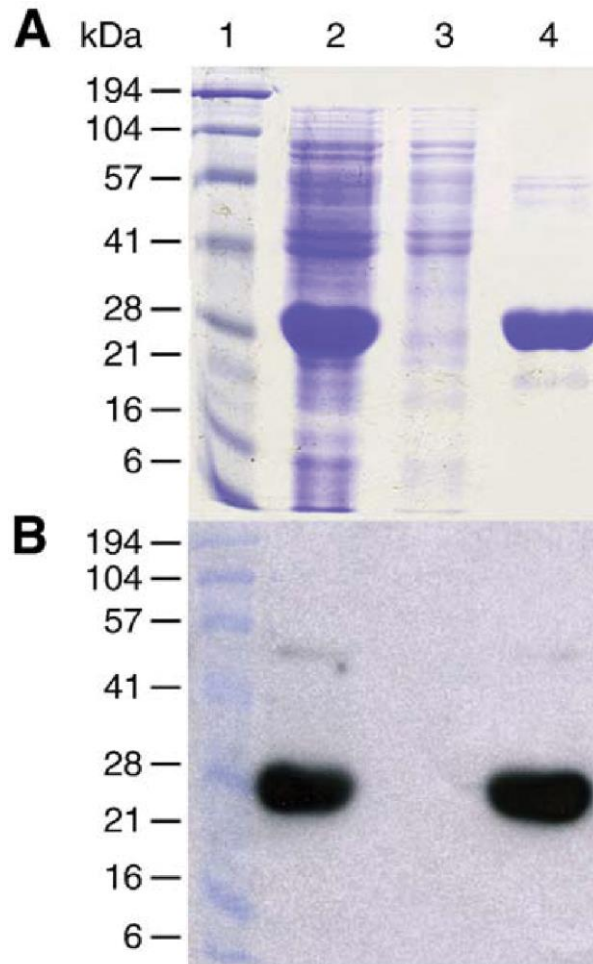
The immunoblot also detected two additional protein species with approximate molecular masses of 10 and 55 kDa. The 10 kDa species, detected in both the un-induced and 3 h-induced whole cell protein extracts, is not consistent with any expected size of the SBT Prx 2 protein. The 10 kDa protein species may represent an SBT Prx 2 degradation product or it may indicate non-specific detection by the anti-His antibodies. The 55 kDa protein species, detected only in the 3 h-induced whole cell protein extract, is consistent with the expected size of an SBT Prx 2 dimer.



**Fig. 3.5.** Reducing SDS-PAGE (A) and immunoblotting (B) analysis of whole cell protein extracts prepared from un-induced and 3 h-induced *E. coli* BL21 (DE3) cells that contained the pET-30a-SBT-Prx 2 construct. The immunoblotting analysis was performed with rabbit anti-6X His polyclonal antibodies (Rockland). Lane 1, molecular mass markers; Lane 2, un-induced whole cell protein extract; Lane 3, 3 h-induced whole cell protein extract.

### 3.3.5 Ni-affinity purification of SBT Prx 2 protein

*E. coli* BL21(DE3) cells containing the pET-30a-SBT Prx 2 construct were used for protein expression. A high level of expression of a protein of the expected size of the SBT Prx 2 monomer (26.8 kDa, including the tags introduced by the vector) was obtained (Fig. 3.6A, lane 2). The identity of the expressed protein was confirmed by immunoblotting with anti-His antibodies (Fig. 3.6B, lane 2). The recombinantly expressed SBT Prx 2 protein was purified by Ni-affinity chromatography with high yield and enrichment (Fig. 3.6A and B, lanes 2-4). Despite the large number of proteins observed in the SDS-PAGE analysis of the combined flow through and 20 mM imidazole wash, the immunoblotting analysis revealed that no SBT Prx 2 protein was present. This indicated that the SBT Prx 2 protein was able to bind to the Ni-column and remain bound for the duration of the 20 mM imidazole wash, enabling the SBT Prx 2 to be highly purified using a one-step Ni-affinity column purification.



**Fig. 3.6.** Reducing SDS-PAGE (A) and immunoblotting (B) analysis of various fractions from the Ni-affinity purification of SBT Prx 2 protein. The immunoblotting analysis was performed with rabbit anti-6X His polyclonal antibodies (Rockland). Lane 1, molecular mass markers; lane 2, crude cell lysate of *E. coli* BL21 (DE3) expressing the pET-30a-SBT Prx 2 construct; lane 3, Ni-affinity purification, flow through and 20 mM imidazole wash; lane 4, Ni-affinity purification, 500 mM imidazole elution.

### 3.3.6 Development of the Prx kinetic assay

To investigate the affinity of the SBT Prx 2 protein for its substrates, a non-rate limiting assay was developed. The assay was based on the method of Rahlfs and Becker (2001) and measured peroxidase activity by monitoring NADPH oxidation coupled to peroxide reduction in the presence of *E. coli* thioredoxin (Trx) and thioredoxin reductase (TrxR). In a series of experiments the concentrations of the *E. coli* TrxR and SBT Prx 2 proteins were systematically varied to identify non-rate limiting conditions for the SBT Prx 2. The concentrations of the Prx assay components and corresponding rates of reaction for the first round of kinetic assay development are summarised in Table 3.3.

Under the assay conditions tested, the rate of Trx-dependent peroxidase activity was shown to be directly proportional to the concentration of the *E. coli* TrxR protein. Therefore, the *E. coli* TrxR protein was the rate limiting component in the assay.

**Table 3.3.** Effect of the *E. coli* TrxR protein concentration on Trx-dependent peroxidase activity of Ni-affinity purified SBT Prx 2 protein. The Prx assays were performed as outlined in Section 2.15 except that the concentration of the Ni-affinity purified SBT Prx 2 protein, *E. coli* Trx protein and H<sub>2</sub>O<sub>2</sub> were held constant at 2.5, 10 and 37 μM, respectively, and the concentration of the *E. coli* TrxR protein was varied (0.1-0.3 U).

SBT Prx 2 (μM)	<i>E. coli</i> Trx (μM)	<i>E. coli</i> TrxR (U)	NADPH (μM)	H <sub>2</sub> O <sub>2</sub> (μM)	Rate of reaction ΔAbs <sub>340 nm</sub> min <sup>-1</sup>
2.5	10	0.1	250	37	0.033
2.5	10	0.2	250	37	0.075
2.5	10	0.3	250	37	0.116

In an attempt to prevent the *E. coli* TrxR from being rate limiting, the concentration of Ni-affinity purified SBT Prx 2 used in the assay was decreased by an order of magnitude. The final concentrations of Prx assay components and corresponding rates of reaction for the second round of kinetic assay development are summarised in Table 3.4.

The decrease in SBT Prx 2 protein concentration by an order of magnitude significantly decreased the measurable rate of reaction to the point where it was just above the limit of detection. A doubling of the SBT Prx 2 protein concentration to 0.4  $\mu\text{M}$  produced a small increase in peroxidase activity keeping all other parameters constant. Therefore, the assay conditions tested were not rate limiting for the SBT Prx 2 protein when used at a concentration of 0.2  $\mu\text{M}$ . Tripling of the concentration of the *E. coli* TrxR protein was shown to have no effect on the rate of reaction. Therefore, the rate of reaction was no longer limited by the TrxR protein concentration. Despite having found non-rate limiting Trx-dependent peroxidase activity conditions for the Ni-affinity purified SBT Prx 2 protein, the rate of activity was too low to make accurate measurements or test lower substrate concentrations.



**Table 3.4.** Effect of varying the concentrations of SBT Prx 2 and *E. coli* TrxR proteins on Trx-dependent peroxidase activity. The Prx assays were performed as outlined in Section 2.15 except that the concentrations of *E. coli* Trx protein and H<sub>2</sub>O<sub>2</sub> were held constant at 20 and 110  $\mu$ M, respectively, and the concentrations of Ni-affinity purified SBT Prx 2 (0.2-0.4  $\mu$ M) and *E. coli* TrxR (0.1-0.3 U) proteins were varied.

SBT Prx 2 ( $\mu$ M)	<i>E. coli</i> Trx ( $\mu$ M)	<i>E. coli</i> TrxR (U)	NADPH ( $\mu$ M)	H <sub>2</sub> O <sub>2</sub> ( $\mu$ M)	Rate of reaction $\Delta$ Abs <sub>340 nm</sub> min <sup>-1</sup>
0.2	20	0.1	250	110	0.018
0.4	20	0.1	250	110	0.024
0.2	20	0.3	250	110	0.015

In an attempt to obtain a higher rate of reaction whilst maintaining non-rate limiting Trx-dependent peroxidase activity conditions, the concentrations of the SBT Prx 2 and *E. coli* TrxR proteins were increased from 0.2  $\mu\text{M}$  to 0.4  $\mu\text{M}$  and 0.1 U to 0.5 U, respectively. The TrxR concentration was increased more than the Prx concentration to try and enable a doubling of Prx activity with a doubling in Prx concentration. This would ensure that no other assay component in addition to the TrxR would be rate limiting. The final concentrations of the Prx assay components and the corresponding rates of reaction for the third round of kinetic assay development are summarised in Table 3.5.

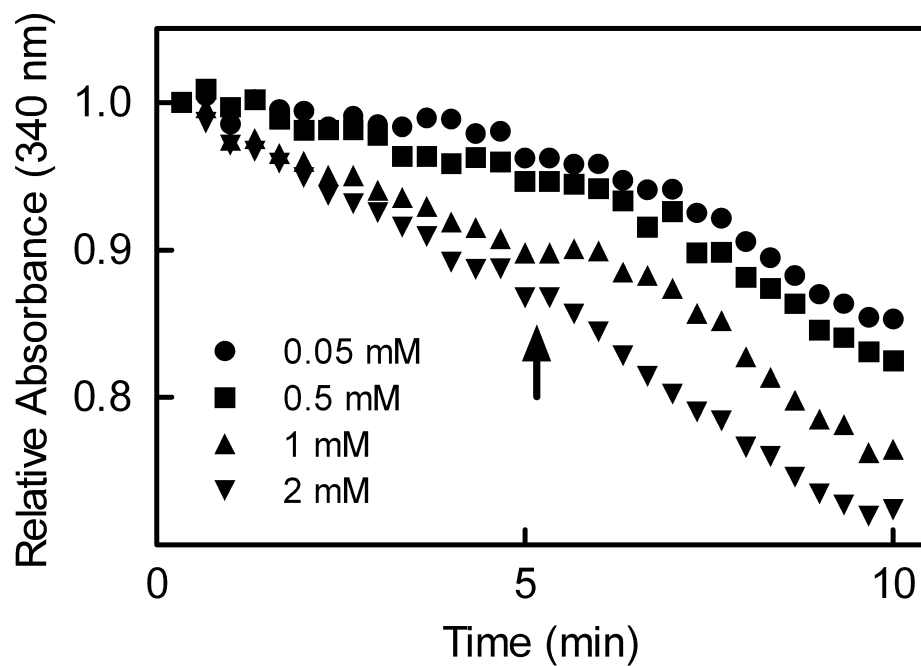
The increase in the SBT Prx 2 and *E. coli* TrxR protein concentrations gave a rate of reaction that was well within detection limits, enabling future testing of a range of lower substrate concentrations. The doubling of the TrxR protein concentration from 0.5 U to 1 U whilst keeping all other experimental parameters constant had no effect on the rate of reaction. Therefore, under the assay conditions tested the use of 0.5 U of TrxR did not limit the rate of Trx-dependent peroxidase activity. Doubling of the SBT Prx 2 protein concentration from 0.4 to 0.8  $\mu\text{M}$  increased the rate of reaction by 67%. Although a doubling in Trx-dependent peroxidase activity was not observed with a doubling of the Prx concentration, it certainly indicated that under these assay conditions that use of the SBT Prx 2 protein at a concentration of 0.4  $\mu\text{M}$  would not be rate limited by any other assay component.

**Table 3.5.** Effect of varying the concentrations of SBT Prx 2 and *E. coli* TrxR proteins on Trx-dependent peroxidase activity. The Prx assays were performed as outlined in Section 2.15 except that the concentrations of the *E. coli* Trx protein and H<sub>2</sub>O<sub>2</sub> were held constant at 20 and 132  $\mu$ M, respectively, and the concentrations of the Ni-affinity purified SBT Prx 2 (0.4-0.8  $\mu$ M) and *E. coli* TrxR (0.5-1 U) proteins were varied.

SBT Prx 2 ( $\mu$ M)	<i>E. coli</i> Trx ( $\mu$ M)	<i>E. coli</i> TrxR (U)	NADPH ( $\mu$ M)	H <sub>2</sub> O <sub>2</sub> ( $\mu$ M)	Rate of reaction $\Delta$ Abs <sub>340 nm</sub> min <sup>-1</sup>
0.4	20	0.5	250	132	0.031
0.4	20	1	250	132	0.030
0.8	20	0.5	250	132	0.052

### 3.3.7 SBT Prx 2 kinetics

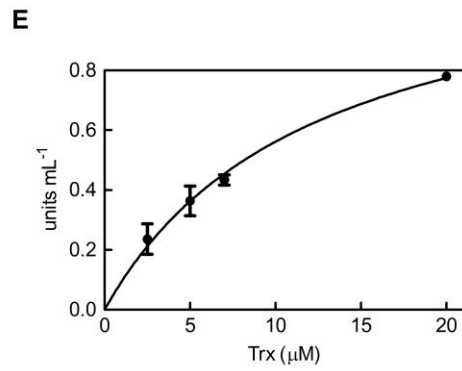
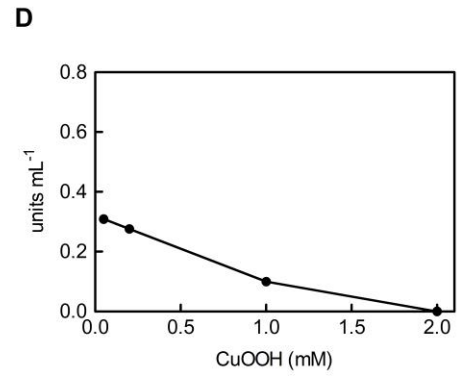
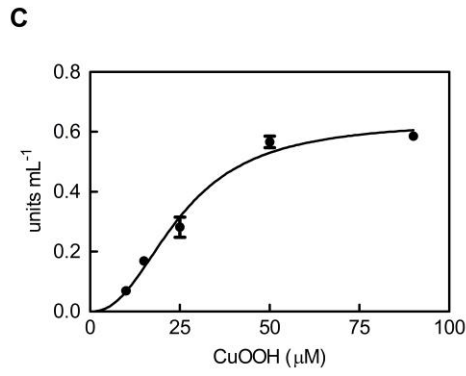
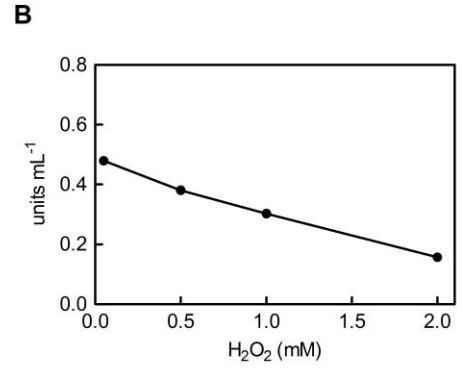
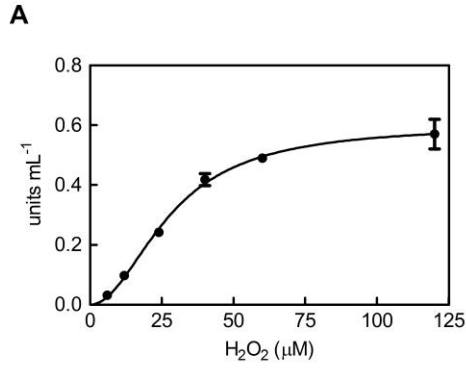
The recombinant SBT Prx 2 protein expressed in *E. coli* and purified by Ni-affinity chromatography was assayed for Prx enzyme activity by monitoring NADPH oxidation coupled to H<sub>2</sub>O<sub>2</sub> reduction in the presence of *E. coli* thioredoxin (Trx) and thioredoxin reductase (TrxR) (Fig. 3.7). At low H<sub>2</sub>O<sub>2</sub> concentrations ( $\leq 50 \mu\text{M}$ ), Prx-independent NADPH oxidation was negligible whereas at higher H<sub>2</sub>O<sub>2</sub> concentrations (0.5 – 2.0 mM) it became quite significant, presumably due to direct oxidation of NADPH by H<sub>2</sub>O<sub>2</sub>. Thus, for all kinetic analyses with H<sub>2</sub>O<sub>2</sub>, the Prx-independent rate was subtracted from the rate obtained with all assay components present.



**Fig. 3.7.** Effect of H<sub>2</sub>O<sub>2</sub> concentration on Trx-dependent peroxidase activity of Ni-affinity purified SBT Prx 2. The Prx assays were performed as outlined in Section 2.15. The H<sub>2</sub>O<sub>2</sub> substrate was added at time zero and SBT Prx 2 protein was added as indicated by the solid arrow. The SBT Prx 2 protein concentration in the assay was 0.4 μM.

The response of SBT Prx 2 enzyme activity to increasing  $\text{H}_2\text{O}_2$  concentration in the range 6 – 120  $\mu\text{M}$  was sigmoidal with a Hill coefficient of 2.0 indicating positive cooperativity and a  $S_{0.5}(\text{H}_2\text{O}_2)$  value of 29  $\mu\text{M}$  (Fig. 3.8A). In contrast, when the  $\text{H}_2\text{O}_2$  concentration was increased into the mM range (0.5 – 2.0 mM), there was a decrease in Prx enzyme activity with increasing  $\text{H}_2\text{O}_2$  concentration (Fig. 3.8B). The SBT Prx could also use cumene hydroperoxide (CuOOH) as a substrate (Fig. 3.8C). The response of SBT Prx activity to increasing CuOOH concentration in the  $\mu\text{M}$  range was also sigmoidal as it was for  $\text{H}_2\text{O}_2$  (Fig. 3.8C). The Hill coefficient for CuOOH was 2.3, again indicating positive cooperativity, and the  $S_{0.5}(\text{CuOOH})$  was 25  $\mu\text{M}$ , very similar to the value obtained for  $\text{H}_2\text{O}_2$ . When the CuOOH concentration was increased into the mM range (0.5 – 2.0 mM), there was a decrease in Prx enzyme activity with increasing CuOOH concentration (Fig. 3.8D). Thus, the peroxidase activity of the SBT Prx was progressively lost as both the  $\text{H}_2\text{O}_2$  and CuOOH concentrations were increased into the mM range. The  $V_{\text{max}}$  values obtained for  $\text{H}_2\text{O}_2$  and CuOOH were also very similar. Thus, overall, there was no marked preference for one substrate over the other. In contrast to the complex kinetics observed with the peroxide substrates, the kinetics observed with Trx were typical Michaelis-Menten giving a  $K_m(\text{Trx})$  of 12  $\mu\text{M}$  (Fig. 3.8E). Thus, the SBT Prx was shown to be a genuine Trx-dependent peroxidase.

**Fig. 3.8.** Effect of (A) low  $\text{H}_2\text{O}_2$  (6–120  $\mu\text{M}$ ), (B) high  $\text{H}_2\text{O}_2$  (0.05–2.0 mM), (C) low  $\text{CuOOH}$  (10–90  $\mu\text{M}$ ), (D) high  $\text{CuOOH}$  (0.05–2.0 mM) and (E) Trx concentration on Trx-dependent peroxidase activity of Ni-affinity purified SBT Prx 2. The Prx assays were performed as outlined in Section 2.15 except that either Trx or peroxide substrate concentration was varied. When Trx concentration was varied,  $\text{H}_2\text{O}_2$  was held constant at 120  $\mu\text{M}$ . When either of the peroxide substrates was varied, Trx was held constant at 20  $\mu\text{M}$ . The SBT Prx protein concentration in the assay was 10  $\mu\text{g mL}^{-1}$ .

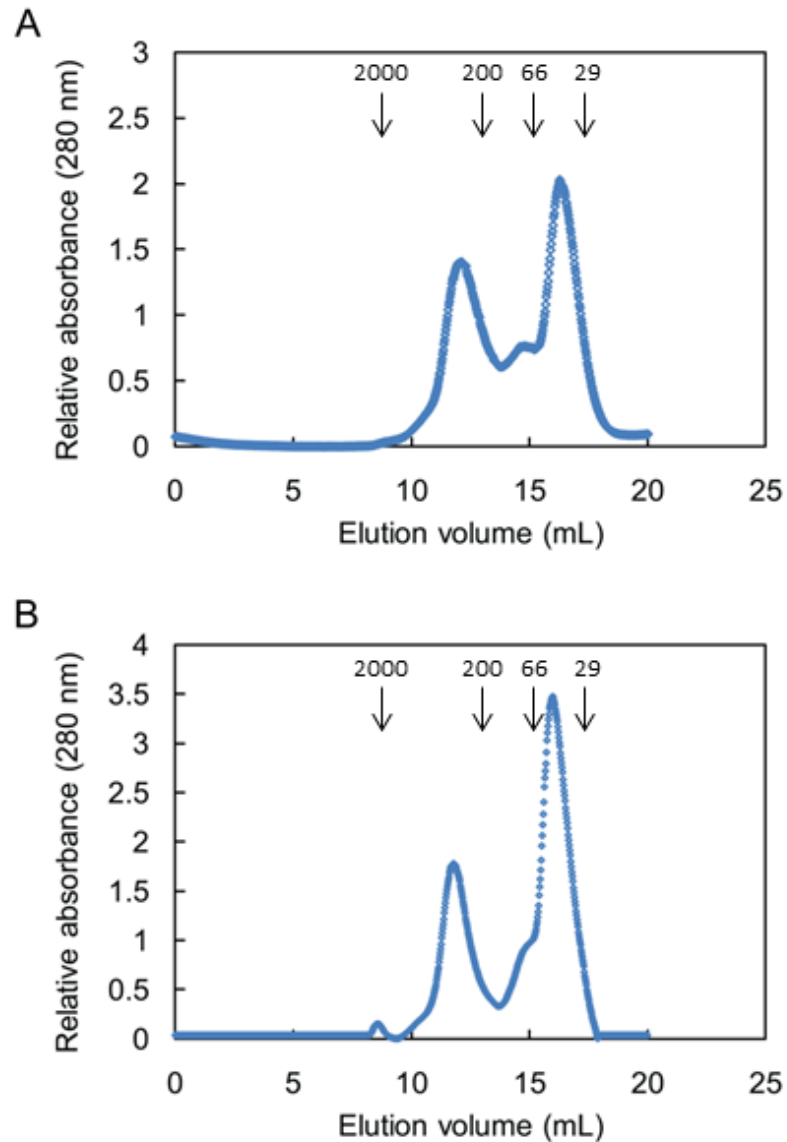




### 3.3.8 Gel filtration chromatography of SBT Prx 2 protein

#### 3.3.8.1 Native molecular mass of SBT Prx 2 protein under oxidised and reduced conditions

The native molecular mass of Ni-affinity purified SBT Prx 2 protein was investigated using gel filtration chromatography under reduced and oxidised conditions (Fig. 3.9). Under both reduced and oxidised conditions, the SBT Prx 2 protein was found to exist as 3 distinct oligomeric forms with approximate molecular masses that corresponded to decamer, tetramer and dimer. Regardless of the redox conditions the dimer was the most abundant oligomeric form. However, the proportion of dimer appeared to be slightly higher under oxidised conditions compared to under reduced conditions.

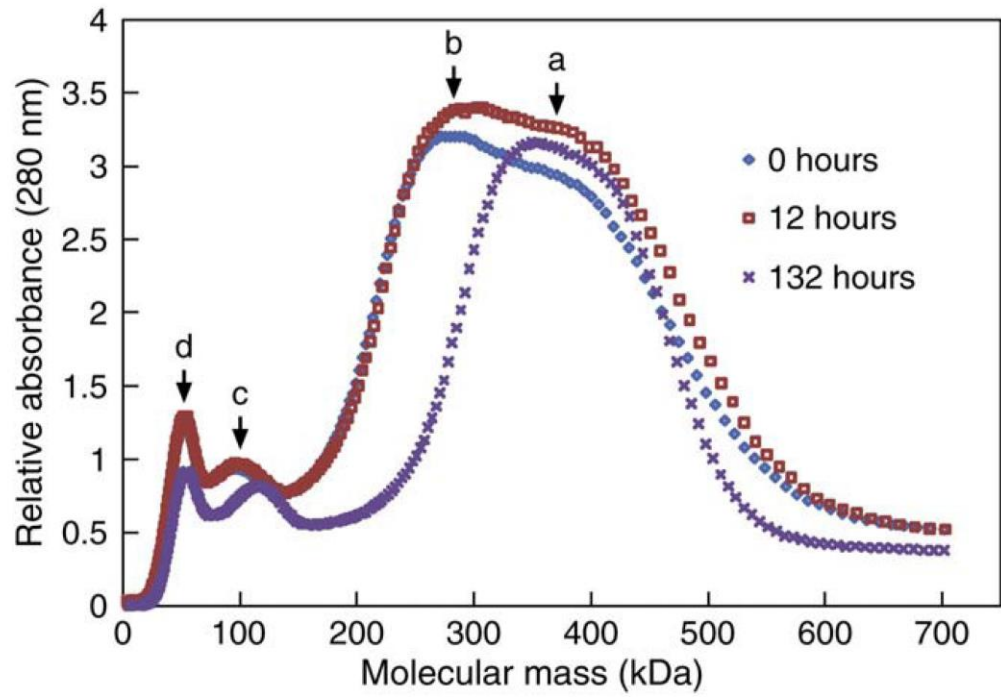
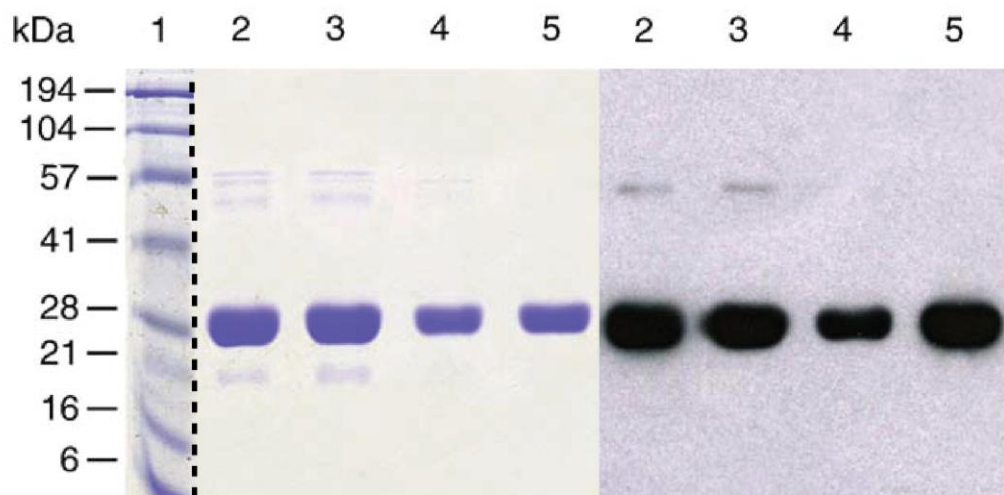


**Fig. 3.9.** Effect of reduced (A) and oxidised (B) conditions on the native molecular mass of Ni-affinity purified SBT Prx 2 protein. SBT Prx 2 protein was purified by Ni-affinity chromatography, concentrated and desalted into a buffer containing 20 mM Tris-base (pH 7.5), 150 mM NaCl and 5 mM DTT for reduced gel filtration analysis or the same buffer except that it lacked DTT for oxidised gel filtration analysis, giving a final protein concentration of 12 mg mL<sup>-1</sup>. The buffer exchanged protein (200  $\mu$ L) was loaded onto a gel filtration column that had been equilibrated with the same buffer. The arrows indicate the elution positions of the molecular mass standards (kDa).

### 3.3.8.2 Effect of storage on native molecular mass of SBT Prx 2 protein

The native molecular mass of SBT Prx 2 protein was determined by gel filtration chromatography immediately following Ni-affinity purification and also following 12 and 132 hours storage at 4°C (Fig. 3.10A). The storage buffer and the gel filtration column buffer were the same except that the storage buffer contained 5 mM DTT whereas the column buffer lacked DTT. Immediately following Ni-affinity purification, the SBT Prx protein appeared at sizes roughly corresponding to dimer (peak d), tetramer (peak c), decamer (peak b) and a higher order aggregate (peak a). The decameric form appeared to be more abundant than the dimeric form. The tetrameric form gave only a minor peak. Storing the Ni-affinity purified SBT Prx protein at 4°C for up to 132 h resulted in a progressive shift of the decameric form to the higher order aggregate. The composition of each gel filtration peak was analysed by SDS-PAGE (Fig. 3.10B) and the identity of the protein was confirmed by immunoblotting (Fig. 3.10C).

**Fig. 3.10.** Effect of storage on the native molecular mass of Ni-affinity purified SBT Prx 2 protein. SBT Prx 2 was purified by Ni-affinity chromatography, concentrated and desalted into a buffer containing 20 mM Tris-base (pH 7.5), 150 mM NaCl and 5 mM DTT, giving a final protein concentration of 30 mg mL<sup>-1</sup>. The concentrated SBT Prx 2 protein was stored at 4 °C for 0, 12 and 132 h. At each of these time-points, 200 µL containing 6 mg protein was loaded onto a gel filtration column equilibrated with the same buffer except that it lacked DTT (A). The content of the gel filtration peaks was analysed by reducing SDS-PAGE (B) and immunoblotting (C). The immunoblotting analysis was performed with rabbit anti-6X His polyclonal antibodies (Rockland). Lane 1, molecular mass markers; lane 2, gel filtration peak a; lane 3, gel filtration peak b; lane 4, gel filtration peak c; lane 5, gel filtration peak d.

**A****B****C**

### 3.3.9 SBT Prx 2 Cys mutant cloning, expression, purification and characterisation

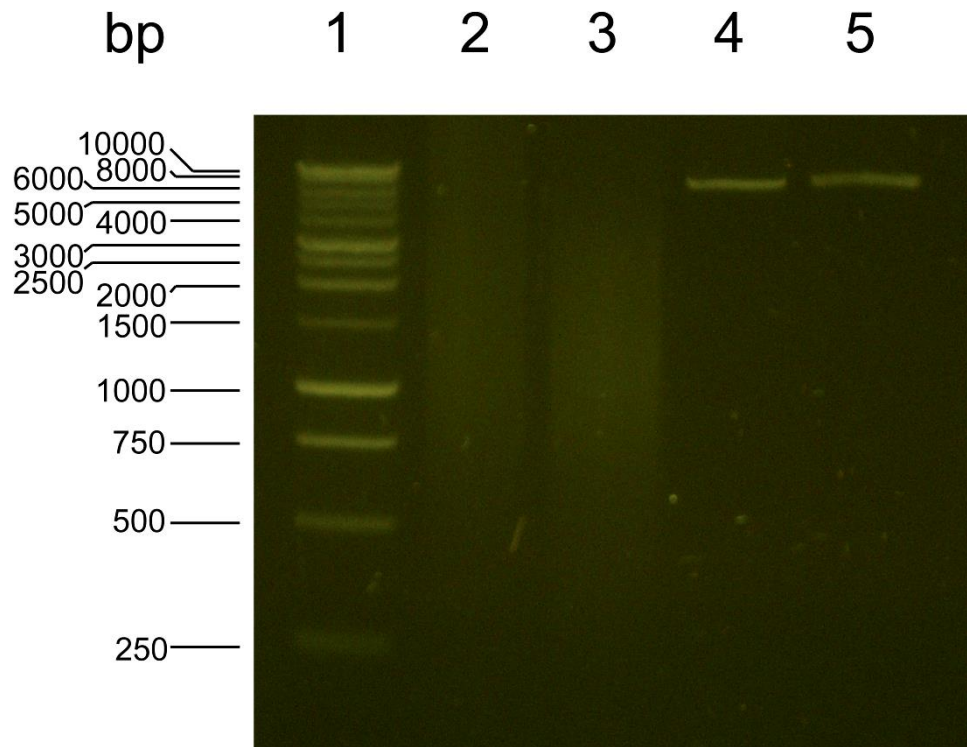
Amino acid sequence alignments between the SBT Prx 2 protein and other members of the 2-Cys Prx protein family from fish and mammals (Fig.3.1) revealed that in addition to the highly conserved peroxidatic and resolving Cys residues some fish species, including SBT, have a unique Cys residue at position 75. The influence of the peroxidatic Cys (Cys<sup>51</sup>) and the unique non-catalytic Cys (Cys<sup>75</sup>) residues on the oligomeric properties of the SBT Prx 2 protein were investigated using site directed mutagenesis (SDM). SDM PCR primers were designed to mutate the Cys<sup>51</sup> and Cys<sup>75</sup> residues of the SBT Prx 2 protein to Ser residues (referred to as C51S and C75S, respectively) and are outlined in Fig. 3.11.

C51S primer pair	C75S primer pair
SEQUENCE:	SEQUENCE:
5'- CACGTTTGTGTCCCCCACTGAG -3'	5'- GGTTATTGGCTCCTCCATCGACTCTC -3'
COMPLEMENT:	COMPLEMENT:
5'- CTCAGTGGGGGACACAAACGTG -3'	5'- GAGAGTCGATGGAGGAGCCAATAACC -3'
LENGTH: 22	LENGTH: 26
GC CONTENT: 59.1 %	GC CONTENT: 53.8 %
MELT TEMP: 60.3 °C	MELT TEMP: 60.4 °C
MOLECULAR WEIGHT: 6662.4 g/mole	MOLECULAR WEIGHT: 7864.1 g/mole
EXTINCTION COEFFICIENT: 197200 L/(mole·cm)	EXTINCTION COEFFICIENT: 229300 L/(mole·cm)
nmole/OD <sub>260</sub> : 5.07	nmole/OD <sub>260</sub> : 4.36
µg/OD <sub>260</sub> : 33.78	µg/OD <sub>260</sub> : 34.30

**Fig. 3.11.** Characteristics of the SDM PCR primers designed to mutate the Cys<sup>51</sup> and Cys<sup>75</sup> residues of the SBT Prx 2 protein to Ser residues. Analysis of the primer pairs was performed using the IDT<sup>®</sup> SciTools OligoAnalyzer 3.1.

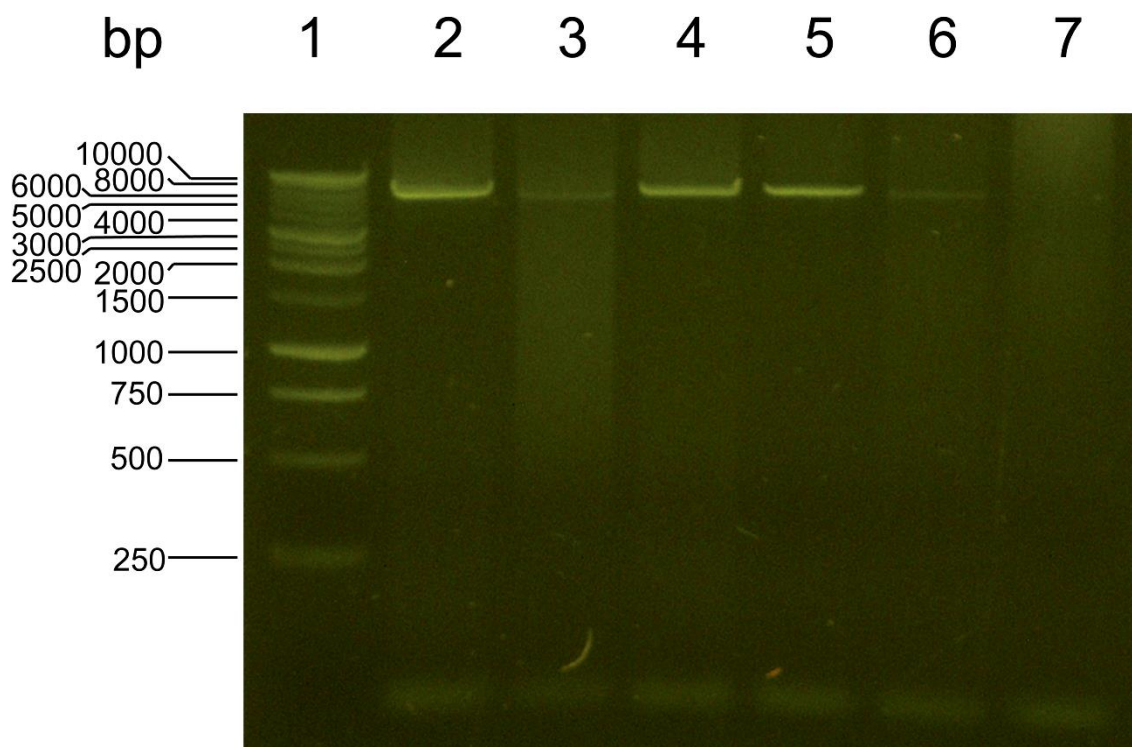
Following amplification of the pET-30a-SBT-Prx 2 construct using the C51S and C75S SDM primers, the PCR products were visualised using agarose gel electrophoresis before and after *DpnI* restriction enzyme digestion (Fig. 3.12). Before *DpnI* restriction enzyme digestion, the C75S SDM PCR reaction produced a product of 6 kb which is consistent with the expected size of the pET-30a-SBT-Prx 2 construct. The C75S SDM PCR product was retained following *DpnI* digestion indicating that it was composed of unmethylated, *in vitro* synthesised DNA and not the original, methylated construct template DNA. In contrast, the C51S SDM PCR did not produce a distinct product but rather a smear. This suggested non-specific binding of the C51S primers to the pET-30a-SBT-Prx 2 template which might be attributed to the annealing temperature being too low.





**Fig. 3.12.** Agarose gel electrophoresis of C51S and C75S SDM PCR products, amplified from purified pET-30a-SBT Prx 2 construct, before and after *DpnI* restriction enzyme digestion. Lane 1, DNA size standards; Lane 2, C51S PCR products prior to *DpnI* digestion; Lane 3, C51S PCR products after *DpnI* digestion; Lane 4, C75S PCR products prior to *DpnI* digestion; Lane 5, C75S PCR products after *DpnI* digestion.

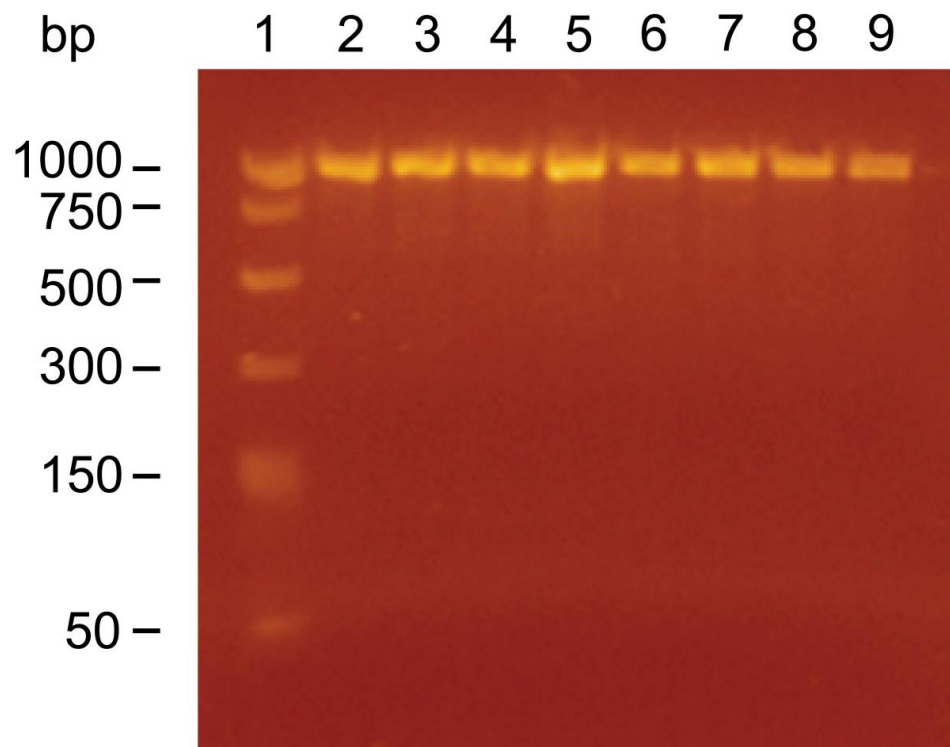
To investigate the effect of higher annealing temperatures on the C51S SDM primers' ability to amplify the pET-30a-SBT-Prx 2 construct, a gradient PCR was performed with temperatures of between 60°C and 69.8°C in varying increments ranging from 1.5 °C to 3°C (Fig. 3.13). Annealing temperature was shown to have a significant effect on the C51S SDM primers' ability to amplify the pET-30a-SBT Prx 2 construct. An annealing temperature of ~65.5°C was found to be optimal because it produced a distinct product at the expected size of the pET-30a-SBT Prx 2 construct and minimal non-specific amplification. The optimal annealing temperature of ~65.5°C was significantly higher than the original annealing temperature of 60°C that was trialled in Fig. 3.12.



**Fig. 3.13.** Effect of higher annealing temperatures on the PCR amplification of pET-30a-SBT Prx 2 plasmid construct using C51S SDM primers. The C51S SDM PCR products were analysed by agarose gel electrophoresis according to Section 2.6. Lane 1, DNA size standards; Lane 2, 60°C; Lane 3, 60.9°C; Lane 4, 62.9°C; Lane 5, 65.5°C; Lane 6, 68.4°C; Lane 7, 69.8°C.

The C51S and C75S pET-30a-SBT Prx 2 constructs digested with *DpnI* restriction enzyme were used to transform *E. coli* DH5 $\alpha$  cells. Purified plasmid DNA was prepared from 4 colonies of *E. coli* cells containing the C51S pET-30a-SBT Prx 2 construct and 5 colonies of *E. coli* cells containing the C75S pET-30a-SBT Prx 2 construct. Alignment of the forward and reverse sequencing results for each colony with the SBT Prx 2 ORF revealed that the C51S and C75S pET-30a-SBT Prx 2 insert sequences contained a single base substitution of a guanine to a cytosine at position 153 and 225, respectively. The single base substitution changed the corresponding codons from TGC to TCC and therefore, the amino acids at positions 51 and 75 from the N-terminus were changed from Cys to Ser. Therefore, both the C51S and C75S mutations had been successfully introduced into the pET-30a-SBT Prx 2 insert sequence. No additional substitutions, deletions or additions were detected in the insert sequences of any of the constructs sequenced.

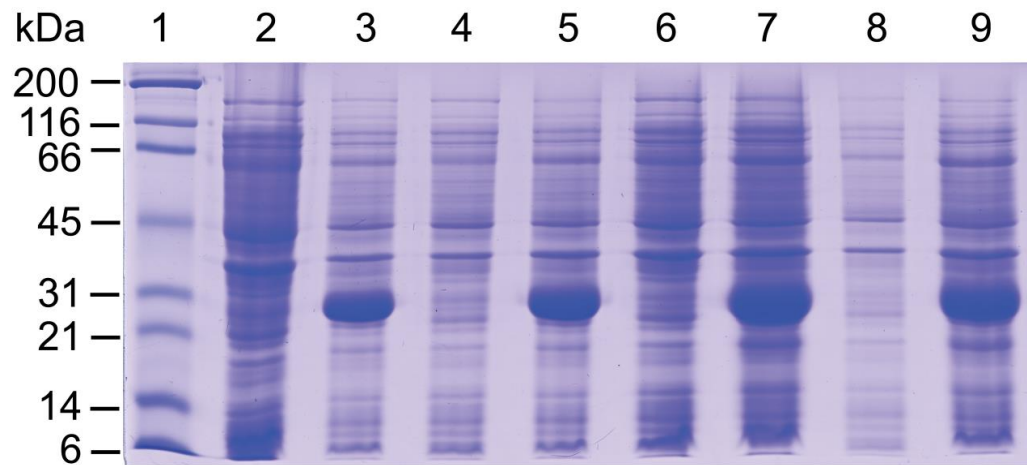
In order to produce C51S and C75S SBT Prx 2 proteins, the corresponding constructs were used to transform the *E. coli* BL21 (DE3) expression host. The transformants were screened for the mutated pET-30-SBT Prx 2 construct by PCR. Agarose gel electrophoresis of the PCR products revealed the presence of a single band of approximately 1000 bp. The expected size of the amplicon was 964 bp, consisting of the SBT Prx 2 ORF and flanking regions of the pET-30a multiple cloning region contained between the T7 promoter and terminator primer binding sites. Thus, the C51S and C75S pET-30a-SBT Prx 2 constructs were successfully introduced into the *E. coli* BL21 (DE3) expression host.



**Fig. 3.14.** Agarose gel electrophoresis of PCR products obtained by PCR screening of *E. coli* BL21 (DE3) cells that had been transformed with the C51S and C75S pET-30a-SBT Prx 2 constructs. The PCR screening was performed as outlined in Section 2.10. Lane 1, DNA size standards; Lane 2, C51S colony 1; Lane 3, C51S colony 2; Lane 4, C51S colony 3; Lane 5, C51S colony 4; Lane 6, C75S colony 1; Lane 7, C75S colony 2; Lane 8, C75S colony 3; Lane 9, C75S colony 4.

Large scale protein expression was performed with *E. coli* BL21 (DE3) cells containing the C51S and C75S pET-30a-SBT Prx 2 constructs as per Section 2.11, to produce recombinant protein for subsequent purification and characterisation. The level of recombinant C51S and C75S protein expression before and after induction was investigated by analysing whole cell protein extracts using SDS-PAGE (Fig. 3.15).

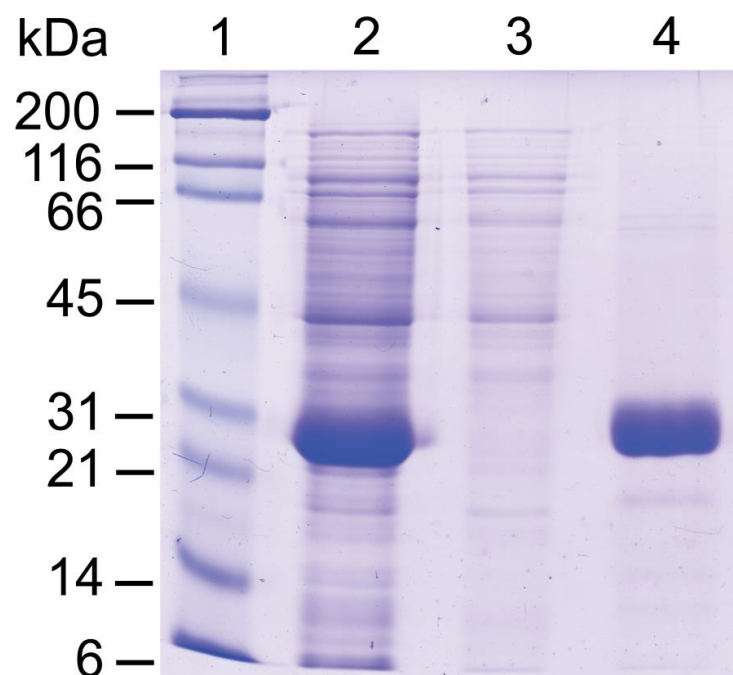
SDS-PAGE analysis of whole cell protein extracts prepared from induced *E. coli* BL21 (DE3) cells containing the C51S and C75S pET-30a-SBT Prx 2 constructs produced prominent bands with an approximate molecular mass of 27 kDa. The size of these prominent protein bands is consistent with the expected size of recombinant SBT Prx 2 monomer. No prominent protein bands were observed in any of the whole cell protein extracts produced from un-induced cells. Therefore, the C51S and C75S SBT Prx 2 proteins were able to be expressed in *E. coli* with high abundance.



**Fig. 3.15.** Reducing SDS-PAGE analysis of whole cell protein extracts prepared from un-induced and 3 h induced *E. coli* BL21 (DE3) cells that contained the C51S and C75S pET-30a-SBT Prx 2 constructs. Lane 1, molecular mass markers; Lane 2, un-induced C51S colony 1; Lane 3, 3 h induced C51S colony 1; Lane 4, un-induced C51S colony 2; Lane 5, 3 h induced C51S colony 2; Lane 6, un-induced C75S colony 1; Lane 7, 3 h induced C75S colony 1; Lane 8, un-induced C75S colony 2; Lane 9, 3 h induced C75S colony 2.

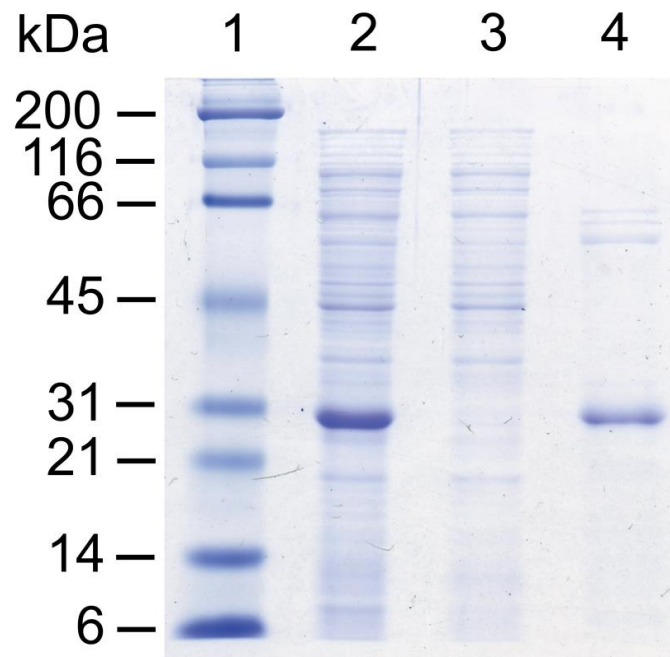
The recombinantly expressed C51S SBT Prx 2 protein was purified by Ni-affinity column chromatography and various fractions were analysed by SDS-PAGE (Fig. 3.16). A single prominent band of the expected size of recombinant C51S SBT Prx 2 protein was present in the Ni-affinity purification 500 mM imidazole wash but was absent from the combined flow-through and 20 mM imidazole wash. Therefore, the C51S SBT Prx 2 protein was able to be purified with high abundance by Ni-affinity chromatography.





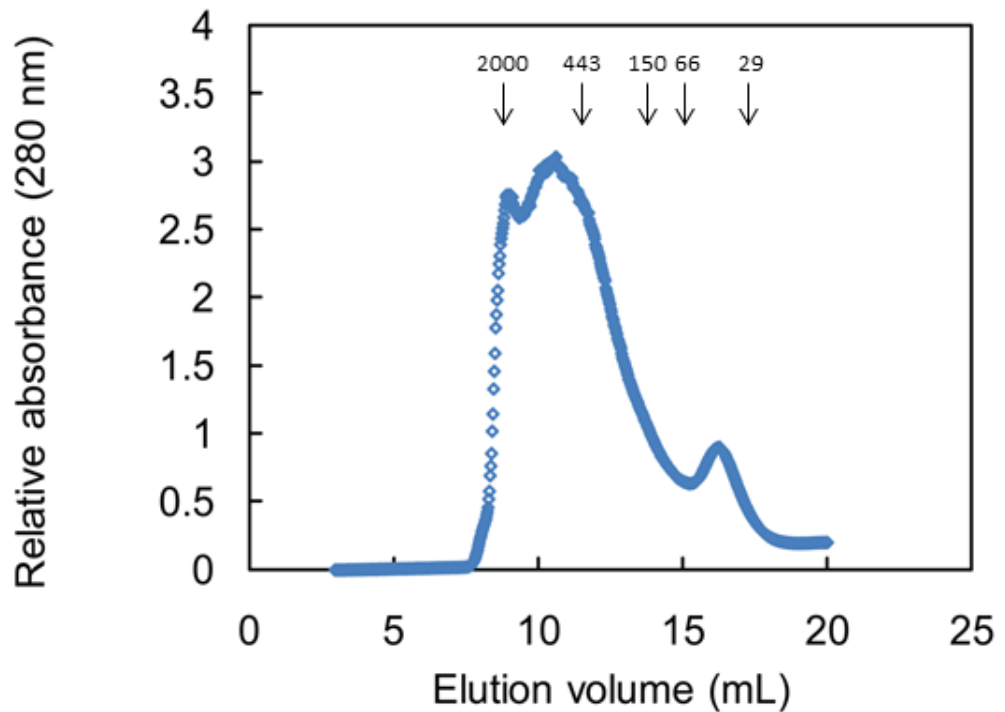
**Fig. 3.16.** Reducing SDS-PAGE analysis of various fractions produced from Ni-affinity purification of recombinant C51S SBT Prx 2 protein. Lane 1, molecular mass markers; Lane 2, whole cell protein extract prepared from 3 h induced *E. coli* BL21 (DE3) cells that contained the C51S pET-30a-SBT Prx 2 construct; Lane 3, Ni-affinity purification, combined flow through and 20 mM imidazole wash; Lane 4, Ni-affinity purification, 500 mM imidazole wash.

The recombinantly expressed C75S SBT Prx 2 protein was purified by Ni-affinity chromatography (Fig. 3.17). However, despite the high level of C75S SBT Prx 2 expression the yield of protein obtained in the 500 mM imidazole wash was significantly less than expected. This expectation was based on the high yield of Ni-affinity purified C51S SBT Prx 2 protein that was obtained from a level of protein expression similar to that obtained for the C75S SBT Prx 2 protein. The C75S SBT Prx 2 protein was not present to any significant extent in either the Ni-column flow-through or 20 mM imidazole wash. As a result, the low yield of Ni-affinity purified C75S SBT Prx 2 protein was not due to loss of unbound protein in the flow-through or premature elution of the protein in the 20 mM imidazole wash. Although the yield of C75S SBT Prx 2 protein in the 500 mM imidazole wash was low, the protein was enriched by the Ni-affinity purification.



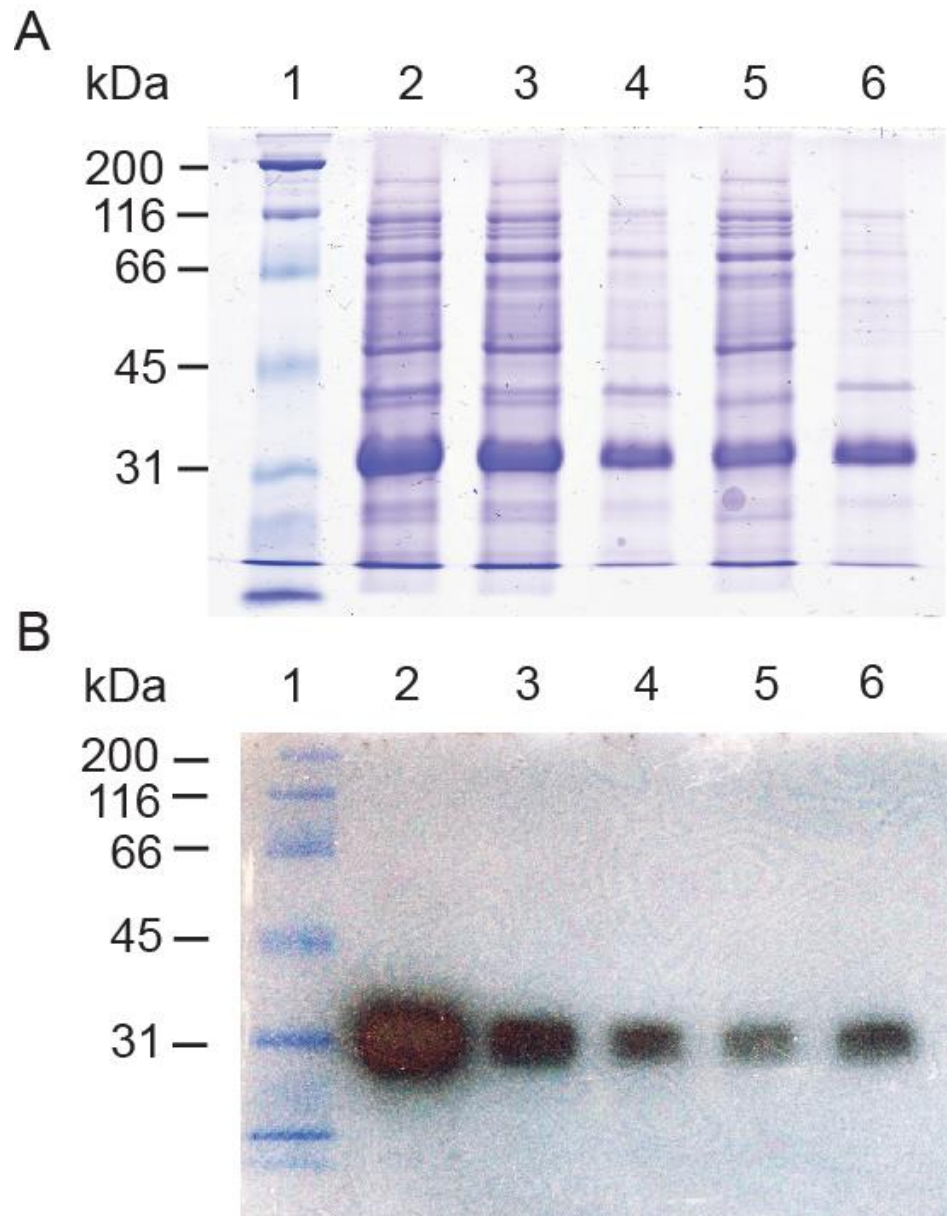
**Fig. 3.17.** Reducing SDS-PAGE analysis of various fractions produced from Ni-affinity chromatography purification of recombinant C75S SBT Prx 2 protein. Lane 1, molecular mass markers; Lane 2, whole cell protein extract prepared from 3 h induced *E. coli* BL21 (DE3) cells that contained the C75S pET-30a-SBT Prx 2 construct; Lane 3, Ni-affinity purification, combined flow through and 20 mM imidazole wash; Lane 4, Ni-affinity purification, 500 mM imidazole wash.

To further investigate the cause of the low yield of Ni-affinity purified C75S SBT Prx 2 protein and to determine its native molecular mass, gel filtration chromatography was performed (Fig. 3.18). Gel filtration chromatography analysis of the C75S SBT Prx 2 protein revealed that under reducing conditions it existed predominantly as large aggregates. The molecular mass of the aggregates ranged from approximately 250 kDa, all the way through to protein being eluted in the void volume with an approximate molecular mass of 2,000 kDa. Therefore, the C75S mutation in the SBT Prx 2 protein appeared to promote the formation of both insoluble and soluble protein aggregates.



**Fig. 3.18.** Gel filtration chromatography analysis of the native molecular mass of Ni-affinity chromatography purified C75S SBT Prx 2 protein. The C75S SBT Prx 2 protein was purified by Ni-affinity chromatography, concentrated and desalted into a buffer containing 20 mM Tris-base (pH 7.5), 150 mM NaCl and 5 mM DTT, giving a final protein concentration of  $12 \text{ mg mL}^{-1}$ . The buffer exchanged protein ( $200 \text{ }\mu\text{L}$ ) was loaded onto a gel filtration column that had been equilibrated with the same buffer. The arrows indicate the elution positions of the molecular mass standards (kDa).

To investigate the nature of the C75S protein aggregates, differential centrifugation was performed on whole cell protein extract produced from *E. coli* BL21 (DE3) cells expressing the C75S SBT Prx 2 protein. The differential centrifugation supernatant and pellet fractions were analysed by SDS-PAGE and immunoblotting (Fig. 3.19). The C75S SBT Prx 2 protein was found to be equally distributed in the 12,000 g and 100,000 g centrifugation supernatants and pellets. The presence of C75S SBT Prx 2 in the 12,000 g centrifugation pellet indicated that a proportion of the expressed protein was insoluble aggregate while the presence of C75S SBT Prx 2 in the 12,000 g centrifugation supernatant indicated that a proportion of the expressed protein was soluble. These results are consistent with those of the gel filtration chromatography analysis (Fig. 3.18). The soluble portion of C75S SBT Prx 2 protein isolated by the 12,000 g centrifugation was subsequently detected in both the supernatant and pellet produced by the 100,000 g centrifugation. The presence of C75S SBT Prx 2 in the 100,000 g centrifugation pellet was most likely the result of the formation of insoluble protein aggregates during the centrifugation or due to the protein being associated with membranes. The results of the differential centrifugation and gel filtration chromatography analyses suggested that the recombinant C75S SBT Prx 2 was expressed as a mixture of insoluble and soluble protein that had a propensity to form large aggregates or associate with cell membranes.



**Fig. 3.19.** Reducing SDS-PAGE (A) and immunoblotting (B) analysis of fractions produced from the differential centrifugation of whole cell protein extracts produced from *E. coli* BL21 (DE3) cells expressing the C75S SBT Prx 2 protein. The differential centrifugation fractions were produced from an equal number of cells as outlined in Section 2.17. The immunoblotting analysis was performed with rabbit anti-6X His polyclonal antibodies (Rockland). Lane 1, molecular mass markers; Lane 2, whole protein extract; Lane 3, 12,000 g, 4°C and 15 min supernatant; Lane 4, 12,000 g, 4°C and 15 min pellet; Lane 5, 100,000 g, 4°C and 1 hr supernatant; Lane 6, 100,000 g, 4°C and 1 hr pellet.

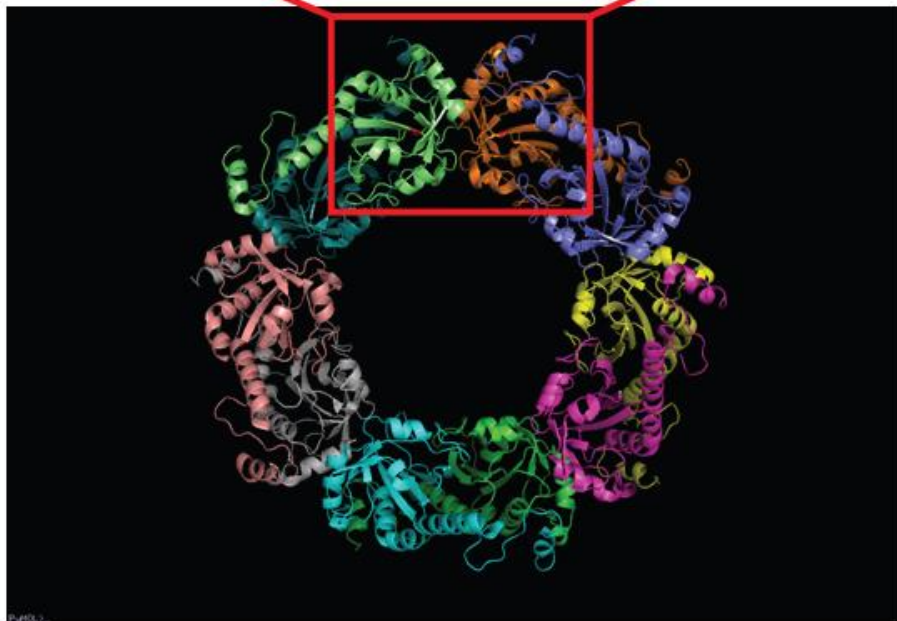
Some insight into the structural changes that could have been induced by the C75S mutation in the SBT Prx 2 protein was gained from analysis of the crystal structure of Rat Prx 1 (RCSB Protein Data Bank (PDB) accession no. 2Z9S). The Rat Prx 1 protein was selected as a putative model for the SBT Prx 2 protein based on the fact that they share 81% amino acid identity. Based on the multiple sequence alignment of these proteins (Fig. 3.1), the A<sup>76</sup> residue from the Rat Prx 1 is equivalent in terms of position to the C<sup>75</sup> residue from the SBT Prx 2. The position of the A<sup>76</sup> residue in the Rat Prx 1 crystal structure was investigated using pyMOL™ (DeLano Scientific) (Fig. 3.20). Analysis of the Rat Prx 1 crystal structure revealed that the A<sup>76</sup> residues of each monomer are positioned in a  $\beta$ -sheet, just beneath the dimer-dimer interface. Rendering of the crystal structure model to view the solvent accessible surface showed that the A<sup>76</sup> residues were buried within each monomer. Therefore, it would appear that the C75S mutation in the SBT Prx 2 protein may have had an effect on both the dimer-dimer interface and the internal organisation of the monomer protein core.



A

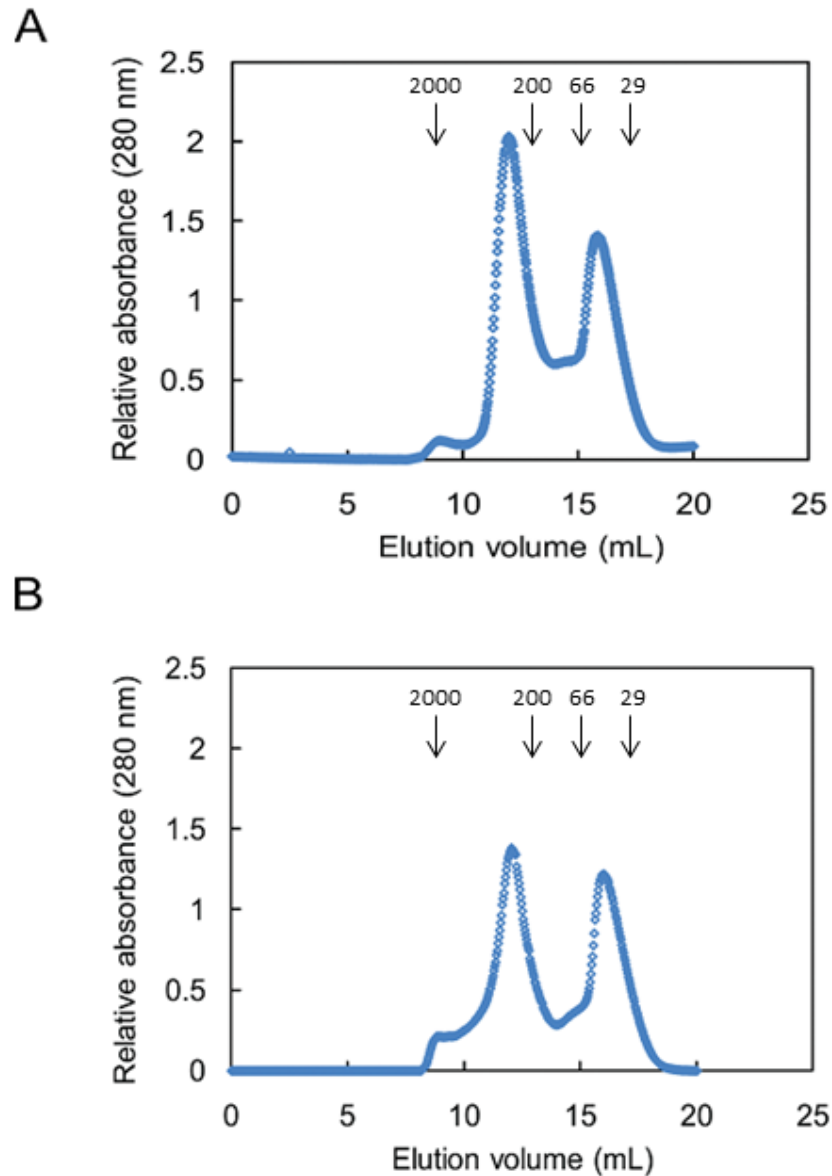


B



**Fig. 3.20.** A schematic model of the C52S Rat Prx 1 (PDB acc., 2Z9S) dimer-dimer interface (A) and overall decamer (B) displayed using pyMOL™ (DeLano Scientific). Each monomer chain is shown in a different colour and the A<sup>76</sup> residues of chains 1 (Green) and 2 (orange) are highlighted in red.

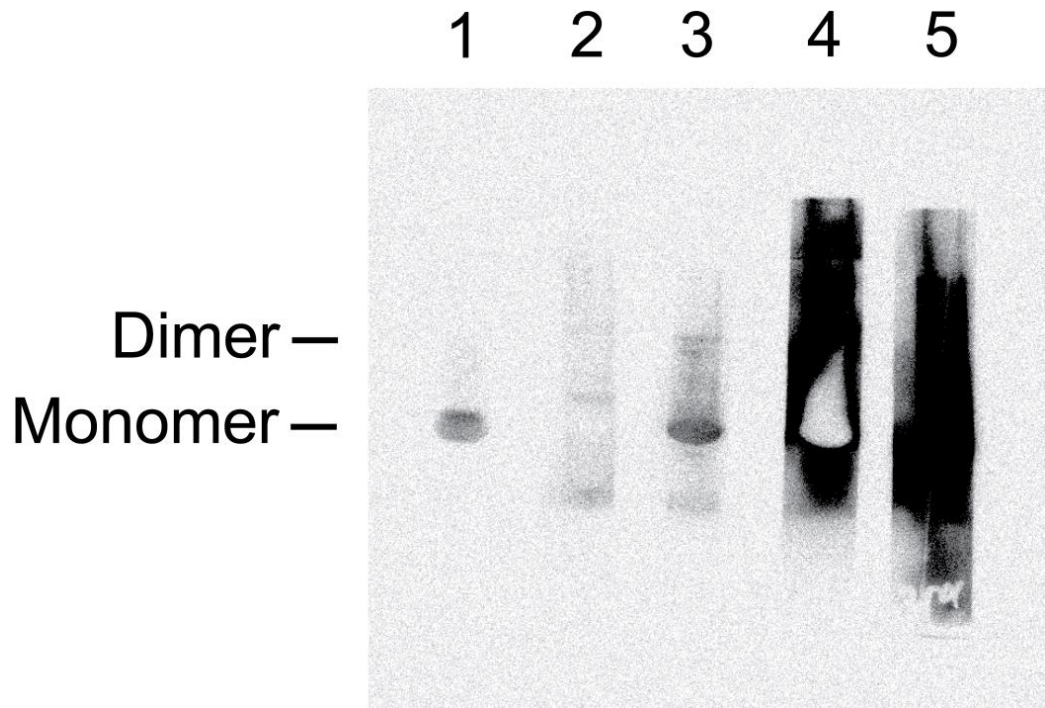
The native molecular mass of Ni-affinity purified C51S SBT Prx 2 protein was investigated using gel filtration chromatography (Fig. 3.21). Under reduced and oxidised conditions the C51S SBT Prx 2 protein was found to exist as two distinct oligomeric forms with molecular masses that corresponded to dimer and decamer. Under reduced conditions the C51S SBT Prx 2 protein appeared to preferentially form decamer while under oxidised conditions this preference was reduced with the decamer and dimer forms being present in almost equal proportions. Therefore, the redox state of the C51S SBT Prx 2 did not appear to have a significant effect on the oligomeric properties of the protein.



**Fig. 3.21.** Effect of reduced (A) and oxidised (B) conditions on the native molecular mass of Ni-affinity purified C51S SBT Prx 2 protein. C51S SBT Prx 2 protein was purified by Ni-affinity chromatography, concentrated and desalted into a buffer containing 20 mM Tris-base (pH 7.5), 150 mM NaCl and 5 mM DTT for reduced gel filtration analysis or the same buffer except that it lacked DTT for oxidised gel filtration analysis, giving a final protein concentration of  $12 \text{ mg mL}^{-1}$ . The buffer exchanged protein ( $200 \text{ }\mu\text{L}$ ) was loaded onto a gel filtration column that had been equilibrated with the same buffer. The arrows indicate the elution positions of the molecular mass standards (kDa).

### 3.3.10 SBT Prx 2 antibody preparation and evaluation

Polyclonal antibodies against Ni-affinity purified SBT Prx 2 protein were raised in rabbit. The SBT Prx 2 antibody titre of the rabbit serum was assessed before the first immunisation and fortnightly following the first three immunisations using immunoblotting (Fig. 3.22). Pre-immune serum did not detect any specific proteins to any significant extent in whole cell protein extract produced from *E. coli* BL21 (DE3) expressing recombinant SBT Prx 2 protein. This suggested that there was limited cross reactivity between the pre-immune rabbit serum and the SBT Prx 2 protein and any *E. coli* BL21 (DE3) proteins. The rabbit serum collected following the first immunisation detected a protein with a molecular mass corresponding to SBT Prx 2 monomer. This indicated that immunisation of the rabbit with Ni-affinity purified SBT Prx 2 protein had triggered an immune response and subsequent production of antibodies. The sensitivity of the antibodies obtained following the first immunisation was comparable to that of the anti-His antibodies that were used as a positive control. Following the second immunisation, the antibody titre increased dramatically with the rabbit serum samples taken following the second and third immunisations producing very strong signals.

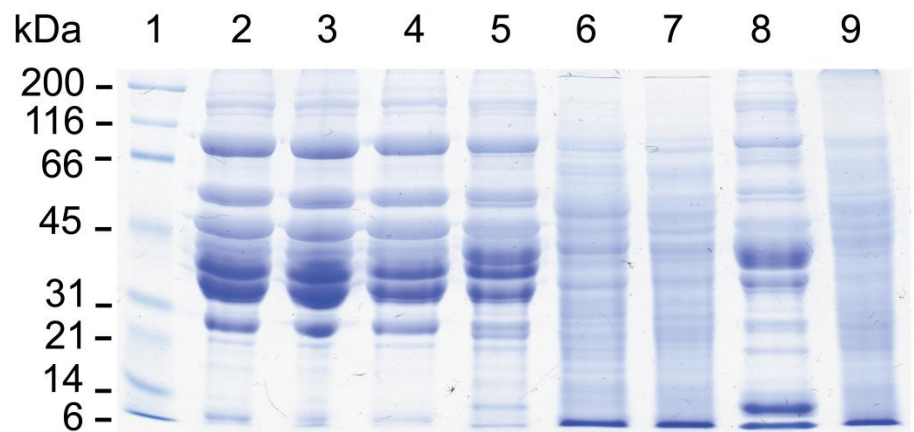


**Fig. 3.22.** Analysis of SBT Prx 2 antibody titre in rabbit serum using immunoblotting. Whole cell protein extracts prepared from *E. coli* BL21 (DE3) expressing recombinant SBT Prx 2 protein were probed with rabbit serum taken before and after fortnightly immunisations with Ni-affinity purified SBT Prx 2 protein. Lane 1, anti-His antibodies; Lane 2, pre-immune rabbit serum; Lane 3, post-1<sup>st</sup> immunisation rabbit serum; Lane 4, post-2<sup>nd</sup> immunisation rabbit serum; Lane 5, post-3<sup>rd</sup> immunisation rabbit serum.

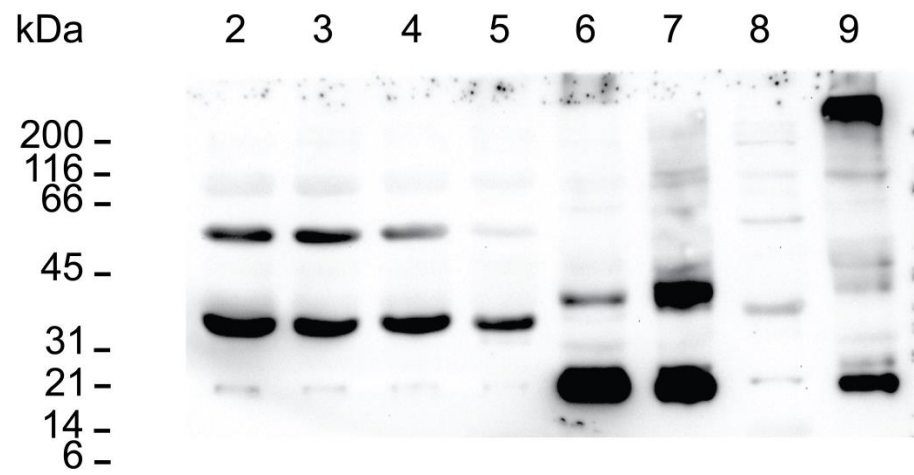
The ability of the anti-SBT Prx 2 antibodies to detect Prx protein in extracts from a variety of fish species and tissues was investigated (Fig. 3.23). SDS-PAGE analysis of fish tissue extracts revealed that proteins were able to be recovered with high abundance. The protein banding patterns obtained for liver and muscle tissue extracts were distinctly different but each type of tissue extract displayed a similar protein banding pattern for all of the fish species analysed. The anti-SBT Prx 2 antibodies detected several protein bands in both muscle and liver tissue protein extracts from all of the fish investigated. Like the SDS-PAGE results, the pattern of detected proteins appeared to be related more strongly to the tissue type rather than the origin of the fish tissue protein extract. Having said this, the barramundi liver tissue protein extract banding pattern appeared to be different to that obtained for SBT and YTK. The prominent protein bands detected in muscle tissue protein extracts were estimated to have molecular masses corresponding to monomer, dimer, tetramer and pentamer configurations of typical 2-Cys Prxs. In the YTK and SBT liver tissue protein extracts prominent bands with approximate molecular masses of 22 and 45 kDa were detected. The sizes of these bands are consistent with the expected sizes of monomer and dimer of 2-Cys Prx proteins. However, both of these proteins were slightly larger than those observed in the muscle tissue extracts. The banding pattern detected in the barramundi liver tissue extract contained two prominent protein bands corresponding to 2-Cys Prx monomer and decamer. The differences in banding pattern detected between liver and muscle tissue protein extracts suggests that in addition to the anti-SBT Prx 2 antibodies being able to detect Prx in different fish species, they may also be able to detect different Prx isoforms. The cross reactivity of the anti-SBT Prx 2 antibodies with Prx from different fish species and possibly multiple Prx isoforms is not surprising given the high degree of protein sequence similarity between Prx proteins from different fish species and different Prx isoforms.

**Fig. 3.23.** Reducing SDS-PAGE (A) and immunoblotting (B) analysis of muscle and liver tissue protein extracts from a variety of fish species. The proteins from fish tissue that had been stored at -70°C were extracted into a buffer containing 50 mM HEPES (pH 7.5), 150 mM NaCl, 10 mM DTT, 1 mM phenylmethanesulfonyl fluoride (PMSF) and 1 mM EDTA using a Polytron® homogeniser (Kinematica, Switzerland). Two SDS-PAGE gels were loaded with 220 µg of each fish tissue protein extract per well. One SDS-PAGE gel was stained with Coomassie blue whilst the other was used for immunoblotting. The immunoblotting was performed with anti-SBT Prx 2 antibodies followed by horseradish peroxidase antibody conjugate. The chemiluminescent signal was captured using a BioRad® VersaDoc™ Model 4000 imaging system. Lane 1, molecular mass markers; Lane 2, SBT Akami muscle tissue; Lane 3, SBT Chutoro muscle tissue; Lane 4, SBT O-toro muscle tissue; Lane 5, YTK muscle tissue; Lane 6, YTK liver tissue; Lane 7, SBT liver tissue; Lane 8, Barramundi muscle tissue; Lane 9, Barramundi liver tissue.

A



B





### 3.3.11 Crystallisation of SBT Prx 2 protein

#### 3.3.11.1 Identification of crystallisation conditions

Crystallisation conditions for the SBT Prx 2 protein were screened for using the Qiagen<sup>®</sup> NeXtal<sup>®</sup> Classic and PEG suites in small scale crystallisation trials. After 3 days incubation, the PEG suite crystallisation trial plates set up with SBT Prx 2 protein immediately following Ni-affinity purification and after 5 days storage at 4°C did not contain any observable crystallisation phenomena while both of the Classic suite crystallisation plates contained a single crystallisation drop that produced small crystalline objects. The most promising solution for protein crystallisation contained 0.1 M HEPES (pH 7.5) and 70% (v/v) ( $\pm$ )-2-Methyl-2,4-pentanediol (MPD). The crystals obtained had a plate-like morphology with maximum dimensions of approximately 5 x 10  $\mu$ m.

#### 3.3.11.2 Up-scaling and optimisation of crystallisation conditions

A grid screen was developed around the most promising crystallisation solution identified in Section 3.3.11.1 and was used to set up large scale crystallisation trials with SBT Prx 2 protein immediately following Ni-affinity purification and with SBT Prx 2 protein that had been stored at 4°C for 10 days. Immediately following addition of SBT Prx 2 protein to each of the crystallisation solutions a precipitate formed. The crystallisation drops were monitored over the following 4 weeks, however, no crystals were observed for any crystallisation condition. Therefore, the promising small scale crystallisation conditions identified in Section 3.3.11.1 were not able to be directly up-scaled into a large scale format and the length of storage of SBT Prx 2 protein following Ni-affinity purification had no effect on crystallisation outcome.

### 3.3.11.3 Effect of varying the ratio of protein solution volume to crystallisation solution volume on large scale crystallisation outcome

In an attempt to upscale the crystallisation drop size whilst preventing the formation of precipitates, a large scale crystallisation trial was set up where the ratio of the volume of Ni-affinity purified protein solution to volume of crystallisation solution was varied (refer to Section 3.2.10.3). In addition to manipulating the crystallisation drop conditions the effect of incubation temperature was also investigated by setting up three replicate plates and incubating them at 4, 22 and 37°C. Five days post-setup, the crystallisation drops were inspected. The plate incubated at 4°C had precipitate in all of the crystallisation drops, however, less precipitate was observed in the conditions which had low ratios of volume of protein solution to volume of crystallisation solution. The plate incubated at 22°C also had precipitate in all of the crystallisation drops but to a lesser extent compared with the crystallisation drops that had been incubated at 4°C. At 37°C the crystallisation drops were much clearer of precipitate compared to those incubated at 4°C or 22°C. The majority of the crystallisation conditions when incubated at 37°C contained very light precipitate except for the drops containing a high ratio of volume of protein solution to volume of crystallisation solution, which remained clear. Due to the predicted increase in equilibration time of the larger-volume crystallisation drops, observations were continued on a weekly basis for total of 4 weeks. During this time the only change observed was an increase in precipitation.

### 3.3.11.4 Small scale crystallisation optimisation

In light of the unsuccessful attempts to upscale the crystallisation drop size, optimisation of the original promising crystallisation condition identified in Section 3.3.11.1 was continued using the small scale crystallisation format. The grid screen developed around the promising Qiagen® NeXtal® Classic suite B10 crystallisation

solution for the first round of large scale protein crystallisation (Section 3.3.11.2) was used to set up a small scale crystallisation trial. Observations of the small scale crystallisation optimisation were performed at 5 and 14 days post-setup (Table 3.6). The trends in crystallisation observations were similar after 5 and 14 days post-setup. Within both sets of observations, the crystallisation condition with the lowest MPD concentration (60% (v/v)) did not produce any crystals regardless of pH. MPD concentrations of 65-75% (v/v) produced regularly-shaped, well-formed single crystals in a pH dependent fashion. In general the best crystallisation outcomes within this range were produced with a higher MPD concentration in combination with a lower pH, or the exact opposite of this, a lower MPD concentration combined with a higher pH. Crystallisation conditions with the highest MPD concentration (80% (v/v)) favoured the formation of irregularly-shaped, poorly-formed crystals at a lower pH and phase separation at a higher pH. Therefore, small scale crystallisation optimisation afforded regularly-shaped, well-formed single crystals, however, no significant improvement in size was made.












**Table 3.6.** SBT Prx 2 small scale crystallisation trial observations after 5 days (A) and 14 days (B) post-setup. SBT Prx 2 protein was purified by Ni-affinity chromatography (Section 2.14) and desalted into a buffer containing 20 mM Tris-base (pH 7.5), 150 mM NaCl and 5 mM DTT. The concentrated SBT Prx 2 protein solution ( $25 \text{ mg mL}^{-1}$ ) was used to set up a small scale crystallisation trial with a grid screen based around the Qiagen<sup>®</sup> NeXtal<sup>®</sup> Classic suite B10 crystallisation solution, composed of 0.1 M HEPES (pH 7.5) and 70% (v/v) MPD. The crystallisation drop phenomena observed are indicated according to colour while the letter code gives more detail on the specific nature of the observed phenomenon. The numerical dimensions, if stated, relate to the dimensions ( $\mu\text{m}$ ) of observed crystalline objects.

## A

		MPD% (v/v)				
		60	65	70	75	80
pH	7	C	C	r 5x30	5-10x15-20	mf
	7.5	C	vL	r 10x15	5x20	Ph
	8	m?	vL	r 5x15	mf	mf nc
	7	L	vL		5-10x20	Ph
	7.5	L	vL		mf	Ph
	8	m?	10x20		mf	Ph

## B

		MPD% (v/v)				
		60	65	70	75	80
pH	7	C	C	m	s r	Ph+mf
	7.5	C	C	s/m r	s r+L	Ph+mf
	8	C	m	s/m r	mf+nc	Ph+nc
	7	L	C	C	s r	M
	7.5	L	m	L	s/m r + L	Ph
	8	L	m r	L+m	s/m r + L	Ph+M

	0	clear
	1	heavy precipitate
	2	medium Precipitate
	3	light precipitate
	4	Micro Crystals
	5	
	6	Needle Clusters / Plates
	7	
	8	Misformed Single Crystals
	9	
	10	Single Well Formed Crystals

C	Clear
H	Heavy Precipitate
M	Medium Precipitate
L	Light Precipitate
S	Skin
Ph	Phase Separation
P	Plate
m	Micro-crystals
f	faint
nc	Needle Cluster
n	Needle
r	Rod
v	Very
s	Small
l	Large
mf	Mis-formed

### 3.3.11.5 Broadening the search for crystallisation conditions that utilise MPD

Although small scale crystallisation optimisation of the original promising crystallisation condition was able to improve the reproducibility and morphology of the crystals produced, neither small-scale nor large-scale crystallisation trials were able to improve the size of the crystals produced. Therefore, to expand the search for crystallisation conditions whilst maintaining MPD as the precipitant, the SBT Prx 2 protein was screened for crystallisation conditions using the Qiagen<sup>®</sup> NeXtal<sup>®</sup> MPD suite. Each crystallisation drop was imaged 6 times over the first 12 days of incubation. Due to the poor quality of the images the clarity of the drop could be assessed but it was difficult to identify if any crystal formation was occurring. On the 12<sup>th</sup> day of incubation post-setup the crystallisation drops were manually observed using a polarised light microscope (Table 3.7). The first 48 conditions (A1-D12) of the Qiagen<sup>®</sup> NeXtal<sup>®</sup> MPD Suite contained different salts in combination with 40% (v/v) MPD. This sub-set of conditions enabled the identification of co-crystallising salts that could be used to optimise the crystallisation conditions. Of the 48 salts tested sodium malonate, lithium sulphate and di-Ammonium tartrate were found to produce crystals in combination with MPD in the 0.5  $\mu$ L crystallisation drops. Of these salts the only one that translated into favourable crystallisation conditions in the larger 2.5  $\mu$ L crystallisation drop was lithium sulphate. Therefore, lithium sulphate was identified as a promising co-crystallising salt.

**Table 3.7.** SBT Prx 2 crystallisation trial 0.5  $\mu\text{L}$  (A) and 2.5  $\mu\text{L}$  (B) crystallisation drop observations after 12 days post-setup. SBT Prx 2 protein was purified by Ni-affinity chromatography and desalted into a buffer containing 20 mM Tris-base (pH 7.5), 150 mM NaCl and 5 mM DTT. The concentrated SBT Prx 2 protein solution (20  $\text{mg mL}^{-1}$ ) was used to set up a crystallisation trial with the Qiagen<sup>®</sup> NeXtal<sup>®</sup> MPD Suite (refer to Appendix for composition table). The crystallisation drop phenomena observed are indicated according to colour while the letter code gives more detail on the specific nature of the observed phenomenon.

A

	1	2	3	4	5	6	7	8	9	10	11	12
A	M/H	C	C	L/mf?	C/L	L	mn/spl	L/C	H	C/L	L	C
B	L	C/L	L/mf?	C/L	L	L/m?	M	MH	L	L/1xmnc	L/C	M
C	M/H	L/C/m?	M	H	L/M	L/C	sr	C	C	H	sr	C
D	C/mf?	vsr/C	L	C/L	C	C	M	C	n?mf?/C	C	C	C
E	M/H	L/M	L/m?	C/mf?	C/mr?	C	H	H	H	L/M	L/M	L/m?
F	L/m?	H	L	L	L	L	L	M	L	C	C/1xr?	L
G	C/m?	C/m?	M	C/m?	H	H	L/m?	C/L	L	L/m?	M	M
H	M/H	C/m	C	L	C/L	H	L/m?	L	C	C/mr?	L	L/C

B

	1	2	3	4	5	6	7	8	9	10	11	12
A	H/S	M/H	H	H	L/m?	H	L/m	H	H	H/S	H/S	H/S
B	M	H	H	M	H	H	H	H/Ph	H	H	H	H
C	M	L/m?	H	L/m?	H	H	L/m?	L/M	H	L/M	MH	L/M mp?
D	L/M	H	H	H	L/m?	vL m?	H	L/m?	C/L	L	L/m?	L
E	H	H	H	L/M	C/L/m?	C/L	H	H	H	H	M	L
F	H	H	H	H	M/H	M	L/M	H/M	MH	L/M	M	L/M/m?
G	L	L/inc	M/mf?	M/H	M	M	M	M	M	M/H	L/M	M
H	L/M	L/M	L/M	H/M	L/m?	C/L	L/m?	L/M	L	L/M	L/M	M

Crystallisation Scoring Legend

0	0	clear
1	1	heavy precipitate
2	2	medium Precipitate
3	3	light precipitate
4	4	Micro Crystals
5	5	
6	6	Needle Clusters / Plates
7	7	
8	8	Misformed Single Crystals
9	9	
10	10	Single Well Formed Crystals

C	Clear
H	Heavy Precipitate
M	Medium Precipitate
L	Light Precipitate
S	Skin
Ph	Phase Separation
P	Plate
m	Micro-crystals
f	faint
nc	Needle Cluster
n	Needle
r	Rod
v	Very
s	Small
l	Large
mf	Mis-formed



Conditions 49-72 (E1-F12) of the Qiagen® NeXtal® MPD Suite contained crystallisation solutions that combined varying concentrations of MPD with varying pH. This sub-set of conditions enabled refinement of the crystallisation pH and MPD concentration. To identify any correlation between MPD concentration, pH and crystallisation outcome the data for these three parameters were re-arranged to produce Table 3.8. For both the small and large crystallisation drops there was an overall trend towards a decrease in precipitate with an increase in pH. This trend was also true for the lowest and highest MPD concentrations. Therefore, based on these observations a pH range of 8-9 was determined to be most likely optimal for crystallisation of the SBT Prx 2 protein.

**Table 3.8.** Effect of varying MPD concentration and pH on the crystallisation of SBT Prx 2 protein in 0.5  $\mu\text{L}$  (A) and 2.5  $\mu\text{L}$  (B) crystallisation drops. SBT Prx 2 protein was purified by Ni-affinity chromatography and desalted into a buffer containing 20 mM Tris-base (pH 7.5), 150 mM NaCl and 5 mM DTT (Section 2.14). The concentrated SBT Prx 2 protein solution (20 mg mL<sup>-1</sup>) was screened for crystallisation conditions using the Qiagen<sup>®</sup> NeXtal<sup>®</sup> MPD suite (conditions 49-72). Refer to Appendix for the Qiagen<sup>®</sup> NeXtal<sup>®</sup> MPD suite composition table. The crystallisation drop phenomena observed are indicated according to colour and number.

**A**

		2	4	2	1	1	1
MPD	65	2	6	2	2	2	2
(%v/v)	40	6	6	6	3	3	2
	20	5	3	2	1	1	1
	10	4	5	6	7	8	9
		pH					

**B**

		3	6	5	3	4	3
MPD	65	6	6	6	6	5	4
(%v/v)	40	6	6	6	6	4	2
	20	6	6	6	3	1	1
	10	4	5	6	7	8	9
		pH					

**Crystallisation Scoring Legend**

	1	Clear
	2	Light precipitate
	3	Light/Medium precipitate
	4	Medium precipitate
	5	Medium/Heavy precipitate
	6	Heavy precipitate

Conditions 73-96 (G1-H12) of the Qiagen<sup>®</sup> NeXtal<sup>®</sup> MPD Suite are a compilation of the most popular and successful crystallisation conditions reported in the Biological Macromolecule Crystallization Database. Of these crystallisation conditions the most promising observations were obtained using condition 74 (G2) and condition 86 (H2) in a large and small crystallisation drop, respectively. Condition 74 contained 0.05 M MgCl<sub>2</sub>, 0.1 M Tris-HCL (pH 8.5) and 12% (w/v) MPD and condition 86 contained 0.5 M (NH<sub>4</sub>)<sub>2</sub>SO<sub>4</sub>, 0.1 M HEPES (pH 7.5) and 30% (w/v) MPD. Therefore, a salt in combination with a relatively low concentration of MPD appeared to promote crystallisation.

### 3.3.11.6 Effect of lithium sulphate on large scale crystallisation outcome

The crystallisation screening of SBT Prx 2 protein with the Qiagen<sup>®</sup> NeXtal<sup>®</sup> MPD suite identified lithium sulphate as a promising co-crystallising salt. Incorporation of lithium sulphate into the crystallisation solution appeared to decrease precipitate formation in the larger crystallisation drop format. To further investigate this, a large scale crystallisation trial was set up with SBT Prx 2 protein and a crystallisation grid screen containing varying concentrations of MPD and lithium sulphate (Table 3.10). Immediately after setup, the crystallisation drops containing 0.2 M Li<sub>2</sub>SO<sub>4</sub>, regardless of MPD concentration, appeared clear while only the crystallisation drops containing no lithium sulphate and a concentration of ≤15% (v/v) MPD appeared clear. In the crystallisation drops containing no lithium sulphate and an MPD concentration of ≥20% (v/v) a light precipitate formed which looked milky white to the naked eye. The crystallisation phenomena observed over the 8 days following setup did not appear to change significantly. It was clear however that the lithium sulphate had a significant effect on reducing the formation of precipitate in the large scale crystallisation drops. The addition of lithium sulphate resulted in crystallisation drops that were clear or contained very light precipitate all the way up to the

maximum MPD concentration of 30% (v/v), whereas, in the absence of lithium sulphate, crystallisation drops that were clear or contained very light precipitate only occurred with the lowest MPD concentration of 10% (v/v). Despite lithium sulphate reducing the formation of precipitate, no crystals were able to be produced.

**Table 3.10.** Effect of lithium sulphate on large scale crystallisation of SBT Prx 2 protein after 1 (A), 2 (B), 3 (C), 6 (D) and 8 (E) days post-setup. SBT Prx 2 protein was purified by Ni-affinity chromatography and desalted into a buffer containing 20 mM Tris-base (pH 7.5), 150 mM NaCl and 5 mM DTT (Section 2.14). The concentrated SBT Prx 2 protein solution ( $20 \text{ mg mL}^{-1}$ ) was screened for crystallisation conditions using varying concentrations of MPD and  $\text{Li}_2\text{SO}_4$  in 0.1 M HEPES (pH 7.5). The crystallisation drops consisted of 2  $\mu\text{L}$  of protein solution combined with 2  $\mu\text{L}$  of crystallisation solution. The crystallisation drop phenomena observed are indicated according to colour while the letter code gives more detail on the specific nature of the observed phenomenon.

A

		MPD% (v/v)				
		10	15	20	25	30
Lithium sulphate (M)	0	L	L	L/M	M	H
	0	L m?	L	L/M	M	H
	0.2	C	C	C?	vL	L
	0.2	C	C m?	C?	vL	L

B

		MPD% (v/v)				
		10	15	20	25	30
Lithium sulphate (M)	0	vL m?	L/M	M	M/H	H
	0	vL m?	L/M	M	M/H	H
	0.2	C	C	vL	vL	L
	0.2	C m?	C	vL	vL	L

C







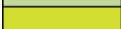




		MPD% (v/v)				
		10	15	20	25	30
Lithium sulphate (M)	0	L	L	L/M	M/H	H
	0	L m?	L	L/M	M/H	H
	0.2	C	C?	L	L	L
	0.2	C	C?	L	L	L

D

		MPD% (v/v)				
		10	15	20	25	30
Lithium sulphate (M)	0	L	L	M	M/H	H
	0	L/m?	L	M	M/H	H
	0.2	C	C?	vL	L	L
	0.2	C m?	C?	vL	L	L

E

		MPD% (v/v)				
		10	15	20	25	30
Lithium sulphate (M)	0	L	L/M	M	H	H
	0	L	L/M	M	H	H
	0.2	C	C	C/vL	C/vL	C/vL
	0.2	C	C	C/vL	C/vL	C/vL

	0	clear
	1	heavy precipitate
	2	medium Precipitate
	3	light precipitate
	4	Micro Crystals
	5	
	6	Needle Clusters / Plates
	7	
	8	Misformed Single Crystals
	9	
	10	Single Well Formed Crystals

C	Clear
H	Heavy Precipitate
M	Medium Precipitate
L	Light Precipitate
S	Skin
Ph	Phase Separation
P	Plate
m	Micro-crystals
f	faint
nc	Needle Cluster
n	Needle
r	Rod
v	Very
s	Small
l	Large
mf	Mis-formed

### 3.3.11.7 Effect of increased MPD concentration combined with high pH on large scale crystallisation outcome

A large scale crystallisation trial was set up to investigate the effect of higher MPD concentrations and higher pH, combined with lithium sulphate, on large scale crystallisation outcome. Immediately after the crystallisation drops were set up they were observed and all were found to be clear with no sign of precipitation. The crystallisation drops were observed over a 4 week period. After 3 days incubation at 20°C, a crystalline object of 20 x 40 µm was found in the crystallisation drop that was prepared with a crystallisation solution containing 30% (v/v) MPD, 0.2 M Li<sub>2</sub>SO<sub>4</sub> and 0.1 M Tris-base (pH 8.5). No other conditions were found to produce crystals. Therefore, it appeared that the combination of lithium sulphate, higher MPD concentration and high pH in a large scale crystallisation drop was able to improve the size of the crystals produced.

### 3.3.11.8 X-ray crystallography analysis

To investigate the structure of the SBT Prx 2 protein, the crystals grown in small and large scale crystallisation trials were analysed using the X-ray crystallography beam-line at the Australian Synchrotron. Each crystal was mounted in the beam-line and images were captured at 0° and +90°  $\Phi$  (angle of rotation perpendicular to the axis that the pin containing the mounted crystal lies upon). The captured images did not show any signs of diffraction.

### 3.4 Discussion

NKEF A and B (Prx 1 and 2) genes have been cloned from a number of fish species but to date none of these genes have been functionally characterized except for those in the current study (Sutton et al., 2010; Loo et al., 2012). Here we report the sequence analysis and functional and structural characterisation of a Prx 2 protein from southern bluefin tuna (SBT).

In addition to the sequencing of the pET-30a-SBT Prx construct confirming that it contained a Prx insert sequence that was mutation free and in-frame with the start site for translation, it also identified an unknown nucleotide in the SBT Prx ORF (GenBank accession no. EU093980) as being an adenine. This in turn identified the unknown residue in the SBT Prx 2 protein sequence at position 193 as being a Leu. This feature of the SBT Prx protein appears to be a unique feature amongst Prx sequences from other fish and mammals which have Phe and Tyr residues at this position, respectively. The significance of this residue in combination with its C-terminal neighbouring Phe residue is discussed later.

The deduced amino acid sequence of the SBT Prx contained the canonical peroxidatic and resolving Cys residues characteristic of typical 2-Cys Prxs. The former was embedded within the highly conserved F-motif (FTFVCPTEI) and the latter was adjacent to a highly conserved hydrophobic region (VCPAGW). These features are highly conserved amongst all typical 2-Cys Prxs from all phyla studied to date, including plants, mammals, fungi, bacteria and fish (Hofmann et al., 2002; König et al., 2003; Dong et al., 2007; Sutton et al., 2010). Pairwise comparisons and phylogenetic analysis revealed that the SBT Prx should be classified as a Prx 2.

Numerous 2-Cys Prx proteins have been able to be expressed with high abundance in *E. coli* (Gourlay et al., 2003, Boucher et al., 2006) and the SBT Prx 2 protein is no exception. SDS-PAGE and immunoblotting analysis of *E. coli* BL21 (DE3) cells



expressing the SBT Prx 2 protein revealed two distinct forms with molecular masses that corresponded to monomer and dimer. This result is consistent with the work carried out by Sekiya et al., 2006, in which SDS-PAGE and immunoblotting analysis of a recombinantly expressed 2-Cys Prx protein from liver fluke revealed two distinct forms with molecular masses corresponding to monomer and dimer. The detection of 2-Cys Prx dimers in the current and afore mentioned study is surprising given the denaturing and reducing conditions of SDS-PAGE. However, these observations may be able to be explained by the extreme chemical resistance of 2-Cys Prx proteins. For example, the bovine mitochondrial Prx (SP-22) was shown to remain folded even when incubated in the presence of 20 mM DTT and up to 3M urea (Gourlay et al., 2003). It needs to be acknowledged that the identification of the two SBT Prx 2 protein forms based on anti-His antibody reactivity is only provisional without confirmation by mass spectrometry.

To investigate its functionality, the SBT Prx 2 protein was purified by Ni-affinity chromatography. The purified protein was assayed in a steady-state system in which peroxide substrate reduction was coupled with NADPH oxidation in the presence of commercially sourced *E. coli* Trx and TrxR. The SBT Prx exhibited thioredoxin-dependent peroxidase activity and it could use H<sub>2</sub>O<sub>2</sub> or CuOOH as the peroxide substrate. Thioredoxin-dependent peroxidase activity is the defining activity of typical 2-Cys Prxs from yeast and mammals (Hofmann et al., 2002; Rhee et al., 2005). Thus, the SBT Prx 2 was confirmed to be a genuine thioredoxin-dependent peroxidase.

The kinetic behaviour of the SBT Prx was investigated by varying either the Trx or the peroxide substrate concentration in the standard steady-state assay system. When the H<sub>2</sub>O<sub>2</sub> concentration was held constant and the Trx concentration was varied, SBT Prx activity exhibited typical Michaelis-Menten kinetics and a K<sub>m</sub> (Trx) value of 12 µM. This was similar to the values of 5.5, 2.7 and 4.3 µM obtained for

human Prx 1, human Prx 2 and mouse Prx 3, respectively (Chae et al., 1999). It was also similar to the values of 8.7, 9.5 and 7.3 obtained for three different 2-Cys Prxs from *Schistosoma mansoni*, a parasitic trematode worm (Sayed and Williams, 2004). Other well studied 2-Cys Prxs come from the apicomplexan parasites *Toxoplasma gondii* and *Plasmodium falciparum* (Akerman and Müller, 2005). These had  $K_m(\text{Trx})$  values of 4.2 and 13.4  $\mu\text{M}$ , respectively. Thus, the  $K_m(\text{Trx})$  value obtained for SBT Prx was within the commonly reported range.

In contrast to the typical Michaelis-Menten kinetics observed with Trx, the kinetics observed with the peroxide substrates  $\text{H}_2\text{O}_2$  and  $\text{CuOOH}$  were much more complex. At low peroxide substrate concentrations ( $\leq 120 \mu\text{M}$ ), the response of SBT Prx activity to increasing peroxide substrate concentration was sigmoidal with Hill coefficients of 2.0 and 2.3 for  $\text{H}_2\text{O}_2$  and  $\text{CuOOH}$ , respectively. However, at higher peroxide substrate concentrations (0.5 – 2.0 mM) there was a progressive decline in SBT Prx activity with increasing peroxide substrate concentration. The latter phenomenon has been observed before for eukaryotic typical 2-Cys Prxs and will be discussed later. However, the former phenomenon (sigmoidal kinetics at lower peroxide substrate concentrations) appears to be novel. Other typical 2-Cys Prxs have been reported to exhibit either non-saturable peroxidase kinetics or typical saturable Michaelis-Menten kinetics with various peroxide substrates (Chae et al., 1999; Hofmann et al., 2002; Munhoz and Netto, 2004; Sayed and Williams, 2004; Akerman and Müller, 2005; Boucher et al., 2006). The  $S_{0.5}$  values calculated for SBT Prx for  $\text{H}_2\text{O}_2$  and  $\text{CuOOH}$  were 29 and 25  $\mu\text{M}$ , respectively. This compares with  $K_m$  values for these substrates of less than 20  $\mu\text{M}$  for human Prx 1 and 2 and mouse Prx 3 (Chae et al., 1999). Chae et al. (1999) observed no change in Prx activity as the peroxide substrate concentration was decreased from 100 to 20  $\mu\text{M}$ . Thus, the SBT Prx had  $S_{0.5}$  values which were at least 10 times greater than the  $K_m$  values observed for mammalian typical 2-Cys Prxs. For further comparison, yeast cTPxl (a

typical 2-Cys Prx) had  $K_m$  values of 12.0 and 17.1  $\mu\text{M}$  for  $\text{H}_2\text{O}_2$  and  $\text{CuOOH}$ , respectively, and yeast cTPxII (also a typical 2-Cys Prx) had  $K_m$  values of 13.8 and 4.5  $\mu\text{M}$ , respectively (Munhoz and Netto, 2004). These values are approaching the  $S_{0.5}$  values obtained for the SBT Prx but they are still somewhat lower. There is great variation in the literature in the  $K_m$  values for peroxide substrates. For example, the  $K_m(\text{H}_2\text{O}_2)$  values reported for *T. gondii* and *P. falciparum* 2-Cys Prxs were 0.38 and 0.25  $\mu\text{M}$ , respectively (Akerman and Müller, 2005) whereas for *S. mansoni* 2-Cys Prxs they were in the range 150 to 350  $\mu\text{M}$  (Sayed and Williams, 2004). This may be due to different methods being used between different laboratories but apparently there is also significant species to species variation.

It is now well established that typical 2-Cys Prxs can be divided into two different types commonly referred to as “sensitive” and “robust” (Wood et al., 2003a; Chae et al., 1994c, 1999; Yang et al., 2002; Lee et al., 2007; Cox et al., 2009; Manta et al., 2009). Most eukaryotic typical 2-Cys Prxs (including yeast and mammalian) belong to the “sensitive” type and most prokaryotic typical 2-Cys Prxs (including the well studied *Salmonella typhimurium* AhpC) belong to the “robust” type. “Sensitive” typical 2-Cys Prxs lose their peroxidase activity at mM concentrations of  $\text{H}_2\text{O}_2$  whereas “robust” typical 2-Cys Prxs remain active. Thus, the SBT Prx belongs to the “sensitive” type as would be expected for a eukaryotic typical 2-Cys Prx. Inactivation of “sensitive” typical 2-Cys Prxs has been shown to be due to overoxidation of the peroxidatic Cys such that Cys– $\text{S}_\text{P}\text{OH}$  (the oxidized sulfenic acid form) becomes oxidized to Cys– $\text{S}_\text{P}\text{O}_2\text{H}$  (the overoxidized sulfinic acid form). This occurs when a second molecule of  $\text{H}_2\text{O}_2$  reacts with Cys– $\text{S}_\text{P}\text{OH}$  before intermolecular disulphide bond formation can occur with the resolving Cys (Cys– $\text{S}_\text{R}\text{H}$ ). Thus, the inactivation of the SBT Prx protein in response to mM concentrations of  $\text{H}_2\text{O}_2$  was most likely due to overoxidation of the peroxidatic Cys. However, direct validation of the

overoxidised peroxidatic Cys residue by mass spectrometry would need to occur before any firm conclusions can be drawn.

It has been observed that “sensitive” eukaryotic typical 2-Cys Prxs possess highly conserved GGLG and YF motifs, whereas “robust” prokaryotic typical 2-Cys Prxs lack these sequence features (Wood et al., 2003a). Structural studies have shown that the GGLG and YF motifs are associated with “sensitivity” because they hinder disulphide bond formation between Cys-S<sub>P</sub>OH and Cys-S<sub>R</sub>H. This makes Cys-S<sub>P</sub>OH longer lived and therefore more susceptible to attack by a second peroxide molecule. It is interesting to note that the SBT Prx 2 sequence contained the conserved GGLG motif but lacked the associated YF motif. In place of the YF motif, the SBT Prx 2 sequence had a LF motif and the other fish Prx sequences, except for the carp sequence, had a FF motif. Thus in SBT, the tyrosine (Y) residue was replaced with a leucine (L) residue whereas in most of the other fish species it was replaced with a phenylalanine (F) residue. Tyrosine and phenylalanine both have aromatic R groups and all three of these amino acids are non-polar. Thus, they should all participate readily in hydrophobic interactions. Therefore the consequences for protein folding should be minimal. However, tyrosine also has a hydroxyl group which can participate in hydrogen bonding. Thus, it will be interesting to determine whether or not these different residues are functionally equivalent in terms of the packing of the GGLG and XF motifs in fish Prx crystal structures.

It is well established that typical 2-Cys Prx proteins from bacteria, yeast, plants and mammals can exist either as homodimers or toroid-shaped decamers that consist of five homodimers. When both the peroxidatic and the resolving Cys residues are in the reduced state, the decamer is favoured. In contrast, when the peroxidatic Cys is in the oxidised state (Cys-S<sub>P</sub>OH), the dimer is favoured. In addition, over-oxidation of the peroxidatic Cys (Cys-S<sub>P</sub>O<sub>2</sub>H) favours the formation of decamer. If oxidising conditions persist, decamers can associate to form higher order aggregates

(Barranco-Medina et al., 2009; Hall et al., 2009). Under both oxidised and reduced conditions the SBT Prx 2 protein was present as a mixture of oligomeric species with molecular masses corresponding to dimer, tetramer and decamer. The most prominent oligomeric protein form in the oxidised and reduced gel filtration chromatography analyses was the dimer. Therefore, it appears that reducing conditions alone are not sufficient to promote the favourable formation of the SBT Prx decamer. Interestingly, gel filtration analysis performed with reduced SBT Prx 2 at a higher concentration favoured the formation of decamer and higher order oligomers. Thus, a lower SBT Prx 2 protein concentration ( $12 \text{ mg mL}^{-1}$ ) appeared to favour the formation of dimer while a higher SBT Prx 2 protein concentration ( $30 \text{ mg mL}^{-1}$ ) appeared to favour the formation of decamer. In *Salmonella typhimurium* the AhpC protein has also been shown to display protein concentration dependent oligomerisation. Under oxidised conditions, low AhpC protein concentration favoured the formation of dimer while high AhpC protein concentration favoured the formation of decamer (Wood et al., 2002).

Gel filtration analysis of SBT Prx 2 protein stored for extended periods revealed a progressive shift from decamer to a higher order aggregate. Although the Ni-affinity purification and subsequent storage at  $4^{\circ}\text{C}$  were both performed in the presence of DTT, the DTT may have become oxidised over time and this may explain the shift from the decamer to the higher order aggregate. Previous gel filtration analyses of PfTrx-Px1 (a typical 2-Cys Prx from *Plasmodium falciparum*) have shown that under oxidising conditions this protein eluted as a single peak of  $\sim 400 \text{ kDa}$  (corresponding to a dimer of decamers) whereas under reducing conditions (i.e., in the presence of  $1 \text{ mM DTT}$ ) it eluted predominantly as a  $250 \text{ kDa}$  species (corresponding to a decamer). Scanning electron microscopy confirmed that the  $250$  and  $400 \text{ kDa}$  species corresponded to a decamer and a dimer of decamers, respectively (Akerman and Müller, 2003). Based on these findings and others, it is possible that

the SBT Prx 2 gel filtration peaks 'b' and 'a' in Fig. 3.10 correspond to a decamer and a dimer of decamers, respectively. In other species such as *Helicobacter pylori*, *Saccharomyces cerevisiae* and *Homo sapiens*, similar higher order aggregates of typical 2-Cys Prx proteins have been shown to have chaperone activity which may be involved in the recovery of proteins damaged by oxidative stress (Hall et al., 2009).

Mutation of particular Cys residues in typical 2-Cys Prxs has been demonstrated to have a dramatic effect on the oligomeric forms of the protein (Matsumura et al., 2008; Hirotsu et al., 1999). A multiple sequence alignment of the SBT Prx 2 protein with other typical 2-Cys Prx proteins from mammals and fish revealed that in addition to the SBT Prx 2 possessing both the highly conserved peroxidatic (Cys<sup>51</sup>) and resolving Cys (Cys<sup>172</sup>) residues it also contained an additional Cys residue at position 75, a property shared with other fish Prx 2 proteins. Interestingly, the Cys<sup>75</sup> residue was absent in the mammal Prx 2 proteins where it was replaced by a Val residue and in Prx 1 proteins from both mammals and fish where it was replaced by an Ala residue. However, the Prx 1 proteins from mammals and some fish possessed an additional Cys residue at the nearby location of position 83 which was first noted by Lee et al. (2007) as a feature that distinguished human Prx 1 from Prx 2. Mutation of the SBT Prx 2 Cys<sup>75</sup> residue to Ser (C75S) resulted in a protein that was able to be highly expressed but was not able to be purified to any significant extent using Ni-affinity chromatography. Gel filtration chromatography analysis of the C75S SBT Prx 2 protein under reduced conditions revealed that it existed as different sized aggregates, ranging from 250 kDa, a size consistent with a decamer, all the way up to 2,000 kDa. In contrast to this, gel filtration chromatography analysis of a C83S Prx 1 mutant from rat revealed that it existed predominantly as monomer under reducing conditions (Matsumura et al., 2008). This suggested that despite the close proximity of the non-catalytic Cys<sup>75</sup> residue of the SBT Prx 2 and other fish Prx

2 proteins to the Cys<sup>83</sup> residue of the Prx 1 from mammals and fish, they have distinctly different structural roles. Analysis of both the rat and human Prx 1 crystal structures revealed that the Cys<sup>83</sup> residue was positioned in the dimer-dimer interface (Matsumura et al., 2008; Lee et al., 2007). The latter crystal structure was found to possess Cys<sup>83</sup>-Cys<sup>83</sup>-linked disulphide bonds at each of the five dimer-dimer interfaces, whilst the former crystal structure was found to contain a Cys<sup>83</sup>-Cys<sup>83</sup>-linked disulphide bond at only one out of the five dimer-dimer interfaces. As a result of these analyses it appeared that the Cys<sup>83</sup> residue forms an integral part of the bonding network in the dimer-dimer interface of Prx 1 proteins. Therefore, the C83S mutation in the rat Prx 1 most likely disrupted the dimer-dimer interface Cys<sup>83</sup>-Cys<sup>83</sup>-linked disulphide bonds, triggering dissociation of the decamer into dimer and the dimer was subsequently reduced by DTT to form monomer. Based on a high degree of protein sequence similarity, the rat Prx 1 crystal structure was used as a model for predicting the structural position and role of the Cys<sup>75</sup> residue in the SBT Prx 2 protein. In this model, the Cys<sup>75</sup> residue appeared to be positioned behind the dimer-dimer interface, contributing to the internal core of the protein monomer. Thus, the C75S mutation in the SBT Prx 2 most likely destabilised the protein through disruption of its internal organisation, giving rise to a mixture of smaller soluble aggregates such as decamer and larger insoluble aggregates. Analytical ultracentrifugation of whole cell protein extract produced from *E. coli* cells expressing the C75S SBT Prx 2 protein confirmed that the aggregates, as indicated from the structure analysis, were comprised of approximately equal proportions of soluble and insoluble protein. Therefore, the Cys<sup>75</sup> residue was found to be essential for the correct folding and maintenance of the SBT Prx 2 protein structure and it plays a distinctly different structural role compared to the Cys<sup>83</sup> residue of mammal and, most likely, fish Prx 1 proteins.

Mutation of the peroxidatic Cys residue of typical 2-Cys Prx proteins has been shown to promote the formation of decamer and higher order oligomers (Gourlay et al., 2003; Matsumura et al., 2008). Gel filtration analysis of the C51S SBT Prx 2 protein revealed, in agreement with published findings, that mutation of the peroxidatic Cys to a Ser residue promoted the formation of decamer compared to wild-type protein. The favourable formation of decamer by peroxidatic Cys mutants stems from an inability to accept peroxide substrates and participate in subsequent disulphide bond formation with the resolving Cys residue. The prevention of intermolecular disulphide bond formation locks the loop-helix motif containing the mutated peroxidatic Cys residue in a folded conformation, stabilising the dimer-dimer interface and therefore, the decamer structure (Matsumura et al., 2008; Wood et al., 2003b). Although formation of the decamer was favoured by the C51S SBT Prx 2 protein, a significant amount of the dimer was also present. This suggested that in addition to the peroxidatic Cys there may be other factors influencing the oligomeric properties of the SBT Prx 2 protein.

In order to investigate the distribution of Prx 2 protein in different SBT tissues, polyclonal antibodies were raised against Ni-affinity purified SBT Prx 2 protein in rabbit. In addition to the anti-SBT Prx 2 antibodies being able to detect appropriately sized proteins in SBT tissue protein extracts, they were also able to detect appropriately sized proteins in tissue protein extracts from other teleost fishes including yellow-tail kingfish and barramundi. The apparent cross-reactivity of the anti-SBT Prx 2 antibodies with other teleost fishes is not surprising given the high degree of Prx protein sequence conservation. The bands detected in the muscle tissue protein extracts were estimated to have molecular masses corresponding to monomer, dimer, tetramer and pentamer configurations of typical 2-Cys Prx proteins. The detection of several 2-Cys Prx configurations is consistent with the SDS-PAGE analysis of glutaraldehyde cross-linked bovine Prx 3 which revealed that



the protein existed as several different configurations with molecular masses corresponding to dimer, tetramer, hexamer, octamer, decamer and double-decamer (Gourlay et al., 2003). The detection of several 2-Cys Prx configurations by the anti-SBT Prx 2 antibodies despite the denaturing and reducing conditions of SDS-PAGE can most likely be attributed to the extreme chemical resistance of 2-Cys Prx proteins. For example, an oligomer of a bovine mitochondrial 2-Cys Prx has been shown to be able to retain ~25% of its native ellipticity when treated with 9.5 M urea (Gourlay et al., 2003). The banding pattern of proteins detected in muscle and liver fish tissue protein extracts was similar between different teleost fishes however they were distinctly different for each type of tissue. Therefore, the anti-SBT Prx 2 antibodies appear to be able to detect Prx protein in a number of different teleost fishes and tissue types.

Although these preliminary data indicate that the anti-SBT Prx 2 antibodies are a useful tool for studying finfish Prxs, further work is required to validate the immunoblotting signals detected and the specificity of the antibodies. To determine if the immunoblotting signals are dependent upon the use of anti-SBT Prx 2 antibodies, immunoblotting could be performed with secondary antibody alone. The specificity of the anti-SBT Prx 2 antibodies could be investigated by using them to immunoprecipitate Prx proteins from various finfish tissue protein extracts. The resulting immunoprecipitations could then be analysed by SDS-PAGE and the proteins present identified by mass spectrometry.

To investigate the structure of the SBT Prx 2 protein using X-ray crystallography, promising crystallisation conditions were screened for using small scale crystallisation trials. Immediately following Ni-affinity purification and after 5 days storage at 4°C the SBT Prx 2 protein was used to set up small scale crystallisation trials with the Qiagen® NeXtal® Classic and PEG crystallisation solution suites. Both the freshly purified and reduced, and stored, most likely oxidised, SBT Prx 2 protein

samples were screened for crystallisation conditions due to possessing different oligomeric species as shown by gel filtration chromatography analysis. The crystallisation drops of both the reduced and oxidised SBT Prx 2 protein samples in combination with condition 22 of the Qiagen<sup>®</sup> NeXtal<sup>®</sup> Classic suite, containing 0.1 M HEPES (pH 7.5) and 70% (v/v) MPD, were found to produce small crystalline objects. The thioredoxin peroxidase B from *Homo sapiens* was found to crystallise under similar conditions which consisted of 16% (v/v) PEG 400, 100 mM Tris-HCl (pH 7.5), 10% (v/v) 2-propanol and 10 mM DTT (Schröder et al., 2000). These conditions are similar to those identified for SBT Prx 2 based on the reported interchangeability of PEG 400 and MPD, and the pH of the crystallisation solutions. Analysis of crystals of the thioredoxin peroxidase B using X-ray crystallography revealed that they were composed of decamer (PDB accession, 1QMV). Therefore, the crystals of the SBT Prx 2 protein are most likely composed of decamer based on the similar crystallisation conditions used and the fact that the decamer protein species was the most abundant SBT Prx 2 form, as shown by gel filtration chromatography. The crystals of SBT Prx 2 obtained in the small scale crystallisation trials were very small and were deemed to be unsuitable for further analysis using X-ray crystallography. In light of this, a strategy to increase the size of the crystals was developed using observations by Mikol et al., (1990) and Gernert et al., (1987). Mikol et al., (1990) investigated the effect of the initial crystallisation drop size on the rate of equilibration with the crystallisation reservoir solution. They found that a smaller initial crystallisation drop size equilibrated at a higher rate with the crystallisation reservoir solution compared to a larger initial crystallisation drop size. This phenomenon was found to be quite pronounced in crystallisation trials that were set up with crystallisation solutions containing MPD. Gernert et al. (1987) investigated the effect of crystallisation drop equilibration time on the crystallisation outcome of hen egg white lysozyme chloride. They found through manipulation of the crystallisation drop conditions that an increase in equilibration time resulted in

fewer and larger crystals. Therefore, based on these observations an improvement in the size of the SBT Prx 2 protein crystals was most likely achievable by using a larger initial crystallisation drop size, thus increasing the crystallisation drop equilibration time.

Using the remaining Ni-affinity purified SBT Prx 2 protein from the small scale crystallisation trial which had been stored at 4°C, a large scale crystallisation trial was set up using crystallisation solutions based on the promising crystallisation condition identified in the initial small scale crystallisation trials. After completing the large scale crystallisation setup the crystallisation drops were inspected and the majority were found to contain varying degrees of precipitation, including the crystallisation drop that was set up with the original promising crystallisation solution. The formation of precipitate in the crystallisation drops so soon after being set up was unexpected due to the larger drop size in theory slowing down the rate of equilibration. The early formation of precipitate in the large scale crystallisation drops was possibly a result of the destabilisation of the SBT Prx 2 protein due to prolonged storage at 4°C prior to being set up, differences in the chemicals and method used to produce the promising crystallisation solution compared to the commercially available crystallisation solution or differences in the physical properties of small and large volume crystallisation drops. To investigate the former, the large scale crystallisation trial was repeated except that it was set up with SBT Prx 2 protein immediately following Ni-affinity purification. As was observed in the first large scale crystallisation trial, the majority of the crystallisation drops including the one that was set up with the original promising crystallisation solution formed precipitate to varying degrees immediately after setup. Therefore, failure to reproduce the small scale crystallisation outcome in a large scale crystallisation format was not due to the length of storage of the Ni-affinity purified SBT Prx 2 protein prior to setup of the crystallisation experiment.

The two remaining hypotheses left to explain the difference between the crystallisation outcome of the small and large scale crystallisation drops were a difference in the physical properties of the different sized crystallisation drops or a difference in the chemicals or method used to produce the promising crystallisation solutions versus the chemicals or method used to produce the commercially available Qiagen® NeXtal® Classic suite B10 crystallisation solution. To investigate the latter, the SBT Prx 2 protein was purified by Ni-affinity chromatography and immediately used to set up a large scale crystallisation drop with the commercially available Qiagen® NeXtal® Classic B10 crystallisation solution in place of a solution of the same composition that had been prepared from stock solutions. Immediately following setup, a heavy precipitate formed in the crystallisation drop. Therefore, a difference in the chemicals or method used to reproduce the promising commercially available crystallisation solution was not able to explain the difference between the crystallisation outcome of the small and large crystallisation drops.

To eliminate protein purification batch to batch variation as a possible factor influencing the large scale crystallisation outcome, the Ni-affinity purified SBT Prx 2 protein used to setup the last round of large scale crystallisation trials was used to set up a small scale crystallisation trial with the promising crystallisation solution. Immediately following setup, the small scale crystallisation drop was clear of precipitation and after 3 days incubation at 22°C small rod shaped crystals were observed. Therefore, the SBT Prx 2 protein sample used to set up the last round of large scale crystallisation trials behaved in the same way as the first batch of Ni-affinity purified SBT Prx 2 and as such, batch to batch variation in Ni-affinity purified SBT Prx 2 protein did not appear to be a factor influencing the large scale crystallisation outcome.

The remaining hypothesis left to explain the observation of crystals in the small scale crystallisation trials versus precipitate in the large scale crystallisation trials

was a difference in the physical properties of the different sized crystallisation drops. Luft et al. (2007) described an efficient optimisation of crystallisation conditions by manipulating the physical properties of the crystallisation drop. They were able to show that by systematically varying the ratio of the volume of protein solution to the volume of crystallisation solution in the crystallisation drop, in addition to temperature, that a single crystallisation solution could give rise to a full spectrum of crystallisation outcomes. Using an experimental design based on the work of Luft et al. (2007) the ratio of the volume of protein solution to the volume of crystallisation solution was systematically varied in a large scale crystallisation trial. The manipulation of the physical properties of the crystallisation drop in this way was shown to have little effect on preventing the formation of precipitate. In contrast to this, the incubation temperature of the large scale crystallisation trials did have an effect on the formation of protein precipitate. A lower incubation temperature of 4°C appeared to favour the formation of precipitate while a higher incubation temperature of 37°C appeared to favour very light or no precipitation. Despite the higher incubation temperature preventing heavy protein precipitation, no crystalline objects were grown in any of the crystallisation solutions tested.

In light of being unable to upscale the SBT Prx 2 protein crystallisation drop size, the opinion of an experienced protein crystallographer was sought. After discussion with Dr Alan Riboldi-Tunncliffe from the Australian Synchrotron Macromolecular Crystallography beam-line it became clear that in his experience scaling up the volume of the crystallisation drop is often problematic because the crystallisation phenomenon observed in a small scale crystallisation drop cannot be replicated or improved upon in a large scale crystallisation drop. Therefore, at this point in time the optimisation of the SBT Prx 2 protein crystallisation was continued using small scale crystallisation drops.

The grid screen developed for the first round of large scale crystallisation trials which contained 60-80% (v/v) MPD and 0.1 M HEPES (pH 7-8) was used to set up a small scale crystallisation trial with Ni-affinity purified SBT Prx 2 protein. MPD concentrations in the range of 65-70% (v/v) produced promising crystallisation outcomes in a pH dependent fashion. Although this crystallisation trial was able to produce regularly-shaped, well-formed single crystals that had overall larger dimensions than those grown using the original promising crystallisation solution, further improvements in the size of the crystals were still necessary in order for them to be suitable for X-ray crystallography analysis.

Screening of the SBT Prx 2 protein for crystallisation conditions using the Qiagen<sup>®</sup> NeXta<sup>®</sup> MPD screening suite enabled an extensive search of crystallisation conditions based on the original promising MPD containing crystallisation solution. By broadening the screening of MPD-containing crystallisation solutions, it was hoped that crystallisation conditions might be able to be identified that could be more easily translated from a small scale to large scale crystallisation drop format. In addition to this, the MPD suite also enabled systematic analysis of the effect of each of the crystallisation solution parameters, including co-crystallising salts, MPD concentration and pH, on the crystallisation outcome. Of the MPD/salt combinations tested, the only one to produce a promising crystallisation outcome in both the small and large volume crystallisation drops was lithium sulphate. Identification of lithium sulphate as a co-crystallising salt was important as it provided another means by which the physical properties of the crystallisation drop could be manipulated, possibly enabling the use of larger volume crystallisation drops and subsequent production of larger crystals. Analysis of the effect of pH on the crystallisation outcome revealed that in general a higher pH (pH 8-9) favoured light or no precipitation compared to a lower pH (pH 4-5) which favoured the formation of medium to heavy precipitation. Therefore, these results indicated that a pH of 8-9

would most likely be required for the crystallisation of the SBT Prx 2 protein. Kantardjieff and Rupp (2004) investigated if the isoelectric point of a protein was able to be used to predict the optimum pH at which it would crystallise. Their analysis of 9596 unique protein crystal forms revealed a significant relationship between the calculated pI of a protein and the reported pH at which it crystallised. Using the program Pepstat available in the Biomanager suite of programs, the pI of the SBT Prx 2 protein was predicted to be 6.9. According to Kantardjieff and Rupp (2004) a protein with a predicted pI of <7 is most likely to crystallise at a pH of approximately 1 unit higher than its predicted pI value. Therefore, the pH range of 8-9 for the crystallisation of the SBT Prx 2 protein, as determined by the MPD screening suite, was consistent with the findings of Kantardjieff and Rupp (2004). The remaining sparse matrix component of the MPD screening suite was less informative than the rest of the screen but it did enable screening of the most successful crystallisation conditions that utilise MPD as a precipitant. None of the sparse matrix crystallisation solutions were found to be able to better the crystals that were produced using the original promising crystallisation solution.

Screening of the SBT Prx 2 protein for crystallisation conditions using the Qiagen<sup>®</sup> NeXtal<sup>®</sup> MPD suite identified lithium sulphate as a co-crystallising salt. Incorporation of lithium sulphate into the crystallisation solution did not interfere with crystal growth in the small scale crystallisation drops but did appear to prevent the formation of precipitate in the large scale crystallisation drops. To further investigate the effect of lithium sulphate on the up-scaling of the crystallisation drop size, a large scale crystallisation trial was set up with varying concentrations of MPD and lithium sulphate. Lithium sulphate was shown to have a significant effect on decreasing precipitation in the large scale crystallisation drops, however, no crystals were produced. Weiss et al. (2000) investigated the crystallisation of lysozyme using MPD as the precipitant. They found that when MPD was used as the precipitant, crystals

of lysozyme could be grown at an alkaline pH but not at an acidic pH. X-ray crystallography analysis of these crystals revealed that a molecule of MPD was bound tightly between the surfaces of two lysozyme molecules, constituting an integral part of the crystalline lattice. Weiss et al. (2000) suggested that the MPD may only be able to bind to the lysozyme protein surface at high pH values and/or at high MPD concentrations, enabling the subsequent formation of a crystal lattice. Therefore, the large scale crystallisation trial most likely did not produce crystals, despite the limited formation of precipitate, because it did not have a high enough pH and/or concentration of MPD.

To follow this up, a large scale crystallisation trial was set up to investigate the effect of higher MPD concentrations and higher pH on the crystallisation of the SBT Prx 2 protein in the presence lithium sulphate. All of the large scale crystallisation drops remained clear for the duration of the experiment except for the crystallisation solution that contained 30% (v/v) MPD, 0.2 M lithium sulphate and 0.1 M Tris-base (pH 8.5), which after 3 days incubation produced a well formed, single, plate-like crystal of approximately 20 x 40  $\mu\text{M}$ . It was quite clear from the results of this experiment that the combination of lithium sulphate and a higher pH enabled the use of an MPD concentration approximately 3-5 fold higher than previously achieved. The combination of a higher pH and MPD concentration in the presence of lithium sulphate was also able to produce the first crystal in the large scale crystallisation drop format.

To investigate the structure of the SBT Prx 2 protein, the crystals grown in the small and large scale crystallisation trials were analysed by X-ray crystallography at the Australian Synchrotron. Images captured from the small plate-like rod crystals gave no signs of diffraction at  $0^\circ$  and  $+90^\circ$   $\Phi$ . The lack of diffraction from the crystals was most likely a result of the crystals overall very small size and plate like morphology.



In light of not being able to collect data from the crystals, the structure of the SBT  
Prx 2 protein was not able to be determined.

# Chapter 4

Expression, purification, and characterisation  
of a peroxiredoxin 1 from Atlantic salmon  
(*Salmo salar*)

## 4.1 Introduction

Human Prx 1 was originally identified and characterised without reference to antioxidant function as a cytosolic factor from red blood cells that enhanced the activity of natural killer cells (Shau et al., 1994). As such, it was referred to as natural killer enhancing factor A (NKEF A) (Shau et al., 1993). Later, the human NKEF A protein was also found to possess antioxidant function by providing protection to protein and DNA against oxidative damage (Sauri et al., 1995). Based on this antioxidant activity and a high degree of amino acid sequence identity, the human NKEF A was found to belong to a large new family of antioxidant enzymes referred to as peroxiredoxins (Prxs) (Rhee et al., 2005). As a cytosolic typical 2-Cys Prx, the human NKEF A has been classified and is widely referred to in the literature as a Prx 1.

In finfish, the NKEF A rather than the Prx 1 nomenclature has been assigned to genes because this is the role in which they have been investigated. NKEF A genes have been characterised in four finfish species including carp (*Cyprinus carpio*), channel catfish (*Ictalurus punctatus*), rainbow trout (*Oncorhynchus mykiss*) and gilthead sea bream (*Sparus aurata*) (Shin et al., 2001; Li and Waldbieser, 2006; Zhang et al., 2001; Pérez-Sánchez et al., 2011). The carp, rainbow trout and channel catfish NKEF A open reading frames (ORFs) were found to encode 199 amino acids. Similarly, the gilthead sea bream NKEF A ORF was found to encode 198 amino acids. Phylogenetic analyses revealed that the carp, channel catfish and gilthead sea bream NKEF A deduced amino acid sequences clustered together with other finfish NKEF A sequences while all four finfish NKEF A deduced amino acid sequences were closely related to mammalian NKEF A/Prx 1 sequences. The four finfish NKEF A deduced amino acid sequences were found to contain two VCP motifs and an additional Cys residue at position 71, all of which are characteristic

features of mammalian NKEF A/Prx 1 amino acid sequences. With the exception of gilthead sea bream, the finfish NKEF A deduced amino acid sequences were also found to contain a Cys residue at position 83, a characteristic feature shared with mammalian NKEF A/Prx 1 sequences. Although the NKEF A genes of all four finfish were found to be constitutively expressed in a range of different tissues, the levels of expression in different tissue types appeared to be species specific.

Despite the comprehensive characterisation of finfish NKEF A genes, there have been no investigations into the antioxidant function or structure of the corresponding proteins. In the current study, I present the first functional and structural characterisation of a Prx 1 protein from the finfish, Atlantic salmon (AS) (*Salmo salar*). A portion of the AS Prx 1 protein characterisation presented in the current study has been published and includes the amino acid sequence analysis, phylogenetic analysis, recombinant expression and Ni-affinity purification (Loo et al., 2012). The current study also details analysis of the AS Prx 1 protein structure using gel filtration chromatography and kinetic characterisation of the AS Prx 1 protein at high substrate concentrations.

## 4.2 Materials and Methods

### 4.2.1 Gene Construct

*Escherichia coli* BL21 (DE3) cells containing a plasmid construct composed of a Novagen pET-30a backbone and a putative Atlantic salmon peroxiredoxin (AS Prx) open reading frame (ORF) (referred to as pET-30a-AS Prx) were generated and kindly provided by Grace Loo (School of Biological Sciences, Flinders University) (Loo et al., 2012). In brief, the cloning of the putative AS Prx ORF initially involved identification of two highly conserved regions in the amino acid sequences of several fish Prxs. Based on these highly conserved regions, PCR primers were designed to amplify an internal fragment of the AS Prx cDNA using cDNA synthesised from AS liver tissue RNA. Using the sequence of this internal fragment as a search term, the sequence of the AS Prx ORF was able to be retrieved from the Consortium for Genomics Research on All Salmon Project (cGRASP) database. Based on the complete AS Prx cDNA sequence, PCR primers were designed to amplify the AS Prx ORF and incorporate *Nco*I and *Bam*HI restriction enzyme sites into the 5' and 3' ends, respectively. The AS Prx ORF and pET-30a expression vector (Novagen®) were digested with the *Nco*I and *Bam*HI restriction enzymes and ligated to produce the pET-30a-AS Prx construct. The pET30a-AS Prx construct was transformed into *Escherichia coli* BL21 (DE3) cells and provided to me as a glycerol stock that had been stored at -70°C.

### 4.2.2 Sequencing of pET-30a-AS Prx construct

Plasmid DNA was prepared from two colonies of *E. coli* BL21 (DE3) cells containing the pET-30a-AS Prx construct as per Section 2.5.2 and the inserts were subsequently sequenced according to Section 2.8. The AS Prx nucleotide sequence was retrieved from the *Salmo salar* expressed sequence tag (EST) cluster database

available at the consortium for Genomics Research on All Salmon website (<http://web.uvic.ca/grasp/>) by using a consensus sequence generated from the alignment of the pET-30a-AS Prx insert sequences as a BLAST search query. The pET-30a-AS Prx insert sequences were aligned with the two most similar nucleotide sequences returned by the BLAST search using Gene Codes Corporation Sequencher™ software.

#### 4.2.3 Optimisation of recombinant AS Prx 1 protein expression

Small scale AS Prx 1 recombinant protein expression was performed with two colonies of *E. coli* BL21 (DE3) cells containing the pET-30a-AS Prx 1 construct according to Section 2.11. After 3 and 18 h induction, a 1 mL sample from each culture was removed, centrifuged at 5000 *g* and 25°C for 10 min and the resulting cell pellets were stored at -20°C. The level of AS Prx 1 protein expression in the un-induced, 3 h induced and 18 h induced cell pellets was investigated using SDS-PAGE and immunoblotting according to Sections 2.12 and 2.13, respectively. The chemiluminescent immunoblot signal was detected using a BioRad® VersaDoc™ imaging system.

#### 4.2.4 Large scale recombinant AS Prx 1 protein expression

Three colonies of *E. coli* BL21 (DE3) cells were screened for the pET-30a-AS Prx 1 construct using the polymerase chain reaction (PCR) protocol outlined in Section 2.10. A negative control PCR reaction was included in the PCR screening and it contained 0.22 µm filter-sterilised water in the place of lysed cell supernatant as template. The PCR screening products were analysed using agarose gel electrophoresis as per Section 2.6. A colony of *E. coli* BL21 (DE3) found to possess the pET-30a-AS Prx 1 construct was used for large scale protein expression as per Section 2.11 using a 4 L fermentor vessel. The level of AS Prx 1 protein expression

was assessed by SDS-PAGE and immunoblotting according to Sections 2.12 and 2.13, respectively.

#### 4.2.5 Ni-affinity purification of AS Prx 1 protein

AS Prx 1 protein was purified from *E. coli* BL21 (DE3) cells expressing the pET-30a-AS Prx 1 construct by Ni-affinity chromatography according to Section 2.14.

Following Ni-affinity purification, the AS Prx 1 protein was exchanged into a buffer containing 20 mM Tris-base (pH 7.5), 450 mM NaCl and 5 mM DTT, concentrated and then either used immediately or frozen in liquid nitrogen and stored at -70°C until needed.

#### 4.2.6 AS Prx 1 kinetic assays

AS Prx 1 kinetic assays were performed as described in Section 2.15.

#### 4.2.7 Gel filtration chromatography of AS Prx 1 protein

The native molecular mass of Ni-affinity purified AS Prx 1 protein (prepared according to Section 4.2.5) was analysed by gel filtration chromatography according to Section 2.16 under reducing and oxidising conditions. For gel filtration chromatography analysis under reducing conditions, 200  $\mu\text{L}$  of Ni-affinity purified AS Prx 1 protein ( $10 \text{ mg mL}^{-1}$ ) was loaded onto a gel filtration column that had been equilibrated with a buffer containing 20 mM Tris-base (pH 7.5), 450 mM NaCl and 5 mM DTT. For gel filtration chromatography analysis under oxidising conditions, Ni-affinity purified AS Prx 1 protein was exchanged into a buffer containing 20 mM Tris-base (pH 7.5) and 450 mM NaCl. Following buffer exchange, 200  $\mu\text{L}$  of concentrated Ni-affinity purified AS Prx 1 ( $10 \text{ mg mL}^{-1}$ ) was loaded onto a gel filtration column that had been equilibrated with the same buffer that was used for the protein buffer exchange.

## 4.2.8 Crystallisation of AS Prx 1 protein

### 4.2.8.1 Identification of crystallisation conditions

In preparation for crystallisation trials, the AS Prx 1 protein was purified by Ni-affinity chromatography followed by gel filtration chromatography under reducing conditions (refer to Sections 4.2.5 and 4.2.7, respectively). The gel filtration chromatography column fractions containing the AS Prx 1 protein as a decamer were pooled and then concentrated using a Sartorius centrifugal concentrator with a 5 kDa molecular weight cut-off, giving a final protein concentration of 7.5 mg mL<sup>-1</sup>. Potential crystallisation conditions for the AS Prx 1 protein were screened for using small scale protein crystallisation as described in Section 2.18.1. The crystallisation drops consisted of 0.4 µL of purified AS Prx 1 protein, 0.1 µL of 20 mM Tris-base (pH 7.5) and 40 mM DTT and 0.3 µL of crystallisation solution. The crystallisation solutions used consisted of the Hampton Research Crystal Screen and Crystal Screen 2 and Qiagen® Nextal® Classic, PEG and MPD Suites (refer to Appendix for composition tables). The crystallisation drops were observed at 2, 7 and 16 days following setup using a polarised light microscope.

### 4.2.8.2 Up-scaling and optimisation of crystallisation conditions

A large scale crystallisation trial was setup according to Section 2.18.2 in which the AS Prx 1 protein and MPD concentrations were systematically varied. The crystallisation drops contained 4 µL of purified AS Prx 1 protein at a concentration of 5-10 mg mL<sup>-1</sup> in 2.5 mg mL<sup>-1</sup> increments, 1 µL of 20 mM Tris-base (pH 7.5) and 40 mM DTT and 3 µL of crystallisation solution containing 0.1 M Bicine (pH 9) and 57.5-70% (v/v) MPD in 2.5% (v/v) increments. The crystallisation plate was incubated at 22°C and observations were taken 1, 6 and 12 days post-setup.



## 4.3 Results

### 4.3.1 Sequencing of pET-30a-AS Prx construct

A BLAST search of the *Salmo salar* EST cluster database using the pET-30a-AS Prx insert sequence as the query returned a number of highly matched nucleotide sequences including contigs 38678 and 29851 which shared 100% and 99% identity, respectively. Alignment of the ORF from contigs 38678 and 29851 identified a single nucleotide mismatch at position 557 bp from the 5' terminus and a difference in the length of the 3' terminus. The nucleotide at position 557 bp for contig 38678 was a thymine (T), therefore giving a CTC codon and a Leu residue translation. Whereas the nucleotide at position 557 bp for contig 29851 was a cytosine (C), therefore giving a CCC codon and Pro residue translation. Both of the pET-30a-AS Prx inserts contained a C at position 557 bp from the 5' terminus, therefore matching contig 29851. The 3' terminus of contig 38678 was found to be shorter than that of contig 29851, matching the 3' terminus of both pET-30a-AS Prx insert sequences. A translated nucleotide alignment revealed that the AS Prx insert sequence in the pET-30a expression vector was in frame and in the correct orientation relative to the start site for translation.

### 4.3.2 AS Prx protein sequence analysis

Alignment of the deduced amino acid sequence of AS Prx with natural killer enhancing factor (NKEF) A (Prx 1) and NKEF B (Prx 2) amino acid sequences from other fish and from a selection of mammals revealed a high degree of sequence conservation (Fig. 4.1). The conserved sequence included features that are characteristic of typical 2-Cys Prxs, including the peroxidatic (C<sup>52</sup>) and resolving (C<sup>173</sup>) Cys residues contained within the F motif (FTFVCPTEI) and a hydrophobic region (VCPAGW), respectively. Therefore, the AS Prx sequence was also a typical

2-Cys Prx sequence. The AS Prx sequence also contained the highly conserved GGLG motif (residues 95-98, underlined in Fig. 4.1) which, in mammals, has been associated with a highly conserved YF motif (residues 194–195, broken underlining in Fig. 4.1). The majority of the fish Prx sequences contained an FF motif in place of the YF motif except for the carp sequence which contained the YF motif.

**Fig. 4.1.** A multiple sequence alignment of AS Prx with other members of the Prx family from fish, mammals and fleshy prawn. The alignment was performed using ClustalX software (Larkin et al., 2007) and shading was done using GeneDoc software (Nicholas et al., 1997). The degree of amino acid conservation is indicated by three levels of shading with black, dark grey and light grey shading indicating 100, 80 and 60% conservation, respectively. The two active site motifs containing the redox active Cys residues are boxed. The conserved 'GGLG' and XF' motifs are highlighted with a solid and a dashed line, respectively. GenBank nucleotide sequence accession numbers for the protein sequences are as follows. Salmon Prx 1, NM001141386; Turbot NKEF B, DQ472128; Pufferfish NKEF B, DQ323504; Zebrafish NKEF B-like, BC076347; Rat Prx 1, D30035; Rainbow trout NKEF A, AF250194; Human NKEF A, X67951; Mouse Prx 1, AK083243; Pufferfish NKEF A, DQ003333; Carp NKEF A, AB010959; Zebrafish NKEF A-like, BC091459; Human NKEF B, BC003022; Rat Prx 2, BC058481; Mouse Prx 2, AK008433; Fleshy prawn Prx 1, DQ205423.

```

*          20          *          40          *          60
Salmon Prx 1 : MAAGKRIRIGHLAPGFTAKAVMPDGGFKDLSMSDYRGKYVVFYFPLDFTFVCPTEIIAFA : 60
Rainbow trout NKEF A : MAAGKRIRIGHLAPGFTAKAVMPDGGFKDLSMSDYRGKYVVFYFPLDFTFVCPTEIIAFA : 60
Pufferfish NKEF A : MAAGKRIRIGHLAPGFTAKAVMPDGGFKDLSMSDYRGKYVVFYFPLDFTFVCPTEIIAFA : 60
Carp NKEF A : MAAGRAHIGKPADFTAKAVMPDGGFKDLSMSDYRGKYVVFYFPLDFTFVCPTEIIAFA : 60
Zebrafish NKEF A-like : MAAGNAHIGKPADFTAKAVMPDGGFGDVRLSDYKGYVVFYFPLDFTFVCPTEIIAFA : 60
Human NKEF A : MSSGNAKIGHAPAPFKATAVMPDGGFKDLSMSDYKGYVVFYFPLDFTFVCPTEIIAFA : 60
Rat Prx 1 : MSSGNAKIGHAPAPFKATAVMPDGGFKDLSMSDYKGYVVFYFPLDFTFVCPTEIIAFA : 60
Zebrafish NKEF B-like : MSAGNAKIGQAPAPFKATAVV-DGGFKDLSMSDYRGKYVVFYFPLDFTFVCPTEIIAFA : 59
Pufferfish NKEF B : MSSGNAKIGQAPAPFKATAVV-DGGFKDLSMSDYRGKYVVFYFPLDFTFVCPTEIIAFA : 59
Turbot NKEF B : MSSGNAKIGQAPAPFKATAVV-DGGFKDLSMSDYRGKYVVFYFPLDFTFVCPTEIIAFA : 59
Mouse Prx 1 : MSSGNAKIGHAPAPFKATAVMPDGGFKDLSMSDYKGYVVFYFPLDFTFVCPTEIIAFA : 60
Mouse Prx 2 : MASGNAQIGKSAPDFIATAVV-DGAFREIKLSDYRGKYVVFYFPLDFTFVCPTEIIAFA : 59
Rat Prx 2 : MASGNAHIGKPADFTAKAVV-DGAFREIKLSDYRGKYVVFYFPLDFTFVCPTEIIAFA : 59
Human NKEF B : MASGNARIGKPADFKATAVV-DGAFREIKLSDYKGYVVFYFPLDFTFVCPTEIIAFA : 59
Fleshy prawn Prx 1 : MSNTVPAIGKPAVFKGTAVV-DGGFKDLSMSDYKGYVVFYFPLDFTFVCPTEIIAFA : 59

```

```

*          80          *          100          *          120
Salmon Prx 1 : DAAEFRKIGCEVIGASVDSFCHLAWINTPRKGGGLGAMRIPLVADTLRSTIDYGVVK : 120
Rainbow trout NKEF A : DAAEFRKIGCEVIGASVDSFCHLAWINTPRKGGGLGAMRIPLVADTLRSTIDYGVVK : 120
Pufferfish NKEF A : DAAEFRKIGCEVIGASVDSFCHLAWINTPRKGGGLGAMRIPLVADTLRSTIDYGVVK : 120
Carp NKEF A : DAAEFRKINCEVIGASVDSFCHLAWINTPRKGGGLGAMRIPLVADTLRSTIDYGVVK : 120
Zebrafish NKEF A-like : DAAEGRKINCEVIGASVDSFCHLAWINTPRKGGGLGAMRIPLVADTLRSTIDYGVVK : 120
Human NKEF A : DRAEFRKLNCCQVIGASVDSFCHLAWINTPRKGGGLGAMRIPLVADTLRSTIDYGVVK : 120
Rat Prx 1 : DRAEFRKLNCCQVIGASVDSFCHLAWINTPRKGGGLGAMRIPLVADTLRSTIDYGVVK : 120
Zebrafish NKEF B-like : ERAEFRKINCEVIGASVDSFCHLAWINTPRKGGGLGAMRIPLVADTLRSTIDYGVVK : 119
Pufferfish NKEF B : DRVDFRKNCEVIGASVDSFCHLAWINTPRKGGGLGAMRIPLVADTLRSTIDYGVVK : 119
Turbot NKEF B : DRAEFRKLNCCQVIGASVDSFCHLAWINTPRKGGGLGAMRIPLVADTLRSTIDYGVVK : 119
Mouse Prx 1 : DRAEFRKLNCCQVIGASVDSFCHLAWINTPRKGGGLGAMRIPLVADTLRSTIDYGVVK : 120
Mouse Prx 2 : DHAEDFRKLGCEVLGVSDSDFTHLAWINTPRKGGGLGAMRIPLVADTLRSTIDYGVVK : 119
Rat Prx 2 : DHAEDFRKLGCEVLGVSDSDFTHLAWINTPRKGGGLGAMRIPLVADTLRSTIDYGVVK : 119
Human NKEF B : NRAEDFRKLGCEVLGVSDSDFTHLAWINTPRKGGGLGAMRIPLVADTLRSTIDYGVVK : 119
Fleshy prawn Prx 1 : DRVEFRKIGCEVVACSTDSFCHLAWINTPRKGGGLGAMRIPLVADTLRSTIDYGVVK : 119

```

```

*          140          *          160          *          180
Salmon Prx 1 : EDEGIAYRGLFVIDDKGVLROITINDLPVGRSVEELRLVQAFQTDKHGEVCPAGWKPG : 180
Rainbow trout NKEF A : EDEGIAYRGLFVIDDKGVLROITINDLPVGRSVEELRLVQAFQTDKHGEVCPAGWKPG : 180
Pufferfish NKEF A : EDEGIAYRGLFVIDDKGVLROITINDLPVGRSVEELRLVQAFQTDKHGEVCPAGWKPG : 180
Carp NKEF A : EDEGIAYRGLFVIDDKGVLROITINDLPVGRSVEELRLVQAFQTDKHGEVCPAGWKPG : 180
Zebrafish NKEF A-like : EDEGIAYRGLFVIDDKGVLROITINDLPVGRSVEELRLVQAFQTDKHGEVCPAGWKPG : 180
Human NKEF A : ADEGISFRGLFVIDDKGVLROITINDLPVGRSVEELRLVQAFQTDKHGEVCPAGWKPG : 180
Rat Prx 1 : ADEGISFRGLFVIDDKGVLROITINDLPVGRSVEELRLVQAFQTDKHGEVCPAGWKPG : 180
Zebrafish NKEF B-like : EDDGIAYRGLFVIDDKGVLROITINDLPVGRSVEELRLVQAFQTDKHGEVCPAGWKPG : 179
Pufferfish NKEF B : EDDGIAYRGLFVIDDKGVLROITINDLPVGRSVEELRLVQAFQTDKHGEVCPAGWKPG : 179
Turbot NKEF B : EDDGIAYRGLFVIDDKGVLROITINDLPVGRSVEELRLVQAFQTDKHGEVCPAGWKPG : 179
Mouse Prx 1 : ADEGISFRGLFVIDDKGVLROITINDLPVGRSVEELRLVQAFQTDKHGEVCPAGWKPG : 180
Mouse Prx 2 : NDEGIAYRGLFVIDAKGVLROITINDLPVGRSVEELRLVQAFQTDKHGEVCPAGWKPG : 179
Rat Prx 2 : NDEGIAYRGLFVIDAKGVLROITINDLPVGRSVEELRLVQAFQTDKHGEVCPAGWKPG : 179
Human NKEF B : TDEGIAYRGLFVIDGKGVLRQITVNDLPVGRSVEELRLVQAFQTDKHGEVCPAGWKPG : 179
Fleshy prawn Prx 1 : EDEGIAYRGLFVIDGKQDLRQVITINDLPVGRSVEELRLVQAFQTDKHGEVCPAGWKPG : 179

```

```

*
Salmon Prx 1 : SDTIKPDVQKSKDEFFSQQ : 199
Rainbow trout NKEF A : SDTIKPDVQKSKDEFFSQQ : 199
Pufferfish NKEF A : SDTIKPDVQKSKDEFFSKH : 198
Carp NKEF A : RDTIKPDVQKSKDEFFSKQH : 199
Zebrafish NKEF A-like : RDTIKPDVQKSKDEFFSKQN : 199
Human NKEF A : SDTIKPDVQKSKDEFFSKQK : 199
Rat Prx 1 : SDTIKPDVQKSKDEFFSKQK : 199
Zebrafish NKEF B-like : SDTIKPDVQKSKDEFFSKQ : 197
Pufferfish NKEF B : SDTIKPDVQKSKDEFFSKQN : 198
Turbot NKEF B : SDTIKPDVQKSKDEFFSKQ : 197
Mouse Prx 1 : SDTIKPDVQKSKDEFFSKQK : 199
Mouse Prx 2 : SDTIKPDVQKSKDEFFSKHN : 198
Rat Prx 2 : SDTIKPDVQKSKDEFFSKHN : 198
Human NKEF B : SDTIKPDVQKSKDEFFSKHN : 198
Fleshy prawn Prx 1 : AKTMKADPAGSKDEFFSQNEN : 198

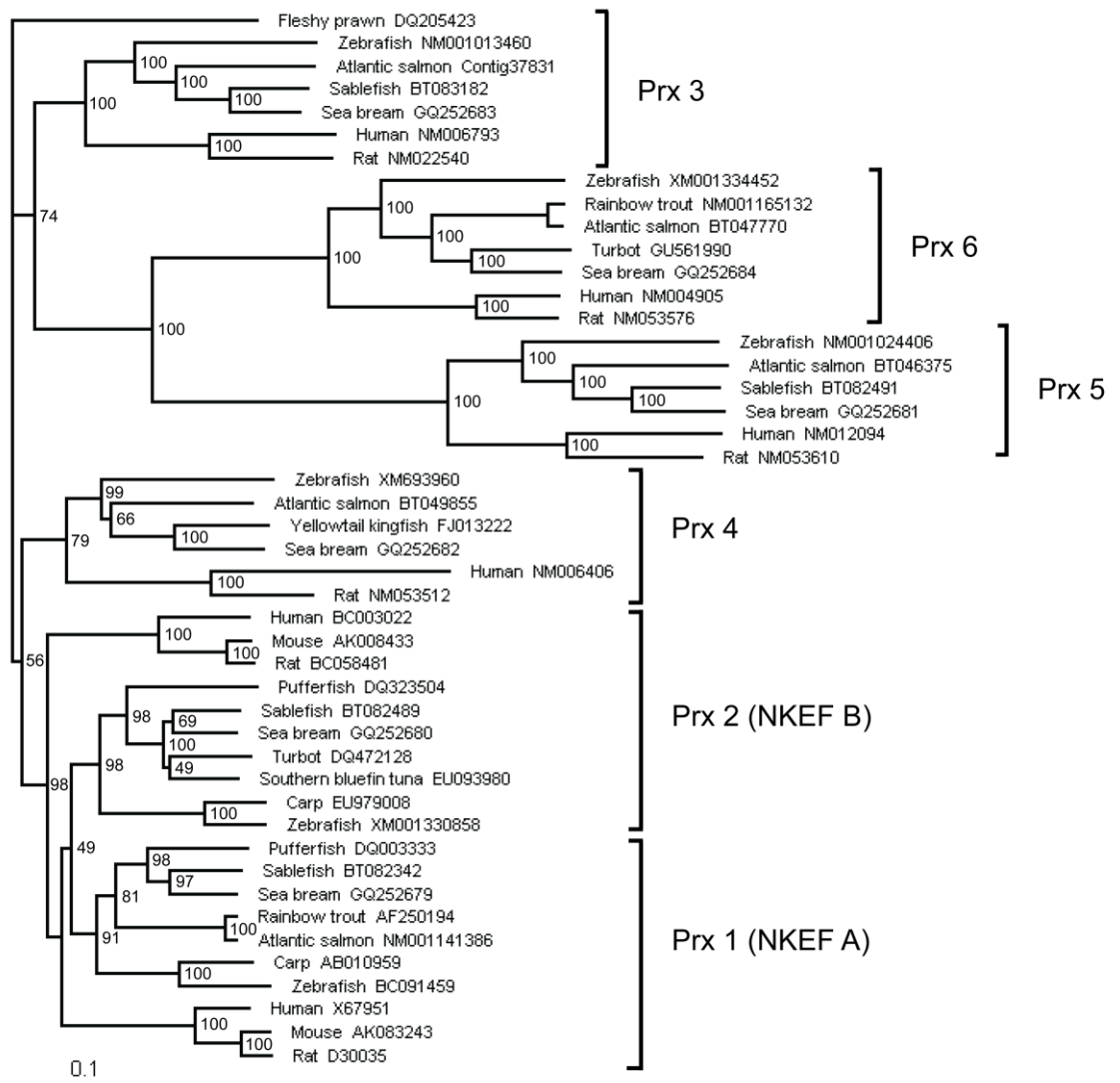
```

Pairwise comparisons of deduced amino acid sequences revealed that the AS Prx sequence was more similar to NKEF A (Prx 1) than NKEF B (Prx 2) sequences (Table 4.1). In particular the AS Prx sequence was most similar to NKEF A sequences from rainbow trout (98% identity), pufferfish (88% identity) and carp (87% identity).

**Table 4.1.** Deduced amino acid sequence identity matrix comparing the AS Prx with other members of the 2-Cys Prx family from fish, mammals and fleshy prawn. The ClustalX amino acid sequence alignment shown in Fig. 4.1 was analysed using Bioedit (Hall, 1999).

	Salmon Prx 1	Rainbow trout NKEF A	Pufferfish NKEF A	Carp NKEF A	Zebrafish NKEF A-like	Human NKEF A	Rat Prx 1	Zebrafish NKEF B-like	Pufferfish NKEF B	Turbot NKEF B	Mouse Prx 1	Mouse Prx 2	Rat Prx 2	Human NKEF B	Fleshy prawn Prx 1
Salmon Prx 1	100	98	88	87	86	82	82	82	81	79	79	76	76	75	70
Rainbow trout NKEF A		100	88	88	87	83	82	82	81	80	80	77	77	76	70
Pufferfish NKEF A			100	84	84	80	79	81	79	80	77	77	76	75	69
Carp NKEF A				100	92	83	83	80	80	77	82	76	77	76	70
Zebrafish NKEF A-like					100	81	81	80	79	77	79	76	77	77	67
Human NKEF A						100	97	80	77	79	95	76	76	77	70
Rat Prx 1							100	80	77	80	97	76	76	77	71
Zebrafish NKEF B-like								100	83	85	79	76	76	76	72
Pufferfish NKEF B									100	85	75	77	78	76	71
Turbot NKEF B										100	78	77	78	77	71
Mouse Prx 1											100	74	75	76	69
Mouse Prx 2												100	99	93	70
Rat Prx 2													100	94	70
Human NKEF B														100	71
Fleshy prawn Prx 1															100

The evolutionary relationships between the AS Prx protein and other members of the 2-Cys Prx protein family from fish and mammals were investigated (Fig. 4.2). The phylogenetic analysis produced six distinct clusters representing each of the Prx isoforms. As expected, based on the high degree of amino acid sequence identity, the AS Prx clustered together with Prx 1 (NKEF A) sequences from other finfish and mammals. As a result of the evidence outlined above the AS Prx was classified as a Prx 1 protein.



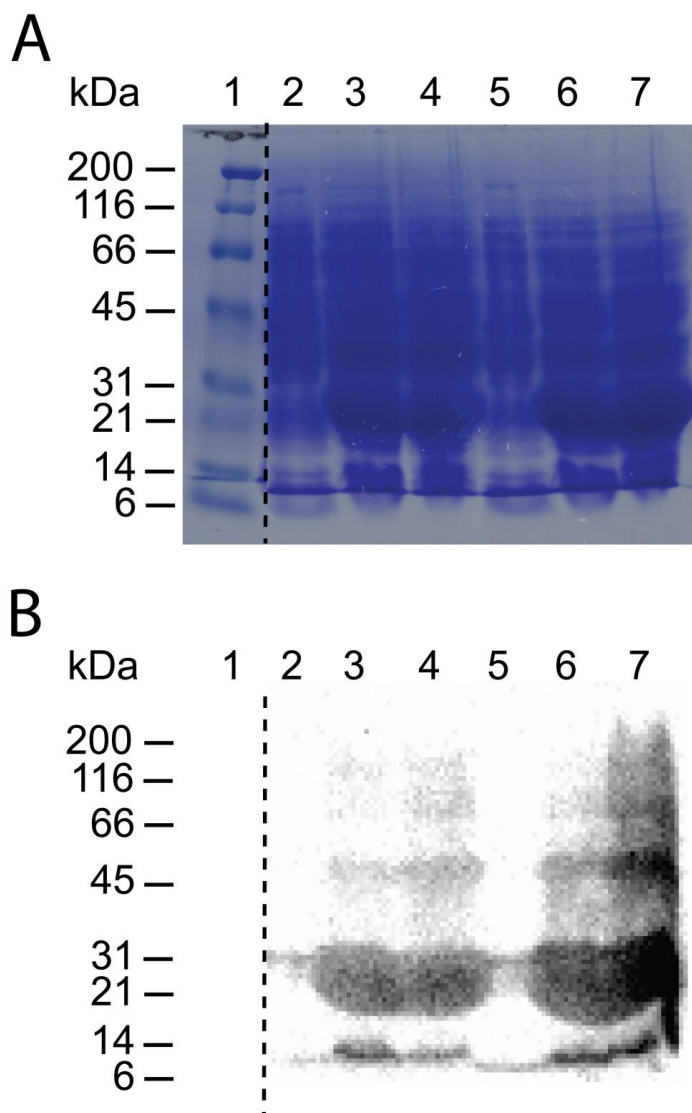
**Fig. 4.2.** A phylogenetic tree comparing Prx amino acid sequences from fish and a selection of mammals. The sequences are from the GenBank database except for the Atlantic salmon Prx 3 sequence (Contig 37831) which is from the cGRASP database. The figures at the branches of the tree are bootstrap values calculated from 1000 replicates.



### 4.3.3 Optimisation of recombinant AS Prx 1 protein expression

Whole cell protein extracts produced from un-induced, 3 h induced and 18 h induced *E. coli* BL21 (DE3) cells containing the pET-30a-AS Prx 1 construct were analysed by SDS-PAGE and immunoblotting (Fig. 4.3). The Coomassie Blue stained SDS-PAGE gel revealed that a prominent protein band of approximately 27 kDa was produced by both cell cultures after 3 h and 18 h induction. The molecular mass of this highly abundant protein was consistent with the expected size of the recombinant AS Prx 1 monomer and its putative identity was confirmed by immunoblotting with anti-His antibodies. Comparison of the intensity of the AS Prx 1 monomer band after 3 h and 18 h induction of both cell cultures revealed no difference, indicating that a maximum yield of AS Prx 1 protein was obtained after 3 h.

In addition to the 27 kDa AS Prx 1 monomer species, two additional species with approximate molecular masses of 10 and 55 kDa were detected by immunoblotting. The 10 kDa species is not consistent with any expected size of the AS Prx 1 protein and may be a degradation product or it may indicate non-specific detection by the anti-His antibodies. The size of the 55 kDa species is consistent with a dimer species of the recombinant AS Prx 1 protein. A single faint band of 27 kDa was detected in the un-induced whole cell protein extracts of both colonies. These bands are presumably the result of a background level of expression brought about by a basal level of T7 RNA polymerase activity despite the transcription of the AS Prx 1 gene being under the tight control of a T7 *lac* promoter.

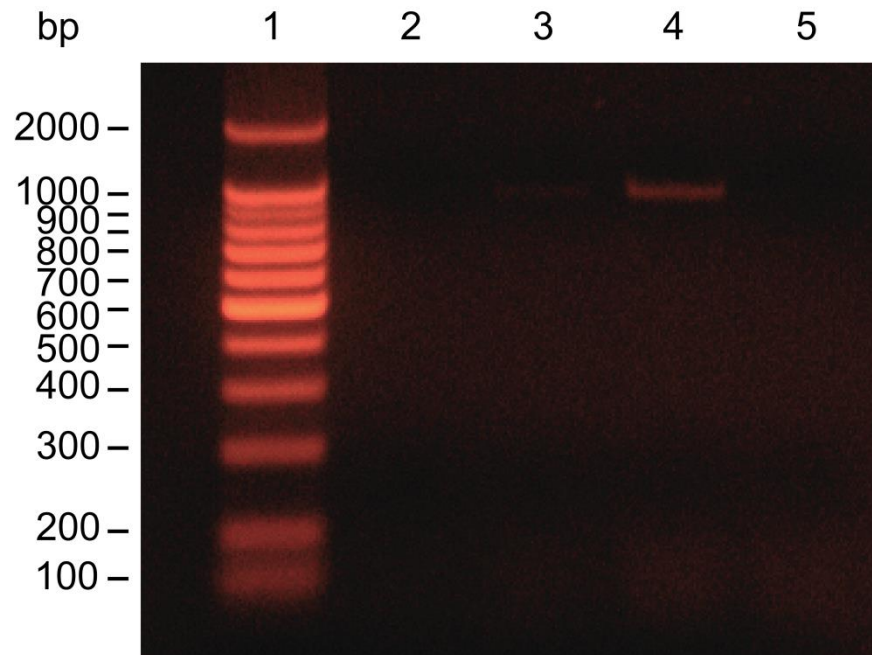


**Fig. 4.3.** Reducing SDS-PAGE (A) and immunoblotting (B) analysis of whole cell protein extracts produced from two cultures of *E.coli* BL21(DE3) cells that contained the pET-30a-AS Prx 1 construct. The immunoblotting analysis was performed with rabbit anti-6X His polyclonal antibodies (Rockland). Samples of both cell cultures were taken prior to induction, 3 h post-induction and 18 h post-induction. The immunoblotting signal was detected using a Bio-Rad® VersaDoc™ imaging system. Lane 1, molecular mass markers; Lane 2, un-induced colony 1; Lane 3, 3 h post-induction colony 1; Lane 4, 18 h post-induction colony 1; Lane 5, un-induced colony 2; Lane 6, 3 h post-induction colony 2; Lane 7, 18 h post-induction colony 2.

#### 4.3.4 Large scale recombinant expression of AS Prx 1 protein

Prior to large scale protein expression, three colonies of *E. coli* BL21 (DE3) cells were PCR screened for the pET-30a-AS Prx 1 construct. The resulting PCR screening products were analysed by agarose gel electrophoresis (Fig. 4.4).

Colonies 1 and 2 produced a faint and a prominent PCR screening product of approximately 1000 bp, respectively. The size of this PCR product is consistent with the expected size of the pET-30a multiple cloning site containing an AS Prx 1 insert. Neither the Colony 3 nor the negative control PCR screening reactions produced products.

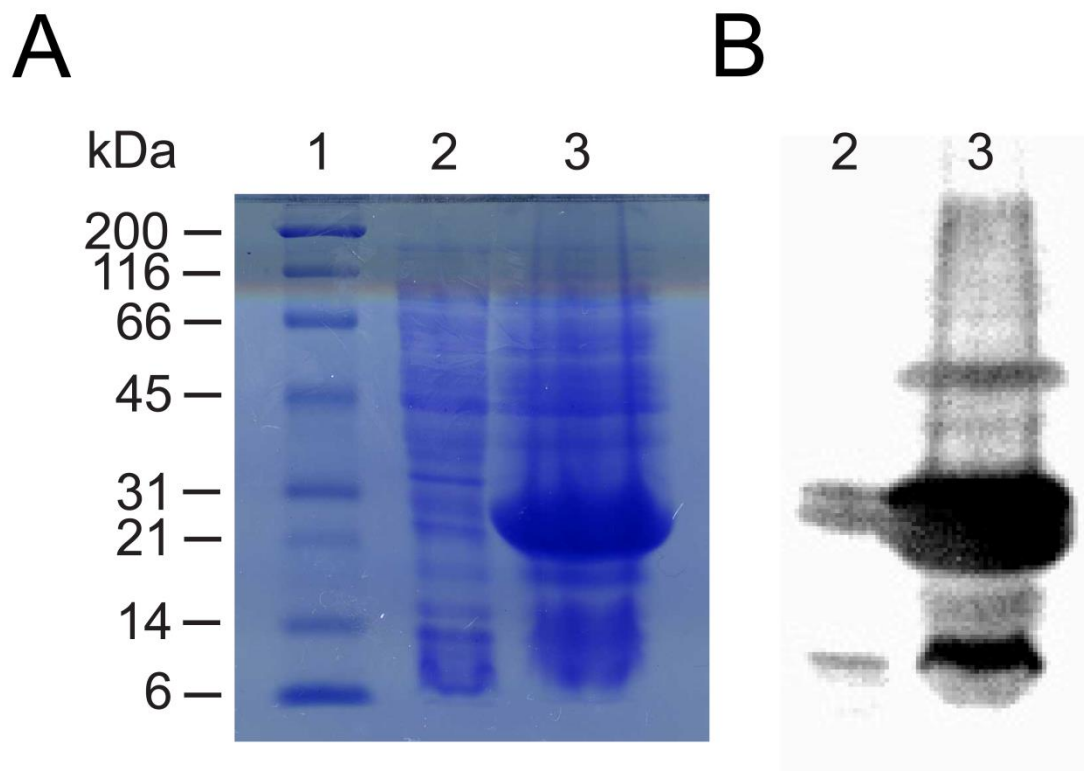


**Fig. 4.4.** Agarose gel electrophoresis of PCR colony screening products produced from three colonies of *E. coli* BL21 (DE3) cells containing the pET-30a-AS Prx 1 construct. The construct insert and flanking multiple cloning region was amplified using T7 promoter and terminator plasmid specific primers. Lane 1, DNA size standards; Lane 2, negative control PCR products; Lane 3, colony 1 PCR products; Lane 4, colony 2 PCR products; Lane 5, colony 3 PCR products.

A colony of *E. coli* BL21 (DE3) cells found to contain the pET-30a-AS Prx 1 construct was used for large scale protein expression. Whole cell protein extracts produced from un-induced and 3 h induced cultures were analysed by SDS-PAGE and immunoblotting (Fig. 4.5).

SDS-PAGE analysis of the whole cell protein extracts produced from cells that had been induced for 3 h revealed a prominent band of approximately 27 kDa. The molecular mass of the 27 kDa protein was consistent with the expected molecular mass of the AS Prx 1 monomer. Immunoblotting analysis revealed that the prominent band observed in the SDS-PAGE analysis actually consisted of two proteins with approximate molecular masses of 27 and 24 kDa. Thus, the putative identity of the 27 kDa protein species was confirmed as being His-tagged AS Prx 1 monomer in addition to identifying a 24 kDa, truncated form of the AS Prx 1 protein. A relatively low level of expression of both of these proteins was also detected in the un-induced whole cell protein extract and is presumably the result of background protein expression.

The immunoblotting analysis also detected two additional protein species with approximate molecular masses of 10 and 54 kDa. The 10 kDa species, detected in both the un-induced and 3 h induced whole cell protein extracts, is not consistent with any expected size of the AS Prx 1 protein. The 10 kDa protein may represent an AS Prx 1 degradation product or it may indicate nonspecific detection by the anti-His antibodies. The 54 kDa protein, detected only in the 3 h induced whole cell protein extract, was consistent with the expected size of an AS Prx 1 dimer.



**Fig. 4.5.** Reducing SDS-PAGE (A) and immunoblotting (B) analysis of whole cell protein extracts prepared from un-induced and 3 hour induced *E. coli* BL21 (DE3) cells containing the pET-30a-AS Prx 1 construct. The immunoblotting analysis was performed with rabbit anti-6X His polyclonal antibodies (Rockland). Lane 1, molecular mass markers; Lane 2, un-induced whole cell protein extract; Lane 3, 3 hour induced whole cell protein extract.

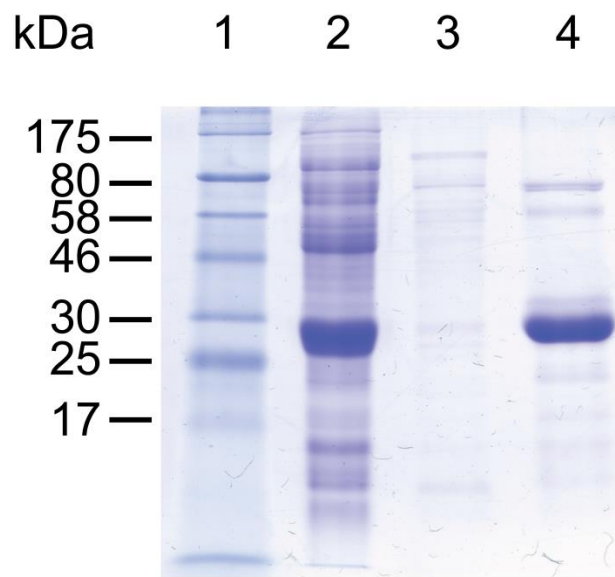
#### 4.3.5 Ni-affinity purification of AS Prx 1 protein

The recombinant AS Prx 1 protein was purified by Ni-affinity column chromatography and various fractions were analysed by SDS-PAGE and immunoblotting (Fig. 4.6). SDS-PAGE analysis revealed a prominent protein band with an approximate molecular mass of 27 kDa in the whole cell crude extract that had been purified and enriched in the 500 mM imidazole elution. Immunoblotting confirmed that the 27 kDa protein species was AS Prx 1 monomer. In addition, the immunoblotting also detected two larger forms of the AS Prx 1 protein with molecular masses of approximately 54 and 81 kDa. The molecular masses of these AS Prx 1 protein forms are consistent with dimer and trimer. Immunoblotting did not detect any of the AS Prx 1 protein forms in the combined Ni-affinity column flowthrough and 20 mM imidazole wash. This indicated that the AS Prx 1 protein was able to bind efficiently to the Ni-affinity column and remain bound for the duration of the 20 mM imidazole wash. As a result, the AS Prx 1 protein was able to be purified by Ni-affinity chromatography with high yield and enrichment.

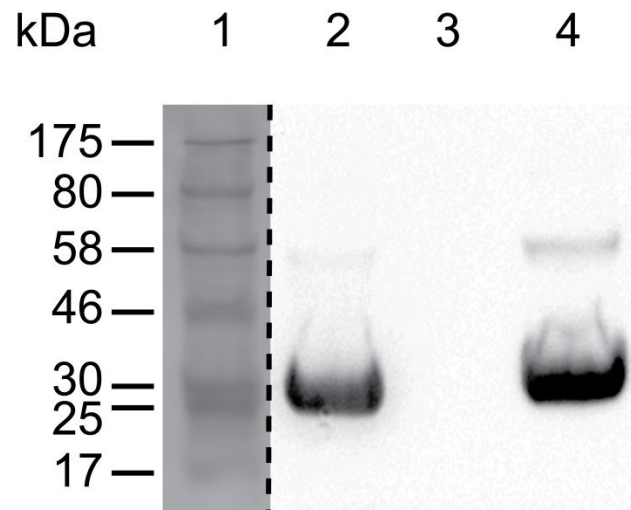
**Fig. 4.6.** Reducing SDS-PAGE (A) and immunoblotting analysis using primary anti-His antibodies (B) or anti-(southern bluefin tuna Prx 2) antibodies (C) of various fractions produced from the Ni-affinity chromatography purification of recombinant AS Prx 1. Lane 1, molecular mass markers; Lane 2, whole cell crude lysate produced from *E. coli* BL21 (DE3) cells expressing the AS Prx 1 protein; Lane 3, Ni-affinity purification, column flow-through and 20 mM imidazole wash; Lane 4, Ni-affinity purification, 500 mM imidazole elution.



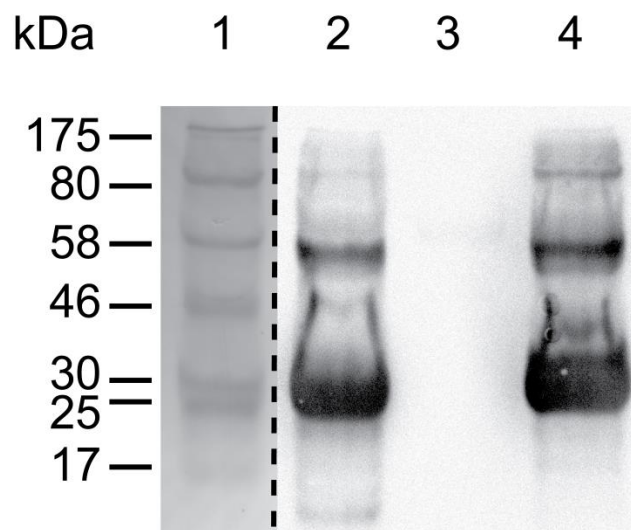
**A**



**B**



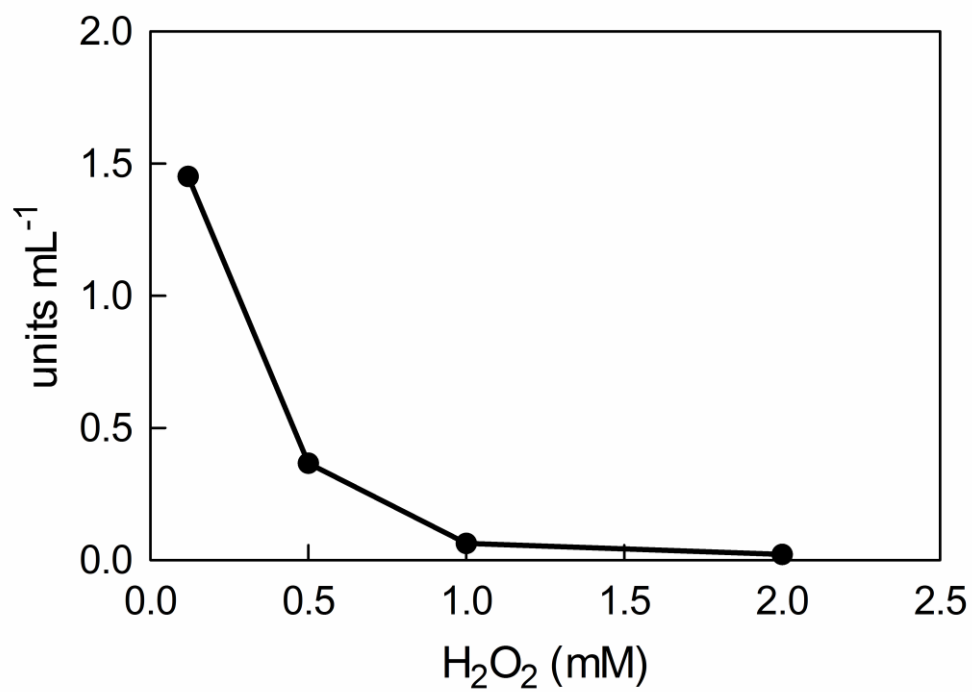
**C**



Immediately following Ni-affinity purification, the AS Prx 1 protein was exchanged into a buffer containing 20 mM Tris-base (pH 7.5), 150 mM NaCl and 5 mM dithiothreitol (DTT). The buffer exchange resulted in the formation of a milky white precipitate, presumably composed of the AS Prx 1 protein. To promote re-solubilisation of the precipitate, ~ 250  $\mu$ L aliquots of 1 M NaCl were added to the buffer exchanged AS Prx 1 solution. After each NaCl addition, the protein solution was mixed by inversion and incubated on ice for 5 min. After a total of 2.44 mL of 1 M NaCl had been added, giving a final concentration of 450 mM NaCl, the precipitate in the AS Prx 1 protein solution had been re-solubilised. As a result the standard AS Prx 1 exchange buffer became 20 mM Tris-base (pH 7.5), 450 mM NaCl and 5 mM DTT.

#### 4.3.6 AS Prx 1 kinetics

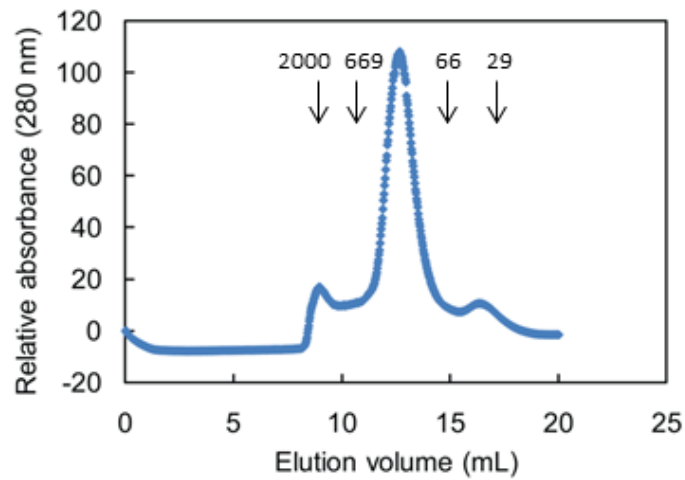
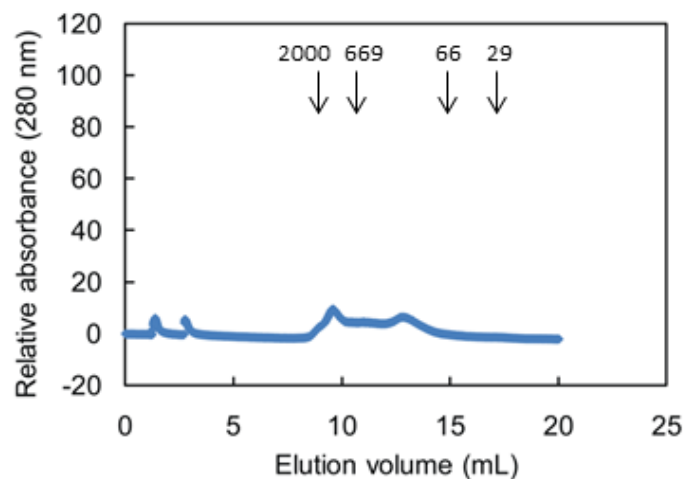
The effect of peroxide substrate at mM concentrations on Trx-dependent peroxidase activity of AS Prx 1 protein was investigated (Fig. 4.7). The Trx-dependent peroxidase activity of AS Prx 1 protein was progressively lost as the peroxide concentration was increased into the mM range (0.12-2.0 mM).



**Fig. 4.7.** Effect of high H<sub>2</sub>O<sub>2</sub> concentrations (0.12-2.0 mM) on Trx-dependent peroxidase activity of Ni-affinity purified AS Prx 1 protein. The Prx assays were performed as outlined in Section 2.15 except that the peroxide substrate concentration was varied. The AS Prx 1 protein concentration in the assay was 10  $\mu\text{g mL}^{-1}$ .

#### 4.3.7 Gel filtration chromatography of AS Prx 1 protein

The native molecular mass of Ni-affinity purified AS Prx 1 protein was investigated using gel filtration chromatography under reducing and oxidising conditions (Fig. 4.8). Under reducing conditions, AS Prx 1 protein was found to exist predominantly as a 244 kDa oligomer. The molecular mass of this AS Prx 1 protein form is consistent with decamer. In addition to decamer, two far less abundant AS Prx 1 protein forms were observed in the void volume and at an elution volume corresponding to a molecular mass of 46 kDa. The protein in the void volume was very large and was not consistent with the expected molecular mass of any known AS Prx 1 form while the 46 kDa species was consistent with the expected molecular mass of an AS Prx 1 dimer. In contrast, under oxidising conditions only two minor peaks of AS Prx 1 protein were observed in the void volume and at an elution volume corresponding to decamer. The heights of the protein peaks obtained for the oxidising gel filtration analysis were approximately an order of magnitude smaller than those obtained for the reducing gel filtration analysis, suggesting that only a tenth of the oxidised AS Prx 1 protein was able to enter the gel filtration column. Upon completion of the oxidising gel filtration run, the residual AS Prx 1 protein remaining in the tip of the loading syringe was inspected and found to contain a white precipitate. This indicated that in the absence of reducing agent, the AS Prx 1 protein was destabilised, leading to the formation of an insoluble aggregate that was not able to pass through the pre-gel filtration column filters.

**A****B**






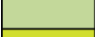





**Fig. 4.8.** Effect of reducing (A) and oxidising (B) conditions on the native molecular mass of Ni-affinity purified AS Prx 1 protein. The AS Prx 1 protein was purified by Ni-affinity chromatography, concentrated and desalted into a buffer containing 20 mM Tris-base (pH 7.5), 450 mM NaCl and 5 mM DTT for reducing gel filtration analysis or the same buffer except that it lacked DTT for oxidising gel filtration analysis, giving a final protein concentration of  $10 \text{ mg mL}^{-1}$ . The buffer exchanged protein ( $200 \mu\text{L}$ ) was loaded onto a gel filtration column that had been equilibrated with the same buffer. The arrows indicate the elution positions of the molecular mass standards (kDa).

## 4.3.8 Crystallisation of AS Prx 1 protein

### 4.3.8.1 Identification of crystallisation conditions

Crystallisation conditions for the gel filtration chromatography purified AS Prx 1 protein were screened for in a small scale format using the Hampton Research Crystal Screen and Crystal Screen 2 and Qiagen® Nextal® Classic, PEG and MPD Suite crystallisation solutions (Table 4.2). After two days the majority of the crystallisation drops were clear or contained light precipitation indicating that the protein concentration chosen was appropriate. At this early stage, no crystallisation phenomena were observed in the crystallisation drops. Seven days post setup, the phenomena observed in the crystallisation drops was more complex and included some crystalline objects. Of the seven crystallisation drops containing crystalline objects, six contained ( $\pm$ )-2-Methyl-2,4-pentanediol (MPD) and one contained  $(\text{NH}_4)_2\text{SO}_4$  as the precipitant. Sixteen days post setup, 3 additional crystallisation drops were observed to contain crystalline objects all of which contained MPD as the precipitant. The concentration of MPD in these crystallisation conditions was less compared to the promising MPD containing crystallisation conditions identified in the 7 days post-setup observations. Therefore, it was clear from the small scale crystallisation trial that MPD was the most promising crystallisation precipitant.

**Table 4.2.** AS Prx 1 protein small scale crystallisation trial observations at 2 (A), 7 (B), and 16 (C) days post-setup using the Hampton Research Crystal Screen and Crystal Screen 2 (1) and Qiagen® Nextal® Classic (2), MPD (3) and PEG (4) crystallisation solution suites (refer to Appendix for composition tables). AS Prx 1 protein was purified by Ni-affinity chromatography followed by gel filtration chromatography. The purified AS Prx 1 protein, in a buffer composed of 20 mM Tris-base (pH 7.5), 450 mM NaCl and 10 mM DTT, was concentrated to 7.5 mg mL<sup>-1</sup>. Crystallisation drops contained 0.4 µL of AS Prx 1 protein, 0.1 µL of 20 mM Tris-base (pH 7.5) and 40 mM DTT and 0.3 µL of crystallisation solution. The crystallisation drop phenomena observed are indicated according to colour while the letter code gives more detail on the specific nature of the observed phenomenon.

	0	clear
	1	heavy precipitate
	2	medium Precipitate
	3	light precipitate
	4	Micro Crystals
	5	
	6	Needle Clusters / Plates
	7	
	8	Misformed Single Crystals
	9	
	10	Single Well Formed Crystals

C	Clear
H	Heavy Precipitate
M	Medium Precipitate
L	Light Precipitate
S	Skin
Ph	Phase Separation
P	Plate
m	Micro-crystals
f	faint
nc	Needle Cluster
n	Needle
r	Rod
v	Very
s	Small
l	Large
mf	Mis-formed

# A

## 1

	1	2	3	4	5	6	7	8	9	10	11	12
A	L	c	c	MH	L	vL	M	L-moon	C/m?	MH	C	M-moon
B	vL	c	vL/m?	C/m?	C	M	L/M-moon	L/M	MH	C/pocket M	C	H
C	M	vL	H	MH	L/M	L	vL	C/fbre	vL	MH	C	C
D	vL	m?/C	MH	M	L-chunky	m?/C	C	L	M	H	M	C/m?
E	L	L	L/M	C	C	L	C	C	C	L	M	vL
F	L	L/M	L/M	C/m?	C	C	L	C	C	C	C	C
G	c	c	L-chunky	c	c	c	c	c	c	L-chunky	L chunky	CvL
H	spray	spray	spray	spray	spray	spray	spray	spray	spray	mf	C	vL

## 2

	1	2	3	4	5	6	7	8	9	10	11	12
A	Lb	Cb	c	L	L	L/M	L/M	L/M	L/M	L/M	L/M	L/M
B	Lb	C/L/m?	L	L	L	L	L	L	vL	L	L	L/M
C	CL	C/L/m?	C/L/m?	L-chunky	Lb	C	L	spray-vL	spray-vL	spray-vL	spray-vL	spray-vL
D	spray	spray	spray	spray	spray/C	spray/C	spray/C	spray/C	spray/C	spray/C	spray/C/m?	spray-vL
E	L	spray/C	spray/vL	spray/vL	spray/vL	spray/vL	spray/vL	spray	spray	spray	spray	spray
F	CL	CvL	C	C	L	L/M	L/M	C/b/mf	spray	spray	spray	spray
G	M	vL	L/M	C/mf	C/mf	C/mf	C/mf	C/b/mf	C/b/mf	spray	L/b/mf	spray
H	C/b/o	C/b/o	C/b/o	spray	spray	spray	spray	spray	spray	spray	spray	spray

## 3

	1	2	3	4	5	6	7	8	9	10	11	12
A	L/M-moon	vL	c	vL	L	vL	L	L	L	L	L	L
B	L	vL	L	L	vL	CvL	L	MH	L	L	L	L/M
C	L	vL/m?	L	L/M	L	vL	L	C	C	H	L	vL
D	spray	spray	spray	spray	vL	vL	vL	Cb	C	vL	L	C
E	spray	spray	Cb	C	C	C	CvL	MH	vL	C	C	C
F	spray L/m?	spray L/m?	spray L	spray L	spray L	Lb	Lb	L	L	L	L	L
G	spray	spray	spray	spray	spray	spray	spray	spray	spray	spray	spray	spray
H	spray	spray	spray	spray	spray	spray	spray	spray	spray	spray	spray	spray

## 4

	1	2	3	4	5	6	7	8	9	10	11	12
A	Lb	Lb	Lb	Lb	L	vL/b	Cb	Cb	Cb	Cb	Cb	vL/b
B	C/mf	C/mf	C/mf	C/mf	C/m?	C/m?	C/mf	C/mf	C/mf	C/mf	C/mf	CvL
C	L	L	L	L/mf	L/mf	vL	CvL	CvL	CvL	CvL	1x L Rod?	CvL/mf
D	C/L/mf	C/L/mf	C/L/mf	C/L/mf	C/L/mf	C/L/mf	CvL	CvL	CvL	CvL	CvL	CvL
E	C/mf	C/mf	CvL	C/L-chunky	vL/b	vL/b	vL/b	Cb	Cb	Cb	Cb	Cb
F	spray	spray	spray	spray	spray	spray	spray	spray	spray	spray	spray	spray
G	spray	spray-L-moon	spray-L-moon	spray-L-moon	spray-L-moon	bo?	L/mf	L/mf/b	L/mf/b	L/b/n?	Lb	Cb
H	spray	spray	spray	spray	spray/L	spray/m?	Cb?	C	Cb	C	C	C



# B

1

	1	2	3	4	5	6	7	8	9	10	11	12
A	L/Mb	C/m?	vL	H chunky	L	L	L/M	L-moon	CvL	H	C	L/M-moon
B	L	C	vL	C	C	M	L-moon	MH	M	vL/patchy MH	C/m?	H
C	L/M	M	H	MH	MH	L	L	C/fibre	CvL	M	C	vL/b
D	L	vL	H chunky	H	L/M chunky	C/m?	C	L	MH	MH	M	C
E	L	L	L/M	CvL	C	vL	L	L-moon	C	C	L/M	L
F	L	L/M	L/M	crystals	C	C	vL	C/m?	vL	C	C	vL/mf
G	C	C	L/m needles?	C	C	C/vL/m?	vL	C	C	L-chunky	L-chunky	C/m needles?
H	spray	spray	spray	spray	spray	spray	spray	spray	vL	spray/mf	C-spray	spray/d

2

	1	2	3	4	5	6	7	8	9	10	11	12
A	L/b	vL	CvL	L	L	L/M	L/M	L/M	L/M	L/M	H	L
B	L/M	C/mf	L	L	L	L	L	L	L	Rods	L	L/M
C	C/L/m?	C/mf	C/mf	L/m?/b	L/b	C/b	L	spray/C	spray/L/m?	spray/C	spray/C	spray/vL
D	spray/C	spray/vL	spray/C	CvL	C	spray/C/b	C/b	spray/C	C/b	spray/C	spray/vL	spray/vL
E	spray/L/M	spray/vL	spray/vL	spray/vL	spray/C	vL	d?	spray/vL	spray/C	spray/vL	spray/C	spray
F	C/mf	C	C	C	C	C	L/M	C/mf/b	spray/vL	spray/vL	spray/C	spray/L
G	L chunky	vL/mf	L	C/mf	C/mf	C/mf	C/mf	vL/b/mf	vL/b/mf	spray	spray/L/b/mf	spray/C
H	spray/b/Ph	spray/b/Ph	spray/b/Ph	spray/C	spray	spray/C	spray/vL	spray/C	spray/C	spray/C	spray/C	spray/C

3

	1	2	3	4	5	6	7	8	9	10	11	12
A	L-moon	L	L	L	L	L	L	L	L	L	L	L
B	L	L	L	L	L	L	L	L/M	L	L	L	L
C	L	L/fibre	L/M	L/M	L	L	L	vL	L	H	L	L
D	spray	spray	spray/vL	spray/vL	vL/b	vL	vL	vL/b	vL	vL	vL	C
E	spray	spray	C/b	CvL/b	C	C	vL	H	L/m?/b	vL	C	C
F	m?	m?	m?	vL	vL	vL/b	vL/b	L/b	Rods	Rods	Rods	Rods
G	spray/C	spray	spray/C	spray/C	spray/C	spray/C	spray/C	spray/C	spray/C	spray/C	spray/C	spray/C
H	spray/C	spray/C	spray/C	spray/C	spray/C	spray/C	spray/C	spray/C	spray/vL	spray/C	spray/C	spray/C

4

	1	2	3	4	5	6	7	8	9	10	11	12
A	L/b	L/b	L/b	L/b	L	L/b	L/b	L/b/mf	L/b	C/b	CvL/b	C/b
B	C/mf	C/mf	C/mf/rods?	C/mf/ Rods	C/mf?	C/mf?	C/mf?	C/mf?	C/mf	CvL	C/b	CvL/b
C	L	L	L	L	L	L	L/M	L/fibre	C/mf	CvL	CvL/1xRod?	vL/mf
D	C/mf/f	C/mf/f	C/mf	C/mf	C/mf	C/mf	vL	CvL	C/L/mf	CvL	CvL	vL
E	L	L chunky	L	L	L/mf-b	L/m?	L	b-mf	C/b-mf	C/b-mf	C/b-mf	L/C/b-mf
F	spray	spray	spray	spray	spray	spray	spray	spray	spray	spray	spray	spray
G	spray	spray/L-moon	spray/L-moon	spray	b-o?	L/b-plate?	L/b	L/b	L/b/straw s	L/b/mf	C/L/b/mf	Cb
H	spray	spray/C	spray/L	CvL	spray/L	spray/C	C/b	C	C/b/mf	C	C	C

C

1

	1	2	3	4	5	6	7	8	9	10	11	12
A	L/b	c	vL	L/M	L	L	L/M	L/M	c	H	c	L/M-moon
B	L/M	c	vL	c	vL	M	L/M-moon	M	H	L/patch M	c	H
C	L/M	MH	H	L/M	M	vL	vL	C/fibre	vL	M	c	vL/mf
D	vL	vL	MH	H	M	c	vL	L	M	MH	L/M	c
E	L	L	L/M	vL	c	L	L	Cf needles?	c	L/M	L/M	L/M
F	L	L/M	L/M	c	c	c	L-moon	L	L	c	c	vL/mf
G	c	c	L	c	c	c	L/Rods-tw in	c	c	L	L	vL
H	spray	spray	spray	spray	spray	spray	spray	spray	vL	L/mf	c	d

2

	1	2	3	4	5	6	7	8	9	10	11	12
A	M/b	L/b	c	L/mf	L/Mmf	M	L/M	L/M	L/M	M	MH	L/M
B	H	vL	M	M	L/M	L/M	L	L	L/m needle	vL Rods	L	MH
C	L chunky	C/mf	C/mf	L chunky	L/b	vL/b	L	c	L	c	vL	vL
D	c	c	c	vL/mf	C/b	c	C/b	c	C/mf	vL	vL	c
E	L/M	c	c	vL	c	vL-moon	L-moonish	L	c	vL	c	spray
F	c	c	c	C/mf	L	L/Mmf	L	vL/mf	c	c	c	vL
G	M	vL/mf	M	C/mf	C/mf	C/mf	C/mf	C/mf/b?	C/mf/b	vL	L/mf/b	C/spray
H	C/b/Ph	C/b/Ph	C/b/Ph	spray/C	spray	spray/C	spray/vL	spray/C	spray/C	spray/C	spray/C	spray/C

3

	1	2	3	4	5	6	7	8	9	10	11	12
A	L/M	vL	vL/L	vL	vL	vL	vL	vL	L/M	vL	vL	L
B	L	vL/L	L	L	vL	vL	L	M	vL	L	L	L
C	L	vL	L/M	L/M	vL	L	s Rods/needles	vL	vL	H	L	vL
D	vL-spray	vL-spray	vL/m?	vL-spray	vL/b	vL	vL	vL/mf	vL	vL	vL/s Rods?	vL
E	vL-spray	C-spray	C-spray	vL	c	c	H	H	L	L	MH	CvL
F	m?	vL/m?	L/m?	vL	vL	vL	vL/b	vL/b	vL/s Rods	vL/s Rods	vL/s Rods	vL/s Rods
G	C-spray	C-spray	C-spray	C-spray	C-spray	C-spray	C-spray	C-spray	C-spray	C-spray	C-spray	C-spray
H	C-spray	C-spray	C-spray	C-spray	C-spray	C-spray	C-spray	C-spray	C-spray	C-spray	C-spray	C-spray

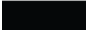










4

	1	2	3	4	5	6	7	8	9	10	11	12
A	L/b	L/b	L/b	L/b	L	vL/b	L/b	C/mf	C/mf	C/mf	C/mf	C/mf
B	C/mf	C/mf	C/mf	C/mf	C/mf	C/mf	C/mf	C/mf	C/mf	C/mf	C/mf	C/mf
C	L	L	L	L	L	L	L/M	L/mf	C/mf	C/mf	L/M	C/mf
D	C/mf	vL/mf	vL/mf	C/mf	L/M	M	L	vL	C/mf	C/mf	vL	C/mf
E	L/mf	L/mf	C/mf	L	L/mf	L/mf	L/mf	C/mf	C/mf	C/mf	C/mf	C/mf
F	C/spray	C/spray	C/spray	C/spray	C/spray	C/spray	C/spray	C/spray	C/spray	C/spray	C/spray	vL
G	C/spray	L-moon/spray	C/spray	C/spray	C/spray	L/b	vL/mf	vL/mf	L/mf	C/mf	L/mf	C/mf
H	C/spray	C/spray	vL/spray	vL/spray	vL/spray/mf	vL/L	vL	c	C/mf	c	C/mf	c

#### 4.3.8.2 Up-scaling and optimisation of crystallisation conditions

Based on the most promising small scale crystallisation conditions identified in Section 4.3.8.1, a large scale crystallisation trial was set up in which the concentrations of MPD and AS Prx 1 protein were systematically varied (Table 4.3). One day post setup, the crystallisation drops were observed and found to contain varying degrees of light precipitation with some evidence of micro-crystalline objects in the crystallisation conditions containing ~65% (v/v) MPD in combination with all of the AS Prx 1 protein concentrations tested. These observations remained essentially unchanged at 6 and 12 days post setup. However, at 6 days post setup, crystallisation drops composed of ~60-62.5% (v/v) MPD in combination with all of the AS Prx 1 protein concentrations tested were found to contain small individual rod-shaped crystals. The size and morphology of the crystals appeared to be related to both the MPD and AS Prx 1 protein concentrations. The formation of larger crystals with more clearly defined edges was favoured by the relatively lower concentrations of MPD and AS Prx 1 protein. Conversely, the relatively higher concentrations of MPD and AS Prx 1 protein favoured the formation of smaller crystals with less defined edges. Ultimately, the largest crystals with the most defined edges were observed at 16 days post setup in crystallisation drops composed of 57.5% (v/v) MPD and 10 mg mL<sup>-1</sup> AS Prx 1 protein. Therefore, the promising small scale crystallisation conditions identified in Section 4.3.8.1 were able to be successfully up-scaled and the quality of the crystals produced improved upon using large scale crystallisation. Despite the significant increase in the size of the crystals produced, they were still considered to be too small for X-ray crystallography analysis.

**Table 4.3.** AS Prx 1 protein large scale crystallisation trial observations at 1 (A), 6 (B) and 12 (C) days post setup. AS Prx 1 protein was purified by Ni-affinity chromatography followed by gel filtration chromatography. The purified AS Prx 1 protein, in a buffer composed of 20 mM Tris-base (pH 7.5), 450 mM NaCl and 10 mM DTT, was concentrated to 10 mg mL<sup>-1</sup>. The crystallisation drops contained 4 µL of purified AS Prx 1 protein decamer at a concentration of 5-10 mg mL<sup>-1</sup> in 2.5 mg mL<sup>-1</sup> increments, 1 µL of 20 mM Tris-base (pH 7.5) and 40 mM DTT and 3 µL of crystallisation solution containing 0.1 M Bicine (pH 9) and 57.5-70 % (v/v) MPD in 2.5 % (v/v) increments. The crystallisation drop phenomena observed are indicated according to colour while the letter code gives more detail on the specific nature of the observed phenomenon.

	0	clear
	1	heavy precipitate
	2	medium Precipitate
	3	light precipitate
	4	Micro Crystals
	5	
	6	Needle Clusters / Plates
	7	
	8	Misformed Single Crystals
	9	
	10	Single Well Formed Crystals

C	Clear
H	Heavy Precipitate
M	Medium Precipitate
L	Light Precipitate
S	Skin
Ph	Phase Separation
P	Plate
m	Micro-crystals
f	faint
nc	Needle Cluster
n	Needle
r	Rod
v	Very
s	Small
l	Large
mf	Mis-formed

A

		MPD% (v/v)					
		57.5	60.0	62.5	65.0	67.5	70.0
Protein (mg mL <sup>-1</sup> )	5.0	L	L/O	L/O	vL/m	vL/m	vL/m?
	5.0	L/O/1kr?	L/O	L/O	vL/m	vL/m	vL
	7.5	L/O	L/O	L/O	L/m	L/O/m?	L/m?
	7.5	L/mf	L	L/mf	L/m	L/m	L/m?
	10.0	L	L/O	L/O	L/O/m	L/m?	L
	10.0	L	L/O	L/O	L/m	L/m?	L/m?

B

		MPD% (v/v)					
		57.5	60.0	62.5	65.0	67.5	70.0
Protein (mg mL <sup>-1</sup> )	5.0	L	Lr (15x30)	s r	m	m	L
	5.0	L/O/1kr?	m	s r	m	m	L
	7.5	L/O	L/m im m . R	s r	vs r/m	m/O	L/O/m?
	7.5	L/mf	Lr (15x30)	s r	vs r/m	m?	L/O/m?
	10.0	s im m . R	f im m . r/O	s/m r	m	m?/O	m?/O
	10.0	?	f im m . r/O	s/m r	m	m?/O	m?/O

C

		MPD% (v/v)					
		57.5	60.0	62.5	65.0	67.5	70.0
Protein (mg mL <sup>-1</sup> )	5.0	L/s r	L/nc/s r	L/s-m r	L/m	Lm?	L
	5.0	L/s r (mf)	L/m	L/s-m r/o	L/m	Lm?	L
	7.5	m r+s r twin	f im m . r	L/vs-m r	L/m	L/m?	L
	7.5	L/s-m f r	L/l r	L/vs-m r	L/m	L/m?	L
	10.0	L/l r	f im m . r	L/m	m	m?	L
	10.0	L/l r	f im m . r	L/vs-m r	m	L	L

## 4.4 Discussion

In the absence of an Atlantic salmon Prx nucleotide sequence in GenBank to make comparisons to the pET-30a-AS Prx insert, a putative AS Prx nucleotide sequence was used as a query in a BLAST search of the *Salmo salar* expressed sequence tag (EST) cluster database available at the consortium for Genomics Research on All Salmon website (<http://web.uvic.ca/grasp/>). The BLAST search returned two contigs annotated as Prxs, contigs 38678 and 29851, that shared  $\geq 99\%$  nucleotide identity to the pET-30a-AS Prx insert sequence. A nucleotide sequence alignment revealed that the pET-30a-AS Prx insert and contig 38678 were identical except for a single nucleotide mismatch. Similarly the nucleotide sequences of the pET-30a-AS Prx insert and contig 29851 were found to be identical except that the contig 29851 possessed a 3' nucleotide extension. Both contigs may be derived from AS Prx genes with the observed differences in sequence a result of the evolutionary divergence between separate populations of the same species. The single nucleotide mismatch between the nucleotide sequences of the pET-30a-AS Prx insert and contig 38678 was not believed to be the result of a mutation in the insert sequence but rather the result of either a single nucleotide polymorphism in the AS Prx coding sequence or a miscalled nucleotide in the sequencing of the ESTs corresponding to contig 38678. Evidence for this comes from the fact that contig 29851 contained the same nucleotide as the pET-30a-AS Prx insert at this position. Therefore, the pET-30a-AS Prx construct was found to contain a putative 2-Cys Prx ORF that was mutation free, in frame relative to the start site for translation and in the correct orientation.

The alignment of the predicted AS Prx protein sequence with other members of the 2-Cys Prx family from other fish and mammals revealed that it contained two highly conserved 'VCP' motifs containing the peroxidatic and resolving Cys residues

characteristic of 2-Cys Prx proteins. The 'VCP' motifs and their associated peroxidatic and resolving Cys residues were found to be embedded within the highly conserved F-motif (FTFVVCPTEI) and adjacent to a highly conserved hydrophobic region (VCPAGW), respectively. Pairwise comparisons and phylogenetic analyses of the deduced amino acid sequences for fish and mammalian Prxs revealed that the AS Prx should be classified as a Prx 1.

The AS Prx 1 was able to be recombinantly expressed on a large scale in the *E. coli* (BL21) expression host as three distinct proteins with molecular masses of approximately 24, 27 and 54 kDa. It needs to be acknowledged that the identification of the three AS Prx 1 protein forms based on anti-His antibody reactivity is only provisional without confirmation by mass spectrometry. The molecular masses of the 27 and 54 kDa AS Prx 1 proteins correspond to monomer and dimer sizes. However, the molecular mass of the 24 kDa protein did not correspond to any expected AS Prx 1 protein form. Similarly, recombinant Prx 1 protein from *Plasmodium falciparum* (PfTPx1) was found to exist as two different forms with molecular masses of ~25 and ~23 kDa when stored for > 1 week or purified in the absence of DTT (Rahlfs and Becker, 2001). The larger ~25 kDa protein corresponded to PfTPx1 monomer while the smaller ~23 kDa protein did not correspond to any expected PfTPx1 protein form. Despite this, the smaller and most likely oxidised PfTPx1 protein displayed antioxidant activity but the pH optimum for the reaction shifted from 7.2 to 8.0 and the approximated  $K_m$  values for  $H_2O_2$ , t-Butylhydroperoxide and cumene hydroperoxide increased by a factor of 5 compared to the larger PfTPx1 protein. As a result of its stability and activity, it was speculated that the smaller PfTPx-1 protein could be part of a regulatory process that has relevance *in vivo*. It was proposed that the smaller PfTPx-1 protein might be produced by an intramolecular reaction or partial degradation of the larger PfTPx1 protein. Therefore, based on this proposal, the smaller and most likely oxidised 24

kDa AS Prx 1 protein might be produced from an intramolecular reaction or partial degradation of the larger 27 kDa AS Prx 1 protein. If the 24 kDa AS Prx 1 protein was produced by partial degradation of the 27 kDa AS Prx 1 protein, then the degradation must have occurred at the C-terminus because the N-terminus (containing the His-tag) of the 24 kDa AS Prx 1 protein remained intact as evidenced by its detection in immunoblotting experiments.

Analysis of the alignment of the AS Prx 1 protein with other members of the 2-Cys Prx protein family from fish and mammals revealed that it contained the highly conserved GGLG motif (residues 95-98, solid underlining in Fig. 4.1) and XF motif (residues 194-195, broken underlining in Fig. 4.1). These motifs confer sensitivity which is defined as a loss of peroxidase activity at milli-molar concentrations of peroxide. Sensitivity occurs as a result of these motifs slowing the intermolecular disulphide bond formation between the peroxidatic Cys that has accepted a peroxide substrate (Cys-S<sub>P</sub>OH) and the resolving Cys (Cys-S<sub>R</sub>H) (Wood et al., 2003a). The slowing of this bond formation makes the Cys-S<sub>P</sub>OH longer lived and thus more susceptible to attack by a second peroxide substrate. In the event that Cys-S<sub>P</sub>OH is attacked by a second peroxide substrate, it is further oxidised to Cys-S<sub>P</sub>O<sub>2</sub>H. In this over-oxidised state the peroxidatic Cys is unable to be reduced by thioredoxin preventing participation in future rounds of catalysis. However, in the presence of a sulphiredoxin protein the over-oxidised peroxidatic Cys can be reduced back to Cys-S<sub>P</sub>OH. Subsequently, Cys-S<sub>P</sub>OH can be reduced by thioredoxin, restoring catalytic function (Biteau et al. 2003). As was expected for a Prx protein containing both the GGLG and XF motifs, the response of Ni-affinity purified AS Prx 1 protein to increasing peroxide concentrations in the range 0.12-2.0 mM was found to be a decrease in peroxidase activity. Thus, the AS Prx 1 protein was classified as a sensitive 2-Cys Prx. Interestingly the XF motif of the AS Prx 1 protein consists of an FF motif, a characteristic shared with the majority of fish 2-Cys



Prx proteins, whereas the XF motif of mammal Prx proteins consists of a YF motif. In humans, the Prx 1 protein has been shown to be sensitive to concentrations of peroxide in the range 0.2-2.0 mM (Lee et al., 2007). Therefore, not only are the FF and YF motifs functionally equivalent they also confer the same degree of sensitivity. This is not surprising given that both phenylalanine (F) and tyrosine (Y) are aromatic amino acids with the only difference being a hydroxyl group.

Investigation into the native molecular mass of the AS Prx 1 protein using gel filtration chromatography revealed that it undergoes dramatic structural changes in response to changes in redox state. Under reducing conditions, the AS Prx 1 protein was found to exist essentially as a single oligomeric form with a molecular mass corresponding to a decamer. This result is consistent with previous gel filtration chromatography analyses of human and rat Prx 1 proteins in which reducing conditions were also found to favour a single oligomeric form with a molecular mass corresponding to a decamer (Lee et al., 2007, Matsumura et al., 2008). The decamer form of typical 2-Cys Prx proteins is favoured under reducing conditions due to stabilisation of the dimer-dimer interface. Stabilisation of the dimer-dimer interface occurs as a result of the loop-helix motif containing the peroxidatic Cys residue adopting a folded conformation (Wood et al., 2002). Under oxidising conditions, the AS Prx 1 protein was destabilised resulting in the formation of insoluble aggregates. In contrast, the response of other Prx 1 proteins to oxidising conditions is complex but does not involve the formation of insoluble aggregates. Under oxidising conditions, the Prx 1 protein from rat preferentially formed decamers at relatively high protein concentrations while it tended to dissociate into tetramers and dimers at relatively low protein concentrations (Matsumura et al., 2008). The basis for these observations, as with those under reducing conditions, lies in the conformation of the loop-helix motif containing the peroxidatic Cys residue. Under oxidising conditions, the peroxidatic Cys (Cys-S<sub>p</sub>H) is oxidised to Cys-S<sub>p</sub>OH,

catalysing the unfolding of the loop-helix motif it is contained within. This structural rearrangement enables intermolecular disulphide bond formation between the peroxidatic and resolving Cys residues. Intermolecular disulphide bond formation disrupts the dimer-dimer interface, initiating dissociation of the decamer into lower order oligomers. However, a relatively high Prx protein concentration can prevent dissociation of the oxidised decamer as evidenced by the crystal structure of an oxidised 2-Cys Prx protein decamer from *Amphibacillus xylanus* (Kitano et al., 2005, Wood et al., 2002). Therefore, under oxidised conditions, the oxidation state of the peroxidatic Cys residue does not appear to be the only force at play influencing the structure of the AS Prx 1 protein.

To further investigate the structure of the AS Prx 1 protein, crystallisation conditions were screened for using commercially available crystallisation solutions. Small scale crystallisation trials identified a number of promising crystallisation conditions all of which contained MPD as the precipitant. Optimisation of the promising crystallisation conditions in a large scale format afforded improvements in both the size and morphology of crystals produced. However, these improvements were not great enough to warrant further investigation of the crystallisation conditions or analysis of the crystals produced using X-ray crystallography.

# Chapter 5

Expression, purification and characterisation  
of a peroxiredoxin 4 from yellowtail kingfish  
(*Seriola lalandi*)

## 5.1 Introduction

In human, Prx 4 was initially identified based on its ability to interact with Prx 1 using the yeast two-hybrid assay (Jin et al., 1997). Analysis of the deduced amino acid sequence of the human Prx 4 revealed that it contained two VCP motifs that are characteristic of 2-Cys Prxs and a distinctly hydrophobic N-terminus consistent with a signal peptide (Jin et al., 1997). The purified recombinant human Prx 4 protein was found to possess thiol peroxidase activity when it was shown to be able to protect glutamine synthetase from inactivation by thiol-dependent metal-catalysed oxidation (Jin et al., 1997). Insight into the function of the putative N-terminal signal peptide was gained when the Prx 4 from rat was investigated by transient expression in COS-1 cells (Matsumoto et al., 1999). Immunoblot analysis detected recombinant rat Prx 4 in the cellular extract and the culture medium and immunofluorescent staining of the COS-1 cells revealed an intra-cellular network-like structure, typical of a protein located in the endoplasmic reticulum. These results suggested that Prx 4 represented the secretory form of the Prx family.

Recently, a Prx 4 from yellowtail kingfish (YTK) was cloned and functionally characterised (Loo and Schuller, 2010). Analysis of the full length YTK Prx 4 deduced amino acid sequence (designated YTK Prx 4-264) using SignalP prediction software (Bendtsen et al, 2004) predicted an N-terminal signal peptide consisting of 33 amino acids, that when removed would result in a protein of 231 amino acids (designated YTK Prx 4-231). In contrast, alignment of YTK Prx 4-264 with other 2-Cys Prx amino acid sequences identified an N-terminal amino acid extension of 67 amino acids, that when removed would result in a protein of 197 amino acids (designated YTK-Prx 4-197). To investigate the predicted N-terminal signal peptides, the YTK Prx 4-197, 231 and 264 proteins were recombinantly expressed and purified. The YTK Prx 4-197 and 231 proteins both displayed thioredoxin-

dependent peroxidase activity whereas the YTK Prx 4-264 protein did not (Loo and Schuller, 2010). This provided evidence that the YTK Prx 4-264 was a pre-protein that needed processing to become active and suggested that either one, if not both, of the predicted N-terminal signal peptides may have relevance *in vivo*.

In the current study I present further sequence analysis of the predicted YTK Prx 4 signal peptides previously identified and the recombinant expression, purification and structural characterisation of the YTK Prx 4-197, 231 and 267 proteins.

## 5.2 Materials and Methods

### 5.2.1 Gene Construct

Purified plasmid construct composed of a Novagen pET-30a backbone and a putative yellowtail kingfish peroxiredoxin (YTK Prx) open reading frame (ORF) insert (referred to as pET-30a-YTK Prx) was generated and kindly provided by Grace Loo (School of Biological Sciences, Flinders University) (Loo and Schuller, 2010). In brief, the cloning of the putative YTK Prx ORF initially involved identification of two highly conserved regions in the amino acid sequences of several fish and mammal Prxs. Based on these highly conserved regions, PCR primers were designed to amplify an internal fragment of the YTK Prx cDNA using cDNA synthesised from YTK muscle tissue RNA. Using the sequence of this internal fragment, the 5' and 3' ends of the YTK Prx cDNA were able to be amplified by rapid amplification of cDNA ends (RACE)-PCR. Based on the complete YTK Prx cDNA sequence, PCR primers were designed to amplify the YTK Prx ORF and incorporate *Nco*I and *Bam*HI restriction enzyme sites into the 5' and 3' ends, respectively. The YTK Prx ORF and pET-30a expression vector (Novagen®) were digested with the *Nco*I and *Bam*HI restriction enzymes and ligated to produce the pET-30a-YTK Prx construct. The YTK Prx ORF insert was believed to be complete, encoding a protein of 264 amino acids. The purified pET-30a-YTK Prx plasmid construct was provided in nuclease-free water and had been stored at -20°C.

### 5.2.2 Sequencing of pET-30a-YTK Prx 4 construct

The purified pET-30a-YTK Prx 4 construct was transformed into *Escherichia coli* (*E. coli*) BL21 (DE3) Singles™ Competent Cells (Novagen®) according to Section 2.9. Colonies of *E. coli* cells that had been transformed were screened for the presence of the pET-30a-YTK Prx 4 construct using the polymerase chain reaction (PCR)

protocol outlined in Section 2.10. PCR screening products were visualised using agarose gel electrophoresis as outlined in Section 2.6. Three colonies of *E. coli* BL21 (DE3) cells found to contain the pET-30a-YTK Prx 4 construct were used to prepare plasmid DNA according to Section 2.5.2. The insert of the purified pET-30a-YTK Prx 4 plasmid was sequenced according to Section 2.8 and aligned with the expected YTK Prx 4 sequence (GenBank nucleotide accession FJ013222) using Gene Codes Corporation Sequencher™ software.

### 5.2.3 Site-directed mutagenesis of pET-30a-YTK Prx 4 construct

Complementary site directed mutagenesis (SDM) PCR primers were designed to introduce a cytosine nucleotide into the pET-30a-YTK Prx 4 insert at a position 443 bp from the 5' terminus. The mutagenic cytosine nucleotide was positioned in the middle of the SDM primers with approximately 10 bp of YTK Prx 4 sequence flanking either side. The SDM primer designs incorporated a 3' G-C rich clamp and an annealing temperature of 62°C which was estimated using the IDT SciTools OligoAnalyzer 3.1 available at [www.idtdna.com/analyzer/applications/oligoanalyzer/](http://www.idtdna.com/analyzer/applications/oligoanalyzer/). The SDM PCR reaction contained 1X Phusion® HF buffer and 1 U Phusion® DNA polymerase (Finnzymes), 200 µM deoxyribonucleotide triphosphates (dNTPs), 3% (v/v) dimethyl sulfoxide (DMSO), 100 ng of pET-30a-YTK Prx 4 plasmid DNA and 100 ng of forward and reverse SDM primer in a final volume of 50 µL. PCR cycling was carried out in a GeneAmp® Applied Biosystems™ Thermocycler. The PCR cycling conditions were 1 cycle of denaturation at 98°C for 30 s followed by 30 cycles of (denaturation at 98°C for 10 s, annealing at 60°C for 20 s and extension at 72°C for 3.5 min), followed by 1 cycle of final extension at 72°C for 5 min. The pET-30a-YTK Prx 4 SDM PCR products were purified using a Promega™ Wizard® SV Gel and PCR Clean-Up System according to the manufacturer's instructions and the concentration of DNA was estimated according to Section 2.5.3. The purified pET-30a-YTK Prx 4 SDM PCR products were digested with the restriction enzyme *DpnI*

supplied by New England Biolabs® (NEB®). The restriction enzyme digestion contained 1X NEB® buffer 4, 60 U *DpnI* and approximately 2.5 µg of pET-30a-YTK Prx 4 SDM PCR products in a final volume of 50 µL. The restriction enzyme digestion was carried out at 37°C for 4 h followed by 80°C for 20 min. The *DpnI* restriction enzyme digested pET-30a-YTK Prx 4 SDM PCR products were used to transform Invitrogen™ sub-cloning efficiency *E. coli* DH5α cells as outlined in Section 2.9. The *E. coli* DH5α cells transformed with the pET-30a-YTK Prx 4 SDM PCR products were used to prepare purified plasmid DNA as per Section 2.5.2. The inserts of the purified plasmids were sequenced according to Section 2.8.

#### 5.2.4 Preparation of constructs with truncated YTK Prx 4 inserts

The YTK Prx 4 nucleotide sequence (GenBank nucleotide accession no. FJ013222) was used to design PCR primers to amplify the regions encoding the YTK Prx 4-197 protein (i.e. the YTK Prx 4-264 protein that lacks the putative N-terminal signal peptide predicted by the multiple sequence alignment) and the YTK Prx 4-231 protein (i.e. the YTK Prx 4-264 protein that lacks the putative N-terminal signal peptide predicted by SignalP software). To facilitate cloning, the design of the forward PCR primers included an *NcoI* restriction enzyme recognition site while the design of the reverse PCR primers included a *NotI* restriction enzyme recognition site. To increase the cutting efficiency of the expected PCR products by the restriction enzymes, two additional nucleotides were incorporated into the 5' termini of both the forward and reverse PCR primers. The length of the YTK Prx 4 ORF portion of each primer was optimised to include a 3' G-C rich clamp and a melting temperature of approximately 60°C. The melting temperature of each primer was estimated using the IDT SciTools OligoAnalyzer 3.1 available at [www.idtdna.com/analyzer/applications/oligoanalyzer/](http://www.idtdna.com/analyzer/applications/oligoanalyzer/).



The pET-30a-YTK Prx 4-264 plasmid DNA was prepared according to Section 2.5.2. Each PCR reaction contained 1X Phusion<sup>®</sup> HF buffer and 1 U Phusion<sup>®</sup> DNA polymerase (Finnzymes), 200 µM dNTPs, 100 ng of pET-30a-YTK Prx 4-264 plasmid DNA and 200 ng of forward and reverse primer in a final volume of 50 µL. PCR cycling was carried out in a GeneAmp<sup>®</sup> Applied Biosystems<sup>™</sup> Thermocycler. The PCR conditions were 1 cycle of denaturation at 98°C for 30 s followed by 30 cycles of (denaturation at 98°C for 10 s, annealing at 60°C for 20 s and extension at 72°C for 30 s), followed by 1 cycle of final extension at 72°C for 3 min.

The YTK Prx 4-197 and 231 PCR products were visualised by agarose gel electrophoresis according to Section 2.6 and the remaining products were purified according to Section 2.5.1. The concentration of purified YTK Prx 4-197 and 231 PCR products was quantified according to Section 2.5.3. Plasmid DNA was prepared from *E. coli* BL21 (DE3) cells containing the pET-30a-YTK Prx 4-264 plasmid according to Section 2.5.2. The purified YTK Prx 4-197 and 231 PCR products, and the pET-30a-YTK Prx 4-264 construct were digested with the *Nco*I and *Not*I restriction enzymes. Each restriction enzyme digestion reaction contained 1 µg of target DNA, 20 U NEB<sup>®</sup> *Not*I-HF, 10 U NEB<sup>®</sup> *Nco*I and 1X NEB<sup>®</sup> Buffer 4 in a total volume of 40 µL. The restriction enzyme digestion reactions were incubated at 37°C for 2 hours followed by 65°C for 20 minutes. The digested YTK Prx 4-197 and 231 PCR products were purified according to Section 2.5.1. The pET-30a plasmid was isolated by agarose gel electrophoresis according to Section 2.6 and subsequently purified according to Section 2.5.1. The concentration of the digested and purified YTK Prx 4-197 and 231 PCR products, and pET-30a plasmid was quantified according to Section 2.5.3.

The prepared YTK Prx 4-197 and 231 PCR products were ligated into the prepared pET-30a plasmid. Each ligation reaction contained 100 ng of pET-30a plasmid, 35 ng of YTK Prx 4-197 or 231 PCR product, 1X NEB<sup>®</sup> Quick Ligation Buffer and 1 µL

NEB® Quick T4 DNA ligase in a total volume of 10 µL. The ligation reactions were incubated at room temperature for 60 min, then directly used to transform competent *E. coli* BL21 (DE3) cells according to Section 2.9. Purified plasmid DNA was prepared from four colonies of *E. coli* BL21 (DE3) cells that had been transformed with the pET-30a-YTK Prx 4-197 plasmid and from one colony of *E. coli* BL21 (DE3) cells that had been transformed with the pET-30a-YTK Prx 4-231 plasmid according to Section 2.5.2. The inserts of each of the purified plasmids were sequenced according to Section 2.8.

### 5.2.5 Expression and purification of YTK Prx 4-197, 231 and 264 proteins

Large scale protein expression was performed with *E. coli* BL21 (DE3) cells containing the pET-30a-YTK Prx 4-197, 231 and 264 plasmids as per Section 2.11 using 0.5 L cultures set up in 2 L Erlenmeyer flasks. The level of YTK Prx 4-197, 231 and 264 protein expression was assessed by SDS-PAGE and immunoblotting as outlined in Sections 2.12 and 2.13, respectively.

The YTK Prx 4-197, 231 and 264 proteins were purified from *E. coli* BL21 (DE3) cells expressing the appropriate YTK Prx 4 construct by Ni-affinity chromatography according to Section 2.14. Following Ni-affinity purification, the YTK Prx 4-197 and 231 proteins were exchanged into a buffer containing 20 mM Tris-base (pH 7.5), 150 mM NaCl and 5 mM DTT, concentrated and then either used immediately or frozen in liquid nitrogen and stored at -70°C until needed.

The solubility of the recombinantly expressed YTK Prx 4-264 protein was investigated by differential centrifugation as outlined in Section 2.17.

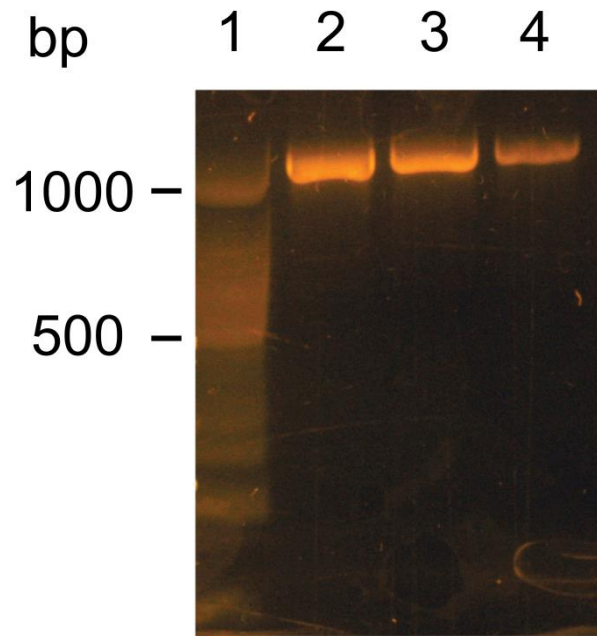
## 5.2.6 Gel filtration chromatography of YTK Prx 4-197 and 231 proteins

The native molecular mass of Ni-affinity purified YTK Prx 4-197 and 231 (prepared according to Section 5.2.5) was analysed by gel filtration chromatography according to Section 2.16 under reducing and oxidising conditions. For gel filtration chromatography analysis under reducing conditions, 200  $\mu\text{L}$  of Ni-affinity purified YTK Prx 4 protein ( $10 \text{ mg mL}^{-1}$ ) was loaded onto a gel filtration column that had been equilibrated with a buffer containing 20 mM Tris-base (pH 7.5), 150 mM NaCl and 5 mM DTT. For gel filtration chromatography analysis under oxidising conditions, Ni-affinity purified YTK Prx 4 protein was exchanged into a buffer containing 20 mM Tris-base (pH 7.5) and 150 mM NaCl. Following buffer exchange, 200  $\mu\text{L}$  of concentrated Ni-affinity purified YTK Prx 4 ( $10 \text{ mg mL}^{-1}$ ) was loaded onto a gel filtration column that had been equilibrated with the same buffer that was used for the protein buffer exchange.

## 5.3 Results

### 5.3.1 Sequencing of pET-30a-YTK Prx 4 construct

A pET-30a plasmid containing a putative YTK Prx 4 insert (referred to as pET-30a-YTK Prx 4), kindly provided by Grace Loo (School of Biological Sciences, Flinders University), was transformed into *E. coli* BL21 (DE3) cells. The transformation produced numerous colonies of *E. coli* cells of which three were screened for the presence of the pET-30a-YTK Prx 4 construct using a PCR-based method. The resulting PCR products were visualised by agarose gel electrophoresis (Fig. 5.1). Agarose gel electrophoresis revealed that each PCR reaction had produced a single product of approximately 1200 base pairs (bp). The size of the products was consistent with the expected size of a YTK Prx 4 insert flanked by the pET-30a multiple cloning site (1189 bp). The PCR screened *E. coli* BL21 (DE3) cells were used to prepare purified pET-30a-YTK Prx 4 plasmid and the inserts sequenced. Alignment of the pET-30a-YTK Prx 4 insert sequences with the expected YTK Prx 4 sequence revealed that they matched except for three silent mutations and a deletion. The silent mutations positioned 201, 699 and 703 bp from the 5' terminus changed the corresponding codons from CTG to CTT, AAA to AAG and CAT to CAC, respectively. The nucleotide deletion located 443 bp from the 5' terminus resulted in a reading frame shift.



**Fig. 5.1.** Agarose gel electrophoresis of PCR screening products produced from three colonies of *E. coli* BL21 (DE3) cells that had been transformed with pET-30a-YTK Prx 4 construct. The YTK Prx 4 insert flanked by the pET-30a multiple cloning site was amplified by PCR using T7 promoter and terminator primers. Lane 1, DNA size standards; Lane 2, colony 1 PCR products; Lane 3, colony 2 PCR products; Lane 4, colony 3 PCR products.

### 5.3.2 Site directed mutagenesis of pET-30a-YTK Prx 4 construct

Sequencing of the pET-30a-YTK Prx 4 insert confirmed its identity in addition to identifying a single cytosine nucleotide deletion positioned 443 bp from the 5' terminus. The primers outlined in Fig. 5.2 were designed to replace the missing cytosine nucleotide in the pET-30a-YTK Prx 4 insert using PCR-based site directed mutagenesis (SDM). Analysis of the SDM PCR products by agarose gel electrophoresis revealed a single product of a size that was consistent with the pET-30a-YTK Prx 4 construct (data not shown). Sequencing of the SDM PCR product revealed that the cytosine nucleotide missing from the pET-30a-YTK Prx 4 insert had been successfully replaced without the introduction of any mutations, deletions or insertions.

SEQUENCE:

5'- CTC CCA GTT CAC CCA CCT GGC C -3'

COMPLEMENT:

5'- GGC CAG GTG GGT GAA CTG GGA G -3'

LENGTH: 22

GC CONTENT: 68.2 %

MELT TEMP: 64.5°C

MOLECULAR

WEIGHT: 6552.3 g/mole

EXTINCTION

COEFFICIENT: 186900 L/(mole-cm)

nmole/OD<sub>260</sub>: 5.35

µg/OD<sub>260</sub>: 35.06

**Fig. 5.2.** Characteristics of SDM PCR primers designed to replace a cytosine nucleotide missing from the pET-30a-YTK Prx 4 insert at a position 443 bp from the 5' terminus. Analysis of the SDM PCR primers was performed using the IDT<sup>®</sup> SciTools OligoAnalyzer 3.1.

### 5.3.3 Sequence analysis of predicted N-terminal YTK Prx 4 signal peptides

Previously, analysis of the full length YTK Prx 4-264 deduced amino acid sequence by SignalP software and alignment with other fish and mammal Prx 4 sequences predicted two possible N-terminal signal peptides of different lengths (Loo and Schuller, 2010). The SignalP software predicted an N-terminal signal peptide of 33 amino acids (referred to as S33), that when removed would result in the YTK Prx 4-231 protein. In contrast, the multiple sequence alignment predicted an N-terminal signal peptide of 67 amino acids (referred to as M67), that when removed would result in the YTK Prx 4-197 protein.

To further investigate the likelihood of the YTK Prx 4-264 predicted N-terminal signal peptides having relevance *in vivo*, their amino acid sequences were compared to rules that have been established for endoplasmic reticulum (ER) signal peptides (Dalbey and von Heijne, 1992). Based on the statistical analysis of signal peptides, the cleavage site is defined by a motif with small residues at positions -1 and -3. In agreement with this, the S33 prediction had Ala and Thr residues at positions -1 and -3, respectively. In contrast, the M67 prediction had a small residue at position -1 but not at position -3. In addition, a signal peptide cleavage site is also normally found 4-6 residues from the end of a central hydrophobic region. The S33 prediction satisfied this requirement by possessing a stretch of 5 Leu residues that preceded the predicted cleavage site by 7 residues. Similarly, the M67 prediction also satisfied this requirement by possessing a stretch of 3 hydrophobic amino acids, Val-Pro-Val, that preceded the predicted cleavage site by 5 residues. Lastly, the transition from the hydrophobic region of a signal peptide is often marked by a helix-breaking residue such as Pro, Gly or Ser. These helix-breaking residues appear to promote binding between the pre-protein and its signal peptidase (Dalbey and von Heijne,



1992). The transition from the hydrophobic region of the S33 prediction did not contain a helix-breaking residue, whereas, the M67 prediction was found to contain a Ser residue. As a result of satisfying more of the requirements of a signal peptide, it was believed that the S33 prediction (i.e. the YTK Prx 4-231 protein) was more likely to be of relevance *in vivo* compared to the M67 prediction (i.e. the YTK Prx 4-197 protein).

#### 5.3.4 Preparation of constructs with truncated YTK Prx 4 inserts

To amplify the regions of the YTK Prx 4 ORF encoding the YTK Prx 4-197 and 231 proteins, PCR primers were designed (Fig. 5.3). The characteristics of the primers were analysed by IDT<sup>®</sup> SciTools OligoAnalyzer 3.1 software.

**Fig. 5.3.** Characteristics of the PCR primers designed to amplify the YTK Prx 4 ORF without the 5' sequence encoding putative N-terminal signal peptides that were predicted from (A) alignment of the YTK Prx 4 deduced amino acid sequence with other 2-Cys Prx proteins and (B) analysis of the YTK Prx 4 deduced amino acid sequence using SignalP software (Bendtsen et al, 2004).

(A) YTK Prx 4-197 Forward Primer

SEQUENCE:

5'-AACCATGGCACACCTCAGCAAAGCCAAGATTTCAAAGCCTTCG-3'

LENGTH:	33
GC CONTENT:	48.5 %
MELT TEMP:	64.1 °C
MOLECULAR WEIGHT:	10035.6 g/mole
EXTINCTION COEFFICIENT:	314600 L/(mole·cm)
nmole/OD <sub>260</sub> :	3.18
µg/OD <sub>260</sub> :	31.90

(B) YTK Prx 4-231 Forward Primer

SEQUENCE:

5'-AACCATGGCAGACGAAGGCGCCAGTGCGAGAAAC-3'

LENGTH:	24
GC CONTENT:	62.5 %
MELT TEMP:	64.4 °C
MOLECULAR WEIGHT:	7445.9 g/mole
EXTINCTION COEFFICIENT:	242700 L/(mole·cm)
nmole/OD <sub>260</sub> :	4.12
µg/OD <sub>260</sub> :	30.68

YTK Prx 4 ORF Reverse Primer

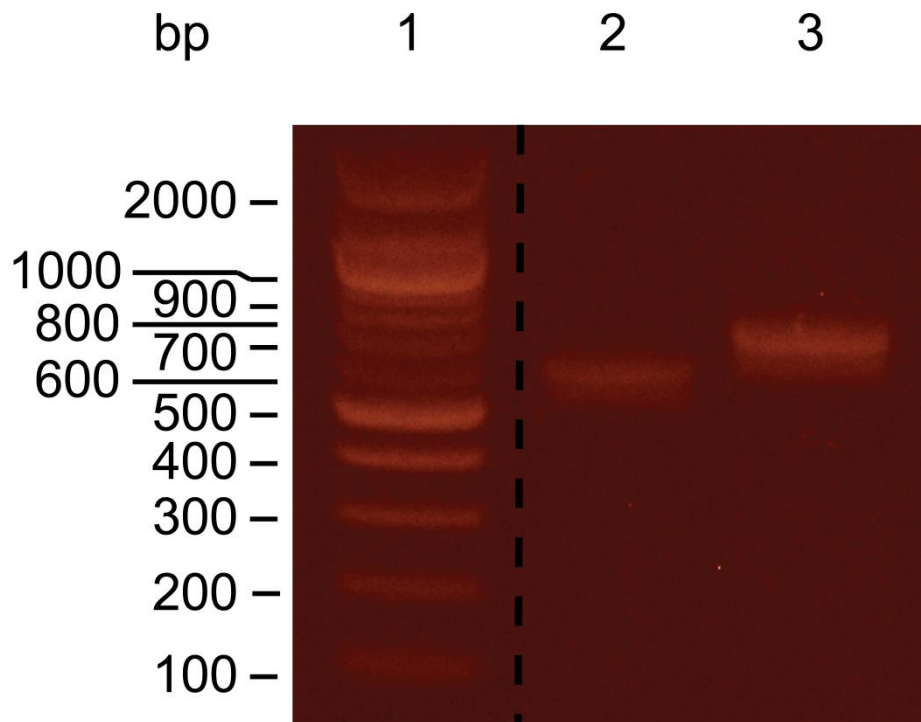
SEQUENCE:

5'-TTGCGGCCGCTCAGTTGAGTTTATCAAATACTTCAGCTTGCCTGAAGGATCAGG-3'

LENGTH:	45
GC CONTENT:	40.0 %
MELT TEMP:	64.4 °C
MOLECULAR WEIGHT:	13874.0 g/mole
EXTINCTION COEFFICIENT:	439800 L/(mole·cm)
nmole/OD <sub>260</sub> :	2.27
µg/OD <sub>260</sub> :	31.55

The portions of the YTK Prx 4 ORF encoding the YTK Prx 4-197 and 231 proteins were amplified by PCR and the resulting products were analysed by agarose gel electrophoresis (Fig. 5.4). Agarose gel electrophoresis revealed that the YTK Prx 4-197 and 231 PCR reactions produced products of approximately 600 bp and 700 bp, respectively. The sizes of the former and later PCR products were consistent with the expected sizes of the portions of the YTK Prx 4 ORF that encoded the YTK Prx 4-197 and 231 proteins, respectively.

The YTK Prx 4-197 and 231 PCR products were ligated into the pET-30a plasmid and the ligation products were used to transform competent *E. coli* BL21 (DE3) cells. Analysis of the transformation plates revealed that the *E. coli* BL21 (DE3) cells that were transformed with the pET-30a-YTK Prx 4-197 and 231 constructs contained 4 colonies and a single colony, respectively. Each colony of transformed cells was used to produce purified plasmid that was sequenced. Sequencing of the pET-30a-YTK Prx 4-197 and 231 constructs revealed that they contained the correct insert sequence that was in frame relative to the start site for translation, in the correct orientation and mutation free.

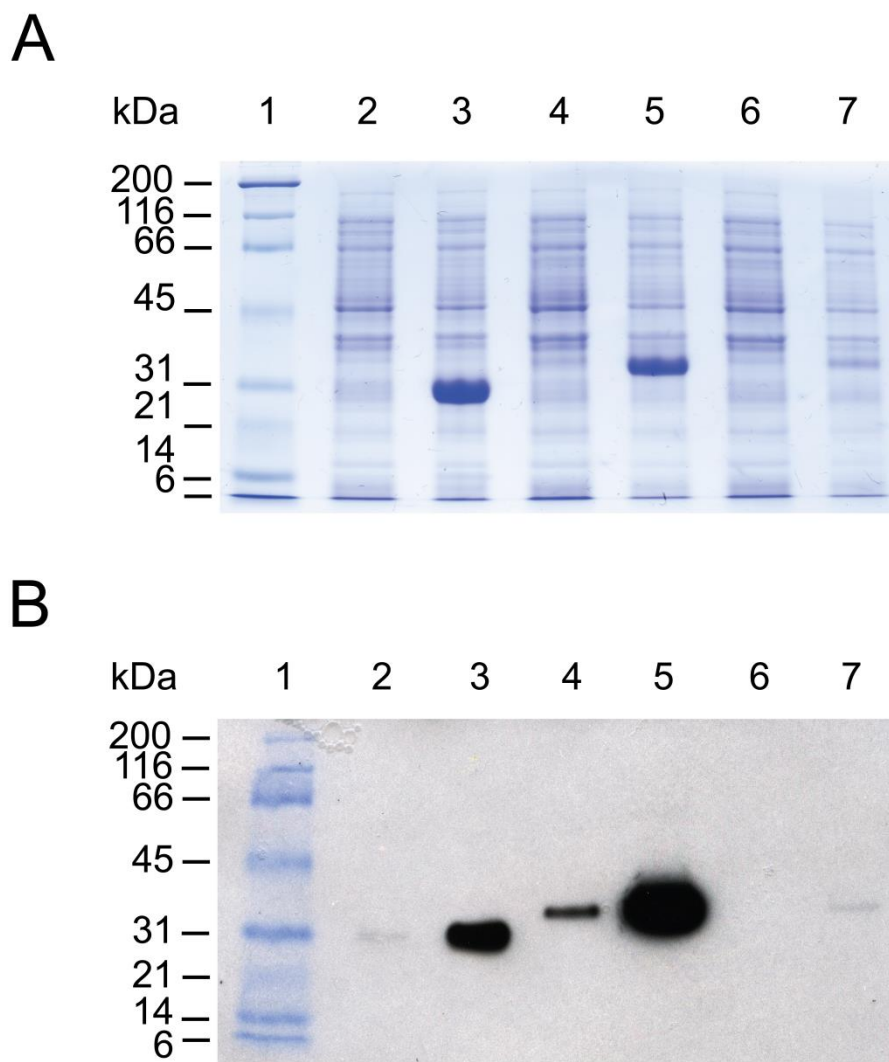


**Fig. 5.4.** Agarose gel electrophoresis of PCR products amplified from the YTK Prx 4-264 construct using the YTK Prx 4-197 and 231 gene specific primer pairs. Lane 1, DNA size standards; Lane 2, YTK Prx 4-197 PCR products; Lane 3, YTK Prx 4-231 PCR products.

### 5.3.5 Large scale expression of YTK Prx 4-197, 231 and 264 proteins

The *E. coli* BL21 (DE3) cells containing the pET-30a-YTK Prx 4-197, 231 and 264 constructs were used for large scale protein expression. The level of recombinant protein expression was investigated by analysing whole cell protein extracts produced from un-induced and 3 h induced cells using SDS-PAGE and immunoblotting (Fig. 5.5). SDS-PAGE analysis of whole cell protein extracts produced from 3 h induced *E. coli* BL21 (DE3) cells that contained the pET-30a-YTK Prx 4-197 and 231 constructs revealed prominent protein bands with approximate molecular masses of 27.5 and 32.5 kDa, respectively (Fig. 5.5A, lanes 3 and 5, respectively). Although the molecular masses of these proteins were 1.5 kDa larger than expected, immunoblotting analysis confirmed that they were His-tagged YTK Prx 4-197 and 231 proteins (Fig. 5.5B, lanes 3 and 5, respectively). Immunoblotting analysis also detected the YTK Prx 4-197 and 231 proteins in the whole cell protein extracts produced from un-induced *E. coli* BL21 (DE3) cells that contained the pET-30a-YTK Prx 4-197 and 231 constructs, respectively (Fig. 5.5B, lanes 2 and 4, respectively). The expression of these proteins prior to induction is presumably caused by a background level of T7 RNA polymerase activity. SDS-PAGE analysis of the whole cell protein extract produced from 3 h induced *E. coli* BL21 (DE3) cells containing the pET-30a-YTK Prx 4-264 construct revealed the absence of a prominent protein band at the expected molecular mass of the YTK Prx 4-264 protein. However, immunoblotting analysis was able to detect a faint protein band with an approximate molecular mass of 32.5 kDa. This molecular mass of the YTK Prx 4-264 protein was 2 kDa smaller than expected. Interestingly, the observed molecular mass of the YTK Prx 4-264 protein was consistent with the observed molecular mass of the YTK Prx 4-231 protein. The level of expression of the YTK

Prx 4-264 protein was significantly lower compared to the level of expression that was observed for the YTK Prx 4-197 and 231 proteins.

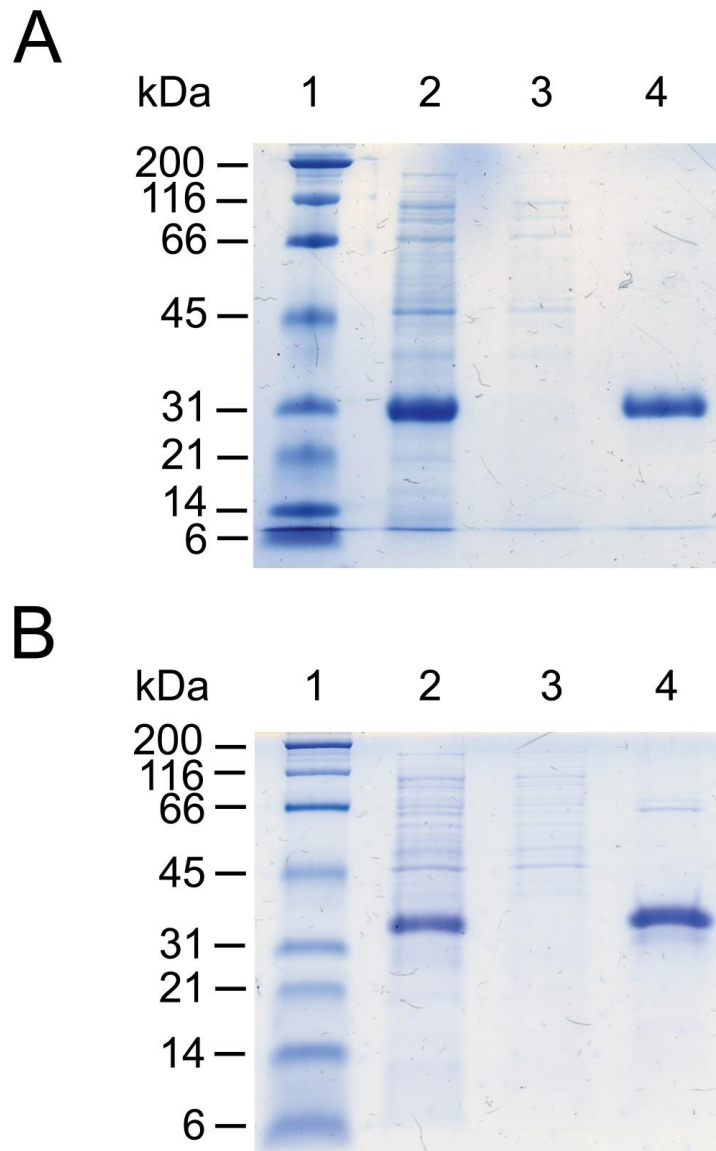


**Fig. 5.5.** Reducing SDS-PAGE (A) and immunoblotting (B) analysis of whole cell protein extracts produced from un-induced and 3 h induced *E. coli* BL21 (DE3) cells that contained the pET-30a-YTK Prx 4-197, 231 and 264 constructs. The immunoblotting analysis was performed with rabbit anti-6X His polyclonal antibodies (Rockland). Lane 1, molecular mass markers; Lane 2, un-induced YTK Prx 4-197; Lane 3, 3 h induced YTK Prx 4-197; Lane 4, un-induced YTK Prx 4-231; Lane 5, 3 h induced YTK Prx 4-231; Lane 6, un-induced YTK Prx 4-264; Lane 7, 3 h induced YTK Prx 4-264.



### 5.3.6 Ni-affinity purification of YTK Prx 4-197, 231 and 264 proteins

The YTK Prx 4-197 and 231 proteins expressed in *E. coli* were purified by Ni-affinity chromatography. Various fractions produced from the Ni-affinity chromatography purifications were analysed by SDS-PAGE (Fig. 5.6). SDS-PAGE analysis of the 500 mM imidazole elution fractions from both purifications revealed the presence a single prominent protein. The molecular masses of these prominent proteins were 1.5 kDa larger than expected for the corresponding recombinant YTK Prx 4 protein, but consistent with previous observations. The combined Ni-affinity column flow-through and 20 mM imidazole wash fractions of both purifications contained numerous *E. coli* proteins but did not appear to contain any significant amount of recombinant YTK Prx 4 protein. This indicated that the YTK Prx 4-197 and 231 proteins were able to bind and remain bound to the Ni-affinity column until eluted in the 500 mM imidazole elution. Therefore, both the YTK Prx 4-197 and 231 proteins were able to be purified by Ni-affinity column chromatography with high yield and enrichment.



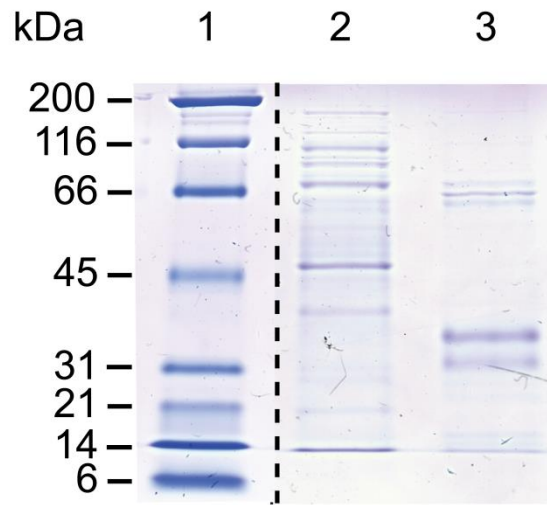
**Fig. 5.6.** Reducing SDS-PAGE analysis of various fractions produced from the Ni-affinity chromatography purification of recombinant (A) YTK Prx 4-197 protein and (B) YTK Prx 4-231 protein. Lane 1, molecular mass markers; Lane 2, whole cell protein extract; Lane 3, combined column flow-through and 20 mM imidazole wash; Lane 4, 500 mM imidazole elution.

Although the level of recombinant YTK Prx 4-264 protein expression was low, the yield of protein recovered following Ni-affinity chromatography purification was lower than expected. To investigate the loss of YTK Prx 4-264 protein, various fractions collected throughout the Ni-affinity purification were analysed by SDS-PAGE and immunoblotting (Fig. 5.7). SDS-PAGE analysis of the 500 mM imidazole elution fraction revealed the presence of several proteins with approximate molecular masses of 32, 36, 64 and 72 kDa (Fig. 5.7A, lane 3). The 36 kDa protein is 1.5 kDa larger than the expected molecular mass of the YTK Prx 4-264 monomer while the 72 kDa protein, possibly a dimer of the 36 kDa protein, is 3 kDa larger than the expected size of the YTK Prx 4-264 dimer. Neither the 32 nor the 64 kDa proteins are consistent with the molecular mass of any expected YTK Prx 4-264 protein forms. However, the 32 kDa protein is consistent with the observed molecular mass of the YTK Prx 4-231 monomer and the 64 kDa protein is consistent with a dimer of the 32 kDa protein. Interestingly, all four of these Ni-affinity purified proteins were detected by immunoblotting using anti-(southern bluefin tuna Prx 2) antibodies. However, only the 36 kDa protein was detected by immunoblotting using anti-His antibodies. Although, the anti-His antibodies also appeared to faintly react with the 32 kDa protein.

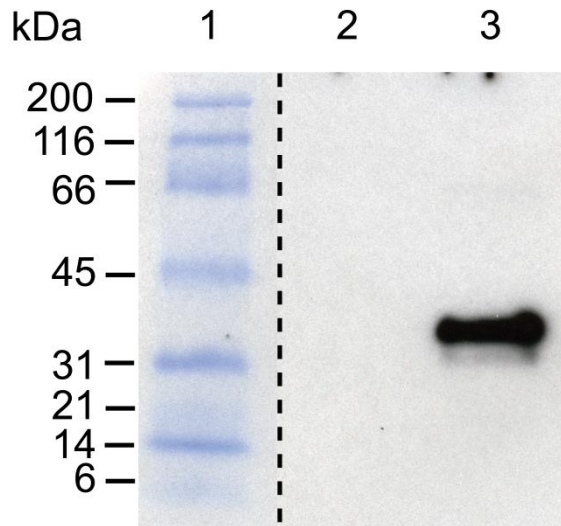
Immunoblotting with both the anti-(southern bluefin tuna Prx 2) and anti-His antibodies detected no YTK Prx 4-264 protein of any form in the combined Ni-affinity column flow-through and 20 mM imidazole wash. Therefore, the lower than expected yield of Ni-affinity purified YTK Prx 4-264 protein was not caused by a loss of unbound protein in the column flow-through or premature elution of the protein from the column by the 20 mM imidazole wash. Although the yield of YTK Prx 4-264 protein in the 500 mM imidazole elution was lower than expected the protein was purified by the Ni-affinity chromatography.

**Fig. 5.7.** Reducing SDS-PAGE (A) and immunoblotting analysis using anti-His (B) and anti-(southern bluefin tuna Prx 2) antibodies (C) of various fractions produced from Ni-affinity chromatography purification of recombinant YTK Prx 4-264 protein. Lane 1, molecular mass markers; Lane 2, Ni-affinity purification, combined flow-through and 20 mM imidazole wash; Lane 3, Ni-affinity purification, 500 mM imidazole elution.

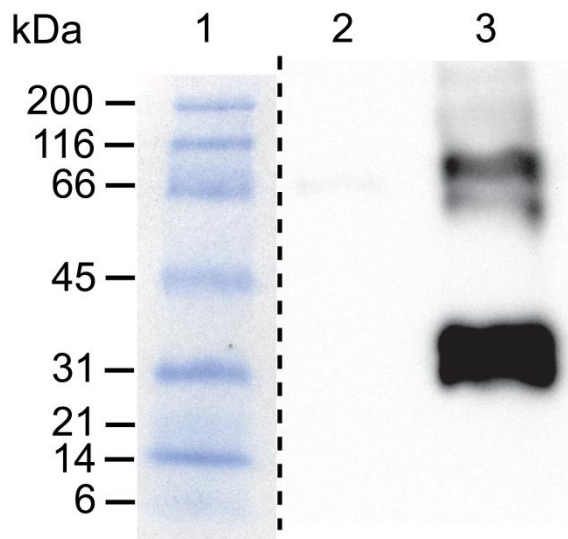
**A**



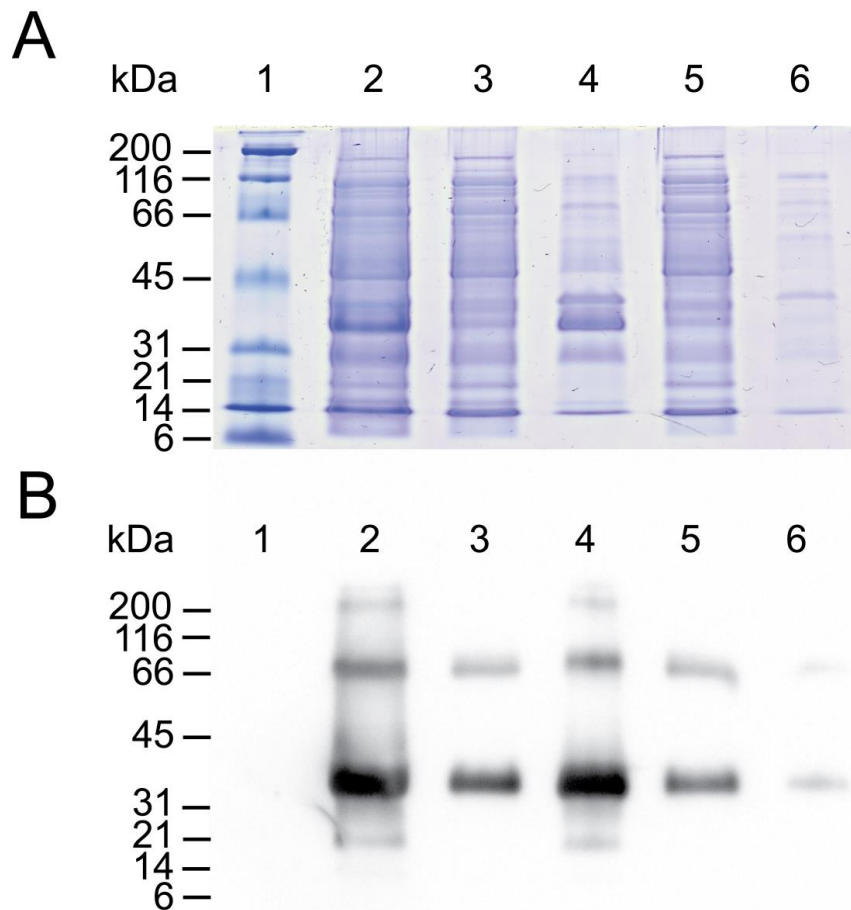
**B**



**C**



Having found that the lower than expected yield of Ni-affinity purified YTK Prx 4-264 protein was not caused by losses that had occurred during the Ni-affinity chromatography, the stability and solubility of the recombinant protein in the expression host was put into question. To investigate this further, whole cell crude lysate produced from *E. coli* cells expressing the YTK Prx 4-264 protein was analysed by differential centrifugation. The resulting centrifugation supernatant and pellet fractions were analysed by SDS-PAGE and immunoblotting (Fig. 5.8). SDS-PAGE analysis revealed that both the whole cell crude lysate and 12,000 g centrifugation pellet fractions contained a prominent protein with an approximate molecular mass consistent with the YTK Prx 4-264 monomer. Immunoblotting analysis confirmed the identity of this prominent protein and also revealed the presence of YTK Prx 4-264 dimer in both of these fractions. YTK Prx 4-264 monomer and dimer were also detected by immunoblotting in all of the remaining fractions except for the 100,000 g pellet fraction which only contained monomer. In all of the fractions containing YTK Prx 4-264 monomer and dimer, the monomer was found to be more abundant compared to the dimer. These results suggest that the YTK Prx 4-264 protein was expressed in the *E. coli* BL21 (DE3) cells as a mixture of soluble and insoluble protein. Therefore, the lower than expected yield of Ni-affinity purified YTK Prx 4-264 protein occurred as a result of a substantial proportion of the protein being expressed in an insoluble form.



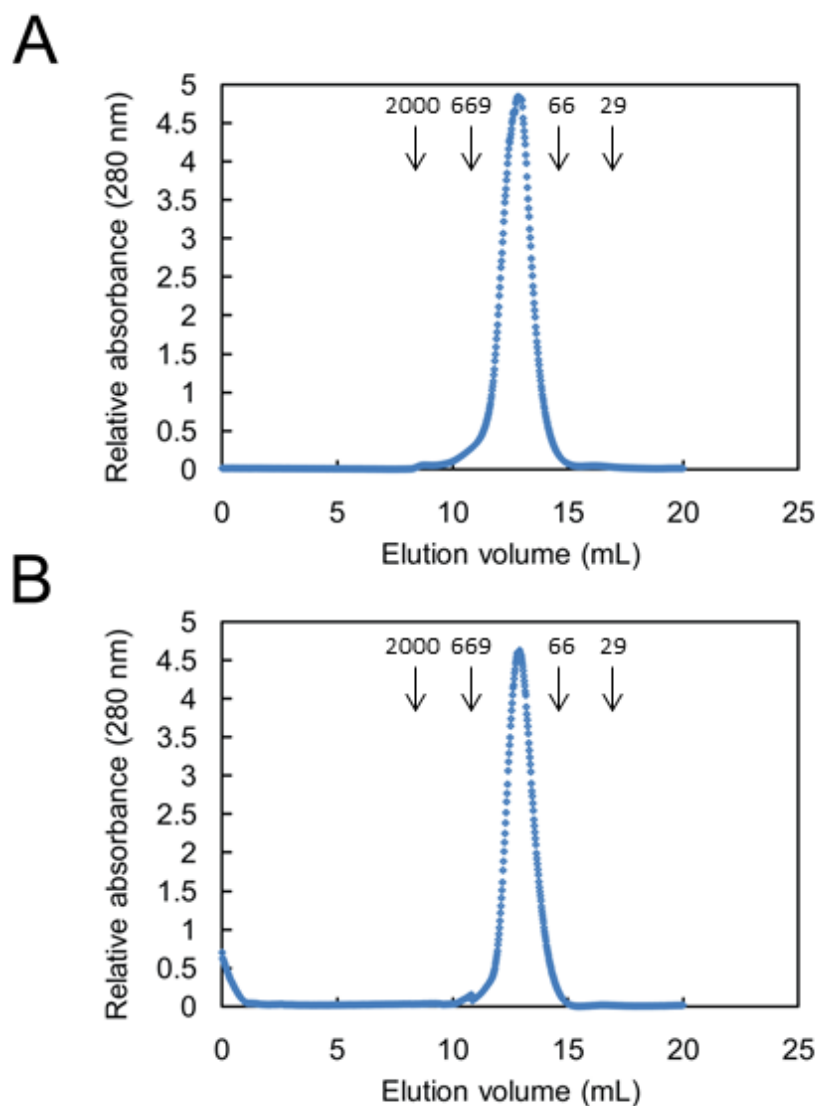
**Fig 5.8.** Reducing SDS-PAGE (A) and immunoblotting (B) analysis of the supernatant and pellet fractions produced from the differential centrifugation of whole cell crude lysate produced from *E. coli* BL21 (DE3) cells expressing the YTK Prx 4-264 protein. The pellet fraction from each centrifugation was resuspended in a volume of 5% (w/v) sodium dodecyl sulphate equal to the volume of the corresponding supernatant. The immunoblotting analysis was performed with anti-(SBT Prx 2) polyclonal antibodies. Lane 1, molecular mass markers; Lane 2, whole cell crude lysate; Lane 3, supernatant produced following centrifugation at 12,000 *g* and 4°C for 15 min; Lane 4, pellet produced following centrifugation at 12,000 *g* and 4°C for 15 min; Lane 5, supernatant produced following centrifugation at 100,000 *g* and 4°C for 1 hr; Lane 6, pellet produced following centrifugation at 100,000 *g* and 4°C for 1 hr.

### 5.3.7 Gel filtration chromatography of YTK Prx 4-197 and 231 proteins

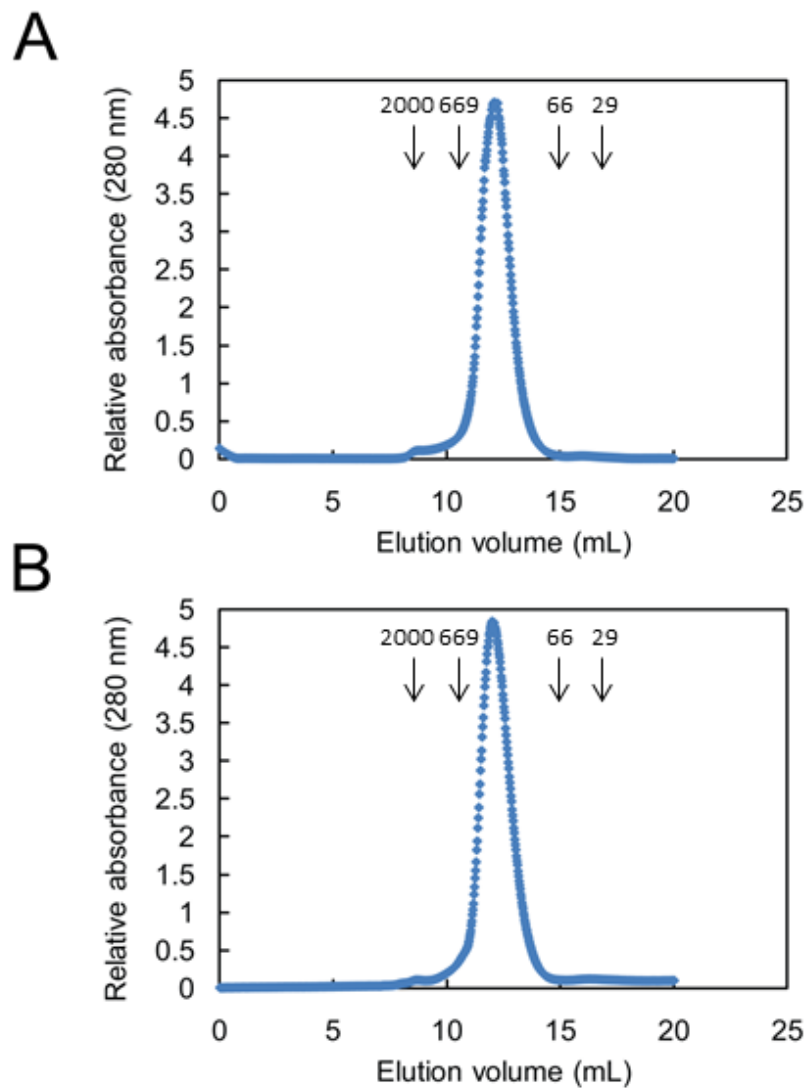
The native molecular mass of the Ni-affinity purified YTK Prx 4-197 protein was investigated by gel filtration chromatography under reducing and oxidising conditions (Fig. 5.9). Under both oxidising and reducing conditions, the YTK Prx 4-197 protein was found to exist as an oligomer with a molecular mass consistent with a decamer. Therefore, changes in the redox environment had no effect on the oligomeric structure of the YTK Prx 4-197 protein.

The native molecular mass of the Ni-affinity purified YTK Prx 4-231 protein was investigated by gel filtration chromatography under reducing and oxidising conditions (Fig. 5.10). Under both oxidising and reducing conditions, the YTK Prx 4-231 protein was found to exist as an oligomer with a molecular mass consistent with a decamer. Therefore, the YTK Prx 4-231 protein favoured a decamer conformation regardless of the redox environment.





**Fig. 5.9.** Effect of oxidising (A) and reducing (B) conditions on the native molecular mass of Ni-affinity purified YTK Prx 4-197 protein. The YTK Prx 4-197 protein was purified by Ni-affinity chromatography, concentrated and desalted into a buffer containing 20 mM Tris-base (pH 7.5), 150 mM NaCl and 5 mM DTT for reducing gel filtration analysis or the same buffer except that it lacked DTT for oxidising gel filtration analysis, giving a final protein concentration of 10 mg mL<sup>-1</sup>. The buffer exchanged protein (200 µL) was loaded onto a gel filtration column that had been equilibrated with the same buffer. The arrows indicate the elution positions of the molecular mass standards (kDa).



**Fig. 5.10.** Effect of oxidising (A) and reducing (B) conditions on the native molecular mass of Ni-affinity purified YTK Prx 4-231 protein. The YTK Prx 4-231 protein was purified by Ni-affinity chromatography, concentrated and desalted into a buffer containing 20 mM Tris-base (pH 7.5), 150 mM NaCl and 5 mM DTT for reducing gel filtration analysis or the same buffer except that it lacked DTT for oxidising gel filtration analysis, giving a final protein concentration of 10 mg mL<sup>-1</sup>. The buffer exchanged protein (200 µL) was loaded onto a gel filtration column that had been equilibrated with the same buffer. The arrows indicate the elution positions of the molecular mass standards (kDa).

## 5.4 Discussion

Sequencing of the pET-30a-YTK Prx 4 plasmid revealed that it contained the expected putative full length YTK Prx 4 ORF insert, encoding 264 amino acids, except for three silent mutations and a single nucleotide deletion. The silent mutations identified may not be artefacts of the cloning procedure but may be the result of evolutionary sequence divergence between isolated populations of yellowtail kingfish. However, the nucleotide deletion was unlikely to have resulted from evolutionary sequence divergence and is more likely to have occurred due to long term storage of the plasmid in the *E. coli* BL21 (DE3) expression host. The single nucleotide deletion was rectified using polymerase chain reaction-based site directed mutagenesis, correcting the reading frame and restoring the expected sequence for the pET-30a-YTK Prx 4 insert.

Previously, the deduced amino acid sequence of the full length YTK Prx 4 open reading frame, designated YTK Prx 4-264, was analysed by alignment with other 2-Cys Prx proteins and SignalP software (Bendtsen et al, 2004). These analyses predicted two putative N-terminal signal peptides of different lengths (Loo and Schuller, 2010). The amino acid composition of each predicted N-terminal signal peptide was compared to the rules that have been established for endoplasmic reticulum (ER) signal peptides (Dalbey and von Heijne, 1992). The putative N-terminal signal peptide predicted by the SignalP software (S33) was found to satisfy more of the requirements of an ER signal peptide compared to the putative signal N-terminal signal peptide predicted by the multiple sequence alignment (M67). Therefore, the YTK Prx 4-231 protein (YTK Prx 4-264 missing S33) is more likely to be of relevance *in vivo* compared to the YTK Prx 4-197 protein (YTK Prx 4 missing M67).

Further evidence in support of the *in vivo* relevance of the putative YTK Prx 4-231 protein over the YTK Prx 4-197 protein, comes from comparison with rat Prx 4 protein. Analysis of a Prx 4 protein from rat that was expressed in Sf21 cells revealed that it was present in both the soluble cellular fraction and the conditioned medium as two proteins with molecular masses of 31 and 27 kDa (Okado-Matsumoto et al., 2000). Amino acid sequence analysis of the N-terminus of the 27 kDa protein revealed that it consisted of Leu-Gln-Gly-Leu-Glu. This indicated that the N-terminal 36 amino acid residues of the 31 kDa protein were removed post-translation to produce the 27 kDa protein. Thus, the 31 kDa protein was a precursor form, whilst the 27 kDa protein was the mature processed form. These sizes correspond closely with the predicted sizes for YTK Prx 4-264 and 231, respectively. Thus, by analogy with rat, the YTK Prx 4-264 protein may be the precursor form and the YTK Prx 4-231 protein may be the processed mature form.

The YTK Prx 4-197 and 231 proteins were expressed in *E. coli* BL21 (DE3) cells and purified by Ni-affinity chromatography utilising an N-terminal His-tag encoded by the pET-30a vector. Immunoblotting analysis of whole cell extracts using anti-His antibodies detected the recombinant YTK Prx 4-197 and 231 proteins with molecular masses of 27 and 32 kDa, respectively. Interestingly, both of these proteins were approximately 1.5 kDa larger than their expected molecular masses. The additional 1.5 kDa of these proteins is consistent with the additional mass that would be incurred if translation was to continue past the YTK Prx 4 stop codon and be terminated at the multiple stop codons incorporated into the 3' end of the pET-30a multiple cloning site. The region between the 3' terminus of the YTK Prx 4 insert and the termination of translation site in the pET-30a multiple cloning site encodes a His-tag. This His-tag is in addition to the one encoded by the 5' region of the pET-30a multiple cloning site that is located upstream of the YTK Prx 4 insert. Therefore, it is quite likely that the recombinant YTK Prx 4-197 and 231 proteins contained both an

N-terminal and a C-terminal His-tag. The termination of translation of the YTK Prx 4 open reading frame is encoded by a single TGA codon. The efficiency of the TGA codon in the termination of translation in *E. coli* was investigated by Mottagui-Tabar et al. (1994). They observed up to a 30-fold difference in read-through of the TGA codon that was dependent upon the nature of the second to last codon that preceded it. The YTK Prx 4 ORF possesses a CTC codon as the second to last codon preceding the TGA stop codon. According to Mottagui-Tabar et al. (1994), the ratio of the formation of a read-through product to the formation of a non-read-through product for the codon usage observed in the YTK Prx 4 ORF was 0.17. This suggests that translational read-through of the YTK Prx 4 stop codon could account for the larger than expected molecular masses of the recombinant YTK Prx 4-197 and 231 proteins.

The YTK Prx 4-264 protein was expressed in *E. coli* BL21 (DE3) cells and purified by Ni-affinity chromatography utilising an N-terminal His-tag encoded by the pET-30a vector. Immunoblotting analysis of the Ni-affinity chromatography 500 mM imidazole elution fraction using anti-His antibodies and anti-(SBT Prx 2) antibodies detected two forms of the YTK Prx 4-264 protein with molecular masses of 32 and 36 kDa. The 36 kDa form is consistent with the expected molecular mass of the YTK Prx 4 -264 protein monomer. However, the 32 form is not consistent with any expected form of the YTK Prx 4-264 protein. Interestingly, the 32 kDa form of the YTK Prx 4-264 is consistent with the observed molecular mass of the recombinant YTK Prx 4-231 protein. It is tempting to speculate that the observed molecular masses of the YTK Prx 4-231 protein and the 32 kDa form of the YTK Prx 4-264 protein were found to be equal for two reasons. Firstly, that the putative N-terminal signal peptide, predicted by the SignalP software, may have been removed from the YTK Prx 4-264 protein (36 kDa form) post translation. Secondly, as proposed for the YTK Prx 4-231 protein, the termination of translation for the YTK Prx 4-264 protein

may have occurred at the multiple stop codons incorporated into the 3' terminus of the pET-30a multiple cloning site rather than at the stop codon incorporated into the YTK Prx 4 ORF. The latter would have led to the incorporation of a C-terminal His-tag into the YTK Prx 4-264 protein. This provided a plausible explanation for the detection of the 32 kDa form of the YTK Prx 4-264 protein by immunoblotting using anti-His antibodies despite the loss of the N-terminal His-tag and associated putative signal peptide. Therefore, it appeared that the N-terminal signal peptide of the 36 kDa form of the YTK Prx 4-264 protein was most likely able to be recognised and cleaved by an *E. coli* signal peptidase. This result is not surprising given that the substrate specificities of signal peptidases are remarkably similar and appear to be conserved in evolution (Dalbey and Gunnar von Heijne, 1992). For example, expression of the preproinsulin protein from rat in *E. coli* demonstrated that a eukaryotic ER/secretion signal peptide was able to direct the recombinant protein to the periplasmic space and be correctly processed to produce proinsulin (Talmadge et al., 1981). Similarly, a signal peptidase from *E. coli* was shown to be able to process the mouse precursor IgG  $\kappa$  fragment into mature protein (Watts et al., 1983).

Although enriched by the Ni-affinity chromatography, recovery of the YTK Prx 4-264 protein was lower than expected compared to the observed recovery of Ni-affinity purified YTK Prx 4-197 and 231 proteins. Having ruled out a loss of protein during the Ni-affinity column purification, the *E. coli* BL21 (DE3) cells expressing the YTK Prx 4-264 protein were analysed by differential centrifugation. Immunoblotting analysis of various fractions produced from the differential centrifugation using anti-(southern bluefin tuna Prx 2) antibodies revealed that the YTK Prx 4-264 protein was expressed as a mixture of soluble and insoluble forms. Therefore, the insoluble portion of the expressed YTK Prx 4-264 protein, presumably lost in the

centrifugation of the whole cell crude lysate, accounted for the lower than expected recovery of the protein following Ni-affinity chromatography purification.

The accumulation of insoluble YTK Prx 4-264 protein within the *E. coli* BL21 (DE3) cells is most likely due to its putative N-terminal secretory signal peptide. As previously discussed, the putative secretory signal peptide of the YTK Prx 4-264 protein appears to be able to be recognised and processed to a limited extent by the *E. coli* BL21 (DE3) cells. According to a review of protein secretion systems in gram-negative bacteria, there are at least eight independently functioning types of systems that catalyse protein transport across or insertion into both the inner and outer membranes (Milton, 2006). These translocation systems use different mechanisms to transport fully unfolded, partially folded or fully folded proteins (Milton, 2006). Of the various transport systems, the signal recognition particle (SRP) pathway of *E. coli* involves cytosolic factors that strongly resemble components involved in protein targeting to the eukaryotic ER membrane (Valent et al., 1998). In both of these systems, the SRP ribonucleoprotein recognises and binds to the N-terminal signal peptide of the nascent polypeptide chain, inhibiting further translational elongation. The ribosomal-nascent peptide in complex with SRP is targeted to the inner membrane where it binds to an SRP receptor. This binding event results in the release of SRP, enabling translational elongation of the nascent peptide to continue while it enters the periplasmic space (Valent et al., 1998). The conditions within the periplasmic space of the *E. coli* may be sufficiently different from that of the lumen of the endoplasmic reticulum that it prevents the YTK Prx 4-264 protein from adopting its correctly folded structure, causing it to form insoluble aggregates. Alternatively, the YTK Prx 4-264 protein may be translated in the cytoplasm and its N-terminal signal peptide recognised by the SecB protein. The SecB protein may bind directly to the signal peptide, although it is more widely accepted that the signal peptide retards protein folding sufficiently to allow the SecB

protein to bind to multiple sites on the protein backbone. Thus, the SecB acts in a similar fashion to general molecular chaperones (Pugsley, 1993). Therefore, the YTK Prx 4 may have been misfolded due to the presence of the signal peptide or by interaction with the SecB protein. Regardless of the possible cause of the misfolding, the YTK Prx 4 protein complexed with the SecB protein would have been delivered to the translocon where its signal peptide would be removed by a signal peptidase as it enters the periplasmic space. The extracellular secretion of proteins delivered to the periplasmic space by both the SRP and SecB pathways is performed by the main terminal branch pathway. The main terminal branch pathway is composed of a poorly defined complex, consisting of 12-16 proteins that are not expressed under normal laboratory conditions (Francetic and Pugsley, 1996). As a result, the most likely misfolded YTK Prx 4 protein would accumulate in the periplasmic space leading to the formation of insoluble aggregates.

The native molecular mass of the Ni-affinity purified YTK Prx 4-197 and 231 proteins was investigated by gel filtration chromatography under reducing and oxidising conditions. Regardless of the redox conditions, the gel filtration analysis of both the YTK Prx 4-197 and 231 proteins revealed that they existed as a single oligomeric form with a molecular mass consistent with a decamer. Similarly, gel filtration analysis of the equivalent Prx 4 proteins (i.e. Prx 4 proteins with and without the characteristic N-terminal amino acid extension) from rat were also found to exist solely as decamer under reducing conditions. However, in contrast to the YTK Prx 4-197 and 231 proteins, the equivalent Prx 4 proteins from rat were found to exist as a mixture of decamer and higher molecular mass forms under oxidising conditions (Ikeda et al., 2010). The Prx 4 protein from rat that lacked the N-terminal amino acid extension was found to display a far higher propensity to form larger molecular mass forms under oxidising conditions compared to the same protein that contained the N-terminal amino acid extension. As such, it was hypothesised that under oxidising



conditions it is likely that the N-terminal amino acid extension regulates the formation of higher molecular mass forms. The discrepancy between the oxidised YTK Prx 4 and oxidised rat Prx 4 results suggests that the N-terminal amino acid extension may not be the only factor regulating the formation of higher molecular mass forms. The difference between these two results may be attributable to differences in the treatment of the proteins prior to gel filtration analysis. The YTK Prx 4-197 and 231 proteins were incubated in a Tris-based buffer that lacked reducing agent while the rat Prx 4 proteins were incubated in a phosphate-buffered saline solution containing 100  $\mu$ M t-BuOOH. The use of t-BuOOH in the absence of a reducing system may have led to the over-oxidation of the rat Prx 4 proteins. The over-oxidation of typical 2-Cys Prx proteins has been shown to promote the association of decamers to form higher order aggregates (Barranco-Medina et al., 2009; Hall et al., 2009). As a result, the N-terminal amino acid extension may act to decrease the formation of higher molecular mass forms by decreasing the sensitivity of the protein to peroxide. Conversely, the removal of the N-terminal amino acid extension may increase the formation of higher molecular mass forms due to an increased sensitivity to peroxides or in other words, an increased chance of over-oxidation.

# Chapter 6

General discussion and conclusion

This thesis has presented the sequence analysis, recombinant expression, purification and characterisation of three typical 2-Cys peroxiredoxins (Prxs) from three finfish species, *Thunnus maccoyii* (southern bluefin tuna, SBT), *Salmo salar* (Atlantic salmon, AS) and *Seriola lalandi* (yellowtail kingfish, YTK). Including the previously reported YTK Prx 4 characterisation performed within our research group (Loo and Schuller, 2010), these studies are the first functional and structural characterisations of typical 2-Cys Prxs from finfish.

The SBT Prx 2 and AS Prx 1 deduced amino acid sequences contained sequence features, including peroxidatic and resolving Cys residues, which are highly conserved amongst typical 2-Cys Prxs (Wood et al., 2003a; König et al., 2003). Phylogenetic analyses of deduced amino acid sequences grouped the SBT Prx 2 and AS Prx 1 with their corresponding Prx homologs from other finfish and mammals. The close evolutionary relationships between the same Prx isoforms from different classes are not surprising given the high degree of amino acid sequence conservation. For example, pairwise comparisons of deduced amino acid sequences revealed that the SBT Prx 2 and AS Prx 1 displayed  $\geq 76\%$  and  $\geq 79\%$  amino acid identity, respectively, with the corresponding Prx homologs from mammals.

In contrast to SBT Prx 2 and AS Prx 1, the YTK Prx 4 deduced amino acid sequence contains an N-terminal extension that most likely constitutes a signal peptide (Loo and Schuller, 2010). The presence of an N-terminal signal peptide is a characteristic feature of mammalian Prx 4 proteins. In mammals, the signal peptide directs the Prx 4 protein to the endoplasmic reticulum for export to the extracellular space (Matsumoto et al., 1999). Previous characterisation of the YTK Prx 4 suggested two possible signal peptides of different lengths that were predicted by SignalP software and alignment with 2-Cys Prxs from other finfish and mammals. The removal of both predicted N-terminal signal peptides resulted in YTK Prx 4

proteins that possessed similar levels of thioredoxin-dependent peroxidase activity. Thus, it was unknown whether either, or both, of the predicted N-terminal signal peptides were relevant *in vivo*. In the current study, the composition of the N-terminal signal peptide predicted by SignalP software satisfied more of the requirements of an ER signal peptide compared to the N-terminal signal peptide predicted by multiple sequence alignment. This suggested that the YTK Prx 4-231 protein (full length YTK Prx 4-264 protein lacking the N-terminal signal peptide predicted by SignalP software) was more likely to be relevant *in vivo* compared to the YTK Prx 4-197 protein (full length YTK Prx 4-264 protein lacking the N-terminal signal peptide predicted by multiple alignment). Further evidence in support of the *in vivo* relevance of the YTK Prx 4-231 protein over the YTK Prx 4-197 protein came from comparison with rat Prx 4 protein. The molecular mass of the YTK Prx 4-231 protein corresponded closely to the processed mature form of the rat Prx 4.

Functional characterisation of the SBT Prx 2 and AS Prx 1 revealed that both proteins exhibited thioredoxin-dependent peroxidase activity. At low concentrations of peroxide substrate ( $\leq 120 \mu\text{M}$ ), the SBT Prx 2 displayed positive cooperativity, a unique feature among typical 2-Cys Prxs. In contrast, at increasing high concentrations of peroxide substrate (0.5-2.0 mM), SBT Prx 2 and AS Prx 1 were progressively inactivated. The progressive inactivation of eukaryotic Prxs by high concentrations of peroxide substrate is attributed to two conserved motifs, GGLG and XF (Wood et al., 2003a). In mammals, the GGLG motif is paired with a YF motif while in most finfish it is paired with a FF motif (Sutton et al., 2010). As expected, the AS Prx 1 contained GGLG and FF motifs. In contrast, the SBT Prx 2 contained a GGLG motif but in place of the expected FF motif it had an LF motif. To determine whether or not these different residues are structurally equivalent in terms of packing of the GGLG and XF motifs, attempts were made to determine the crystal

structures of the SBT Prx 2 and AS Prx 1 proteins. Despite being able to produce crystals, structures were not able to be determined due to a lack of diffraction.

Functional characterisation also revealed that the AS Prx 1 protein was more susceptible to inactivation by high concentrations of peroxide substrate compared to the SBT Prx 2 protein. For example, at 1 mM H<sub>2</sub>O<sub>2</sub>, AS Prx 1 retained only 5% of the peroxidase activity it displayed at 0.1 mM H<sub>2</sub>O<sub>2</sub> whereas SBT Prx 2 retained 63% of the peroxidase activity it displayed at 0.1 mM H<sub>2</sub>O<sub>2</sub>. In humans it has been established that Prx 1 is more susceptible than Prx 2 to inactivation by high concentrations of peroxide substrate because it contains an additional Cys residue located in the dimer-dimer interfaces of its decamer structure (Lee et al., 2007). It has been proposed that this additional Cys residue stabilises the dimer-dimer interface and in doing so, hinders localised unfolding required for disulphide bond formation to occur between the peroxidatic and resolving Cys residues. Thus, the peroxidatic Cys is more prone to inactivation via over-oxidation. As expected, the AS Prx 1 amino acid sequence contained an additional Cys residue at position 83 while the SBT Prx 2 amino acid sequence did not. It is tempting to speculate that in addition to C<sup>83</sup>, the difference in susceptibility to inactivation between SBT Prx 2 and AS Prx 1 could also be influenced by differences in the composition of their corresponding XF motifs.

Analysis of the native molecular mass of SBT Prx 2, AS Prx 1 and YTK Prx 4 by gel filtration chromatography revealed that these proteins form a variety of oligomeric structures. Under reducing and oxidising conditions, the native molecular mass of the SBT Prx 2 and YTK Prx 4 197 and 231 proteins remained relatively unchanged. In contrast, the native molecular mass of the AS Prx 1 protein was severely affected by redox status. Under reducing conditions, the AS Prx 1 protein existed almost exclusively as decamers while under oxidising conditions its structural integrity was compromised resulting in the formation of insoluble aggregates. A similar loss in

structural integrity was also observed in the C75S mutant of the SBT Prx 2 protein. Using the rat Prx 1 crystal structure as a model, the C75S mutation most likely triggered destabilisation of the SBT Prx 2 protein structure through disruption of the dimer-dimer interface and internal organisation of the monomer protein core.

At comparable protein concentrations, AS Prx 1 and YTK Prx 4 existed exclusively as decamer while the SBT Prx 2 existed predominantly as dimer. However, at a higher protein concentration, the native molecular mass of SBT Prx 2 shifted from dimer to higher order oligomeric structures including decamer. For example, at a protein concentration of  $12 \text{ mg mL}^{-1}$  the SBT Prx 2 existed predominantly as dimer while at a protein concentration of  $30 \text{ mg mL}^{-1}$  the SBT Prx 2 existed predominantly as a mixture of decamer and a higher order oligomer that may be a dimer of decamers. It is interesting to note that prolonged storage under presumably oxidising conditions promoted conversion of the decamer into the putative dimer of decamers. The formation of higher order oligomers consisting of stacked decamer subunits has been previously reported to occur in Prxs (Akerman and Müller, 2003). However, the physiological relevance of these higher order oligomers, if any, is not known (Wood et al., 2003b).

This thesis has presented the first functional and structural characterisation of a selection of typical 2-Cys Prx proteins from three finfish species that are important in Australian aquaculture. This work provides a foundation upon which to base further examination of finfish Prx proteins. Future work on finfish Prx proteins could involve investigation into sub-cellular localisation, chaperone activity and the identification and characterisation of any remaining isoforms. In addition to its academic value, this work may also be of benefit to the finfish farming industry through aiding in the development of improved practices and tools that minimise oxidative stress. For example, the overoxidation and consequent inactivation of typical 2-Cys Prx proteins may be able to be developed into a bio-marker that could be used to assess the

level of oxidative stress in farmed finfish. The use of this bio-marker could alert finfish farming operators to the possibility of oxidised feeds, parasite infections or the presence of oxidising pollutants. The early detection and prevention of further oxidative stress in farmed finfish has the potential to decrease rates of disease and mortality while maximising the quality, and hence the value, of end-products.

# References

- Akerman, S.E., Müller, S., 2003. 2-Cys peroxiredoxin PfTrx-Px1 is involved in the antioxidant defence of *Plasmodium falciparum*. *Mol. Biochem. Parasitol.* 130, 75–81.
- Akerman, S.E., Müller, S., 2005. Peroxiredoxin-linked detoxification of hydroperoxides in *Toxoplasma gondii*. *J. Biol. Chem.* 280, 564–570.
- Alvarez, M.J., Lopez-Bote, C.J., Diez, A., Corraze, G., Arzel, J., Dias, J., Kaushik, S.J., Bautista, J.M., 1998. Dietary fish oil and digestible protein modify susceptibility to lipid peroxidation in the muscle of rainbow trout (*Oncorhynchus mykiss*) and sea bass (*Dicentrarchus labrax*). *British Journal of Nutrition.* 80, 281-289.
- Azzam, E.I., de Toledo, S.M., Little, J.B., 2003. Oxidative metabolism, gap junctions and the ionizing radiation-induced bystander effect. *Oncogene.* 22, 7050-7057.
- Babior, B.M., 1995. The respiratory burst oxidase. *Current Opinion in Hematology.* 2, 55-60.
- Barranco-Medina, S., Lázaro, J.-J., Dietz, K.-J., 2009. The oligomeric conformation of peroxiredoxins links redox state to function. *FEBS Letters.* 583, 1809–1816.
- Bartkowiak, A., Grzelińska, E., Varga, I.SZ., 1981. Studies on superoxide dismutase from cod (*Gadus Morhua*) liver. *International Journal of Biochemistry.* 13, 1039-1072.
- Bell, J.G., Cowey, C.B., Youngson, A., 1984. Rainbow trout liver microsomal lipid peroxidation. The effect of purified glutathione peroxidase, glutathione S-transferase and other factors. *Biochimica et Biophysica Acta – Lipids and lipid metabolism.* 795, 91-99.



- Belló, A.R.R., Fortes, E., Belló-Klein, A., Belló, A.A., Llesuy, S.F., Robaldo, R.B., Bianchini, A., 2000. Lipid peroxidation induced by *Clinostomum detruncatum* in muscle of freshwater fish *Rhamdia quelen*. *Diseases of Aquatic Organisms*. 42, 233-236.
- Bendtsen, J.D., Nielsen, H., von Heijne, G., Brunak, S., 2004. Improved prediction of signal peptides: SignalP 3.0. *Journal of Molecular Biology*. 340, 783-795.
- Bernier-Villamor, L., Navarro, E., Sevilla, F. and Lázaro, J.J., 2004. Cloning and characterization of a 2-Cys peroxiredoxin from *Pisum sativum*. *J. Exp. Bot.* 55, 2191–2199.
- Biteau, B., Labarre, J., Toledano, M.B., 2003. ATP-dependent reduction of cysteine-sulphinic acid by *S. cerevisiae* sulphiredoxin. *Nature*. 425, 980-984.
- Boucher, I.W., McMillan, P.J., Gabrielsen, M., Akerman, S.E., Brannigan, J.A., Schnick, C., Brzozowski, A.M., Wilkinson, A.J., Müller, S., 2006. Structural and biochemical characterization of a mitochondrial peroxiredoxin from *Plasmodium falciparum*. *Mol. Microbiol.* 61, 948–959.
- Boveris, A., Oshino, N., Chance, B., 1972. The cellular production of hydrogen peroxide. *Biochemical Journal*. 128, 617-630.
- Bradford, M., 1976. A rapid and sensitive method for the quantitation of microgram quantities of protein utilizing the principle of protein dye-binding. *Anal. Biochem.* 72, 248–254.
- Butler, R.E., Cihlarova, V., Stewart, G.R., 2010. Effective generation of reactive oxygen species in the mycobacterial phagosome requires K<sup>+</sup> efflux from the bacterium. *Cellular Microbiology*. 12, 1186-1193.

- Chae, H.Z., Chung, S.J., Rhee, S.G., 1994c. Thioredoxin-dependent peroxide reductase from yeast. *J. Biol. Chem.* 269, 27670–27678.
- Chae, H.Z., Kim, H.J., Kang, S.W., Rhee, S.G., 1999. Characterization of three isoforms of mammalian peroxiredoxin that reduce peroxides in the presence of thioredoxin. *Diabetes Res. Clin. Pract.* 45, 101–112.
- Chae, H.Z., Kim, I., Kim, K., Rhee, S.G., 1993. Cloning, sequencing, and mutation of thiol-specific antioxidant gene of *Saccharomyces cerevisiae*. *The Journal of Biological Chemistry.* 268, 16815-16821.
- Chae, H.Z., Robison, K., Poole, L.B., Church, G., Storz, G., Rhee, S.G., 1994a. Cloning and sequencing of thiol-specific antioxidant from mammalian brain: Alkyl hydroperoxide reductase and thiol-specific antioxidant define a large family of antioxidant enzymes. *Proceedings of the National Academy of Sciences of the United States of America.* 91, 7017-7021.
- Chae, H.Z., Uhm, T.B., Rhee, S.G., 1994b. Dimerisation of thiol-specific antioxidant and the essential role of Cysteine 47. *Proceedings of the National Academy of Sciences of the United States of America.* 91, 7022-7026.
- Chance, B., Oshino, N., 1971. Kinetics and mechanisms of catalase in peroxisomes of the mitochondrial fraction. *Biochemical Journal.* 122, 225-233.
- Chaudière, J., Ferrari-Iliou, R., 1999. Intracellular antioxidants: from chemical to biochemical mechanisms. *Food and Chemical Toxicology.* 37, 949-962.
- Cochemé, H.M., Murphy, M.P., 2009. Mitochondria as a source of reactive oxygen species. *Biochemical Journal (Classics).* 1-4.

- Cooke, M.S., Evans, M.D., Dizdaroglu, M., Lunec, J., 2003. Oxidative DNA damage: mechanisms, mutations, and disease. *The Journal of the Federation of American Societies for Experimental Biology*. 17, 1195-1214.
- Cox, A.G., Pearson, A.G., Pullar, J.M., Jönsson, T.J., Lowther, W.T., Winterbourn, C.C., Hampton, M.B., 2009. Mitochondrial peroxiredoxin 3 is more resilient to hyperoxidation than cytoplasmic peroxiredoxins. *Biochem. J.* 421, 51–58.
- Dalbey, R.E. and von Heijne, G., 1992. Signal peptidases in prokaryotes and eukaryotes – a new protease family. *Trends in Biochemical Sciences*. 17, 474-478.
- D'Autréaux, B., Toledano, M.B., 2007. ROS as signalling molecules: mechanisms that generate specificity in ROS homeostasis. *Nature Reviews: Molecular Cell Biology*. 8, 813-824.
- Dautremepuits, C., Betoulle, S., Vernet, G., 2003. Stimulation of antioxidant enzymes levels in carp (*Cyprinus carpio* L.) infected by *Ptychobothrium* sp. (Cestoda). *Fish and Shellfish Immunology*. 15, 467-471.
- De Duve, C., Baudhuin, P., 1966. Peroxisomes (microbodies and related particles). *Physiological Reviews*. 46, 323-357.
- Dong, W., Xiang, L., Shao, J., 2007. Cloning and characterization of two natural killer enhancing factor genes (NKEF-A and NKEF-B) in pufferfish, *Tetraodon nigroviridis*. *Fish and Shellfish Immunology*. 22, 1-15.
- Errede, B., Kamen, M.D., Hatefi, Y., 1978. Preparation and properties of complex IV (Ferrocytochrome c :Oxygen Oxidoreductase EC 1.9.3.1). *Methods in enzymology*. 53, 40-47.

Fatima, M., Ahmad, I., Sayeed, I., Athar, M., Raisuddin, S., 2000. Pollutant-induced over-activation of phagocytes is concomitantly associated with peroxidative damage in fish tissues. *Aquatic Toxicology*. 49, 243-250.

Fenton, H.J.H., 1894. Oxidation of tartaric acid in the presence of iron. *Journal of the Chemical Society, Transactions*. 65, 899-910.

Fisher, A.B., 2011. Peroxiredoxin 6: A bifunctional enzyme with glutathione peroxidase and phospholipase A<sub>2</sub> activities. *Antioxidants and Redox Signalling*. 15, 831-844.

Fitz-Gerald, C.H., Bremner, H.A., 1998. The oxidative stability of chilled and frozen pilchards used as feed for captive southern bluefin tuna. *Journal of Aquatic Food Product Technology*. 7, 27-44.

Francetic, L. and Pugsley, A.P., 1996. The cryptic general secretory pathway (gsp) operon of *Escherichia coli* k-12 encodes functional proteins. *J. Bacteriol.* 178, 3544-3549.

Garrett, R.H., Grisham, C.M., 2008. *Biochemistry*, 4<sup>th</sup> edition. Brooks/Cole, Boston, USA.

Gernert, K.M., Smith, R. and Carter, D.C., 1987. A simple apparatus for controlling nucleation and size in protein crystal growth. *Analytical Biochemistry*. 168, 141-147.

Gillette, J.R., Brodie, B.B., La Du, B.N., 1956. The oxidation of drugs by liver microsomes: On the role of TPNH and oxygen. *The Journal of Pharmacology and experimental therapeutics*. 119, 532-540.

Gough, D.R., Cotter, T.G., 2011. Hydrogen peroxide: a Jekyll and Hyde signalling molecule. *Cell Death and Disease*. 2, October 06, 1-8.

Gourlay, L.J., Bhella, D., Kelly, S.M., Price, N.C., Lindsay, J.G., 2003. Structure-function analysis of recombinant substrate protein 22 kDa (SP-22). *The Journal of Biological Chemistry*. 278, 32631-32637.

Gutteridge, J.M.C., 1995. Lipid peroxidation and antioxidants as biomarkers of tissue damage. *Clinical Chemistry*. 41, 1819-1828.

Haber, F., Weiss, J., 1934. The catalytic decomposition of hydrogen peroxide by iron salts. *Proceedings of the Royal Society A*. 147, 332-351.

Hall, T.A., 1999. BioEdit: a user-friendly biological sequence alignment editor and analysis program for Windows 95/98/NT. *Nucl. Acids Symp. Ser.* 41, 95–98.

Hall, A., Karplus, P.A., Poole, L.B., 2009. Typical 2-Cys peroxiredoxins — structures mechanisms and functions. *FEBS J*. 276, 2469–2477.

Halliwell, B., 1978. Biochemical mechanisms accounting for the toxic action of oxygen on living organisms: The key role of superoxide dismutase. *Cell Biology International Reports*. 2, 113-128.

Halliwell, B., Chirico, S., 1993. Lipid peroxidation: its mechanism, measurement, and significance. *The American Journal of Clinical Nutrition*. 57 (suppl), 715S-725S.

Halliwell, B., Gutteridge, J.M.C., 1989. *Free Radicals in Biology and Medicine*, 2<sup>nd</sup> edition. Clarendon Press, Oxford, UK.

Harrison, R., 2002. Structure and function of xanthine oxidoreductase: Where are we now? *Free Radical Biology and Medicine*. 33, 774-797.

Higgins, S.J. and Hames, B.D., 2003. *Protein expression: a practical approach*. Oxford University Press. 80.

Hirotsu, S., Abe, Y., Okada, K., Nagahara, N., Hori, H., Nishino, T. and Hakoshima, T., 1999. Crystal structure of a multifunctional 2-Cys peroxiredoxin heme-binding protein 23 kDa/proliferation-associated gene product. PNAS. 96, 12333-12338.

Hofmann, B., Hecht, H.-J., Flohé, L., 2002. Peroxiredoxins. Biol. Chem. 383, 347–364.

Huang, R., Gao, L., Wang, Y., Hu, W., Guo, Q., 2009. Structure, organization and expression of common carp (*Cyprinus carpio* L.) NKEF-B gene. Fish and shellfish immunology. 26, 220-229.

Ikeda, Y., Ito, R., Ihara, H., Okada, T., Fujii, J., 2010. Expression of N-terminally truncated forms of rat peroxiredoxin-4 in insect cells. Protein Expression and Purification. 72, 1-7.

Jacobson, F.S., Morgan, R.W., Christman, M.F., Ames, B.N., 1989. An alkyl hydroperoxide reductase from *Salmonella typhimurium* involved in the defense of DNA against oxidative damage. The Journal of Biological Chemistry. 264, 1488-1496.

Jensen, P.K., 1966. Antimycin-insensitive oxidation of succinate and reduced nicotinamide-adenine dinucleotide in electron transport particles .I. pH dependency and hydrogen peroxide formation. Biochemica Et Biophysica Acta. 122, 157-166.

Jin, D-Y., Chae, H.Z., Rhee, S.G., Jeang, K-T., 1997. Regulatory role for a novel human thioredoxin peroxidase in NF- $\kappa$ B activation. The Journal of Biological Chemistry. 272, 30952-30961.

Jönsson, T.J., Lowther, W.T., 2007. The peroxiredoxin repair proteins. Subcellular Biochemistry. 44, 115-141.

- Jos, Á., Pichardo, S., Prieto, A.I., Repetto, G., Vázquez, C.M., Moreno, I., Cameán, A.M., 2005. Toxic cyanobacterial cells containing microcystins induce oxidative stress in exposed tilapia fish (*Oreochromis* sp.) under laboratory conditions. *Aquatic Toxicology*. 72, 261-271.
- Kantardjieff, K.A. and Rupp, B., 2004. Protein isoelectric point as a predictor for increased crystallization screening efficiency. *Bioinformatics*. 20, 2162-2168.
- Kehrer, J.P., 2000. The Haber-Weiss reaction and mechanisms of toxicity. *Toxicology*. 149, 43-50.
- Ken, C., Weng, D., Duan, K., Lin, C., 2002. Characterization of copper/zinc-superoxide dismutase from *Pagrus major* cDNA and enzyme stability. *Journal of Agricultural and Food Chemistry*. 50, 784-789.
- Kim, K., Kim, I.H., Lee, K., Rhee, S.G., Stadtman, E.R., 1988. The isolation and purification of a specific "protector" protein which inhibits enzyme inactivation by a thiol/Fe(III)/O<sub>2</sub> mixed-function oxidation system. *The Journal of Biological Chemistry*. 263, 4704-4711.
- Kirkman, H.N., Gaetani, G.F., 2007. Mammalian catalase: a venerable enzyme with new mysteries. *Trends in Biochemical Sciences*. 32, 44-50.
- Kitano, K., Kita, A., Hakoshima, T., Niimura, Y., Miki, K., 2005. Crystal structure of decameric peroxiredoxin (AhpC) from *Amphibacillus xylanus*. *Proteins: Structure, function, and bioinformatics*. 59, 644-647.
- König, J., Lotte, K., Plessow, R., Brockhinke, A., Baier, M., Dietz, K.-J., 2003. Reaction mechanism of plant 2-Cys peroxiredoxin. Role of the C terminus and the quaternary structure. *J. Biol. Chem*. 278, 24409–24420.

Lambeth, J.D., 2004. NOX enzymes and the biology of reactive oxygen. *Nature Reviews Immunology*. 4, 181-189.

Larkin, M.A., Blackshields, G., Brown, N.P., Chenna, R., McGettigan, P.A., McWilliam, H., Valentin, F., Wallace, I.M., Wilm, A., Lopez, R., Thompson, J.D., Gibson, T.J., Higgins, D.G., 2007. Clustal W and Clustal X version 2.0. *Bioinformatics* 23, 2947–2948.

Lee, W., Choi, K.-S., Riddell, J., Ip, C., Ghosh, D., Park, J.-H., Park, Y.-M., 2007. Human peroxiredoxin 1 and 2 are not duplicate proteins. The unique presence of Cys83 in Prx1 underscores the structural and functional differences between Prx1 and Prx2. *J. Biol. Chem.* 282, 22011–22022.

Lehnert, B.E., Goodwin, E.H., 1997. Extracellular factor(s) following exposure to  $\alpha$  particles can cause sister chromatid exchanges in normal human cells. *Cancer Research*. 57, 2164-2171.

Li, R.W. and Waldbieser, G.C., 2006. Genomic organisation and expression of the natural killer cell enhancing factor (NKEF) gene in channel catfish, *Ictalurus punctatus* (Rafinesque). *Fish and Shellfish Immunology*. 20, 72-82.

Lin, C.T., Lee, T.L., Duan, K.J., Ken, C.F., 2000. Molecular cloning, characterization and expression of a cDNA coding copper/zinc superoxide dismutase from Black Porgy. *Journal of Agricultural and Food Chemistry*. 48, 4444-4447.

Lodish, H., Berk, A., Kaiser, C.A., Krieger, M., Scott, M.P., Bretscher, A., Ploegh, H., Matsudaira, P., 2008. *Molecular Cell Biology*. W.H. Freeman and company. Figure 5-23.



- Loo, G.H. and Schuller, K.A., 2010. Cloning and functional characterization of a peroxiredoxin 4 from yellowtail kingfish (*Seriola lalandi*). *Comparative Biochemistry and Physiology. Part B.* 156, 244-253.
- Loo, G.H., Sutton, D.L., Schuller, K.A., 2012. Cloning and functional characterisation of a peroxiredoxin 1 (NKEF A) cDNA from Atlantic salmon (*Salmo salar*) and its expression in fish infected with *Neoparamoeba perurans*. *Fish and Shellfish Immunology.* 32, 1074-1082.
- Loschen, G., Azzi, A., Richter, C., Flohé, L., 1974. Superoxide radicals as precursors of mitochondrial hydrogen peroxide. *FEBS Letters.* 42, 68-72.
- Manta, B., Hugo, M., Ortiz, C., Ferrer-Sueta, G., Trujillo, M., Denicola, A., 2009. The peroxidase and peroxynitrite reductase activity of human erythrocyte peroxiredoxin 2. *Arch. Biochem. Biophys.* 484, 146–154.
- Marklund, S.L., 1984. Extracellular superoxide dismutase and other superoxide dismutase isoenzymes in tissues from nine mammalian species. *Biochemical Journal.* 222, 649-655.
- Marnett, L.J., 2000. Oxyradicals and DNA damage. *Carcinogenesis.* 21, 361-370.
- Martínez-Álvarez, R.M., Morales, A.E., Sanz, A., 2005. Antioxidant defenses in fish: Biotic and abiotic factors. *Reviews in Fish Biology and Fisheries.* 15, 75-88.
- Matés, J.M., 2000. Effects of antioxidant enzymes in the molecular control of reactive oxygen species toxicology. *Toxicology.* 153, 83-104.
- Matsumoto, A., Okado, A., Fujii, T., Fujii, J., Egashira, M., Niikawa, N., Taniguchi, N., 1999. Cloning of the peroxiredoxin gene family in rats and characterization of the fourth member. *FEBS letters.* 443, 246-250.

Matsumura, T., Okamoto, K., Iwahara, S., Hori, H., Takahashi, Y., Nishino, T., Abe, Y., 2008. Dimer-oligomer interconversion of wild-type and mutant rat 2-Cys peroxiredoxin: disulphide formation at dimer-dimer interfaces is not essential for decamerization. *The Journal of Biological Chemistry*. 283, 284-293.

May, J.M., 1998. Ascorbate function and metabolism in the human erythrocyte. *Frontiers in Bioscience*. 3, d1-10.

McCord, J.M., Fridovich, I., 1968. The reduction of cytochrome *c* by milk xanthine oxidase. *The Journal of Biological Chemistry*. 243, 5753-5760.

McCord, J.M., Fridovich, I., 1969. An enzymic function for erythrocyte cuprein (Hemocuprein). *The Journal of Biological Chemistry*. 244, 6049-6055.

Mikol, V., Rodeau, J-L., Giegé, 1990. Experimental determination of water equilibration rates in the hanging drop method of protein crystallization. *Analytical Biochemistry*. 186, 332-339.

Milton, S.H., 2006. Protein secretion systems in gram-negative bacteria. *Microbe*. 1, 414-419.

Miwa, S., St-Pierre, J., Partridge, L., Brand, M.D., 2003. Superoxide and hydrogen peroxide production by *Drosophila* mitochondria. *Free Radical Biology and Medicine*. 35, 938-948.

Montemartini, M., Kalisz, H.M., Hecht, H, Steinert, P. and Flohé, L., 1999. Activation of active-site cysteine residues in the peroxiredoxin-type trypanothione peroxidase of *Crithidia fasciculata*. *Eur. J. of Biochem*. 264, 516-524.

Mottagui-Tabar, S., Björnsson, A., Isaksson, L.A., 1994. The second to last amino acid in the nascent peptide as a codon context determinant. *The EMBO Journal*. 13, 249-257.

Mourente, G., Díaz-Salvago, E., Tocher, D.R., Bell, J.G., 2000. Effects of dietary polyunsaturated fatty acid/vitamin E (PUFA/tocopherol) ratio on antioxidant defence mechanisms of juvenile gilthead sea bream (*Sparus aurata* L., Osteichthyes, Sparidae). *Fish Physiology and Biochemistry*. 23, 337-351.

Munhoz, D.C., Netto, L.E.S., 2004. Cytosolic thioredoxin peroxidase I and II are important defenses of yeast against organic hydroperoxide insult. Catalases and peroxiredoxins cooperate in the decomposition of H<sub>2</sub>O<sub>2</sub> by yeast. *J. Biol. Chem.* 279, 35219–35227.

Murphy, M.P., 2009. How mitochondria produce reactive oxygen species. *Journal of Biochemistry*. 417, 1-13.

Nagai, T., Yukimoto, T., Suzuki, N., 2002. Glutathione peroxidase from the liver of Japanese sea bass *Lateolabrax japonicas*. *Z. Naturforsch.* 57c, 172-176.

Nakano, T., Sato, M., Takeuchi, M., 1992. Partial purification and properties of glutathione peroxidase from carp hepatopancreas. *Comparative Biochemistry and Physiology Part B*. 102, 31-35.

Narayanan, P.K., Goodwin, E.H., Lehnert, B.E., 1997. A particles initiate biological production of superoxide anions and hydrogen peroxide in human cells. *Cancer Research*. 57, 3963-3971.

Nicholas, K.B., Nicholas Jr., H.B., Deerfield II, D.W., 1997. Genedoc: analysis and visualization of genetic variation. *embnet.news* 4 (2), 1.

Nordberg, J., Arnér, E.S.J., 2001. Reactive oxygen species , antioxidants, and the mammalian thioredoxin system. *Free Radical Biology & Medicine*. 31, 1287-1312.

- Okado-Matsumoto, A., Matsumoto, A, Fujii, J., Taniguchi, N., 2000. Peroxiredoxin IV is a secretable protein with heparin-binding properties under reduced conditions. *J. Biochem.* 127, 493-501.
- Paiva, S.A.R., Russell, R.M., 1999.  $\beta$ -Carotene and other carotenoids as antioxidants. *Journal of the American College of Nutrition.* 18, 426-433.
- Pérez-Sánchez, J., Bermejo-Nogales, A., Calduch-Giner, J.A., Kaushik, S., Sitjá-Bobadilla, A., 2011. Molecular characterization and expression analysis of six peroxiredoxin paralogous genes in gilthead sea bream (*Sparus aurata*): Insights from fish exposed to dietary, pathogen and confinement stressors. *Fish and Shellfish Immunology.* 31, 294-302.
- Petasne, R.G., Zika, R.G., 1987. Fate of superoxide in coastal sea water. *Nature.* 325, 516-518.
- Pikaev, A.K., Ershov, B.G., 1987. Primary products of the radiolysis of water and their reactivity. *Russian Chemical Reviews.* 36, 602-620.
- Pugsley, A.P., 1993. The complete general secretory pathway in gram-negative bacteria. *Microbiological Reviews.* 57, 50-108.
- Rada, B., Leto, T.L., 2008. Oxidative innate immune defences by Nox/Duox family NADPH oxidases. *Contrib. Microbiol.* 15, 164-187.
- Rahlfs, S., Becker, K., 2001. Thioredoxin peroxidases of the malarial parasite *Plasmodium falciparum*. *Eur. J. Biochem.* 268, 1404–1409.
- Rhee, S.G., 2006. H<sub>2</sub>O<sub>2</sub>, a necessary evil for cell signalling. *Science.* 321, 1882-1883.

- Rhee, S.G., Chae, H.Z., Kim, K., 2005. Peroxiredoxins: a historical overview and speculative preview of novel mechanisms and emerging concepts in cell signalling, *Free Radic. Biol. Med.* 38, 1543–1552.
- Rhee, S.G., Woo, H.A., 2011. Multiple functions of peroxiredoxins: Peroxidases, sensors and regulators of the intracellular messenger H<sub>2</sub>O<sub>2</sub>, and protein chaperones. *Antioxidants and Redox Signalling.* 15, 781-794.
- Riley, P.A., 1994. Free radicals in biology: oxidative stress and the effects of ionising radiation. *International Journal of Radiation Biology.* 65, 27-33.
- Roald, S.O., Armstrong, D., Landsverk, T., 1981. Histochemical, fluorescent and electron microscopical appearance of hepatocellular ceroidosis in the Atlantic salmon *Salmo salar* L. *Journal of Fish Diseases.* 4, 1-14.
- Saitou, N., Nei, M., 1987. The neighbor-joining method: a new method for reconstructing phylogenetic trees. *Mol. Biol. Evol.* 4, 406–425.
- Sambrook, J., Fritsch, E.F. and Maniatis, T., 1989. *Molecular Cloning: A Laboratory Manual.* Cold Spring Harbor Laboratory Press, NY.
- Sauri, H., Butterfield, L., Kim, A., Shau, H.Y., 1995. Antioxidant function of recombinant human natural killer enhancing factor. *Biochemical and biophysical research communications.* 208, 964-969.
- Sayeed, I., Parvez, S., Pandey, S., Bin-Hafeez, B., Haque, R., Raisuddin, S., 2003. Oxidative stress biomarkers of exposure to deltamethrin in freshwater fish, *Channa punctatus* Bloch. *Ecotoxicology and Environmental Safety.* 56, 295-301.
- Sayed, A.A., Williams, D.L., 2004. Biochemical characterization of 2-Cys peroxiredoxins from *Schistosoma mansoni*. *J. Biol. Chem.* 229, 26159–26166.

- Scandalious, J.G., 1993. Oxygen stress and superoxide dismutase. *Plant Physiology*. 101, 7-12.
- Schrader, M., Fahimi, H.D., 2004. Mammalian peroxisomes and reactive oxygen species. *Histochemistry and Cell Biology*. 122, 383-393.
- Schröder, E., Littlechild, J.A., Lebedev, A.A, Errington, N., Vagin, A.A. and Isupov, M.N., 2000. Crystal structure of a decameric 2-Cys peroxiredoxin from human erythrocytes at 1.7 Å resolution, *Structure*. 8, 605-615.
- Schröder, E., Willis, A.C., Ponting, C.P., 1998. Porcine natural-killer-enhancing factor B: oligomerisation and identification as a calpain substrate *in vitro*. *Biochimica Et Biophysica Acta*. 1383, 279-291.
- Sekiya, M., Mulcahy, G., Irwin, J.A., Stack, C.M., Donnelly, S.M., Xu, W., Collins, P., Dalton, J.P., 2006. Biochemical characterization of the recombinant peroxiredoxin (FhePrx) of the liver fluke, *Fasciola hepatica*. *FEBS Letters*. 580, 5016-5022.
- Serbinova, E., Kagan, V., Han, D., Packer, L., 1991. Free radical recycling and intermembrane mobility in the antioxidant properties of alpha-tocopherol and alpha-tocotrienol. *Free Radical Biology and Medicine*. 10, 263-275.
- Shau, H., Butterfield, L.H., Chiu, R., Kim, A., 1994. Cloning and sequence analysis of candidate human natural killer-enhancing factor genes. *Immunogenetics*. 40, 129-134.
- Shau, H., Gupta, R.K., Golub, S.H., 1993. Identification of a natural killer enhancing factor (NKEF) from human erythroid cells. *Cell Immunology*. 147, 1-11.
- Shin, D., Fujiki, k., Nakao, M., Yano, T., 2001. Organisation of the NKEF gene and its expression in the common carp (*Cyprinus carpio*). *Developmental and comparative immunology*. 25, 597-606.

- Sies, H., 1997. Oxidative stress: Oxidants and antioxidants. *Experimental Physiology*. 82, 291-295.
- Sies, H., Stahl, W., 1995. Vitamins E and C,  $\beta$ -carotene, and other carotenoids as antioxidants. *The American Journal of Clinical Nutrition*. 62 (suppl), 1315S-1321S.
- Stadtman, E.R., Levine, R.L., 2000. Protein oxidation. *Annals of the New York Academy of Sciences*. 899, 191-208.
- Stohs, S.J., Bagchi, D., 1995. Oxidative mechanisms in the toxicity of metal ions. *Free Radical Biology and Medicine*. 18, 321-336.
- Sutton, D.L., Loo, G.H., Menz, R.I., Schuller, K.A., 2010. Cloning and functional characterization of a typical 2-Cys peroxiredoxin from southern bluefin tuna (*Thunnus maccoyii*). *Comparative Biochemistry and Physiology, Part B*. 156, 97-106.
- Talmadge, K., Brosius, J., Gilbert, W., 1981. An internal signal sequence directs secretion and processing of proinsulin in bacteria. *Nature*. 294, 176-178.
- Thannickal, V.J., Fanburg, B.L., 2000. Reactive oxygen species in cell signalling. *Am. J. Physiol. Lung Cell Mol. Physiol.* 279, L1005-L1028.
- Thompson, J.L., Thomas, P.M., Schuller, K.A., 2006. Purification and properties of a glutathione peroxidase from southern bluefin tuna (*Thunnus maccoyii*) liver. *Comp. Biochem. Physiol. Part B*. 144, 86-93.
- Toppo, S., Flohé, L., Ursini, F., Vanin, S., Maiorino, M., 2009. Catalytic mechanisms and specificities of glutathione peroxidases: variations of a basic scheme. *Biochimica et Biophysica Acta*. 1790, 1486-1500.

Uhlinger, D.J., Tyagi, S.R., Inge, K.L., Lambeth, J.D., 1993. The respiratory burst oxidase of human neutrophils. *The Journal of Biological Chemistry*. 268, 8624-8631.

Valent, Q.A., Scotti, P.A., High, S., de Gier, J.L., von Heijne, G., Lentzen, G., Wintermeyer, W., Oudega, B., Luirink, J., 1998. The *Escherichia coli* SRP and SecB targeting pathways converge at the translocon. *The EMBO Journal*. 17, 2504-2512.

Van Baalen, C., Marler, J.E., 1966. Occurrence of hydrogen peroxide in sea water. *Nature*. 211, 951.

Vig, É., Gabrielak, T., Leyko, W., Nemcsók, J., Matkovics, B., 1989. Purification and characterization of Cu,Zn-superoxide dismutase from common carp liver. *Comparative Biochemistry and Physiology Part B: Comparative Biochemistry*. 94, 395-397.

Watts, C., Wickner, W., Zimmermann, R., 1983. M13 procoat and pre-immunoglobulin share processing specificity but use different membrane receptor mechanisms. *Proc. Natl. Acad. Sci. USA*. 80, 2809-2813.

Weisiger, R.A., Fridovich, I., 1973. Superoxide dismutase. *The Journal of Biological Chemistry*. 248, 3582-3592.

Weiss, M.S., Palm, G.J. and Hilgenfeld, R., 2000. Crystallization, structure solution and refinement of hen egg-white lysozyme at pH 8.0 in the presence of MPD. *Acta Cryst. D56*, 952-958.

Winterbourn, C.C., Metodiewa, D., 1999. Reactivity of biologically important thiol compounds with superoxide and hydrogen peroxide. *Free radical biology and medicine*. 27, 322-328.



Wood, Z.A., Poole, L.B., Hantgan, R.R., Karplus, P.A., 2002. Dimers to doughnuts: Redox-sensitive oligomerization of 2-Cysteine peroxiredoxins. *Biochemistry*. 41, 5493-5504.

Wood, Z.A., Poole, L.B., Karplus, P.A., 2003a. Peroxiredoxin evolution and the regulation of hydrogen peroxide signalling. *Science*. 300, 650–653.

Wood, Z.A., Schröder, E., Harris, J.R., Poole, L.B., 2003b. Structure, mechanism and regulation of peroxiredoxins. *TRENDS in Biochemical Sciences*. 28, 32-40.

Yang, K.-S., Kang, S.W., Woo, H.A., Hwang, S.C., Chae, H.Z., Kim, K., Rhee, S.G., 2002. Inactivation of human peroxiredoxin I during catalysis as the result of the oxidation of the catalytic site cysteine to cysteine-sulfinic acid. *J. Biol. Chem*. 277, 38029–38036.

Zhang, H., Evenhuis, J.P., Thorgaard, G.H., Ristow, S.S., 2001. Cloning, characterization and genomic structure of the natural killer cell enhancement factor (NKEF)-like gene from homozygous clones of rainbow trout (*Oncorhynchus mykiss*). *Developmental and comparative immunology*. 25, 25-35.

# Appendix

## Crystallisation suite composition tables

### 1.1 Qiagen<sup>®</sup> NeXtal<sup>®</sup> Classic Suite

Number	Well (96- well plates)	Salt	Buffer	Precipitant
1	A1	0.01 M Cobalt chloride	0.1 M Sodium acetate pH 4.6	1.0 M 1,6-Hexanediol
2	A2		0.1 M tri-Sodium citrate pH 5.6	2.5 M 1,6-Hexanediol
3	A3	0.2 M Magnesium chloride	0.1 M TRIS pH 8.5	3.4 M 1,6-Hexanediol
4	A4	2.0 M Ammonium sulfate		5 %(v/v) Isopropanol
5	A5		0.1 M HEPES sodium salt pH 7.5	10 %(v/v) Isopropanol 20 %(w/v) PEG 4000
6	A6	0.2 M Calcium chloride	0.1 M Sodium acetate pH 4.6	20 %(v/v) Isopropanol
7	A7		0.1 M tri-Sodium citrate pH 5.6	20 %(v/v) Isopropanol 20 %(w/v) PEG 4000
8	A8	0.2 M tri-Sodium citrate	0.1 M HEPES sodium salt pH 7.5	20 %(v/v) Isopropanol
9	A9	0.2 M tri-Sodium citrate	0.1 M Sodium cacodylate pH 6.5 0.1 M HEPES sodium salt pH 7.5	30 %(v/v) Isopropanol
10	A10	0.2 M Magnesium chloride	7.5	30 %(v/v) Isopropanol

11	A11	0.2 M Ammonium acetate	0.1 M TRIS.HCl pH 8.5	30 %(v/v) Isopropanol
12	A12	1.5 M Sodium chloride		10 %(v/v) Ethanol
13	B1		0.1 M TRIS pH 8.5	20 %(v/v) Ethanol
14	B2			25 %(v/v) Ethylene glycol
15	B3	0.02 M Calcium chloride	0.1 M Sodium acetate pH 4.6	30 %(v/v) MPD
16	B4	0.2 M Sodium chloride	0.1 M Sodium acetate pH 4.6	30 %(v/v) MPD
17	B5	0.2 M Ammonium acetate	0.1 M tri-Sodium citrate pH 5.6	30 %(v/v) MPD
18	B6	0.2 M Magnesium acetate	0.1 M Sodium cacodylate pH 6.5	30 %(v/v) MPD
19	B7	0.2 M tri-Sodium citrate	0.1 M HEPES sodium salt pH 7.5	30 %(v/v) MPD
20	B8	0.5 M Ammonium sulfate	0.1 M HEPES pH 7.5	30 %(v/v) MPD
21	B9	0.2 M Ammonium phosphate	0.1 M TRIS pH 8.5	50 %(v/v) MPD
22	B10		0.1 M HEPES pH 7.5	70 %(v/v) MPD
23	B11		0.1 M TRIS pH 8.5	25 %(v/v) tert-Butanol
24	B12		0.1 M tri-Sodium citrate pH 5.6	35 %(v/v) tert-Butanol
25	C1			0.4 M Ammonium phosphate
26	C2		0.1 M tri-Sodium citrate pH 5.6	1.0 M Ammonium phosphate
27	C3		0.1 M TRIS.HCl pH 8.5	2.0 M Ammonium phosphate
28	C4		0.1 M HEPES pH 7.5	2.0 M Ammonium formate
29	C5		0.1 M Sodium acetate pH 4.6	2.0 M Ammonium sulfate
30	C6		0.1 M TRIS.HCl pH 8.5	2.0 M Ammonium sulfate
31	C7			2.0 M Ammonium sulfate
32	C8	0.1 M Sodium chloride	0.1 M HEPES pH 7.5	1.6 M Ammonium sulfate
33	C9	0.01 M Cobalt chloride	0.1 M MES pH 6.5	1.8 M Ammonium sulfate
34	C10	0.2 M K/Na tartrate	0.1 M tri-Sodium citrate pH 5.6	2.0 M Ammonium sulfate
35	C11			1.0 M Imidazole pH 7.0
36	C12			0.4 M K/Na tartrate
37	D1		0.1 M HEPES sodium salt pH 7.5	0.8 M K/Na tartrate
38	D2		0.1 M Imidazole pH 6.5	1.0 M Sodium acetate
39	D3	0.05 M Cadmium sulfate	0.1 M HEPES pH 7.5	1.0 M Sodium acetate
40	D4		0.1 M Sodium cacodylate pH 6.5	1.4 M Sodium acetate

41	D5		0.1 M Sodium acetate pH 4.6	2.0 M Sodium chloride
42	D6	0.1 M Sodium phosphate 0.1 M Potassium phosphate	0.1 M MES pH 6.5	2.0 M Sodium chloride
43	D7		0.1 M HEPES pH 7.5 0.1 M HEPES sodium salt pH 7.5	4.3 M Sodium chloride
44	D8			1.4 M tri-Sodium citrate
45	D9			1.6 M tri-Sodium citrate pH 6.5
46	D10		0.1 M HEPES sodium salt pH 7.5	0.8 M Sodium phosphate 0.8 M Potassium phosphate
47	D11		0.1 M Sodium acetate pH 4.6	2.0 M Sodium formate
48	D12			4.0 M Sodium formate
49	E1		0.1 M BICINE pH 9.0	2 %(v/v) Dioxane 10 %(w/v) PEG 20000
50	E2	1.6 M Ammonium sulfate	0.1 M MES pH 6.5	10 %(v/v) Dioxane
51	E3			35 %(v/v) Dioxane 2 %(v/v) Ethylene imine polymer
52	E4	0.5 M Sodium chloride	0.1 M tri-Sodium citrate pH 5.6	
53	E5	1.5 M Ammonium sulfate	0.1 M TRIS pH 8.5	12 %(v/v) Glycerol
54	E6	0.5 M Sodium chloride 0.01 M Magnesium chloride		0.01 M CTAB
55	E7	0.01 M Ferric chloride	0.1 M tri-Sodium citrate pH 5.6	10 %(v/v) Jeffamine M-600
56	E8		0.1 M HEPES pH 7.5	20 %(v/v) Jeffamine M-600
57	E9	0.5 M Ammonium sulfate	0.1 M tri-Sodium citrate pH 5.6	1.0 M Lithium sulfate
58	E10	0.01 M Nickel chloride	0.1 M TRIS pH 8.5 0.1 M HEPES sodium salt pH 7.5	1.0 M Lithium sulfate
59	E11			1.5 M Lithium sulfate
60	E12		0.1 M BICINE pH 9.0	2.0 M Magnesium chloride
61	F1			0.2 M Magnesium formate
62	F2		0.1 M MES pH 6.5	1.6 M Magnesium sulfate
63	F3		0.1 M TRIS.HCl pH 8.5	8 %(w/v) PEG 8000
64	F4		0.1 M HEPES pH 7.5	10 %(w/v) PEG 8000
65	F5	0.5 M Lithium sulfate		15 %(w/v) PEG 8000

66	F6	0.2 M Zinc acetate	0.1 M Sodium cacodylate pH 6.5	18 %(w/v) PEG 8000
67	F7	0.2 M Calcium acetate	0.1 M Sodium cacodylate pH 6.5	18 %(w/v) PEG 8000
68	F8	0.2 M Magnesium acetate	0.1 M Sodium cacodylate pH 6.5	20 %(w/v) PEG 8000
69	F9	0.05 M Potassium phosphate		20 %(w/v) PEG 8000
70	F10	0.2 M Ammonium sulfate	0.1 M Sodium cacodylate pH 6.5	30 %(w/v) PEG 8000
71	F11	0.2 M Sodium acetate	0.1 M Sodium cacodylate pH 6.5	30 %(w/v) PEG 8000
72	F12	0.2 M Ammonium sulfate		30 %(w/v) PEG 8000
73	G1	2.0 M Ammonium sulfate	0.1 M HEPES sodium salt pH 7.5	2 %(v/v) PEG 400
74	G2	0.2 M Calcium chloride	0.1 M HEPES sodium salt pH 7.5	28 %(v/v) PEG 400
75	G3	0.1 M Cadmium chloride	0.1 M Sodium acetate pH 4.6 0.1 M HEPES sodium salt pH 7.5	30 %(v/v) PEG 400
76	G4	0.2 M Magnesium chloride		30 %(v/v) PEG 400
77	G5	0.2 M tri-Sodium citrate	0.1 M TRIS.HCl pH 8.5	30 %(v/v) PEG 400
78	G6	0.1 M Sodium chloride	0.1 M BICINE pH 9.0	20 %(w/v) PEG 550 MME
79	G7	0.01 M Zinc sulfate	0.1 M MES pH 6.5	25 %(w/v) PEG 550 MME
80	G8			10 %(w/v) PEG 1000 10 %(w/v) PEG 8000
81	G9			30 %(w/v) PEG 1500
82	G10	0.01 M Nickel chloride	0.1 M TRIS pH 8.5	20 %(w/v) PEG 2000 MME
83	G11	0.2 M Ammonium sulfate	0.1 M Sodium acetate pH 4.6	30 %(w/v) PEG 2000 MME
84	G12		0.1 M Sodium acetate pH 4.6	8 %(w/v) PEG 4000
85	H1	0.2 M Ammonium sulfate	0.1 M Sodium acetate pH 4.6	25 %(w/v) PEG 4000
86	H2	0.2 M Ammonium acetate	0.1 M Sodium acetate pH 4.6	30 %(w/v) PEG 4000
87	H3	0.2 M Ammonium acetate	0.1 M tri-Sodium citrate pH 5.6	30 %(w/v) PEG 4000
88	H4	0.2 M Magnesium chloride	0.1 M TRIS.HCl pH 8.5	30 %(w/v) PEG 4000
89	H5	0.2 M Lithium sulfate	0.1 M TRIS.HCl pH 8.5	30 %(w/v) PEG 4000
90	H6	0.2 M Sodium acetate	0.1 M TRIS.HCl pH 8.5	30 %(w/v) PEG 4000
91	H7	0.2 M Ammonium sulfate		30 %(w/v) PEG 4000
92	H8	0.2 M Ammonium sulfate	0.1 M MES pH 6.5	30 %(w/v) PEG 5000 MME
93	H9		0.1 M HEPES pH 7.5	10 %(w/v) PEG 6000 5 %(v/v) MPD

94	H10	2.0 M Sodium chloride		10 %(w/v) PEG 6000
95	H11		0.1 M HEPES pH 7.5	20 %(w/v) PEG 10000
96	H12		0.1 M MES pH 6.5	8 %(v/v) Ethylene glycol 12 %(w/v) PEG 20000

## 1.2 Qiagen<sup>®</sup> NeXtal<sup>®</sup> PEGs Suite

Number	Well (96- well Plates)	Salt	Buffer	Precipitant
1	A1		0.1 M Sodium acetate pH 4.6	40 %(v/v) PEG 200
2	A2		0.1 M Sodium acetate pH 4.6	30 %(v/v) PEG 300
3	A3		0.1 M Sodium acetate pH 4.6	30 %(v/v) PEG 400
4	A4		0.1 M Sodium acetate pH 4.6	25 %(v/v) PEG 550 MME
5	A5		0.1 M Sodium acetate pH 4.6	25 %(w/v) PEG 1000
6	A6		0.1 M Sodium acetate pH 4.6	25 %(w/v) PEG 2000 MME
7	A7		0.1 M MES pH 6.5	40 %(v/v) PEG 200
8	A8		0.1 M MES pH 6.5	30 %(v/v) PEG 300
9	A9		0.1 M MES pH 6.5	30 %(v/v) PEG 400
10	A10		0.1 M MES pH 6.5	25 %(v/v) PEG 550 MME
11	A11		0.1 M MES pH 6.5	25 %(w/v) PEG 1000
12	A12		0.1 M MES pH 6.5	25 %(w/v) PEG 2000 MME
13	B1		0.1 M Sodium HEPES pH 7.5	40 %(v/v) PEG 200
14	B2		0.1 M Sodium HEPES pH 7.5	30 %(v/v) PEG 300
15	B3		0.1 M Sodium HEPES pH 7.5	30 %(v/v) PEG 400
16	B4		0.1 M Sodium HEPES pH 7.5	25 %(v/v) PEG 550 MME
17	B5		0.1 M Sodium HEPES pH 7.5	25 %(w/v) PEG 1000
18	B6		0.1 M Sodium HEPES pH 7.5	25 %(w/v) PEG 2000 MME
19	B7		0.1 M TRIS.HCl pH 8.5	40 %(v/v) PEG 200
20	B8		0.1 M TRIS.HCl pH 8.5	30 %(v/v) PEG 300
21	B9		0.1 M TRIS.HCl pH 8.5	30 %(v/v) PEG 400
22	B10		0.1 M TRIS.HCl pH 8.5	25 %(v/v) PEG 550 MME

23	B11		0.1 M TRIS.HCl pH 8.5	25 %(w/v) PEG 1000
24	B12		0.1 M TRIS.HCl pH 8.5	25 %(w/v) PEG 2000 MME
25	C1		0.1 M Sodium acetate pH 4.6	25 %(w/v) PEG 3000
26	C2		0.1 M Sodium acetate pH 4.6	25 %(w/v) PEG 4000
27	C3		0.1 M Sodium acetate pH 4.6	25 %(w/v) PEG 6000
28	C4		0.1 M Sodium acetate pH 4.6	25 %(w/v) PEG 8000
29	C5		0.1 M Sodium acetate pH 4.6	20 %(w/v) PEG 10000
30	C6		0.1 M Sodium acetate pH 4.6	15 %(w/v) PEG 20000
31	C7		0.1 M MES pH 6.5	25 %(w/v) PEG 3000
32	C8		0.1 M MES pH 6.5	25 %(w/v) PEG 4000
33	C9		0.1 M MES pH 6.5	25 %(w/v) PEG 6000
34	C10		0.1 M MES pH 6.5	25 %(w/v) PEG 8000
35	C11		0.1 M MES pH 6.5	20 %(w/v) PEG 10000
36	C12		0.1 M MES pH 6.5	15 %(w/v) PEG 20000
37	D1		0.1 M Sodium HEPES pH 7.5	25 %(w/v) PEG 3000
38	D2		0.1 M Sodium HEPES pH 7.5	25 %(w/v) PEG 4000
39	D3		0.1 M Sodium HEPES pH 7.5	25 %(w/v) PEG 6000
40	D4		0.1 M Sodium HEPES pH 7.5	25 %(w/v) PEG 8000
41	D5		0.1 M Sodium HEPES pH 7.5	20 %(w/v) PEG 10000
42	D6		0.1 M Sodium HEPES pH 7.5	15 %(w/v) PEG 20000
43	D7		0.1 M TRIS.HCl pH 8.5	25 %(w/v) PEG 3000
44	D8		0.1 M TRIS.HCl pH 8.5	25 %(w/v) PEG 4000
45	D9		0.1 M TRIS.HCl pH 8.5	25 %(w/v) PEG 6000
46	D10		0.1 M TRIS.HCl pH 8.5	25 %(w/v) PEG 8000
47	D11		0.1 M TRIS.HCl pH 8.5	20 %(w/v) PEG 10000
48	D12		0.1 M TRIS.HCl pH 8.5	15 %(w/v) PEG 20000
49	E1	0.2 M Sodium fluoride		20 %(w/v) PEG 3350
50	E2	0.2 M Potassium fluoride		20 %(w/v) PEG 3350



51	E3	0.2 M Ammonium fluoride	20 %(w/v) PEG 3350
52	E4	0.2 M Lithium chloride	20 %(w/v) PEG 3350
53	E5	0.2 M Magnesium chloride	20 %(w/v) PEG 3350
54	E6	0.2 M Sodium chloride	20 %(w/v) PEG 3350
55	E7	0.2 M Calcium chloride	20 %(w/v) PEG 3350
56	E8	0.2 M Potassium chloride	20 %(w/v) PEG 3350
57	E9	0.2 M Ammonium chloride	20 %(w/v) PEG 3350
58	E10	0.2 M Sodium iodide	20 %(w/v) PEG 3350
59	E11	0.2 M Potassium iodide	20 %(w/v) PEG 3350
60	E12	0.2 M Ammonium iodide	20 %(w/v) PEG 3350
61	F1	0.2 M Sodium thiocyanate	20 %(w/v) PEG 3350
62	F2	0.2 M Potassium thiocyanate	20 %(w/v) PEG 3350
63	F3	0.2 M Lithium nitrate	20 %(w/v) PEG 3350
64	F4	0.2 M Magnesium nitrate	20 %(w/v) PEG 3350
65	F5	0.2 M Sodium nitrate	20 %(w/v) PEG 3350
66	F6	0.2 M Potassium nitrate	20 %(w/v) PEG 3350
67	F7	0.2 M Ammonium nitrate	20 %(w/v) PEG 3350
68	F8	0.2 M Magnesium formate	20 %(w/v) PEG 3350
69	F9	0.2 M Sodium formate	20 %(w/v) PEG 3350
70	F10	0.2 M Potassium formate	20 %(w/v) PEG 3350
71	F11	0.2 M Ammonium formate	20 %(w/v) PEG 3350
72	F12	0.2 M Lithium acetate	20 %(w/v) PEG 3350
73	G1	0.2 M Magnesium acetate	20 %(w/v) PEG 3350
74	G2	0.2 M Zinc acetate	20 %(w/v) PEG 3350
75	G3	0.2 M Sodium acetate	20 %(w/v) PEG 3350
76	G4	0.2 M Calcium acetate	20 %(w/v) PEG 3350
77	G5	0.2 M Potassium acetate	20 %(w/v) PEG 3350
78	G6	0.2 M Ammonium acetate	20 %(w/v) PEG 3350
79	G7	0.2 M Lithium sulfate	20 %(w/v) PEG 3350
80	G8	0.2 M Magnesium sulfate	20 %(w/v) PEG 3350
81	G9	0.2 M Sodium sulfate	20 %(w/v) PEG 3350
82	G10	0.2 M Potassium sulfate	20 %(w/v) PEG 3350

83	G11	0.2 M Ammonium sulfate	20 %(w/v) PEG 3350
84	G12	0.2 M di-Sodium tartrate	20 %(w/v) PEG 3350
85	H1	0.2 M K/Na tartrate	20 %(w/v) PEG 3350
86	H2	0.2 M di-Ammonium tartrate	20 %(w/v) PEG 3350
87	H3	0.2 M Sodium phosphate	20 %(w/v) PEG 3350
88	H4	0.2 M di-Sodium phosphate	20 %(w/v) PEG 3350
89	H5	0.2 M Potassium phosphate	20 %(w/v) PEG 3350
90	H6	0.2 M di-Potassium phosphate	20 %(w/v) PEG 3350
91	H7	0.2 M Ammonium phosphate	20 %(w/v) PEG 3350
92	H8	0.2 M di-Ammonium phosphate	20 %(w/v) PEG 3350
93	H9	0.2 M tri-Lithium citrate	20 %(w/v) PEG 3350
94	H10	0.2 M tri-Sodium citrate	20 %(w/v) PEG 3350
95	H11	0.2 M tri-Potassium citrate	20 %(w/v) PEG 3350
96	H12	0.18 M tri-Ammonium citrate	20 %(w/v) PEG 3350

### 1.3 Qiagen® NeXtal® MPD Suite

Number	Well (96-well plates)	Salt	Buffer	Precipitant
1	A1	0.2 M Cadmium chloride		40 %(v/v) MPD
2	A2	0.2 M Potassium fluoride		40 %(v/v) MPD
3	A3	0.2 M Ammonium fluoride		40 %(v/v) MPD
4	A4	0.2 M Lithium chloride		40 %(v/v) MPD
5	A5	0.2 M Magnesium chloride		40 %(v/v) MPD
6	A6	0.2 M Sodium chloride		40 %(v/v) MPD
7	A7	0.2 M Calcium chloride		40 %(v/v) MPD
8	A8	0.2 M Potassium chloride		40 %(v/v) MPD
9	A9	0.2 M Ammonium chloride		40 %(v/v) MPD
10	A10	0.2 M Sodium iodide		40 %(v/v) MPD
11	A11	0.2 M Potassium iodide		40 %(v/v) MPD
12	A12	0.2 M Ammonium iodide		40 %(v/v) MPD
13	B1	0.2 M Sodium thiocyanate		40 %(v/v) MPD
14	B2	0.2 M Potassium thiocyanate		40 %(v/v) MPD
15	B3	0.2 M Lithium nitrate		40 %(v/v) MPD
16	B4	0.2 M Magnesium nitrate		40 %(v/v) MPD
17	B5	0.2 M Sodium nitrate		40 %(v/v) MPD
18	B6	0.2 M Potassium nitrate		40 %(v/v) MPD
19	B7	0.2 M Ammonium nitrate		40 %(v/v) MPD
20	B8	0.2 M Zinc sulfate		40 %(v/v) MPD
21	B9	0.2 M Sodium formate		40 %(v/v) MPD
22	B10	0.2 M Potassium formate		40 %(v/v) MPD
23	B11	0.2 M Ammonium formate		40 %(v/v) MPD
24	B12	0.2 M Lithium acetate		40 %(v/v) MPD
25	C1	0.2 M Magnesium acetate		40 %(v/v) MPD
26	C2	0.2 M Sodium malonate		40 %(v/v) MPD

27	C3	0.2 M Sodium acetate	40 %(v/v) MPD
28	C4	0.2 M Calcium acetate	40 %(v/v) MPD
29	C5	0.2 M Potassium acetate	40 %(v/v) MPD
30	C6	0.2 M Ammonium acetate	40 %(v/v) MPD
31	C7	0.2 M Lithium sulfate	40 %(v/v) MPD
32	C8	0.2 M Magnesium sulfate	40 %(v/v) MPD
33	C9	0.2 M Cesium chloride	40 %(v/v) MPD
34	C10	0.2 M Nickel chloride	40 %(v/v) MPD
35	C11	0.2 M Ammonium sulfate	40 %(v/v) MPD
36	C12	0.2 M di-Sodium tartrate	40 %(v/v) MPD
37	D1	0.2 M Potassium/Sodium tartrate	40 %(v/v) MPD
38	D2	0.2 M di-Ammonium tartrate	40 %(v/v) MPD
39	D3	0.2 M Sodium phosphate	40 %(v/v) MPD
40	D4	0.2 M Potassium bromide	40 %(v/v) MPD
41	D5	0.2 M Sodium bromide	40 %(v/v) MPD
42	D6	0.2 M di-Potassium phosphate	40 %(v/v) MPD
43	D7	0.2 M Ammonium phosphate	40 %(v/v) MPD
44	D8	0.2 M di-Ammonium phosphate	40 %(v/v) MPD
45	D9	0.2 M tri-Lithium citrate	40 %(v/v) MPD
46	D10	0.2 M Sodium citrate	40 %(v/v) MPD
47	D11	0.2 M tri-Potassium citrate	40 %(v/v) MPD
48	D12	0.18 M tri-Ammonium citrate	40 %(v/v) MPD
49	E1	0.1 M Citric acid pH 4.0	10 %(v/v) MPD
50	E2	0.1 M Sodium acetate pH 5.0	10 %(v/v) MPD
51	E3	0.1 M MES pH 6.0	10 %(v/v) MPD
52	E4	0.1 M HEPES pH 7.0	10 %(v/v) MPD
53	E5	0.1 M TRIS pH 8.0	10 %(v/v) MPD
54	E6	0.1 M BICINE pH 9.0	10 %(v/v) MPD
55	E7	0.1 M Citric acid pH 4.0	20 %(v/v) MPD
56	E8	0.1 M Sodium acetate pH 5.0	20 %(v/v) MPD
57	E9	0.1 M MES pH 6.0	20 %(v/v) MPD
58	E10	0.1 M HEPES pH 7.0	20 %(v/v) MPD

59	E11		0.1 M TRIS pH 8.0	20 %(v/v) MPD
60	E12		0.1 M BICINE pH 9.0	20 %(v/v) MPD
61	F1		0.1 M Citric acid pH 4.0	40 %(v/v) MPD
62	F2		0.1 M Sodium acetate pH 5.0	40 %(v/v) MPD
63	F3		0.1 M MES pH 6.0	40 %(v/v) MPD
64	F4		0.1 M HEPES pH 7.0	40 %(v/v) MPD
65	F5		0.1 M TRIS pH 8.0	40 %(v/v) MPD
66	F6		0.1 M BICINE pH 9.0	40 %(v/v) MPD
67	F7		0.1 M Sodium acetate pH 4.0	65 %(v/v) MPD
68	F8		0.1 M Sodium acetate pH 5.0	65 %(v/v) MPD
69	F9		0.1 M MES pH 6.0	65 %(v/v) MPD
70	F10		0.1 M HEPES pH 7.0	65 %(v/v) MPD
71	F11		0.1 M TRIS pH 8.0	65 %(v/v) MPD
72	F12		0.1 M BICINE pH 9.0	65 %(v/v) MPD
73	G1	0.1 M Sodium citrate	0.1 M HEPES sodium salt pH 7.5	10 %(w/v) MPD
74	G2	0.05 M Magnesium chloride	0.1 M TRIS.HCl pH 8.5	12 %(w/v) MPD
75	G3	0.02 M Calcium chloride	0.1 M Sodium acetate pH 4.6	15 %(w/v) MPD
76	G4		0.1 M Imidazole.HCl pH 8.0	15 %(w/v) MPD
				5 %(w/v) PEG 4000
77	G5	0.2 M Ammonium acetate	0.1 M Sodium citrate pH 5.6	15 %(w/v) MPD
78	G6	0.2 M Magnesium acetate	0.1 M MES sodium salt pH 6.5	15 %(w/v) MPD
79	G7	0.2 M Sodium citrate	0.1 M HEPES sodium salt pH 7.5	15 %(w/v) MPD
80	G8	0.1 M Sodium citrate	0.1 M HEPES sodium salt pH 7.5	20 %(w/v) MPD
81	G9		0.1 M Imidazole.HCl pH 8.0	20 %(w/v) MPD
82	G10	0.2 M Sodium chloride		20 %(w/v) MPD
				4 %(w/v) Glycerol
83	G11	0.02 M Calcium chloride	0.1 M Sodium acetate pH 4.6	30 %(w/v) MPD
84	G12	0.2 M Ammonium acetate	0.1 M Sodium citrate pH 5.6	30 %(w/v) MPD
85	H1	0.2 M Magnesium acetate	0.1 M MES sodium salt pH 6.5	30 %(w/v) MPD
86	H2	0.5 M Ammonium sulfate	0.1 M HEPES sodium salt pH 7.5	30 %(w/v) MPD
87	H3	0.2 M Sodium citrate	0.1 M HEPES sodium salt pH 7.5	30 %(w/v) MPD
88	H4		0.1 M HEPES sodium salt pH 7.5	30 %(w/v) MPD

89	H5	0.1 M Imidazole.HCl pH 8.0	5 %(w/v) PEG 4000 30 %(w/v) MPD
90	H6		10 %(w/v) PEG 4000 30 %(w/v) MPD 20 %(w/v) Ethanol
91	H7		35 %(w/v) MPD
92	H8	0.1 M Imidazole.HCl pH 8.0	35 %(w/v) MPD
93	H9	0.1 M TRIS.HCl pH 8.5	40 %(w/v) MPD
94	H10	0.1 M HEPES sodium salt pH 7.5	47 %(w/v) MPD
95	H11		47 %(w/v) MPD 2 %(w/v) tert-Butanol

## 1.4 Hampton Research Crystal Screen

Number	Salt	Buffer	Precipitant
1	0.02 M Calcium chloride dihydrate	0.1 M Sodium acetate trihydrate pH 4.6	30 % v/v (+/-)-2-Methyl-2,4-pentanediol
2			0.4 M Potassium sodium tartrate tetrahydrate
3			0.4 M Ammonium phosphate monobasic
4		0.1 M TRIS hydrochloride pH 8.5	2.0 Ammonium sulfate
5	0.2 M Sodium citrate tribasic dihydrate	0.1 M HEPES sodium pH 7.5	30 % v/v (+/-)-2-Methyl-2,4- pentanediol
6	0.2 M Magnesium chloride hexahydrate	0.1 M TRIS hydrochloride pH8.5	30 % v/v Polyethylene glycol 4,000
7		0.1 M Sodium cacodylate trihydrate pH 6.5	1.4 M Sodium acetate trihydrate
8	0.2 M Sodium citrate tribasic dihydrate	0.1 M Sodium cacodylate trihydrate pH 6.5	30 % v/v 2-Propanol
9	0.2 M Ammonium acetate	0.1 M Sodium citrate tribasic dihydrate pH 5.6	30 % v/v Polyethylene glycol 4,000
10	0.2 M Ammonium acetate	0.1 M Sodium acetate trihydrate pH 4.6	30 % v/v Polyethylene glycol 4,000
11		0.1 M Sodium citrate tribasic dihydrate pH 5.6	1.0 M Ammonium phosphate monobasic
12	0.2 M Magnesium chloride hexahydrate	0.1 M HEPES sodium pH 7.5	30 % v/v 2-Propanol
13	0.2 M Sodium citrate tribasic dihydrate	0.1 M TRIS hydrochloride pH8.5	30 % v/v Polyethylene glycol 400
14	0.2 M Calcium chloride dihydrate	0.1 M HEPES sodium pH 7.5	28 % v/v Polyethylene glycol 400
15	0.2 M Ammonium sulfate	0.1 M Sodium cacodylate trihydrate pH 6.5	30 % v/v Polyethylene glycol 8,000
16		0.1 M HEPES sodium pH 7.5	1.5 M Lithium sulfate monohydrate
17	0.2 M Lithium sulfate monohydrate	0.1 M TRIS hydrochloride pH 8.5	30 % w/v Polyethylene glycol 4,000
18	0.2 M Magnesium acetate tetrahydrate	0.1 M Sodium cacodylate trihydrate pH 6.5	20 % w/v Polyethylene glycol 8,000
19	0.2 M Ammonium acetate	0.1 M TRIS hydrochloride pH 8.5	30 % v/v 2-Propanol
20	0.2 M Ammonium sulfate	0.1 M Sodium acetate trihydrate pH 4.6	25 % w/v Polyethylene glycol 4,000
21	0.2 M Magnesium acetate tetrahydrate	0.1 M Sodium cacodylate trihydrate pH 6.5	30% v/v (+/-)-2-Methyl-2,4-pentanediol
22	0.2 M Sodium acetate trihydrate	0.1 M TRIS hydrochloride pH 8.5	30 % w/v Polyethylene glycol 4,000

23	0.2 M Magnesium chloride hexahydrate	0.1 M HEPES sodium pH 7.5	30 % v/v Polyethylene glycol 400
24	0.2 M Calcium chloride dihydrate	0.1 M Sodium acetate trihydrate pH 4.6	20 % v/v 2-Propanol
25		0.1 M Imidazole pH 6.5	1.0 M Sodium acetate trihydrate
26	0.2 M Ammonium acetate	0.1 M Sodium citrate tribasic dihydrate pH 5.6	30 % v/v (+/-)-2-Methyl-2,4-pentaneiol
27	0.2 M Sodium citrate tribasic dihydrate	0.1 M HEPES sodium pH 7.5	20 % v/v 2-Propanol
28	0.2 M Sodium acetate trihydrate	0.1 M Sodium cacodylate trihydrate pH 6.5	30 % w/v Polyethylene glycol 8,000
29		0.1 M HEPES sodium pH 7.5	0.8 M Potassium sodium tartrate tetrahydrate
30	0.2 M Ammonium sulfate		30 % w/v Polyethylene glycol 8,000
31	0.2 M Ammonium sulfate		30 % w/v Polyethylene glycol 4,000
32			2.0 M Ammonium sulfate
33			4.0 M Sodium formate
34		0.1 M Sodium acetate trihydrate pH 4.6	2.0 M Sodium formate
35		0.1 M HEPES sodium pH 7.5	0.8 M Sodium phosphate monobasic monohydrate
			0.8 M Potassium phosphate monobasic
36		0.1 M TRIS hydrochloride pH 8.5	8 % w/v Polyethylene glycol 8,000
37		0.1 M Sodium acetate trihydrate pH 4.6	8 % w/v Polyethylene glycol 4,000
38		0.1 M HEPES sodium pH 7.5	1.4 M Sodium citrate tribasic dihydrate
39		0.1 M HEPES sodium pH 7.5	2 % v/v Polyethylene glycol 400
			2.0 M Ammonium sulfate
40		0.1 M Sodium citrate tribasic dihydrate pH 5.6	20 % v/v 2-Propanol
			20 % w/v Polyethylene glycol 4,000
41		0.1 M HEPES sodium pH 7.5	10 % v/v 2-Propanol
			20 % w/v Polyethylene glycol 4,000
42	0.05 M Potassium phosphate monobasic		20 % w/v Polyethylene glycol 8,000
43			30 % w/v Polyethylene glycol 1,500
44			0.2 M Magnesium formate dihydrate
45	0.2 M Zinc acetate dihydrate	0.1 M Sodium cacodylate trihydrate pH 6.5	18 % w/v Polyethylene glycol 8,000



46	0.2 M Calcium acetate hydrate	0.1 M Sodium cacodylate trihydrate pH 6.5	18 % w/v Polyethylene glycol 8,000
47		0.1 M Sodium acetate trihydrate pH 4.6	2.0 M Ammonium sulfate
48		0.1 M TRIS hydrochloride pH 8.5	2.0 M Ammonium phosphate monobasic
49	1.0 M Lithium sulfate monohydrate		2 % w/v Polyethylene glycol 8,000
50	0.5 M Lithium sulfate monohydrate		15 % w/v Polyethylene glycol 8,000

## 1.5 Hampton Research Crystal Screen 2

Number	Salt	Buffer	Precipitant
1	2.0 M Sodium chloride		10 % w/v Polyethylene glycol 6,000
2	0.5 M Sodium chloride 0.01 M Magnesium chloride hexahydrate		0.01 M Hexadecyltrimethylammonium bromide
3			25 % v/v Ethylene glycol
4			35 % v/v 1,4-Dioxane
5	2.0 M Ammonium sulfate		5 % v/v 2-Propanol
6			1.0 M Imidazole pH 7.0
7			10 % w/v Polyethylene glycol 1,000 10 % w/v Polyethylene glycol 8,000
8	1.5 M Sodium chloride		10 % v/v Ethanol
9		0.1 M Sodium acetate trihydrate pH 4.6	2.0 M Sodium chloride
10	0.2 M Sodium chloride	0.1 M Sodium acetate trihydrate pH 4.6	30 % v/v (+/-)-2-Methyl-2,4-pentanediol
11	0.01 M Cobalt(II) chloride hexahydrate	0.1 M Sodium acetate trihydrate pH 4.6	1.0 M 1,6-Hexanediol
12	0.1 M Cadmium chloride hydrate	0.1 M Sodium acetate trihydrate pH 4.6	30 % v/v Polyethylene glycol 400
13	0.2 M Ammonium sulfate	0.1 M Sodium acetate trihydrate pH 4.6	30 % w/v Polyethylene glycol monomethyl ether 2,000
14	0.2 M Potassium sodium tartrate tetrahydrate	0.1 M Sodium citrate tribasic dihydrate pH 5.6	2.0 M Ammonium sulfate
15	0.5 M Ammonium sulfate	0.1 M Sodium citrate tribasic dihydrate pH 5.6	1.0 M Lithium sulfate monohydrate
16	0.5 M Sodium chloride	0.1 M Sodium citrate tribasic dihydrate pH 5.6	2 % v/v Ethylene imine polymer
17		0.1 M Sodium citrate tribasic dihydrate pH 5.6	35 % v/v tert-Butanol
18	0.01 M Iron(III) chloride hexahydrate	0.1 M Sodium citrate tribasic dihydrate pH 5.6	10 % v/v Jeffamine M-600
19		0.1 M Sodium citrate tribasic dihydrate pH 5.6	2.5 M 1,6-Hexanediol
20		0.1 M MES monohydrate pH 6.5	1.6 M Magnesium sulfate heptahydrate

21	0.1 M Sodium phosphate monobasic monohydrate 0.1 M Potassium phosphate monobasic	0.1 M MES monohydrate pH 6.5	2.0 M Sodium chloride
22		0.1 M MES monohydrate pH 6.5	12 % w/v Polyethylene glycol 20,000
23	1.6 M Ammonium sulfate	0.1 M MES monohydrate pH 6.5	10 % v/v 1,4-Dioxane
24	0.05 M Cesium chloride	0.1 M MES monohydrate pH 6.5	30 % v/v Jeffamine M-600
25	0.01 M Cobalt(II) chloride hexahydrate	0.1 M MES monohydrate pH 6.5	1.8 M Ammonium sulfate
26	0.2 M Ammonium sulfate	0.1 M MES monohydrate pH 6.5	30 % w/v Polyethylene glycol monomethyl ether 5,000
27	0.01 M Zinc sulfate heptahydrate	0.1 M MES monohydrate pH 6.5	25 % v/v Polyethylene glycol monomethyl ether 550
28			1.6 M Sodium citrate tribasic dihydrate pH 6.5
29	0.5 M Ammonium sulfate	0.1 M HEPES pH 7.5	30 % v/v (+/-)-2-Methyl-2,4-pentanediol
30		0.1 M HEPES pH 7.5	10 % w/v Polyethylene glycol 6,000
			5 % v/v (+/-)-2-Methyl-2,4-pentanediol
31		0.1 M HEPES pH 7.5	20 % v/v Jeffamine M-600
32	0.1 M Sodium chloride	0.1 M HEPES pH 7.5	1.6 M Ammonium sulfate
33		0.1 M HEPES pH 7.5	2.0 M Ammonium formate
34	0.05 M Cadmium sulfate hydrate	0.1 M HEPES pH 7.5	1.0 M Sodium acetate trihydrate
35		0.1 M HEPES pH 7.5	70 % v/v (+/-)-2-Methyl-2,4-pentanediol
36		0.1 M HEPES pH 7.5	4.3 M Sodium chloride
37		0.1 M HEPES pH 7.5	10 % w/v Polyethylene glycol 8,000
			8% v/v Ethylene glycol
38		0.1 M HEPES pH 7.5	20 % w/v Polyethylene glycol 10,000
39	0.2 M Magnesium chloride hexahydrate	0.1 M Tris pH 8.5	3.4 M 1,6-Hexanediol
40		0.1 M Tris pH 8.5	25 % v/v tert-Butanol
41	0.01 M Nickel(II) chloride hexahydrate	0.1 M Tris pH 8.5	1.0 M Lithium sulfate monohydrate
42	1.5 M Ammonium sulfate	0.1 Tris pH 8.5	12 % v/v Glycerol
43	0.2 M Ammonium phosphate monobasic	0.1 Tris pH 8.5	50 % v/v (+/-)-2-Methyl-2,4-pentanediol
44		0.1 Tris pH 8.5	20 % v/v Ethanol

45	0.01 M Nickel(II) chloride hexahydrate	0.1 Tris pH 8.5	20 % w/v Polyethylene glycol monomethyl ether 2,000
46	0.1 M Sodium chloride	0.1 BICINE pH 9.0	20 % v/v Polyethylene glycol monomethyl ether 550
47		0.1 BICINE pH 9.0	2.0 M Magnesium chloride hexahydrate
48		0.1 BICINE pH 9.0	2 % v/v 1,4-Dioxane
			10 % w/v Polyethylene glycol 20,000